

**Measurement and Modelling of Volatile  
Organic Compounds in a Tropical  
Rainforest Environment**

**Shani Amber Garraway**

Doctor of Philosophy

University of York  
Chemistry

June 2018



# Abstract

This thesis describes measurements of volatile organic compounds made at the Danum Valley Global Atmosphere Watch station in Sabah, Malaysia using gas chromatography with flame ionization detection. Measurements of 13 VOCs were made between August 2015 and March 2016. A non-negative matrix factorization analysis is performed on the observational data, which identified three main periods within the dataset. A period influenced by the Indonesian biomass burning season characterized by large increases in most VOCs concentrations; background periods where local conditions dominate; and a period influenced by local anthropogenic events where short lived increases in some species were seen.

Biomass burning in the region caused a substantial increase in most VOCs at the measurement site between August and October 2015. Comparison of VOC emission ratios with previous studies indicates that the burning in the region is a combination of peat and forest burning. Combining fire maps with air mass trajectories shows that changes in meteorological conditions, not changes in fire activity, drives the variability in VOC concentrations at the measurement site during the biomass burning period.

The background periods were dominated by biogenic emissions. The two VOCs identified as being mainly biogenic in origin were isoprene and propene, with isoprene being the dominant VOC during the background periods. Comparison of propene observations with the GEOS-Chem model shows that the model substantially overestimates propene concentrations. This shows that the current MEGAN propene emissions algorithm based on mid-latitude observations is not appropriate for the tropics. There was good agreement between measured isoprene concentrations and MEGAN derived GEOS-Chem model concentrations. Most previous studies have shown the MEGAN overestimates isoprene emissions. No clear seasonality was seen in isoprene concentrations at the Danum Valley measurement site. This is unlike previous studies in the Amazon, where strong seasonal cycles are observed.



# Table of Contents

<b>ABSTRACT .....</b>	<b>3</b>
<b>TABLE OF CONTENTS.....</b>	<b>5</b>
<b>LIST OF FIGURES .....</b>	<b>11</b>
<b>LIST OF TABLES .....</b>	<b>19</b>
<b>ACKNOWLEDGEMENTS .....</b>	<b>21</b>
<b>DECLARATION.....</b>	<b>23</b>
<b>1 INTRODUCTION.....</b>	<b>25</b>
1.1 UNDERSTANDING COMPOSITION .....	25
1.2 ATMOSPHERIC NOX.....	27
1.3 VOLATILE ORGANIC COMPOUNDS .....	28
1.4 THE IMPORTANCE OF VOCs.....	29
1.5 EMISSION SOURCES AND ALGORITHMS .....	30
1.5.1 <i>Anthropogenic Emissions</i> .....	30
1.5.2 <i>Biogenic Emissions</i> .....	31
1.5.3 <i>Biomass Burning Emissions</i> .....	34
1.5.4 <i>Tropospheric Ozone</i> .....	35
1.6 VOC CHEMISTRY.....	37
1.7 MEASUREMENT TECHNIQUES .....	40
1.7.1 <i>Sampling Methods</i> .....	41
1.7.2 <i>Whole Air Sampling</i> .....	41
1.7.3 <i>Sorbent Sampling</i> .....	42
1.8 SEPARATION AND ANALYSIS.....	42
1.8.1 <i>Gas Chromatography</i> .....	42
1.8.2 <i>Proton Transfer Reaction Mass Spectrometry</i> .....	44
1.9 PREVIOUS OBSERVATIONS OF VOCs.....	44

1.9.1	<i>OP3 Campaign (7<sup>th</sup> April – 4<sup>th</sup> May and 21<sup>st</sup> June – 27<sup>th</sup> July 2008)</i> .....	44
1.9.2	<i>Measurements in the Amazon</i> .....	46
1.9.3	<i>Satellite Observations</i> .....	47
1.9.4	<i>Biomass Burning Observations</i> .....	48
1.9.5	<i>Global Studies</i> .....	49
1.9.6	<i>South East Asian Burning Season</i> .....	49
1.10	CURRENT KNOWLEDGE GAPS .....	50
1.11	BALI PROJECT OVERVIEW .....	53
1.12	THESIS OUTLINE.....	54
<b>2</b>	<b>INSTRUMENT METHODOLOGY</b> .....	<b>55</b>
2.1	PROJECT OVERVIEW.....	55
2.2	EXPERIMENTAL.....	56
2.2.1	<i>Measurement site set up</i> .....	56
2.3	INSTRUMENTATION SETUP .....	57
2.3.1	<i>Sampling</i> .....	59
2.3.2	<i>Pre-concentration and Trapping</i> .....	61
2.3.3	<i>Water Removal</i> .....	61
2.4	GAS CHROMATOGRAM .....	63
2.5	PEAK IDENTIFICATION .....	65
2.6	CALIBRATION AND INSTRUMENT STABILITY CHECKS.....	66
2.7	LIMITS OF DETECTION.....	70
2.8	ERROR ANALYSIS.....	71
2.9	INSTRUMENT ISSUES.....	73
2.9.1	<i>Power Issues</i> .....	73
2.9.2	<i>Flow Rate Variability</i> .....	74
2.9.3	<i>Chromatography Issues</i> .....	75
2.9.4	<i>Sampling Height</i> .....	77
2.10	CONCLUSIONS.....	78
<b>3</b>	<b>MODEL DESCRIPTION</b> .....	<b>81</b>
3.1	INTRODUCTION .....	81
3.2	USER SELECTED SIMULATION OPTIONS.....	82
3.2.1	<i>Horizontal Grid</i> .....	82
3.3	METEOROLOGICAL DATA.....	84
3.4	VERTICAL GRID .....	85
3.5	MODEL VERSION.....	86

3.5.1	<i>Version 11-02d</i> .....	86
3.6	MODEL INPUTS AND COMPONENTS.....	87
3.6.1	<i>Restart Files</i> .....	87
3.6.2	<i>Boundary Conditions</i> .....	87
3.6.3	<i>Emissions in GEOS-Chem</i> .....	88
3.6.4	<i>Chemistry</i> .....	90
3.7	CONCLUSIONS.....	91
<b>4</b>	<b>DATA OVERVIEW AND NMF ANALYSIS</b> .....	<b>93</b>
4.1	INTRODUCTION.....	93
4.2	TIME SERIES OF OBSERVATIONAL DATA.....	94
4.3	GENERAL DESCRIPTION OF THE TIME SERIES.....	98
4.4	WIDER DATASET.....	99
4.4.1	<i>Isoprene</i> .....	101
4.4.2	<i>Small Alkanes</i> .....	103
4.4.3	<i>Other Alkanes (i-pentane, i-butane &amp; n-butane)</i> .....	105
4.4.4	<i>Alkenes</i> .....	109
4.4.5	<i>Acetylene</i> .....	110
4.4.6	<i>Aromatics</i> .....	110
4.5	NON NEGATIVE MATRIX FACTORISATION (NMF) ANALYSIS.....	112
4.5.1	<i>Non-negative vs Positive Matrix Factorisation and other source analyses</i> 112	
4.5.2	<i>Non-Negative Matrix Factorisation Theory</i> .....	113
4.6	RESULTS.....	114
4.7	NMF ANALYSIS EVALUATION AND METHOD SELECTION.....	117
4.7.1	<i>Normalisation Method Selection</i> .....	117
4.7.2	<i>Selection of Number of Components for Analysis</i> .....	121
4.7.3	<i>Three Component Analysis</i> .....	122
4.8	EVENTS WITHIN THE DATASET.....	126
4.8.1	<i>Biomass burning period</i> .....	127
4.8.2	<i>Background periods</i> .....	128
4.8.3	<i>Local/Anthropogenic time periods</i> .....	128
4.9	MODEL VOC TIME SERIES.....	130
4.9.1	<i>Isoprene</i> .....	130
4.9.2	<i>Small Alkanes</i> .....	131
4.9.3	<i>Other Alkanes</i> .....	132
4.9.4	<i>Alkenes</i> .....	132

4.9.5	<i>Aromatics</i> .....	133
4.10	SUMMARY OF MODEL OBSERVATION COMPARISONS .....	135
4.11	CONCLUSIONS.....	136
<b>5</b>	<b>BIOMASS BURNING</b> .....	<b>139</b>
5.1	INTRODUCTION .....	139
5.2	FIRE MAPS .....	145
5.3	AIR MASS TRAJECTORIES.....	147
5.3.1	<i>Period 1</i> .....	148
5.3.2	<i>Period 2</i> .....	149
5.3.3	<i>Period 3</i> .....	150
5.3.4	<i>Period 4</i> .....	151
5.3.5	<i>Period 5</i> .....	152
5.3.6	<i>Period 6</i> .....	153
5.4	COMPARISON WITH KNOWN BIOMASS BURNING EVENTS.....	155
5.5	KALIMANTAN PEAT FIRES .....	155
5.6	EMISSION RATIOS .....	156
5.6.1	<i>Comparison of Emission Ratios</i> .....	157
5.7	GFAS EMISSION RATIOS.....	161
5.8	MODEL BIOMASS BURNING SIMULATIONS .....	163
5.9	MODEL SCALE FACTORS.....	164
5.10	EVALUATION OF BIOMASS BURNING EMISSION.....	165
5.11	MODELLED INFLUENCE OF BIOMASS BURNING EMISSIONS .....	168
5.11.1	<i>Ethane</i> .....	169
5.11.2	<i>Isoprene</i> .....	172
5.11.3	<i>OH</i> .....	174
5.11.4	<i>Ozone</i> .....	175
5.12	CONCLUSIONS.....	179
<b>6</b>	<b> BIOGENIC VOCS</b> .....	<b>181</b>
6.1	INTRODUCTION .....	181
6.2	PROPENE.....	181
6.2.1	<i>Propene Observations</i> .....	181
6.3	MODELLED PROPENE .....	184
6.3.1	<i>Magnitude of Modelled Propene</i> .....	185
6.4	PROPENE DIURNAL CYCLE.....	187
6.5	ISOPRENE .....	190

6.5.1	<i>Isoprene Observations</i> .....	190
6.5.2	<i>Diurnal Cycles</i> .....	196
6.5.3	<i>Modelled Isoprene</i> .....	197
6.5.4	<i>Diurnal Cycles</i> .....	199
6.6	DISCUSSION OF HIGH ISOPRENE PERIODS .....	201
6.7	EFFECT OF BIOGENIC EMISSIONS IN GEOS-CHEM.....	206
6.7.1	<i>Isoprene</i> .....	206
6.8	OH .....	208
6.9	OZONE.....	209
6.10	PM <sub>2.5</sub> .....	213
6.11	CONCLUSIONS.....	216
<b>7</b>	<b>CONCLUSIONS AND FUTURE WORK.....</b>	<b>219</b>
<b>8</b>	<b>REFERENCES.....</b>	<b>227</b>



## List of Figures

<i>Figure 1.1 Structures of isoprene (left) and limonene (right). Limonene is an example of a monocyclic monoterpene.....</i>	<i>32</i>
<i>Figure 1.2 Isoprene oxidation mechanism, taken from (B. Nguyen et al., 2014).....</i>	<i>38</i>
<i>Figure 1.3 GAW global sites monitoring VOCs. The majority of sites are situated in Europe, with poorer coverage in the Southern hemisphere and around the tropics. Maps obtained from the GAWSIS website <a href="https://gawsis.meteoswiss.ch/GAWSIS">https://gawsis.meteoswiss.ch/GAWSIS</a>.....</i>	<i>51</i>
<i>Figure 1.4 GAW stations measuring VOCs in South East Asia. Map obtained from the GAWSIS website.....</i>	<i>51</i>
<i>Figure 1.5 GAW stations measuring isoprene globally. This map shows that the only stations currently making isoprene measurements are in Europe, with no GAW stations measuring isoprene in the tropics. Map obtained from the GAWSIS website.....</i>	<i>52</i>
<i>Figure 2.1 Location of the Danum Valley site, Sabah, Malaysia.....</i>	<i>56</i>
<i>Figure 2.2 Top down view of the measurement site, showing the building in which the instrument is set up and the sample line running from 30 m up the research tower, through the building wall to the main sample pump.....</i>	<i>57</i>
<i>Figure 2.3 Schematic of the instrumental setup in Borneo. The numbers correspond to the section headings below.....</i>	<i>59</i>
<i>Figure 2.4 View from the research tower at ~10m. There are a few nearby trees, as shown, but the site is above most of the surrounding canopy in the valley below. This is representative of all sides of the tower.....</i>	<i>60</i>
<i>Figure 2.5 (Left) Tower at GAW site where sample inlet is located ~30m above ground level. (Right) Inlet on tower, the inlet is formed from a plastic funnel to minimise damage from the elements, it is also covered in a plastic sheet to prevent rain and large objects from entering the system.....</i>	<i>61</i>
<i>Figure 2.6 The glass (cold) fingers, valve and fan inside the water removal unit. Each cold finger has an inlet for the wet gases and outlet back through the valve for the dry gas. The green wire is the thermocouple, which helps regulate the temperature within the aluminium block.....</i>	<i>63</i>
<i>Figure 2.7 Sample chromatogram showing a strong isoprene peak ~28 minutes. This shows that the peaks are well separated and resolved.....</i>	<i>65</i>
<i>Figure 2.8 Chromatogram showing the NPL standard run on the GC-FID.....</i>	<i>67</i>

*Figure 2.9 Isoprene peak areas for the York working standard run at a range of sample volumes. This plots shows that over this range the instrument response for isoprene is linear. .... 68*

*Figure 2.10 Mixing ratios in ppb of the York working standard run across the measurement period. These mixing ratios are obtained using the peak areas/ppb values found from the National Physical Laboratory certified standard. The standards run throughout January and February were 150 ml sample volume but have been corrected to 500 ml. .... 69*

*Figure 2.11 Timeline showing periods with good measurement coverage (green boxes) and missing data periods (red boxes) for this work and a description of the instrument issues causing the gaps in data..... 73*

*Figure 2.12 Chromatograms during a 'normal' period in late March (top) and during a period of unexplained increased VOCs, early March (bottom). The bottom chromatogram shows an increase in the peak height and area for assigned VOCs but also an increased number of peaks, including multiple peaks inside peak identification windows for a single VOC. This is particularly the case near the end of the chromatogram where benzene and toluene elute. .... 76*

*Figure 2.13 Time series of toluene mixing ratios during March 2016. The early part of the series corresponds to measurements made with the sample inlet at lowered to ~2 m above ground level, a clear increase in mixing ratios is observed during this time 78*

*Figure 3.1 Global 4° x 5° resolution plot of surface isoprene concentrations. The entire island of Borneo is covered by only two boxes..... 83*

*Figure 3.2 Surface isoprene concentrations for the nested Asia grid at 0.5° x 0.625° resolution. There is much finer detail over Borneo than can be seen for the 4° x 5° global simulation..... 83*

*Figure 3.3 Isoprene concentrations for the area covered by the Chinas grid at 4x5 resolution, on the same colour scale as Figure 3.1..... 84*

*Figure 3.4 Vertical levels in GEOS-Chem with MERRA2 meteorology up to 3 km. Adapted from the GEOS-Chem wiki page [http://wiki.seas.harvard.edu/geos-chem/index.php/GEOS-Chem\\_vertical\\_grids#Vertical\\_grids\\_for\\_GEOS-5.2C\\_GEOS-FP.2C\\_MERRA.2C\\_and\\_MERRA-2](http://wiki.seas.harvard.edu/geos-chem/index.php/GEOS-Chem_vertical_grids#Vertical_grids_for_GEOS-5.2C_GEOS-FP.2C_MERRA.2C_and_MERRA-2)..... 86*

*Figure 4.1 Time series of VOC species measured at the Bukit Atur observatory, Malaysian Borneo from August 2015 to March 2016. Gaps in the time series reflect site power failures and a number of instrument issues, which are described in chapter 2. Continued on next page..... 95*

<i>Figure 4.2 Same as Figure 4.1 but shown on a logarithmic scale. Continued on next page.....</i>	<i>97</i>
<i>Figure 4.3 Measurements from this work (new measurements, red dots) and the OP3 project (black dots) presented by month. The year in which the measurements were made has been excluded for comparison purposes. All measurements were made using gas chromatography, with the exception of the second isoprene plot, which is PTR-MS data from the OP3 campaign.....</i>	<i>100</i>
<i>Figure 4.4 Box and whisker plots for isoprene measured in this work and the OP3 campaign separated by the periods indicated in the ethane plot in Figure 4.3. Data from the two OP3 periods is within the black rectangles. The circles represent outliers. These are values that lie outside the nearest quartile <math>\pm 1.5 * IQR</math>. Periods 1, 4 and 5 include data from the BALI project, periods 2 and 3 are from the OP3 project.....</i>	<i>101</i>
<i>Figure 4.5 Same as figure 4.4 for ethane and propane.....</i>	<i>103</i>
<i>Figure 4.6 Correlation plot for ethane and propane mixing ratios for all observations made during this work.....</i>	<i>104</i>
<i>Figure 4.7 Same as figure 4.4 for iso-pentane, iso-butane and n-butane.....</i>	<i>105</i>
<i>Figure 4.8 Box and whisker plot for iso-pentane including outliers.....</i>	<i>108</i>
<i>Figure 4.9 Box and whisker plots for the butanes including outliers.....</i>	<i>109</i>
<i>Figure 4.10 The contribution of all VOCs to each component of the five components from the NMF analysis. This analysis used un-normalized measured mixing ratio VOC data.....</i>	<i>115</i>
<i>Figure 4.11 The relative contribution of all VOCs to each of the five component from the NMF analysis. This analysis used data normalized by dividing the measured mixing ratios by the maximum value for each VOC.....</i>	<i>115</i>
<i>Figure 4.12 The relative contribution of all VOCs to each of the five component from the NMF analysis. This analysis used data normalized by dividing the measured mixing ratios by the mean value for each VOC.....</i>	<i>116</i>
<i>Figure 4.13 The relative contribution of all VOCs to each of the five component from the NMF analysis. This analysis used data normalized by dividing the measured mixing ratios by the median value for each VOC.....</i>	<i>116</i>
<i>Figure 4.14 R<sup>2</sup> values, found from correlation of VOC observations with those predicted by the NMF analysis for differing numbers of components. The modelled values are the product of the two matrices produced by the analysis. For each VOC the R<sup>2</sup> values is calculated for NMF analysis using one to ten components. The analysis was run using four different data analysis methods: measured mixing ratios</i>	

<i>(red), division by the mean (blue), maximum (green) and median (purple) mixing ratios. Continued on next page.....</i>	<i>118</i>
<i>Figure 4.15 Contributions of all VOCs to each component from three component NMF analysis using mixing ratio data normalised through division by the maximum values.....</i>	<i>122</i>
<i>Figure 4.16 Time series for the NMF analysis using three components with data normalised by division with the maximum mixing ratio. Component zero is high during the initial measurement period, when most of the measured VOCs are high and likely reflects biomass burning influence. Component one shows less variability over the time series. This corresponds to high influence from isoprene and propene. Component two is dominated by sharp spikes in the mixing ratio, which occur at several time periods.....</i>	<i>122</i>
<i>Figure 4.17 Correlation plots of the mixing ratio values obtained through the NMF analysis, calculated from the product of the two output matrices (component number, hydrocarbon and component number, time). This gives a simulated time series for each VOC that was then plotted against the observation time series. The <math>R^2</math> value is also given. For most VOCs a high <math>R^2</math> value <math>&gt;0.8</math> was calculated. The reasons for the low <math>R^2</math> values has been discussed above. Continued on next page.....</i>	<i>125</i>
<i>Figure 4.18 Ethane time series overlaid with the three regimes affecting the VOCs mixing ratios. Biomass burning, increase in many VOCs seen as a result of air masses travelling over active fires in the surrounding regions (see chapter 5). Biogenic, VOC mixing ratios are affected mainly by local events with little influence from surrounding regions. Isoprene dominated the VOC composition during these periods. Anthropogenic/local, increases were seen for some VOCs during these periods, often these events were short lived. These periods have been assigned to a change in local conditions but no specific source as been identified, equally there have been no instrument issues found to justify the exclusion of this data. ....</i>	<i>127</i>
<i>Figure 4.19 Comparison between isoprene observations and GEOS-Chem .....</i>	<i>130</i>
<i>Figure 4.20 Same as Figure 4.17 but for ethane.....</i>	<i>131</i>
<i>Figure 4.21 Same as Figure 4.17 but for propane .....</i>	<i>131</i>
<i>Figure 4.22 Same as Figure 4.17 but for the other alkanes. For the model this is alkanes with 4 carbons or more, the observations are iso &amp; n-butane, iso-pentane and n-heptane.....</i>	<i>132</i>
<i>Figure 4.23 Same as Figure 4.17 but for the alkenes. For the model this is alkenes with 3 carbons or more, the observations are propene and butene .....</i>	<i>133</i>
<i>Figure 4.24 Same as Figure 4.17 but for benzene.....</i>	<i>134</i>

<i>Figure 4.25 Same as Figure 4.17 but for toluene</i> .....	134
<i>Figure 4.26 Ethane mixing ratios for two grid boxes in the 0.5° x 0.625° Asia simulation. The line in red includes the coordinates for the measurement site. The line in blue is an adjacent box</i> .....	136
<i>Figure 5.1 Time series for ethane measurements made as part of this work. This chapter focuses on measurements between August and October, where an enhancement in most VOCs was seen</i> .....	139
<i>Figure 5.2 Time series of all VOCs observations over the period defined as being affected by biomass burning in the surrounding region. Continued on next page...</i>	141
<i>Figure 5.3 A map of the area surrounding the measurement site showing fire events. The top panel shows a background period during the first week of January 2016. The bottom panel shows biomass burning occurring in the first week of October 2015 (bottom)</i> .....	145
<i>Figure 5.4 Ethane time series over the biomass burning period, divided into sections by distinct changes in VOC mixing ratios</i> .....	146
<i>Figure 5.5 Fire maps for the periods shown in Figure 5.4. For periods shorter than one week fire maps for seven days are shown so as not to give a downward bias to the number of active fires by the smaller number of days</i> .....	147
<i>Figure 5.6 Trajectories for period one. From left to right are trajectories ending on each day between 25<sup>th</sup> and 31<sup>st</sup> August. The black star represents the approximate location of the Bukit Atur observatory, where measurements were made for this work</i> .....	149
<i>Figure 5.7 Back trajectories run under the same conditions as described previously, finishing on 01/09/2015, 02/09/2015. These plots show that over this period the air mass is travelling over a similar area</i> .....	150
<i>Figure 5.8 Back trajectories, under the same conditions as the previous two figures but finishing on 7<sup>th</sup>, 8<sup>th</sup> and 9<sup>th</sup> of September</i> .....	150
<i>Figure 5.9 Map showing the areas surrounding Borneo, highlighting the Celebes sea where the air mass travels over during this period</i> .....	151
<i>Figure 5.10 Back trajectories run daily between 15<sup>th</sup> and 21<sup>st</sup> September</i> .....	152
<i>Figure 5.11 Back trajectories between the 22<sup>nd</sup> and 27<sup>th</sup> September</i> .....	153
<i>Figure 5.12 Back trajectories for the final period of the biomass burning period. Trajectories were run daily between the 6<sup>th</sup> and 14<sup>th</sup> of October</i> .....	154
<i>Figure 5.13 Emission ratios of different VOCs to propane calculated for this work and previous studies by Lewis et al. (2013) and Simpson et al. (2011), both in Canada. Stockwell et al. results from peat burning in Indonesian Borneo and Andreae and</i>	

<i>Merlet, which reports values from a number of studies in tropical rainforests. A value for this work but corrected for three days of loss via OH has also been included.....</i>	<i>158</i>
<i>Figure 5.14 Emission ratios for each VOC in Figure 5.12, shown at a greater zoom level for individual VOCs. Continues on net page. ....</i>	<i>159</i>
<i>Figure 5.15 Comparison between GEOS-Chem (black line) and observations (red dots) during the biomass burning periods.....</i>	<i>164</i>
<i>Figure 5.16 Comparison between GEOS-Chem scaled using the factors in Table 5.2 (black line) and observations (red dots) during the biomass burning periods.....</i>	<i>166</i>
<i>Figure 5.17 Ethane mixing ratios for the box containing the measurement site in GEOS-Chem, with biomass burning emissions turned on and off.....</i>	<i>169</i>
<i>Figure 5.18 Ethane mixing ratios with biomass burning emissions turned on for September 2015.....</i>	<i>170</i>
<i>Figure 5.19 The absolute change in ethane when biomass burning emissions were turned off in GEOS-Chem. The model was run over September 2015. ....</i>	<i>171</i>
<i>Figure 5.20 The percentage change in ethane when biomass burning emissions were turned off in GEOS-Chem. The model was run over September 2015. ....</i>	<i>171</i>
<i>Figure 5.21 Isoprene mixing ratios for the box containing the measurement site in GEOS-Chem, with biomass burning emissions turned on and off.....</i>	<i>172</i>
<i>Figure 5.22 Isoprene mixing ratios with biomass burning emissions turned on for September 2015.....</i>	<i>173</i>
<i>Figure 5.23 The absolute change in isoprene when biomass burning emissions were turned off in GEOS-Chem. The model was run over September 2015. ....</i>	<i>173</i>
<i>Figure 5.24 OH mixing ratios for the box containing the measurement site in GEOS-Chem, with biomass burning emissions turned on and off.....</i>	<i>175</i>
<i>Figure 5.25 Ozone mixing ratios for the box containing the measurement site in GEOS-Chem, with biomass burning emissions turned on and off.....</i>	<i>176</i>
<i>Figure 5.26 Ozone mixing ratios with biomass burning emissions turned on for September 2015.....</i>	<i>177</i>
<i>Figure 5.27 The absolute change in ozone when biomass burning emissions were turned off in GEOS-Chem. The model was run over September 2015. ....</i>	<i>178</i>
<i>Figure 5.28 The percentage change in ozone when biomass burning emissions were turned off in GEOS-Chem. The model was run over September 2015. ....</i>	<i>179</i>
<i>Figure 6.1 Time resolved propene measurements made during this work. The data is separated into five periods labeled as the nearest month.....</i>	<i>183</i>
<i>Figure 6.2 Diurnal average profiles for the measurement months identified in figure 1. Times shown are local time (GMT+8).....</i>	<i>184</i>

<i>Figure 6.3 Model propene mixing ratios with biogenic emissions switched on (grey) and off (black), with observations over the same time period (red circles).....</i>	<i>187</i>
<i>Figure 6.4 Map of anthropogenic propene emissions over Borneo and the surrounding areas. Colour scale is in <math>10^{11}</math> atomsC <math>cm^{-2}</math> <math>s^{-1}</math>. Values above <math>1 \times 10^{11}</math> atomsC <math>cm^{-2}</math> <math>s^{-1}</math>, have been masked as dark red to remove bias on the colour scale caused by very large anthropogenic emission sources such as major cities.....</i>	<i>188</i>
<i>Figure 6.5 Model (black) and Observations (red) diurnal medians by month. The shaded areas represent the 25<sup>th</sup> to 75<sup>th</sup> percentiles.....</i>	<i>189</i>
<i>Figure 6.6 Average model diurnal over one year for propene (red) and OH (black)</i>	<i>191</i>
<i>Figure 6.7 An isoprene time series showing measurements from this work (solid circles) and measurements made using GC-FID during the OP3 campaign (faded circles).....</i>	<i>192</i>
<i>Figure 6.8 Box and whisker plots for isoprene measurements from this project and the OP3 GC-FID measurements. OP3 measurements are shown in the black box.....</i>	<i>192</i>
<i>Figure 6.9 Same as Figure 6.8 but with OP3 PTR-MS measurements.....</i>	<i>194</i>
<i>Figure 6.10 Isoprene diurnal profiles for March from our work and the April OP3 campaign. The line is the median value, with shaded areas representing the 25<sup>th</sup> and 75<sup>th</sup> percentiles. The OP3 data from April is compared to the March data from our work as this is the nearest available month for comparison.....</i>	<i>194</i>
<i>Figure 6.11 Isoprene diurnal profiles for September from our work and the July OP3 campaign. The line is the median value, with shaded areas representing the 25<sup>th</sup> and 75<sup>th</sup> percentiles. The OP3 data from July is compared to the September data from our work as this is the nearest.....</i>	<i>194</i>
<i>Figure 6.12 Diurnal average profiles for the periods identified in figure 6.1. The OP3 data is shown with dashes lines.....</i>	<i>196</i>
<i>Figure 6.13 Time series for one year of GEOS-Chem isoprene concentrations, coloured by month.....</i>	<i>198</i>
<i>Figure 6.14 Average diurnal profiles for isoprene concentrations from GEOS-Chem.....</i>	<i>199</i>
<i>Figure 6.15 Diurnal isoprene profiles for this work and the GEOS-Chem model. The line represents the median values, with the shaded areas showing the 25<sup>th</sup> and 75<sup>th</sup> percentiles.....</i>	<i>200</i>
<i>Figure 6.16 Maps showing isoprene emissions in South East Asia for clockwise (October, November and December).....</i>	<i>202</i>
<i>Figure 6.17 Same as Figure 6.13 for OH.....</i>	<i>204</i>
<i>Figure 6.18 Same as Figure 6.13 for CO.....</i>	<i>204</i>

<i>Figure 6.19 Same as Figure 6.13 for black carbon.....</i>	<i>205</i>
<i>Figure 6.20 Same as Figure 6.13 for ozone.....</i>	<i>205</i>
<i>Figure 6.21 Isoprene concentrations at the measurement site from GEOS-Chem with biogenic emissions turned on (red ine) and off (black line).....</i>	<i>206</i>
<i>Figure 6.22 Surface isoprene concentrations for the GEOS-Chem China nested grid with biogenic emissions on .....</i>	<i>207</i>
<i>Figure 6.23 The absolute change in isoprene (ppbv) when biogenic emissions were turned off in the GEOS-Chem China nested grid for November 2015.....</i>	<i>207</i>
<i>Figure 6.24 OH concentrations at the measurement site from the GEOS-Chem China nested grid with biogenic emissions turned on (red ine) and off (black line).....</i>	<i>208</i>
<i>Figure 6.25 Surface ozone concentrations from GEOS-Chem for the measurement site, with (red line) and without (black line) biogenic emissions turned on .....</i>	<i>209</i>
<i>Figure 6.26 Surface ozone concentrations for the China nested grid with biogenic emissions on for November 2015. ....</i>	<i>210</i>
<i>Figure 6.27 Daytime average surface ozone concentrations over Asia between 2010-2014. Data is from the TOAR database (Schultz et al. 2017). The map is adapted from the original downloaded from the PANGAEA website (<a href="https://doi.pangaea.de/10.1594/PANGAEA.876109">https://doi.pangaea.de/10.1594/PANGAEA.876109</a>).....</i>	<i>210</i>
<i>Figure 6.28 The mean absolute change in surface ozone (ppbv) when biogenic emissions were turned off in the GEOS-Chem China nested grid for November 2015 .....</i>	<i>212</i>
<i>Figure 6.29 The mean percentage change in surface ozone (ppbv) when biogenic emissions were turned off in the GEOS-Chem China nested grid for November 2015 .....</i>	<i>212</i>
<i>Figure 6.30 Change in PM<sub>2.5</sub> for GEOS-Chem at the measurement site with biogenic emissions turned on off.....</i>	<i>213</i>
<i>Figure 6.31 Surface concentrations of PM<sub>2.5</sub> for the GEOS-Chem China nested grid with biogenic emissions on .....</i>	<i>214</i>
<i>Figure 6.32 The absolute change in PM<sub>2.5</sub> (µg/m<sup>3</sup>) when biogenic emissions were turned off in the GEOS-Chem China nested grid .....</i>	<i>215</i>
<i>Figure 6.33 The percentage change in PM<sub>2.5</sub> (µg/m<sup>3</sup>) when biogenic emissions were turned off in the GEOS-Chem China nested grid.....</i>	<i>215</i>

## List of Tables

<i>Table 1.1 Annual average VOC emissions between 1980-2010. These values were calculated using the Model of Emissions of Gases and Aerosols from Nature (MEGAN) model. Table adapted from (Sindelarova et al., 2014)</i>	32
<i>Table 2.1 Limits of detection for all VOC species measured in this work. The numbers in brackets represent the LOD values for the GC-FID at the Cape Verde Atmospheric Observatory.</i>	71
<i>Table 4.1 Mean, median and inter-quartile range values for the periods identified in figure 3. The number in brackets identifies the measurement period, OP3 and BALI identify the project. The two OP3 instruments (GC and PTR-MS) are shown separately</i>	101
<i>Table 4.2 Mean, median and interquartile range concentrations for all measured hydrocarbons from this work and the OP3 campaign</i>	111
<i>Table 4.3 Mean, median and interquartile range values for all measured hydrocarbons by each of the periods identified</i>	129
<i>Table 5.1 VOCs mean, median and inter-quartile range mixing ratios during the background and biomass burning periods</i>	143
<i>Table 5.2 Scaling factors for each VOC to be applied to model output (model will be divided by these values) to give better agreement with observations during background periods</i>	165
<i>Table 5.3 Mean, median and inter-quartile range values for the observations and GEOS-Chem during non biomass burning (No BB: 05, 06, 07/2015) and biomass burning (BB: 08, 09 &amp; 10/2015) time periods. All values are given in pptv.</i>	168
<i>Table 5.4 Mean, median and inter-quartile range values for GEOS-Chem ethane with and without biomass burning emissions turned on</i>	169
<i>Table 5.5 Mean, median and inter-quartile range values for GEOS-Chem isoprene with and without biomass burning emissions turned on</i>	172
<i>Table 5.6 Mean, median and inter-quartile range values for GEOS-Chem OH with and without biomass burning emissions turned on</i>	175
<i>Table 5.7 Mean, median and inter-quartile range values for GEOS-Chem OH with and without biomass burning emissions turned on</i>	176
<i>Table 6.1 Mean, median and range (5<sup>th</sup> to 95<sup>th</sup> percentiles) for propene from this work, OP3 and GEOS-Chem</i>	186

*Table 6.2 Mean, median and inter-quartile range (25<sup>th</sup> – 75<sup>th</sup> percentiles) values for both the observations and model by month \_\_\_\_\_ 199*

*Table 6.3 Mean, median and inter-quartile range (25<sup>th</sup> – 75<sup>th</sup> percentiles) values for the peak isoprene (11:00-18:00) for both the observations and model by month \_\_200*

*Table 6.4 Mean, median and inter-quartile range values for the measurement site in GEOS-Chem with and without biogenic emissions turned on \_\_\_\_\_208*

*Table 6.5 Mean, median and inter-quartile range values for the measurement site in GEOS-Chem with and without biogenic emissions turned on \_\_\_\_\_209*

*Table 6.6 Mean, median and inter-quartile range values for the measurement site in GEOS-Chem with and without biogenic emissions turned on \_\_\_\_\_213*

# Acknowledgements

Thank you to my family, friends and colleagues who have supported me throughout my PhD. This thesis would not have been possible without you.



## Declaration

I declare that this thesis is a presentation of original work and I am the sole author. This work has not previously been presented for an award at this, or any other, University. All sources are acknowledged as references.



# Chapter 1

## 1 Introduction

### 1.1 Understanding Composition

Understanding the complexities of the Earth's atmosphere is key to developing our knowledge of two of the major issues facing our planet, climate change and air quality. Better understanding of the processes governing these changes enables effective policy to be implemented to mitigate these issues. To improve understanding, work in the field, laboratory and model studies must be combined to create a full picture of the effects of changes in the past, present and going forward.

It is widely accepted that increased concentrations of climate forcers such as CO<sub>2</sub> from anthropogenic sources is the primary cause of increasing average global temperatures (Pachauri et al., 2014). Long term studies such as those at the Mauna Loa observatory have shown a significant upward trend in CO<sub>2</sub> over a number of decades, increasing from 315 ppm in the 1960s to over 400 ppm in the present day (Keeling et al., 2009, Keeling et al., 1995). It is not only CO<sub>2</sub> that is a concern for climate change, methane emitted from the burning of fossil fuels and wetlands among other sources has a global warming potential greater than CO<sub>2</sub> (Lashof and Ahuja, 1990, Bousquet et al., 2006). The potential effects of climate change are wide ranging, from ocean acidification to problems with adequate food production (McNeil and Matear, 2008, Rosenzweig and Parry, 1994). There are important feedbacks from the coupling between the biosphere and atmosphere. For example a warming planet may release more climate forcers such as CO<sub>2</sub> and methane from thawing permafrost (Schuur et al., 2008). The consequences of this would be increased warming. Understanding the emission sources, atmospheric chemistry and effects of these species is key to lessening the effects of climate change and implementing policy to restrict the emissions of climate forcers.

In addition to climate change, atmospheric composition is important for understanding air quality. Poor air quality can affect human health, mortality and damage ecosystems, causing personal, productivity and economic losses (Kampa and Castanas, 2008, Vlachokostas et al., 2010). There are many species that

influence air quality, including ozone, NO<sub>x</sub>, aromatics and particulate matter (Krupnick et al., 1990, Nielsen et al., 1996, Schwarze et al., 2006). It is not only outdoor air quality that can impact upon human health, indoor air quality is a growing concern (Jones, 1999). Understanding air quality requires knowledge of species' emissions, chemistry once emitted, effects of local conditions and impacts on health and ecosystems. This is a complicated task requiring a range of approaches.

Central to understanding the concentration of a pollutant are its emissions. Therefore, emission studies are needed to quantify the flux of species in to the atmosphere (Zhao et al., 2011, Pacyna and Pacyna, 2001). Laboratory, field and model studies can show what products are formed by chemistry after emission and the rate at which they react (Mentel et al., 1996, Laaksonen et al., 2008, Sprengnether et al., 2002). This is useful for knowing what secondary products are formed and the expected lifetimes of species once emitted. Field measurements and model studies can show the effect of changes in conditions on emissions and chemistry (Finlayson-Pitts and Pitts, 1993, Peng et al., 2006). To understand the effects on health and ecosystems epidemiological studies, chamber studies and model simulations can be used (Peters, 2005). All of this information must be considered to gain a full understanding of air quality. Epidemiological studies can be used to create guidelines and inform policy, such as the World Health Organization's air quality guidelines (Krzyzanowski and Cohen, 2008). These guidelines recommend maximum levels for exposure to certain pollutants and provide a target for improving air quality.

The focus of this work is on volatile organic compounds (carbon containing organic compounds that may be present in the air), the chemistry of VOCs and their influences on air quality and climate are discussed in detail in section 5 of this chapter. This thesis measures mixing ratios of a range of VOCs at a remote rainforest site and looks to understand the factors that affect these concentrations. The effects of VOCs on the wider region are investigated with model studies. This requires an understanding of the other species that are involved in the oxidation chemistry of VOCs such as NO<sub>x</sub> and ozone.

This introduction begins with a discussion of atmospheric VOCs as these are the compounds measured in this work. NO<sub>x</sub> and ozone are also discussed as these

species are closely linked to VOC chemistry. Techniques used previously for VOC measurements are then described along with a discussion of previous observations. Finally an outline of this thesis is given.

## **1.2 Atmospheric NO<sub>x</sub>**

Atmospheric NO<sub>x</sub> is the term used for a group of relatively short lived nitrogen oxide species including nitric oxide (NO), nitrogen dioxide (NO<sub>2</sub>) and N<sub>2</sub>O<sub>5</sub>. These species are important in the atmosphere as they are central to understanding tropospheric ozone chemistry, can modify the oxidizing capacity of the atmosphere, contribute to the acidification of ecosystems and have impacts for human health (Sillman, 1999, Galloway, 1995, Samet and Utell, 1990).

The dominant sources of NO<sub>x</sub> are anthropogenic, predominantly from the burning of fossil fuels for power, industry or transport (van Aardenne et al., 1999, Lamsal et al., 2011). Another source of NO<sub>x</sub> is biomass burning (Wang et al., 2002). Total NO<sub>x</sub> emissions are around 22 Tg N yr<sup>-1</sup> (Delmas et al., 1997). Where total anthropogenic emissions account for 70% of NO<sub>x</sub> emissions with 50% from fossil fuels and 20% from biomass burning. Natural sources are thought to account for less than 30% of NO<sub>x</sub> emissions, natural emission sources are from soil and lightning (Schumann and Huntrieser, 2007, Tie et al., 2002, Delmas et al., 1997).

Recent trends in NO<sub>x</sub> emissions vary widely by location. In countries such as India and China where rapid industrialization has occurred emissions of NO<sub>x</sub> along with many pollutants has increased dramatically. In China increases of 70% were observed over a ten year period from 1995, driven by a combination of increasing vehicle and power plant emissions (Zhang et al., 2007). Over a similar time period model predictions showed surface NO<sub>x</sub> in India increased by 20-30% (Beig and Brasseur, 2006). The trend in Europe and parts of North America over this period however showed a reduction in NO<sub>x</sub> concentrations of up to 7% per year (Archibald et al., 2009). Nevertheless, NO<sub>x</sub> concentrations across large parts of Europe have stabilized despite inventories predicting decreasing emissions. This is largely due to emission controls on vehicles not being met in real world driving and highlights the need for robust policy for air quality improvement (Carslaw et al., 2011).

NO<sub>x</sub> contributes to photochemical smog formation events. These events are harmful not only to human health but also impact on plant life (Pope, 2000, Chameides et al., 1999). NO<sub>2</sub> can cause direct adverse health effects, mainly to the lungs after inhalation (Yang and Omaye, 2009). It is therefore important to put controls on NO<sub>x</sub>, particularly in urban areas where NO<sub>x</sub> emissions are greatest and population densities are high (Wang et al., 2014). This is however a more complicated problem than reducing NO<sub>x</sub> alone. It is not only NO<sub>x</sub> that affects ozone or smog formation, VOC concentrations are also important. Therefore a clear understanding of local conditions is needed to properly implement the most effective air quality strategy (Marr and Harley, 2002, Dimitriades, 1972).

### **1.3 Volatile Organic Compounds**

VOC chemistry can have a large effect on atmospheric chemistry, climate and also human health. This chemistry includes formation of secondary organic aerosol (Kroll et al., 2006), which affects radiative forcing and human health (Jacobson, 2001, Mauderly and Chow, 2008) and ground level ozone formation/destruction, which can impact human health and crop yields (Squire et al., 2014). For these reasons volatile organic compounds (VOCs) have an important role in determining the chemistry of the atmosphere.

Other than methane, isoprene is the most emitted VOC and accounts for approximately a third of annual global non-methane NMVOC emissions from both natural and anthropogenic sources (Guenther et al., 2006). Methane has a much longer lifetime (several years for methane compared with a couple of hours for isoprene) than the other VOCs and so is often dealt with separately (Voulgarakis et al., 2013, Atkinson, 2000). It is thought that >90% of atmospheric isoprene is emitted by terrestrial plant foliage, with tropical broadleaf trees having the highest emission rates.

Sources of VOCs are discussed in section 1.5. The chemistry of VOCs, including key sinks is discussed in section 1.6.

## 1.4 The importance of VOCs

The emission of large quantities of VOCs during biomass burning and more widely through direct emissions of organic aerosol and SOA formation contributes to high particulate matter (PM) levels in surrounding areas (Huang et al., 2014). Studies have shown that PM of a range of sizes can impact on human health. These health effects include triggering of asthma symptoms, cardiovascular and pulmonary diseases and mortality (Atkinson et al., 2014, Pope et al., 2004, Brunekreef and Forsberg, 2005).

Studies of the health effects of biomass burning in South East Asia were conducted during the significant events of 1997 and 2015. During the 1997 season studies showed that PM levels increased to above those that were considered to have adverse health effects (Kunii et al., 2002). The study found high reported levels of health effects including respiratory problems, particularly from those with pre-existing conditions such as heart problems. Another study found that the haze resulting from the burning had an impact on peoples physical functioning, with the effects lasting beyond the end of the haze, particularly for women (Frankenberg et al., 2005). However another study in Singapore found that the health effects on lung function during the haze was minimal, with little increase in mortality or hospital admissions (Emmanuel, 2001). These studies highlight the difficulty in quantifying the health effects of events such as errors in self reporting of symptoms and distinguishing health problems caused by haze events with those that have other causes.

Aerosols can contribute to radiative and therefore climatic effects in the atmosphere, which includes SOA formed from VOCs. There are two main routes by which aerosols influence radiation, the direct radiative effect and the aerosol indirect effect. The direct effect occurs when aerosols absorb and scatter radiation (Yu et al., 2006). The indirect effect occurs when aerosols act as nuclei for cloud formation and affect cloud optical properties (Mahowald, 2011).

SOA impacts generally result in an overall net decrease in radiative forcing, leading to cooling. Studies have found that the effects of biogenic SOA are comparable to effects from anthropogenic aerosols and higher than most other natural SOA sources (Scott et al., 2014). It is therefore important to understand the effects of

changes to ecosystems on SOA production, as this has implications for global climate. One study has shown that land cover changes, from forest and grasslands to crops, leads to an overall positive radiative forcing due to a lowering of biogenic SOA productions (Unger, 2014). This demonstrates the complex relationship between land use changes, VOC emissions, SOA formation and radiative effects.

In addition to SOA production, VOC chemistry impacts upon ozone concentrations, which is described in the previous section. Some VOCs have a high ozone formation potential, including isoprene and toluene and so emissions of these species, under the right conditions, can lead to increases in ozone levels (Zeng et al., 2008). This is important because ground level ozone impacts on human health and crop production.

Ozone impacts primarily on the lungs, causing inflammation. This leads to problems such as decreased lung function, even in those who are otherwise healthy and those with existing pulmonary problems such as asthma can see an increase in symptoms (Mudway and Kelly, 2000). Studies have shown that there is a link between ozone exposure and mortality. This is true even for short term exposure including events such as heat waves that result in significantly increased ozone levels (Bell et al., 2004, Filleul et al., 2006).

As well as impacting upon human health, surface ozone can affect plant growth. Damage to crops could cause problems with feeding a growing population in the future. A wide variety of important crops are affected by surface ozone concentrations including wheat, rice and soyabean (Maggs et al., 1995, Ainsworth, 2008, Van Dingenen et al., 2009). Studies have predicted the loss in various crops both for past years and predictions for future changes in ozone. These show that the cost of loss crops in 2000 were in the tens of billions of dollars and predicted that the issue would only increase, showing that surface ozone concentrations are already impacting on crop production (Avnery et al., 2011).

## **1.5 Emission Sources and Algorithms**

### **1.5.1 Anthropogenic Emissions**

Although biogenic emissions are the dominant source of VOCs globally, anthropogenic emissions also contribute, particularly in urban and industrialized areas (Helmig et al., 2011). Anthropogenic VOC sources include vehicle fuels, both production and use (Peng et al., 2012, Chin and Batterman, 2012). VOCs emitted from vehicle use include aromatics such as benzene and toluene with the exact composition depending upon vehicle and fuel type (You et al., 2007). Industrial activities (Zheng et al., 2017) and solvent use (Yuan et al., 2010) are another source of anthropogenic VOCs. VOCs emitted by solvent use include alkanes, aromatics and alcohols (Theloke and Friedrich, 2007). The exact composition of VOCs varies in different regions (Na et al., 2004). Of these sources, transport is the biggest contributor of VOC emissions (Kansal, 2009).

As with biogenic emissions there are inventories used to implement anthropogenic emissions in atmospheric chemistry. Examples of these include the EDGAR (Emissions Database for Global Atmospheric Research anthropogenic emissions) (Olivier et al., 1994) and MIX, which focuses on emissions in Asia (Li et al., 2015). These inventories use activity data such as agricultural or industrial data and combine these with emission factors to calculate emissions for relevant species.

### **1.5.2 Biogenic Emissions**

There are a number of issues when assessing emission quantities of VOCs including lack of knowledge of plant species coverage for different areas and problems in quantifying changes in emissions with varying conditions for different plant types (Simpson et al., 1995, Kuzma and Fall, 1993, Schnitzler et al., 2014). Isoprene oxidation chemistry is complex and relies on laboratory, chamber and field observations combined with model studies to understand the possible reaction pathways. There are still large uncertainties in the yields and products of VOC oxidation (Ervens et al., 2008, Crounse et al., 2011).

The terrestrial biosphere is a large source of atmospheric VOCs. A recent model study estimated the total magnitude of biogenic VOC emissions to be 760 Tg (C) yr<sup>-1</sup> (Sindelarova et al., 2014). These emissions were dominated by isoprene with monoterpenes, sesquiterpenes and many other species including alkanes, alkenes and oxygenated VOCs. Emission quantities for different VOCs are shown in Table

1.1. The structures of isoprene and limonene (a monoterpene) are shown in Figure 1.1. (Sindelarova et al., 2014) estimated that 70% of the total VOC emission was isoprene.

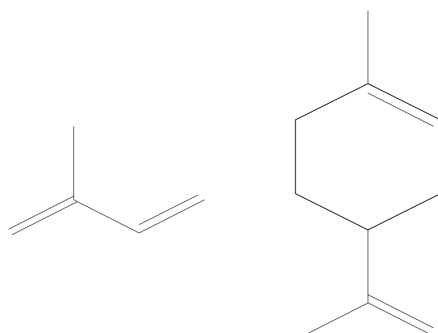


**Figure 1.1 Structures of isoprene (left) and limonene (right). Limonene is an example of a monocyclic monoterpene**

**Table 1.1 Annual average biogenic VOC emissions between 1980-2010. These values were calculated using the Model of Emissions of Gases and Aerosols from Nature (MEGAN) model. Table adapted from (Sindelarova et al., 2014)**

<b>VOC</b>	<b>Mean emission Tg yr<sup>-1</sup></b>	<b>Percentage contribution %</b>
<b>Isoprene</b>	594	69.2
<b>Total monoterpenes</b>	95	10.9
<b>Sesquiterpenes</b>	20	2.4
<b>Methanol</b>	130	6.4
<b>Acetone</b>	37	3.0
<b>Ethanol</b>	19	1.3
<b>Acetaldehyde</b>	19	1.3
<b>Ethene</b>	18.1	2.0
<b>Propene</b>	15	1.7
<b>Formaldehyde</b>	4.6	0.2
<b>Formic acid</b>	3.5	0.1
<b>Acetic acid</b>	3.5	0.1
<b>2-methyl-3-buten-2-ol</b>	1.6	0.1
<b>Toluene</b>	1.5	0.2
<b>Other VOC species</b>	8.5	0.8

There have been a number of different approaches used to quantify the magnitude of emissions and concentration of isoprene and other biogenic VOCs on a regional and global scale. At the leaf level enclosure measurements have been made with a number of techniques, including in-situ enclosure measurements using chambers or bags to enclose the branch or leaves (Matsunaga et al., 2011, Bouvier-Brown et al., 2009). Air is flowed through the system and the outflow analysed with gas chromatography (GC) (Guenther et al., 1996) or proton transfer mass spectrometry (PTR-MS) (Bracho-Nunez et al., 2013).

On a larger scale, flux measurements over a canopy have been made in a number of environments. PTR-MS combined with the eddy covariance technique has been used to study VOC emission rates over a rainforest and oil palm plantations in Malaysian Borneo (Fowler et al., 2011). This study found that VOC emissions over oil palm plantations were three times higher than over the rainforest, with isoprene emissions being higher by a factor of five. This is important in Borneo because there has been a substantial expansion in the number of palm plantations, since the 1980's (Sayer et al., 2012). Palm oil is an important export for Malaysia, in 1998 it accounted for 5.6% of GDP (Yusoff, 2006). This makes palm oil production an important environmental and political issue in the region.

Models are used to scale these leaf level and canopy measurements to a global scale. One such model is the Model of Emissions of Gases and Aerosols from Nature (MEGAN) (Guenther et al., 2012). Results from studies of direct emissions from different plant types using enclosure techniques (Kesselmeier and Staudt, 1999) are combined with meteorological and land type data to calculate the global distribution of emissions. The magnitude of isoprene emissions as calculated by MEGAN range from 500-750 Tg isoprene annually (Guenther et al., 2006).

The activity factor for each class is calculated as follows:

$$\gamma_i = C_{CE} LAI \gamma_{P,i} \gamma_{T,i} \gamma_{A,i} \gamma_{SM,i} \gamma_{C,i} \tag{Equation 1}$$

Where  $C_{CE}$  is the canopy environment coefficient, this has a value that gives  $\gamma_i = 1$  under standard conditions. LAI is the leaf area index and the activity factors  $\gamma$  account for responses to light, temperature, leaf age, soil moisture and  $CO_2$  inhibition respectively.

The dominant local drivers of biogenic VOC emissions are light and temperature. There have been studies on a range of plant types to study the light and temperature dependence of different VOCs. Emission rates of most VOC increase with increasing temperature, up to a threshold where enzymatic activity is inhibited (Peñuelas and Llusà, 2001). Some VOC emission rates are also dependent on photosynthetically active radiation (PAR), including isoprene (Tingey et al., 1979). Several studies have found that it is not only isoprene emissions that depend on both temperature and PAR. A wide range of VOCs exhibit some degree of light dependency including monoterpenes such as  $\alpha$ -pinene (Schuh et al., 1997, Owen et al., 2002).

### **1.5.3 Biomass Burning Emissions**

Another important source of VOCs is from biomass burning. Although much of the global biomass burning is anthropogenic (for land clearance and burning crop residues) it has been included as a separate category here. There are broadly two main categories of burning: open burning, with sources such as land clearance for agricultural purposes or natural burning from lightning strikes (Crutzen and Andreae, 1990, Archibald et al., 2009); and domestic burning (biofuel), for uses such as cooking or heating (Ludwig et al., 2003). Domestic burning emissions are difficult to quantify due to the lack of systematic measurements and data collection (Kituyi et al., 2005). There have been laboratory studies used to quantify the types of emissions from domestic burning such as cooking fires (Stockwell et al., 2015). However our knowledge of the volume and type of wood burning from domestic fires is poor.

Within the open burning category there are different types of natural material burnt during the fire events. These include tropical forests (Ferek et al., 1998, Jonquière et al., 1998), savannahs (Cahoon Jr et al., 1992) and boreal forests (Wentworth et al., 2018). The different types of burning have different VOC emission factors associated with them (Shirai et al., 2003, Andreae and Merlet, 2001).

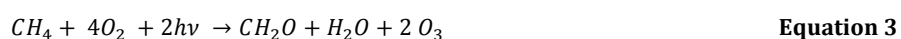
These emission factors are important for including biomass burning emissions in model studies. There are a number of different emissions inventories that can be

used with atmospheric models, the use of which depends upon the desired spatial, temporal and scientific questions and output. Examples of these inventories include GFED, Global Fire Emissions Database (Field et al., 2016), GFAS, Global Fire Assimilation System (Kaiser et al., 2012) and FINN, the Fire INventory from NCAR (Wiedinmyer et al., 2010). These inventories combine satellite observations of fire activity and land cover maps with emission factors of relevant species. For some inventories all species emissions are scaled relative to CO<sub>2</sub>.

#### 1.5.4 Tropospheric Ozone

Tropospheric ozone is a key species in defining the oxidative capacity of the atmosphere. This is because oxidizing reactions with ozone or OH are the main removal route for most important atmospheric species and ozone is key to OH production. It is also a key air pollutant and climate gas in its own right. Understanding the production routes and chemistry of ozone is therefore important because at high concentrations it can have negative impacts on human health, crop production and climate (West et al., 2007, Ainsworth et al., 2012, Fishman et al., 1979). Measurements of ozone are made using satellite data, ground based instruments or ozonesondes (Fishman et al., 2003, Fioletov et al., 2002, Logan, 1999). In addition to the photolytic production of ozone in the troposphere described below, there is a source of ozone from troposphere-stratosphere exchange.

Ozone is formed via the photolysis of NO<sub>2</sub> to create NO and the subsequent reaction of the oxygen atom with an oxygen molecule. There is a rapid recycling of ozone back to NO<sub>2</sub> creating a null cycle. For net ozone production to occur oxidation of NO to NO<sub>2</sub> by a molecule other than ozone is necessary. This could include peroxy radicals from the oxidation of CO or VOCs. The following equations show net ozone production from CO and methane.



Photolysis of ozone leads to the formation of hydroxyl radicals (OH). OH is highly reactive and can react with most species in the atmosphere including volatile organic compounds (VOCs), CO and methane. OH formation from ozone occurs via reaction of an electronically excited oxygen atom O(<sup>1</sup>D) with water vapour, which

is shown in equations 3-5. However, this only accounts for a small fraction of the loss of O(<sup>1</sup>D), most reacts with a third body to give ground state O(<sup>3</sup>P). This can then go on to react with molecular oxygen to reform ozone (equations 6-8).



Tropospheric ozone has a strong seasonal cycle that varies depending on location. In the background Northern hemisphere there is generally a springtime peak. This is attributed primarily to the photochemical production of ozone from anthropogenic precursors, but there is also transport of ozone from the stratosphere to the troposphere (Chan et al., 1998, Derwent et al., 1998). This spring maximum is generally followed by a summertime minimum. In urban and semi urban areas the ozone peaks in the summer are driven by photochemistry (Ding and Wang, 2006). Background ozone generally peaks between July and September in the Southern tropics (Horowitz et al., 2003). This coincides with peak NO<sub>x</sub> emissions, from biomass burning and lightning sources (Moxim and Levy, 2000).

Increases in surface ozone are predicted with increases in global temperature. There are a number of reasons why this may occur, including changes in rate constants at higher temperatures, increased biogenic emissions and changes in meteorology. This will have detrimental effects on air quality and human health and mortality rates as a result (Bell et al., 2007). The same is true for plant growth and health, including impacts on important crops (Mauzerall and Wang, 2001). Studies such as this highlight the need for stringent air quality regulations to reduce concentrations of harmful pollutants.

## 1.6 VOC Chemistry

Once emitted to the atmosphere VOCs can be removed through a number of routes. These include photolysis and reactions with species such as the hydroxyl (OH), ozones or nitrate (NO<sub>3</sub>) radicals as well as removal through physical processes such as deposition (Atkinson and Arey, 2003). There have also been studies in the Arctic that have show removal of VOCs by reaction with halogens occur, which can impact ozone concentrations (Ramacher et al., 1997, Ramacher et al., 1999). (Sherwen et al., 2016) showed that including halogens in a global model reduced ozone concentrations. Under most conditions the dominant removal process in the troposphere is reaction with OH (Atkinson, 2007).

Over forested regions isoprene tends to dominate the OH reactivity (frequency of OH loss, normally in s<sup>-1</sup>) with smaller contributions from monoterpenes and other VOC species (Edwards et al., 2013, Sinha et al., 2010). However, at night other species such as monoterpenes and sesquiterpenes can dominate as isoprene concentrations fall due to the lack of sunlight and short lifetime of isoprene (Ortega et al., 2007). As the non-methane VOC with the largest emissions, isoprene oxidation via OH has possibly been studied in most detail. Rate constants for the reaction of isoprene and its products with OH have been measured in laboratory studies e.g. (Zhang et al., 2000, Jacobs et al., 2013, St. Clair et al., 2016). Isoprene oxidation is complex with many reaction pathways but understanding this chemistry is important for understanding the oxidative capacity of the atmosphere.

In addition to the initial rate constants, understanding the yield of different products from oxidation is important in understanding the chemistry of isoprene and other VOCs. Methacrolein (MACR) and methyl vinyl ketone (MVK) are important oxidation products of isoprene. Chamber studies alongside standard laboratory techniques have allowed the yields of these species from the reaction of isoprene with OH to be quantified under simulated atmospheric conditions (Karl et al., 2006).

The reaction rates and product yields can then be combined and used to develop mechanisms and schemes for VOC oxidation, see Figure 1.2. These can be used in models to simulate the chemical processes in the atmosphere. One such example is

the master chemical mechanism (Jenkin et al., 1997). Detailed mechanisms for different types of VOCs are included from short chain alkanes to aromatics (Bloss et al., 2005).

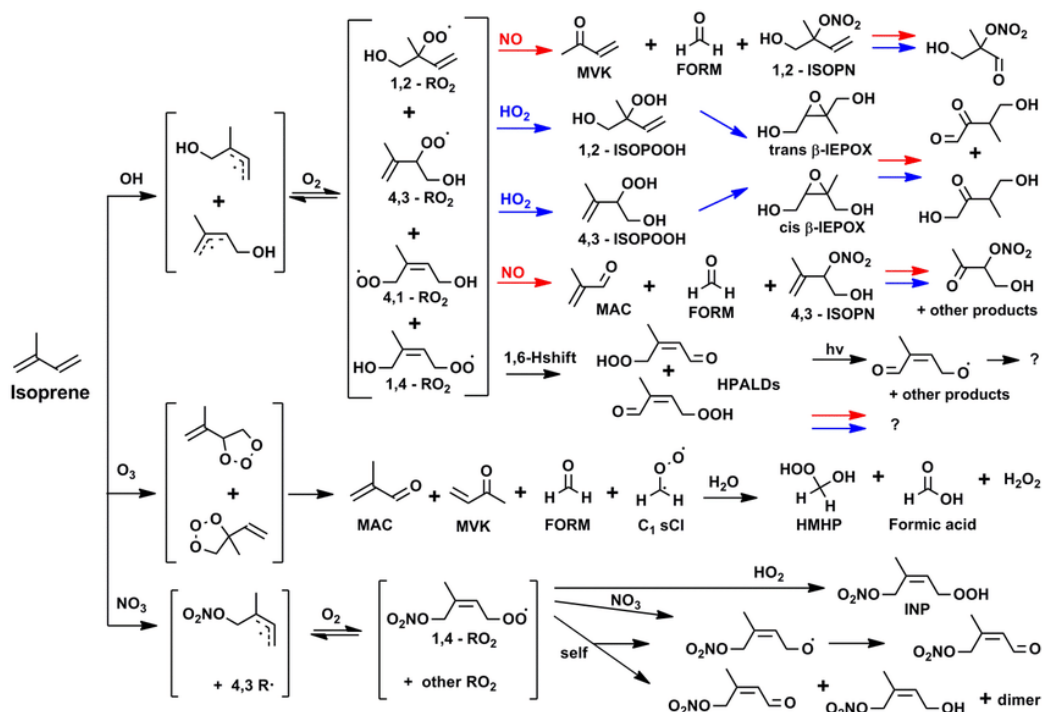


Figure 1.2 Isoprene oxidation mechanism, taken from (B. Nguyen et al., 2014)

Photo-oxidation of isoprene and other VOCs can lead to the formation of secondary organic aerosol (SOA). As the VOCs are oxidized the resulting products can become less volatile as more polar groups such as alcohols or acids are added to the carbon structure and result in partitioning from the gaseous to the aerosol phase (Carlton et al., 2009). For isoprene there are several routes by which aerosol formation can occur (Ng et al., 2008, Liu et al., 2016). It is not only biogenic VOCs that can lead to SOA formation. SOA formed from VOCs, particularly aromatic compounds can lead to the formation of haze in urban areas (Sun et al., 2016, Volkamer et al., 2006).

In addition to SOA formation, VOCs can have an effect on ozone concentrations. The effect of VOC species on ozone concentration depends upon whether the environment is  $\text{NO}_x$  or VOC-limited (Zeng et al., 2008).  $\text{NO}_x$  and VOCs are the precursors to ozone formation. When  $\text{NO}_x$  is in excess the environment is VOC limited, as increasing  $\text{NO}_x$  concentrations does not need to formation of more

ozone. The opposite is true when an environment is  $\text{NO}_x$  limited so VOCs are in excess. Understanding this relationship can lead to better implementation of air quality policy for reduction of tropospheric ozone (Wang and Hao, 2012).

Ozone is formed through the photolysis of  $\text{NO}_2$ , so  $\text{NO}_x$  is a necessary component of tropospheric ozone. However, VOC oxidation can lead to  $\text{HO}_2$  and  $\text{RO}_2$  radical formation and reaction of these species with  $\text{NO}$  leads to formation of  $\text{NO}_2$ . Photolysis of  $\text{NO}_2$  then leads to ozone production (Atkinson, 2000). Under high  $\text{NO}_x$  conditions the reaction between  $\text{OH} + \text{NO}_2$  to form nitric acid can terminate VOC oxidation and remove  $\text{NO}_2$  without production of ozone. Therefore local  $\text{NO}_x$  levels determine the overall rate of ozone production/destruction. The rate of reaction of  $\text{HO}_2$  and  $\text{RO}_2$  radicals with  $\text{NO}$  versus the alternative reaction pathways determines the overall rate of production of ozone. For this reason understanding the local conditions including  $\text{NO}_x$  levels is important for a full understanding of atmospheric VOC- $\text{NO}_x$ - $\text{O}_3$  chemistry.

A study by (Lelieveld et al., 2008) identified problems with simulating  $\text{OH}$  concentrations in a low- $\text{NO}_x$  high VOC environment. Observations over the Amazon showed  $\text{OH}$  concentrations higher than expected and to address this it was suggested that  $\text{OH}$  was recycled from VOC oxidation in low  $\text{NO}_x$  environments. Model simulations found that incorporating this  $\text{OH}$  recycling from isoprene oxidation could help explain the high  $\text{OH}$  concentrations observed. Similar results were found by (Kubistin et al., 2010) over a rainforest in Suriname. Measured  $\text{OH}$  concentrations were higher than expected and agreement between the model and observations improved when isoprene chemistry was removed from the model. This suggests that an  $\text{OH}$  source similar to the  $\text{OH}$  sink provided by VOC oxidation is needed.

Model studies (Stone et al., 2011) combined with measurements of  $\text{OH}$  concentration and reactivity in Borneo (Whalley et al., 2011) have evaluated understanding in regions highly impacted by isoprene. These studies found problems with simulating  $\text{OH}$  and  $\text{HO}_2$  concentrations. Both studies found a large underestimation of modelled  $\text{OH}$  and problems with simulating measured  $\text{HO}_2$ . These studies point towards a lack of understanding of  $\text{HO}_x$  chemistry in low  $\text{NO}_x$ , high biogenic VOC environments. In addition to this, laboratory studies have shown that the oxidation of isoprene by  $\text{OH}$  is not well understood in low  $\text{NO}_x$

environments (Paulot et al., 2009b). All of this shows that current understanding of low-NO<sub>x</sub> isoprene chemistry is poor and further field, laboratory and modeling studies are needed to better characterize this chemistry.

There have been several suggestions of how to reconcile the disagreement between modelled and observed isoprene chemistry in these low-NO<sub>x</sub> environments. Suggested improvements involve OH recycling schemes and include direct OH recycling from OH oxidation of isoprene and production of OH from HO<sub>2</sub> + RO<sub>2</sub> reactions. However when these were included in modeling studies any improvement in agreement with OH concentrations comes at a cost to agreement with HO<sub>2</sub> (Stone et al., 2011). Therefore further laboratory studies are needed to better elucidate isoprene oxidation pathways.

Field studies have provided observations of a wide range of VOCs as well as important species linked to VOC chemistry, such as ozone and OH. Model simulations provide a method for evaluating these datasets and testing our understanding of VOC chemistry under different conditions. These studies have shown a general model underestimation of OH in high VOC low NO<sub>x</sub> environments. The next section gives details on measurement techniques for VOCs and summarizes some key results from previous field studies.

## **1.7 Measurement Techniques**

A range of techniques have been used to make VOC measurement. A number of the key methods are discussed below. The first section outlines techniques used for sampling VOCs, the second gives details on how different VOCs are separated and subsequently detected. Important points when considering VOCs measurements are species separation, time resolution of sampling and analysis and concentration of ambient samples for detection. Species separation is the ability of a technique to resolve individual components of a mixture so that each may be identified individually. Time resolution of sampling and analysis is how often a sample can be taken and then separated giving the output (such as a chromatogram run with GC). Concentrations of VOCs in the atmosphere are generally low, ppt or below for many species of interest. For this reason, large volumes of air must be sampled to obtain high enough VOC mass for detection. Often this is done by passing large

volumes of air over a trapping material that holds the VOCs, so that the VOCs are concentrated before separation.

### **1.7.1 Sampling Methods**

There are two main methods for VOC sample collection, whole air and sorbent sampling (Kumar and Viden, 2007).

### **1.7.2 Whole Air Sampling**

Whole air sampling (WAS) involves the filling of a vessel with the desired sample. One example of this is the use of canisters. This technique is often used for aircraft campaigns where there are restrictions on what instruments can be used on board, or for more remote location where the logistics of transporting a large instrument for online analysis is difficult (Lerner et al., 2017, Baker et al., 2010).

The canisters are stainless steel or glass vessels, normally a couple of litres in size. The canisters will be flushed, normally with nitrogen and evacuated before use to remove any possible contaminants. The canisters collected can then be stored, shipped and analysed on the desired instrument, or multiple instruments (Colman et al., 2001). Given that the canisters are likely to be stored for a period of time before analysis it is important to consider the stability and possible degradation of VOCs in the canisters when analyzing these samples (Sin et al., 2001).

The Global Atmosphere Watch (GAW) programme publishes guidelines for the standard procedures required when using canisters for VOC sampling. This operating procedure ensure consistency across sites (Steinbrecher and Weib, 2012).

An alternative to canisters is the use of bag sampling. Materials such as Tedlar, polyvinylidene fluoride and fluorinated ethylene propylene are available to use. Bag sampling offers more portability than canisters for work in the field. The bags are prepared in a similar way to the canisters with flushing and evacuation. A major issue with bag sampling is loss of VOCs during storage (Wang et al., 1996). The conditions under which the bags are stored has an impact upon the stability of VOCs in the bags (Hsieh et al., 2003).

Despite the issues of stability of VOC samples while stored in canisters or bags, the portability and ease of use, particularly with bag sampling, means both of these techniques are widely used for VOC sample collection.

### **1.7.3 Sorbent Sampling**

Sorbent sampling involves passing air over an adsorbant material to trap VOCs within it. There are a wide variety of adsorbants and sampling options that can be used depending on the desired VOCs and environment (Uhde, 2007). After sampling the VOCs are removed from the trapping material ready for analysis, through either solvent extraction or most often for atmospheric VOC analysis, thermal desorption (Woolfenden, 2010).

For the work in this thesis direct sampling of ambient air from an outside inlet was used. Collecting and storing air samples using WAS or sorbent sampling was not appropriate for this work due to the logistics of working in a remote location and degradation of VOC while stored and transferred. Also, for a species such as isoprene with a strong diurnal profile it is important that samples are taken frequently so that this profile can be observed. Online sampling allows for automated samples to be taken at regular time intervals without the need for manual intervention and the storage and shipping of samples.

## **1.8 Separation and Analysis**

After sample collection the VOC species need to be separated, detected and quantified. Details on the instruments most commonly used are given below.

### **1.8.1 Gas Chromatography**

Gas chromatography is a commonly used separation technique for VOC analysis. It is used in conjunction with a detector such as a mass spectrometer (GC-MS) or a flame ionization detector (GC-FID). Both instruments, with a number of modifications, have been used extensively for the analysis of atmospheric VOCs (Chai and Pawliszyn, 1995, Tani et al., 2003, Bartenbach et al., 2006). GC-FID

works through the combustion of organic species to form ions that are then collected and the current of the electrical signal produced is proportional to the amount of analyte. MS ionizes the species that are then detected based upon their mass-to-charge ratio. There are a number of ionization methods that can be used for mass spectrometry.

Many developments of the GC-detector systems have increased the range of applications for these instruments and give a wide range of VOCs that can now be measured. The use of multiple columns means a wider spread of VOCs can be analysed, an example of this is the simultaneous analysis of hydrocarbons and oxygenated volatile organic compounds (Hopkins et al., 2003). The development of two-dimensional gas chromatography techniques gives greater capacity to separate VOCs and improved sensitivity compared with single column techniques (Bartenbach et al., 2006).

FID detection offers good sensitivity to VOCs, good stability and gives a linear response over a wide range of concentrations (Huang et al., 1990). This linear response is advantageous given the wide range of mixing ratios observed for some VOCs, from almost zero to thousands of ppb. Since FID is non selective in what compounds are oxidized from the sample, good chromatographic separation is required before detection.

GC-MS is sometimes used alongside FID given their often complementary strengths/weaknesses, although it can be used as the only detector. The high selectivity of the mass spectrometry means co-elution of compounds is minimized compared with FID (Poster et al., 2006), although careful selection of column specifications during gas chromatography can reduce co-elution. However, sensitivity of MS detection is reduced if multiple ion masses are desired, which is almost always the case when making atmospheric measurement (Vékey, 2001). Measurement of lower mass hydrocarbons using GC-MS is problematic, whereas these can be detected using FID (Maeda et al., 1995).

### **1.8.2 Proton Transfer Reaction Mass Spectrometry**

An alternative to using gas chromatography with a detector is Proton Transfer Reaction Mass Spectrometry (PTR-MS). This method does not require samples to be separated before analysis, unlike FID and MS detection. PTR-MS uses hydronium ions to ionize the VOC species before they are separated by mass and the ions counted using an electron multiplier detector (Hewitt et al., 2003).

A major advantage of using PTR-MS over GC is that monitoring can be rapidly done online, since there is no need for pre-concentration or separation of samples. This makes it ideal for use in situations where rapid changes in mixing ratios of VOCs are expected (Fall et al., 1999).

However, there are some drawbacks to this technique. For most species soft ionization occurs, meaning that there is no fragmentation of the parent ion. However, for some species including monoterpenes fragmentation does occur and this leads to problems in interpreting the mass spectrum (Tani et al., 2003). In some cases PTR-MS is combined with the GC based techniques to give a more complete picture of the VOC composition (Lindinger et al., 2005).

## **1.9 Previous Observations of VOCs**

Observations of VOC fluxes and mixing ratios have been made in a wide range of locations from temperate forests to the tropics (Fares et al., 2013, Warneke et al., 2001). Studies in the tropics will be the focus of the following sections due to the relevance for this work and because most biogenic VOCs are emitted in the tropics.

### **1.9.1 OP3 Campaign (7<sup>th</sup> April – 4<sup>th</sup> May and 21<sup>st</sup> June – 27<sup>th</sup> July 2008)**

The Oxidant and Particle Photochemical Processes above a south-east Asian tropical rainforest (OP3) made measurements at the Bukit Atur Global Atmosphere Watch site, Malaysian Borneo in 2008 (Hewitt et al., 2010). Of interest to this work are measurements of concentrations and fluxes of a range of VOCs.

Measurements of isoprene and monoterpenes were made using gas chromatography with flame ionization detection during the OP3 campaign (Jones

et al., 2011). This work found isoprene to be the dominant daytime VOC, with monoterpenes being the most abundant species outside of daylight hours.

As part of this work measurements of VOCs were made onboard the facility for airborne atmospheric measurement (FAAM) aircraft. Agreement between the ground based and airborne measurements for isoprene was generally good, apart from some high peak isoprene values seen from the aircraft samples. These high values were attributed to localized effects of extremely high isoprene emissions. The airborne measurements covered the rainforest area but also surrounding oil palm plantations, the mixing ratio of isoprene above the plantations was found to be approximately four times higher than above the rainforest, demonstrating that land use changes can have significant impacts upon local and regional atmospheric composition. The possible effects of land use changes in South East Asia have been studied in detail in other work (Vadrevu et al., 2017).

Measurements of meteorological data were made alongside the VOC mixing ratios at the ground based site. From this it was found that both isoprene and monoterpene mixing ratios were correlated with temperature. Isoprene also showed a dependence on light, specifically photosynthetically active radiation (PAR). This relationship for isoprene is not simply due to emissions as light driven isoprene removal processes were also thought to be important.

In addition to the GC-FID measurements made during OP3, proton transfer reaction mass spectrometry (PTR-MS) measurements of isoprene mixing ratios and fluxes were made (Langford et al., 2010). The PTR-MS sampled from a height of 75 m above ground level, compared with 5 m for the GC-FID measurements. Fluxes were calculated using the eddy covariance technique.

(Langford et al., 2010) found isoprene to be the most abundant hydrocarbon in the rainforest. The extent of isoprene oxidation was calculated from the ratio of (MACR + MVK) to isoprene. MACR and MVK are oxidation products of isoprene. The PTR-MS OP3 data measured values that were consistent with previous studies in the Amazon (Kesselmeier et al., 2002, Kuhn et al., 2007).

An important finding from this study was that the measured isoprene and monoterpene emission fluxes were much lower than those calculated from

(MEGAN) (Guenther et al., 2012). For isoprene the measurements were ~4 times lower and monoterpenes were 70% lower than MEGAN. The model values are based upon emission rates for tropical forests. This suggests that MEGAN base emissions are too high for the rainforests in Borneo, although the work in this thesis found good agreement between measured and modeled isoprene concentrations.

### **1.9.2 Measurements in the Amazon**

Measurements of concentrations and fluxes of VOCs have been made for the Amazon in a number of studies (Rizzo et al., 2010, Kesselmeier et al., 2000, Helmig et al., 1998, Karl et al., 2007, Greenberg et al., 2004, Rinne et al., 2002).

One study at the Reserva Biologica do Cuieiras made measurements of mixing ratios and fluxes of isoprene and monoterpenes (Kuhn et al., 2007). Samples for mixing ratio analysis were collected using a solid absorbant and analysed using GC-FID. This study again found isoprene to be the dominant biogenic VOC. Other species such as benzene and toluene showed consistently low mixing ratios, suggesting influences at the site from anthropogenic emission sources were minimal.

This study used two algorithms for calculating VOC fluxes, surface layer gradient (SLG) and relaxed eddy accumulation (REA) (Pattey et al., 1993, Byun, 1990). The flux calculations found that both isoprene and monoterpenes emissions show some light dependence. For anthropogenic VOCs, such as benzene, negative flux gradients were calculated, meaning there was a net deposition of these species not emission. The fluxes were compared to model values but used a single column chemistry and climate model (SCM), unlike the MEGAN model used for the OP3 comparisons. There was good agreement with modeled fluxes. Even though these fluxes were used to parameterize the SCM model, the model overestimated concentrations of isoprene, MVK and MACR. This showed that there were problems with successfully implementing chemistry and transport processes within the model.

This study also investigated the differences between observational fluxes based upon observations above the canopy and modeled fluxes with algorithms based on

primary plant emission factors. Model studies showed that the difference in simulations at the leaf and canopy scale was around 10% and this fell within the uncertainty of the measurements. Therefore loss processes within the canopy do not cause a discrepancy when calculating observed fluxes.

Other measurement made in the Amazon have used techniques such as balloon sounding (Greenberg et al., 2004) to report isoprene and VOC emissions. This study reported emission rates for a number of different eco regions and found significant differences in emissions between these regions, all of which were in Amazonia. These differences were ascribed to changes in the species present in each area and so the percentage of plants that emitted VOC species varied.

This is important for model studies. Most models use a small number of plant functional types (PFTs) to give the base emissions for different areas. Tropical forest would be one PFT with a single emission factor. Given the high variability observed within one rainforest region and between different ecosystems, using the same emission factors for rainforest on different continents may not be appropriate.

A study by (Rinne et al., 2002) investigated the light and temperature dependence of isoprene and monoterpene emissions. The measured fluxes were lower than those used in global atmospheric chemistry models. Although given that these measurements were made at a single site covering a small footprint area it is difficult to conclude that the fluxes would scale to the larger area represented in models. Monoterpene emissions were found to depend on light and temperature and including a response to both variables in calculating fluxes gave values one-third less than just temperature dependence. More studies of emissions at the leaf level to quantify the relationship between these variables for monoterpenes is important for successful model simulations.

### **1.9.3 Satellite Observations**

In addition to in-situ measurements, satellite observations of formaldehyde can be used to infer isoprene concentrations. The formaldehyde column data is retrieved from satellite measurements from instruments such as the Ozone Monitoring Instrument (OMI) (González Abad et al., 2015). The spectrum between 307 and

383 nm is used for formaldehyde retrievals. The data is processed through spectral fitting and then converted into a vertical column density. The column density is related to isoprene emissions, normally through an assumed relationship with model emissions (Palmer et al., 2006). Formaldehyde is an oxidation product of VOCs, primarily isoprene. The yield of formaldehyde from isoprene oxidation combined with the short lifetime of isoprene, can be used to infer isoprene concentrations from formaldehyde measurements. Other VOCs do oxidize to form formaldehyde, but this is either in very small quantities or the production rate is slower compared with isoprene (Palmer et al., 2003).

The advantage of using satellite data is that it can be used in areas where there is poor availability of VOC data, such as Africa (Marais et al., 2012). It also offers the advantage of offering a long-term, global dataset. This can be used to analyse seasonal variation in isoprene in addition to the impacts of shorter lived events such as biomass burning (Bauwens et al., 2016). These observations can also provide a method for evaluating the success of models in simulating isoprene emissions (Baek et al., 2014).

(Palmer et al., 2006) found strong interannual variability in isoprene from column formaldehyde observations over the United States. This variability was attributed to changes in temperature, which is consistent with the dependence of isoprene emissions on temperature in MEGAN. The inferred seasonal changes in isoprene showed good agreement with in-situ measurements but with a 30% underestimation. This study suggests that column formaldehyde is a useful tool for assessing isoprene emissions, but without an improved understanding of isoprene chemistry in low-NO<sub>x</sub> environments this technique will be limited in its scope.

#### **1.9.4 Biomass Burning Observations**

Biomass burning is a major source of trace gases, aerosol and smoke particles in the atmosphere. It has been estimated that annually 2 to 5 petagrams of carbon is combusted during these burning events (Crutzen and Andreae, 1990). This compares with the ~594 Tg of carbon emitted from isoprene emissions annually. Burning occurs globally due to boreal fires, tropical burning for land clearance and cooking fires (Wentworth et al., 2018, Field et al., 2009, Stockwell et al., 2015). The

effects of biomass burning specifically for the South East Asian biomass burning season will be discussed below in section 1.9.6.

### **1.9.5 Global Studies**

Measurements of emissions of a range of species from biomass burning have been made both in controlled laboratory experiments and in the field (Ito and Penner, 2004, Thompson et al., 2001, Engling et al., 2014). A lot of burning is seasonal and understanding these patterns is important for predicting and mitigating potential impacts (Duncan et al., 2003). Satellite observations of fire locations are important for these longer term global studies, providing good temporal and spatial information on burning events (Edwards et al., 2006). Ground based measurements can provide detailed information on which species are emitted during burning and emission ratios or factors can be calculated from the available data (Greenberg et al., 1984, Andreae and Merlet, 2001). These emission quantities are important input for model studies.

### **1.9.6 South East Asian Burning Season**

In Asia biomass burning is dominated by forest fires not domestic burning (Hao Wei and Liu, 2012). One of the most important sources of biomass burning in this region is from Indonesian fires. The resultant emissions bring widespread problems for air quality and therefore health throughout the region including substantial haze problems in Singapore and Malaysia (Engling et al., 2014, Koplitz et al., 2016).

During 2015 one of the worst biomass burning seasons on record for Indonesia occurred (Huijnen et al., 2016). It was thought this resulted from a strong El Niño that contributed to an extended period of drought. This drought enhanced the normal seasonal biomass burning, with the mean daily CO<sub>2</sub> emission rate from the burning over this period exceeding that of the EU from fossil fuels (Huijnen et al., 2016). In addition to the El Niño effects, it has been suggested that anthropogenic global warming could also increase the likelihood of drought throughout Indonesia and this could lead to an enhancement in future burning (Lestari et al., 2014). Understanding the effects of the burning in this area on the whole of South East Asia is therefore vitally important. In addition to this, preventative measures such as improved land management practices will be important in preserving and

improving the air quality throughout South East Asia as well as minimizing the emission of species with global warming potential.

A specific problem in Indonesia is underground peat burning. These underground fires are difficult to extinguish and there is also an ample supply of fuel for continued burning (Field et al., 2016). These fires are a source of many trace gases including VOCs and are not yet well characterized for model studies due to a lack of detailed measurements.

## **1.10 Current Knowledge Gaps**

The Global Atmosphere Watch (GAW) programme (Schultz, 2015) operates a network of research stations making long-term observations of a range of parameters important for the global atmosphere. One section of this network focuses on reactive gases. This covers species such as ozone and CO but most importantly for this work VOCs. There are a large number of stations monitoring reactive gases globally but the number monitoring VOCs specifically is much less. The monitoring stations are focused mainly in Europe with generally poor coverage around the tropics, Figure 1.3. However, the tropics are believed to be the dominant source of isoprene and monoterpenes globally (Guenther et al., 2012). Globally there are not currently any GAW sites making long-term VOC measurements in the tropical forests, Figure 1.4. The tropical forests are the locations for most of this burning, any influence from these events, particularly on an inter-annual basis will be not be seen without long-term measurement sites.

This project aimed to address this issue by making observations of a number of VOCs over a period of several months in a tropical rainforest environment. It was hoped that this would allow for short term (hourly, daily) changes in VOC mixing ratios to be identified as well as longer term trends over periods of weeks or months. Combined with model studies and knowledge of local events this should increase understanding of how VOCs change in this environment and hopefully be able to explain what is causing these changes.

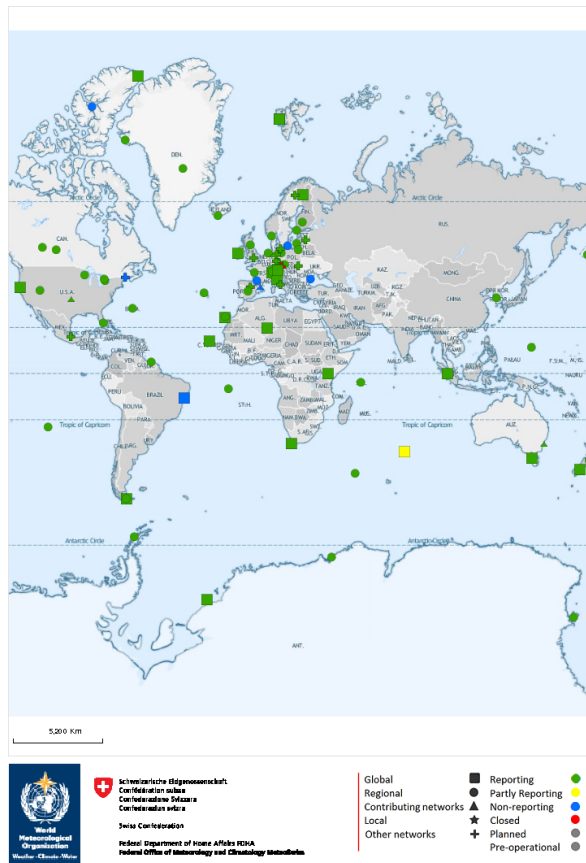


Figure 1.3 GAW global sites monitoring VOCs. The majority of sites are situated in Europe, with poorer coverage in the Southern hemisphere and around the tropics. Maps obtained from the GAW website <https://gawsis.meteoswiss.ch/GAWGIS>

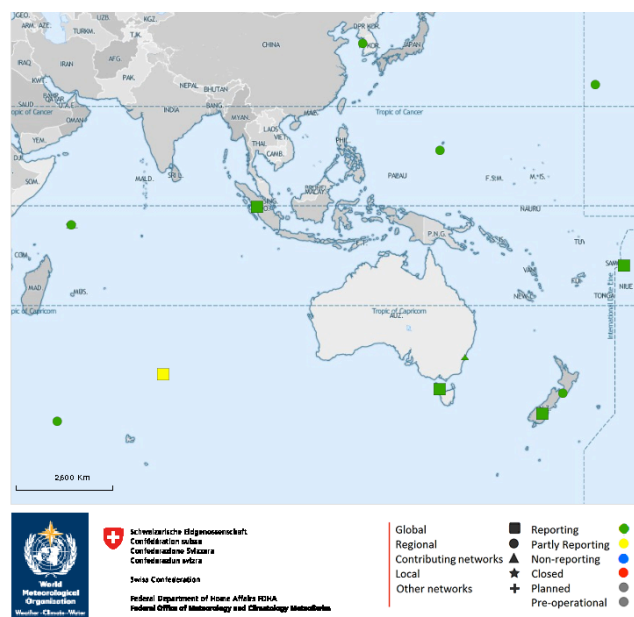


Figure 1.4 GAW stations measuring VOCs in South East Asia. Map obtained from the GAW website.



**Figure 1.5 GAW stations measuring isoprene globally. This map shows that the only stations currently making isoprene measurements are in Europe, with no GAW stations measuring isoprene in the tropics. Map obtained from the GAW SIS website.**

In addition to a lack of observations in the most relevant areas, models have been unable to reconcile observations of both OH and isoprene, particularly in low-NO<sub>x</sub> environments (Pugh et al., 2010, Stone et al., 2011, Lelieveld et al., 2008). This is in part due to a lack of fully comprehensive understanding of isoprene oxidation chemistry, including SOA formation. Laboratory and theoretical studies are continually improving understanding of isoprene oxidation pathways (Peeters et al., 2009, Paulot et al., 2009b, Henze and Seinfeld, 2006, Wennberg et al., 2018). Implementing these updates into global models can then assess the effects of these changes in different environments (Taraborrelli et al., 2012). However, given that there is an underestimation of OH in forested regions (Lu et al., 2012) likely possibly linked to VOC chemistry, more laboratory and model studies looking at the possible pathways of isoprene oxidation and effects on OH chemistry are needed to address this issue.

## 1.11 BALI Project Overview

The work described here is part of a wider consortium of projects funded under the NERC BALI (Biodiversity and Land Use Impacts on Tropical Ecosystem Function) project. The aim of BALI is to improve understanding of how land-use change affects the biodiversity and biogeochemical cycling in tropical forest environments. There is a wide range of research done as part of this project, such as effects of logging, invertebrate species and carbon budgets of different land uses.

The measurement site is situated in the Danum Valley conservation area, an area of lowland rainforest. The site has a building that houses the laboratory areas and a 100 m tall observation tower. The site is situated at the top of a hill. This site was chosen as it is located in an area not currently covered by GAW VOC measurements. In addition to this colleagues had existing collaborations with the Malaysian Meteorology Department who operate the site. Full details on the site are given in chapter 2.

Measurements in this thesis used gas chromatography with flame ionization detection (GC-FID) to make measurements of VOC mixing ratios at a tropical rainforest site in Malaysian Borneo, from August 2015 - March 2016. The instrument is described in detail in chapter 2. These measurements are combined with model studies using the GEOS-Chem chemistry transport model, have been used to better understand VOC chemistry in a low-NO<sub>x</sub> environment. The model is described in chapter 3.

The measurement site has previously been used for the Oxidant and Particle Photochemical Processed (OP3) campaign. Measurements of VOC mixing ratios and fluxes were made during this campaign over two periods, each of three weeks (Jones et al., 2011, Langford et al., 2010). These measurements were made using a gas chromatograph with flame ionization detection, similar to the one used in this work and a proton transfer reaction with mass spectrometry (PTR-MS). The PTR-MS made flux measurements in addition to mixing ratios. Isoprene and some other VOCs were measured in both campaigns and a comparison and discussion of these is given in chapter four.

## 1.12 Thesis Outline

**Chapter two.** Gives details on the instrumentation used to make the VOC measurements. Descriptions of the sampling, separation and analysis of VOCs and instrument errors encountered are given. The measurement site is also described.

**Chapter three.** The GEOS-Chem model used for all simulations in this work is described here. Details about model features, such as emissions algorithms and relevant chemistry schemes are given.

**Chapter four.** Includes an overview of all data collected during this work. Non-negative matrix factorization is used to separate the total dataset into three distinct components and the analysis is described in detail. The components found from the NMF analysis are outlined here and discussed in detail in the following chapters.

**Chapter five.** The biomass burning component identified in chapter four is analysed in further detail. Active fire maps and back trajectories are used to show that burning emissions from Indonesia likely influenced the measurement site. GEOS-Chem biomass burning emissions are evaluated through comparison with the observations.

**Chapter six.** This section focuses on the biogenic component from the observations. This looks mainly at isoprene but also propene, comparing with previous observations such as the OP3 campaign and evaluating the success of GEOS-Chem in simulating VOC chemistry in a low-NO<sub>x</sub> environment.

**Chapter seven.** This contains a summary of the findings of this work and considers ideas for future work.

# Chapter 2

## 2 Instrument Methodology

### 2.1 Project Overview

Measurements were made at Danum Valley GAW station in Sabah, Malaysia. This would not have been possible without the help and support of colleagues at the Malaysian Meteorological Department and the Universiti Kebangsaan Malaysia (UKM). The author would like to acknowledge their assistance with the measurements made as part of this project.

Measurements of thirteen VOCs were made at the Danum Valley Global Atmosphere Watch Station in Sabah Malaysian Borneo (4.98°N, 117.84°E, 426 m above sea level). A list of all measured VOCs with limits of detection is given in Table 2.1. These measurements were made as part of the biodiversity and land-use impacts on tropical ecosystem function (BALI) project. The wider project aimed to study the biogeochemical impacts of land-use changes on Borneo.

Measurements for this work were made using automated gas chromatography with flame ionisation detection (Hopkins et al., 2003). The instrument is capable of measuring a wider range of compounds than those reported (Hopkins et al., 2003). However, these were either not observed at the site or the identity of the peaks could not be confirmed using the NPL standard (Grenfell et al., 2010).

This chapter outlines the experimental techniques used for VOC detection and analysis. A detailed description of the sampling and separation methods is given in section 2.3 & 2.4, including a description of the site and instrumentation used. Section 2.5 discusses the peak identification and how the raw data is processed to give peak areas for each of the VOC species. The calibration method and details on instrument stability are outlined in section 2.6. Finally, there were a number of issues encountered with running the instrument throughout this project. The details of these are given in section 2.9.

## 2.2 Experimental

### 2.2.1 Measurement site set up

The measurement site was chosen as part of the BALI project, which includes research projects in the Danum Valley area as well as other areas in Sabah, Malaysia. The surrounding rainforest is mixed dipterocarp forest, this is the dominant tree type in Sabah rainforests (King et al., 2006). The annual mean temperature is 26.8 °C and precipitation is 2825 mm, with generally light winds, information taken from the GAW website (<https://gawsis.meteoswiss.ch/GAWSIS//index.html#/search/station/stationReportDetails/61>).

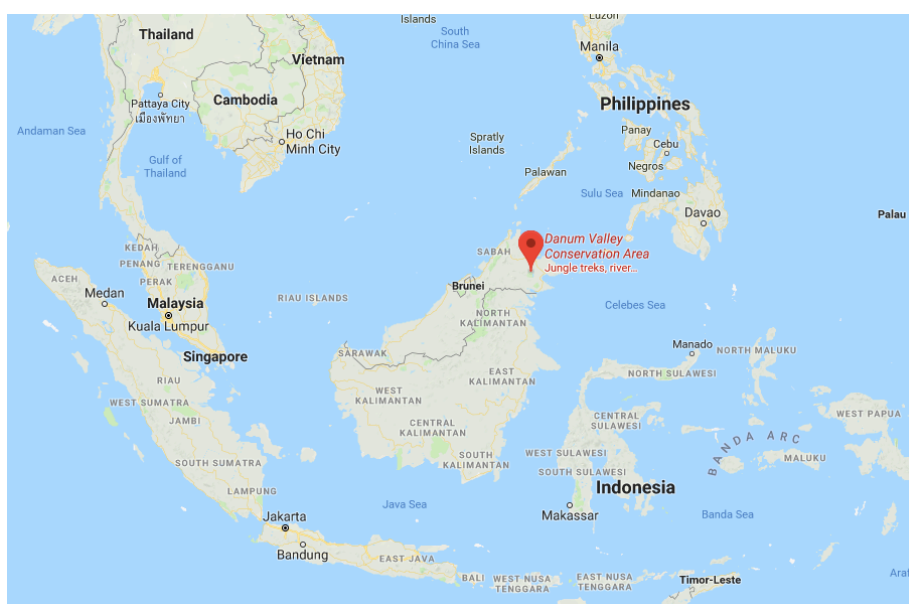
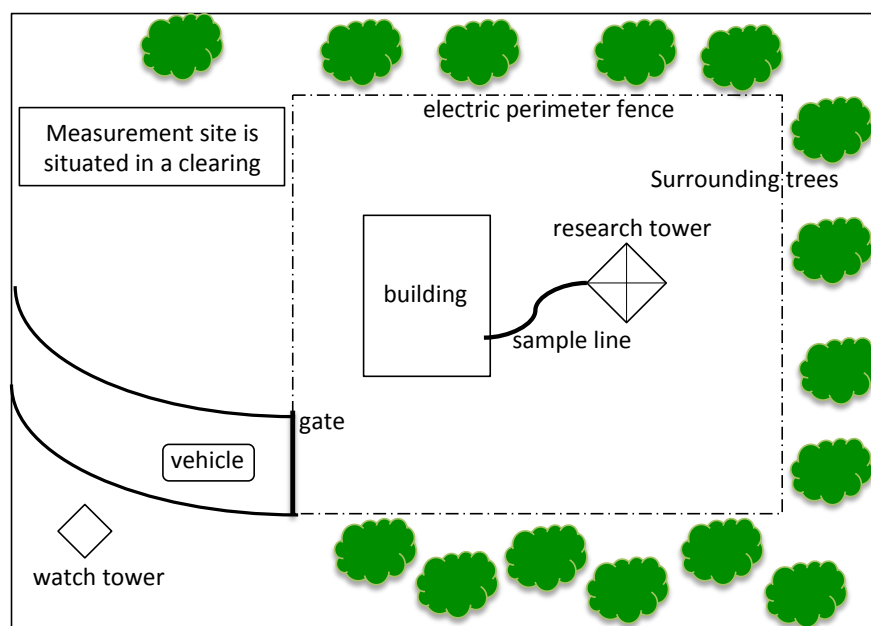


Figure 2.1 Location of the Danum Valley site, Sabah, Malaysia.

The same site was used during the OP3 campaign and this should allow a comparison of measurements between OP3 and our measurements. There was also access to Malaysian Meteorological Department staff who visited the site frequently and internet access to provide remote data access. At the measurement site there is a small, single-storey building that houses the laboratory and staff living quarters. Approximately 20 m away from the building is the 100 m tall research tower. The laboratory is located on the tower side of the building. There is a small wooden watchtower at the top of the entrance to the site. Vehicles park at the gated entrance to the site.



**Figure 2.2 Top down view of the measurement site, showing the building in which the instrument is set up and the sample line running from 30 m up the research tower, through the building wall to the main sample pump**

The building and tower are located within a clearing at the top of a hill. There are trees surrounding the measurement site, at approximately 30 m distance from the tower in all directions except the building side where trees are cleared a greater distance. There is a track (around 300 m long) leading from the road at the foot of the hill, up to the gate at the entrance to the site. The main sample line runs from the research tower, through a hole in the side of the building onto the main sample pump. A detailed overview of the sampling process is given in section 2.3.1.

## 2.3 Instrumentation setup

A schematic of the instrumental setup in Borneo is shown in Figure 2.3. This covers all steps of sampling, separation and detection of VOCs. The numbered sections correspond to the headings in this section from 2.3.1 onwards. The main equipment including important pumps are shown in this diagram. For simplicity, other important components including the compressor and hydrogen generator are described in the relevant section and not included in the schematic.

Sampling covers the processes that take the ambient air from the external sampling point to the units that prepare the air for separation and detection. Pre-concentration and trapping describes the steps that ensure the sampled air deposits adequate amount of VOCs onto the adsorbent trap for detection in subsequent steps. Water removal gives details on the unit that ensures ambient air samples are dried before entering the gas chromatograph. This is important because any water in the samples would limit the effectiveness of the pre-concentration stage, cause problems for the chromatography and risk damaging the columns. The gas chromatograph section outlines the setup and part details for the instrument as well as the methods used to separate and detect different VOCs.

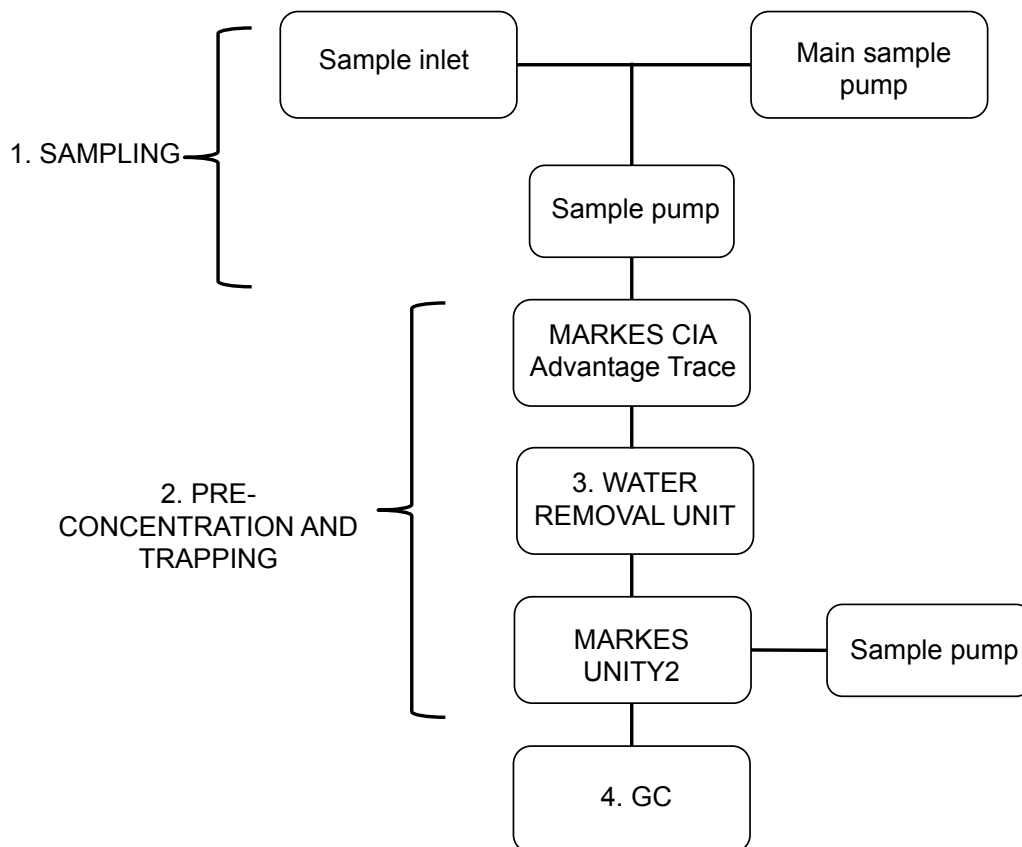


**Figure 2.3 Schematic of the instrumental setup in Borneo. The numbers correspond to the section headings below**

### 2.3.1 Sampling

Ambient air was pulled (KNF vacuum pump, part number 014833/017447) through a manifold at greater than  $\sim 30 \text{ L min}^{-1}$ . This gave a manifold residence time of less than eight seconds before air was sub-sampled from the main line. The main sample line was  $\sim 40\text{m}$  in length and made from  $\frac{1}{2}$ " PFA tubing (Swagelock, part number: PFA-T8\_062-100). The inlet was located at  $\sim 30 \text{ m}$  above ground level on the research tower. This gave a sampling height above the majority of the canopy, with the exception of a few nearby trees. Most of the surrounding canopy is situated in the valley below, as seen in Figure 2.4. Sampling was from above the canopy because there are complicated loss processes for isoprene that occur within the canopy (Karl et al., 2004). Thus sampling above the canopy should give a better representation of the local isoprene concentration not just for a single location within the canopy layer. In addition to this isoprene emissions are known to be highly dependent on the plant species (Owen et al., 1997). Sampling from

above the canopy should mean that the mixing ratios are less likely to be subjected to a large influence from a limited number of trees. Finally sampling from a greater height should minimize any interference from local sources such as the building or any vehicles transporting staff to the site.



**Figure 2.4 View from the research tower at ~10m. There are a few nearby trees, as shown, but the site is above most of the surrounding canopy in the valley below. This is representative of all sides of the tower.**

The inlet was covered with an inverted plastic funnel to prevent rainwater entering the system and a 90  $\mu\text{m}$  stainless steel in-line particulate filter (Swagelok, part number: SS-4F-90) located at the beginning of the tubing to prevent insects and particulates entering the tubing, Figure 2.5. Inside the building the final three metres of tubing was heated to around 40°C to prevent water condensing in the lines. Water in the system would be problematic for achieving sufficient trapping (without breakthrough) of VOCs and good chromatography with well-defined peaks at consistent retention times. For sub-sampling, a t-piece was introduced into the main line and a further line of ¼" Teflon tubing was passed to the instrument using a downstream KNF labport sample pump (type: N86KN.18, serial no: 2.6873043). The target sampling flow rate was 50 ml min<sup>-1</sup> for a sampling time of 10 minutes, giving a sample volume of 500 ml. The sub-sampled air was pre-concentrated (section 2.3.2) and water removed (section 2.3.3) before sample injection.



**Figure 2.5 (Left) Tower at GAW site where sample inlet is located ~30m above ground level. (Right) Inlet on tower, the inlet is formed from a plastic funnel to minimise damage from the elements, it is also covered in a plastic sheet to prevent rain and large objects from entering the system**

### **2.3.2 Pre-concentration and Trapping**

A MARKES International UNITY-2 (serial no: U22035) and MARKES International CIA Advantage Trace (serial no: GB00H40108) were used for sample pre-concentration and injection. Pre-concentration of samples was required due to the relative lack of sensitivity of the detector and low mixing ratios of VOCs in ambient air. The target sample volume was 500 ml.

The sample was injected on to a dual bed trap (Markes International Tenax and carboxen trapping materials), which was cooled to a temperature of -20 °C. Cooling of the trap was achieved using Peltier plates.

### **2.3.3 Water Removal**

An important feature of this system was a water removal unit. Previous measurements show that the humidity drops below 90% only for a couple of hours a day, even for gaps in the canopy such as where the measurement site is located (Brown, 1993). For comparison the annual average humidity in York from the Met Office website is ~80% (<https://www.metoffice.gov.uk/public/weather/climate/>). An important

component of the water removal system was the cold fingers. These are glass vessels that are cylindrical in shape, (approximately 12 cm in length by 2 cm diameter) with a volume of around 80 ml. There are two arms on the top of each cold finger to allow gas flow in and out. Seven cold fingers were held within an aluminium block cooled to -30 °C using a Stirling cooler. A thermocouple was inserted into the aluminium block at a depth similar to the cold fingers, if the temperature exceeded the expected temperature that Stirling cooler would then cool further until the desired temperature was reached again. The top section of the unit was heated to around 35°C to prevent water freezing out in the top of the cold fingers or gas lines and causing a blockage of the flow. The heat was circulated in the upper part of the system using a fan. The cold fingers were connected to the system using a 16 port multi-position Valco valve. This valve allowed for switching between cold fingers when the previous one was blocked without the need to undo any fittings. Once all cold fingers were cycled through and blocked with ice the unit needed to be detached from the instrumental setup, thawed and the water removed. This required manual input from local collaborators. During the measurement period this process was required to be completed on one occasion. Figure 2.6 shows the inside of the water removal system used in Borneo. There are six large cold fingers with one smaller piece of glassware in the center. It was estimated that each cold finger would last for one to two months of continuous sampling before becoming blocked due to ice formation. Before gas flow was blocked, flow through the cold finger in use was stopped and flow moved to the next cold finger. This process can be automated but was done manually due to problems with running the instrument continuously, manual switching of the cold fingers was done using the control box, which also gave a read out of which cold finger was currently in use.

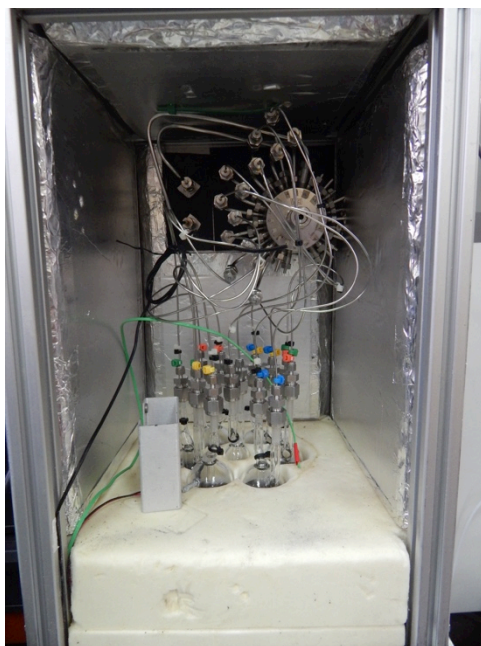


**Figure 2.6** The glass (cold) fingers, valve and fan inside the water removal unit. Each cold finger has an inlet for the wet gases and outlet back through the valve for the dry gas. The green wire is the thermocouple, which helps regulate the temperature within the aluminium block.

## 2.4 Gas Chromatogram

Chromatographic separation was achieved using a dual column Agilent 7890B GC (serial no: CN13383102), with two flame ionisation detectors. The GC was initially fitted with an Agilent DB5 (60 m length, 0.53  $\mu\text{m}$  ID, 5  $\mu\text{m}$  film thickness) and a porous layer open tubular (PLOT) column (50 m length, 0.53  $\mu\text{m}$  ID, 10  $\mu\text{m}$  film). Two columns were used in order to be able to measure speciated monoterpenes in addition to the non-methane hydrocarbons, as was done during the OP3 campaign (Jones et al., 2011). Due to problems experienced with one of the detectors during the observing period the system was simplified to a single PLOT column in order to achieve better quality data from a smaller group of compounds.

Sample flow was split between the two columns with approximately 50:50 flow split. The GC oven was heated from an initial temperature of 40  $^{\circ}\text{C}$  up to 200  $^{\circ}\text{C}$ , at a rate of 5  $^{\circ}\text{C min}^{-1}$ . The carrier flow rate was programmed at 20 ml/min for 15.5 minutes, 5 ml/min for 25 minutes and 25 ml/min until the end of the run. Hydrogen was used as the carrier gas, the hydrogen was produced using a Parker

Balston hydrogen generator (part number H2PD-150, hydrogen purity >99.99999%). The air supply for the GC detectors was supplied using a Jun-Air oil-free compressor (part no: OF302-25MQ2) and an additional dryer to achieve a dewpoint of -70C (CompAir dryer, A1LX desiccant dryer).

Calibration was achieved using a standard mixture of VOCs of known concentration; more details of this procedure are given in section 2.6. GCWerks software was used for analysis of chromatograms; this is described in section 2.5. In addition to running calibrations alongside ambient air samples, blank samples using nitrogen gas were run periodically. The blank runs enabled any interference with desired peaks to be detected and accounted for in subsequent analysis.

Key equipment was run on an uninterruptable power supply (APC smart UPS, part number: SMX3000HV) in an effort to maintain instrument usage through any short-term power losses.

## 2.5 Peak Identification

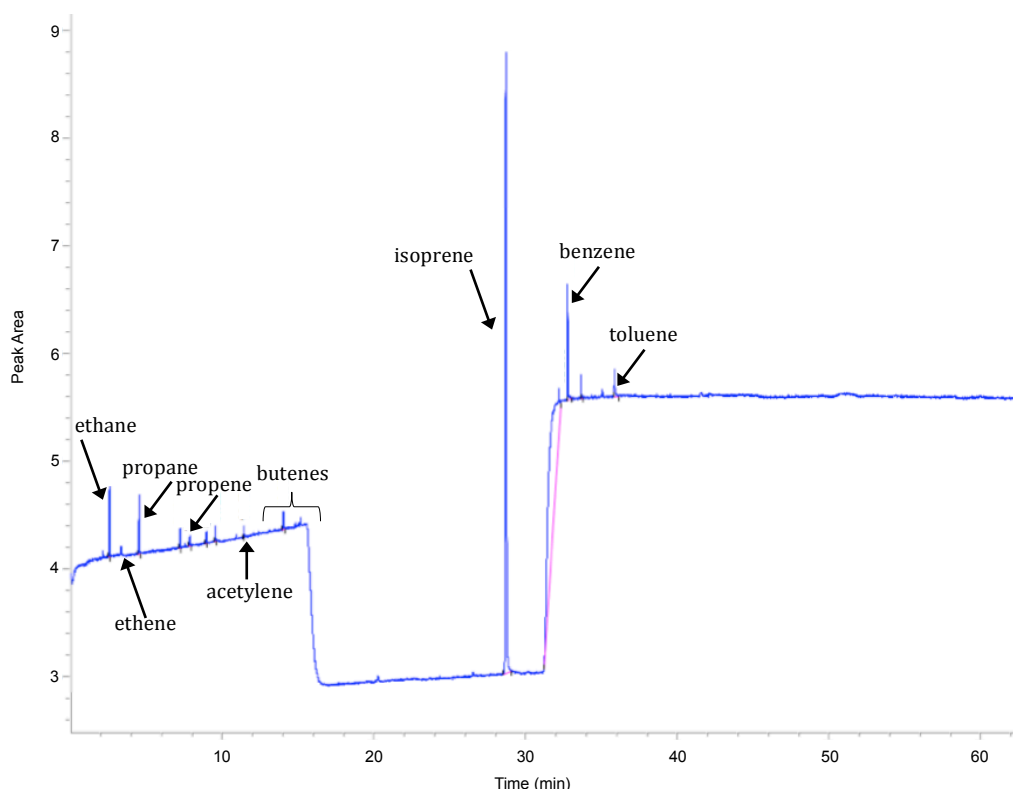


**Figure 2.7** Sample chromatogram showing a strong isoprene peak ~28 minutes. This shows that the peaks are well separated and resolved.

Chromatograms were analysed using GCWerks MD software. This software is used to analyse GC-MS data from the Advanced Global Atmospheric Gases Experiment (AGAGE network, <https://agage.mit.edu/>) and has been adapted for use with GC-FID data. This software processes peaks using an automated integration. There are several parameters that need to be set for integration. The mode, peak width and peak threshold. For this work the model was set to detect by curvature. A number of methods were used for data analysis on similar chromatograms and detection by curvature was found to be the best method for a sloping baseline, which is present in the chromatograms. The peak width and threshold determine what is defined as a peak, accounting for the noise in the baseline and the signal. The peak width also determines how any noise on the peak is smoothed before integration. These parameters were set over a range of values for different sections of the chromatogram, depending on the level of noise in the baseline and closeness of peaks. This allows for changes in the parameters to be made to account for instrument drift or changes in sensitivity, so that automatic integration can still be run for all chromatograms.

The retention times are identified using a certified standard containing all VOCs of interest. The peak widths are chosen to allow for variations in retention time, which are common with this technique so that the peak is still picked up by the software. For isoprene the peak width is set to be fairly large (~2 minutes) as there are no other peaks of interest within this window and isoprene is the dominant peak on most chromatograms. This means that should any other peaks appear within this window only the largest peak will be integrated and this will be the isoprene peak. For other areas of the chromatogram where multiple peaks appear over a short retention time the peak identification windows are set to be much narrower. This is the case for the butenes which appear at ~15 minutes so the peak ID windows for these VOCs are set at 10 secs. Identification of these peaks for integration is very sensitive to variability in the instrument. For this reason, although integration is automated the chromatograms are checked manually for any shift in retention times or changes in instrument sensitivity. If any changes are found the integration parameters will be adjusted to cover the identified time period. For each change identified a new set of parameters can be set and so the peaks can be automatically integrated successfully. This applies not only to changes in retention times but also to other integration parameters such as peak threshold and width that the software uses to identify which signals are identified as a peak.

## **2.6 Calibration and Instrument Stability checks**

For VOC calibration, a National Physical Laboratory (NPL) certified 30-component ozone precursor standard (serial no: D994124) was used. All VOCs reported in this work are calibrated using this standard. This calibration method is tied to the NPL calibration scale for VOCs (Grenfell et al., 2010). The GAW-VOC network also adopts this approach and this allows for direct comparisons between our measurements and those at other sites ([http://www.wmo.int/pages/prog/arep/gaw/gaw\\_home\\_en.html](http://www.wmo.int/pages/prog/arep/gaw/gaw_home_en.html)). A chromatogram of the NPL standard is shown in Figure 2.8.

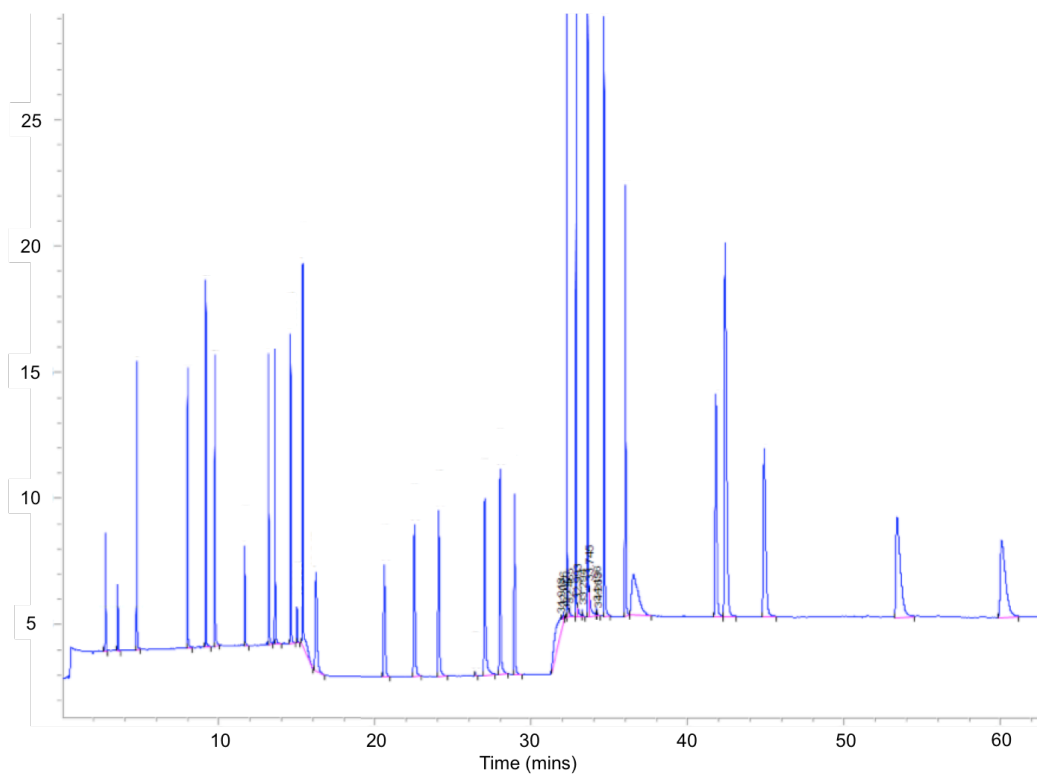


**Figure 2.8 Chromatogram showing the NPL standard run on the GC-FID.**

Working standard samples over a range of volumes were run to test whether the instrument had a linear response for isoprene concentration at different sample volumes. Figure 2.9 shows that the instrument has a strong linear response for isoprene mixing ratios, giving an  $R^2$  value of over 0.99. This means that regardless of sample volume the same calibration factors should be able to be used to quantify the VOC mixing ratios.

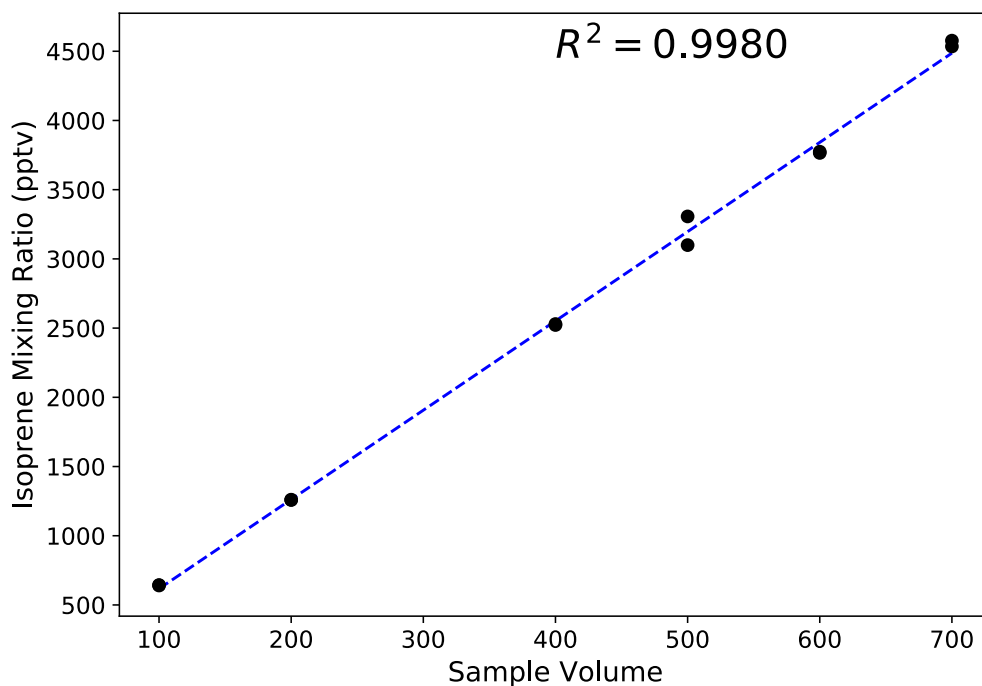


**Figure 2.9 Isoprene peak areas for the York working standard run at a range of sample volumes. This plots shows that over this range the instrument response for isoprene is linear.**

To calibrate the system, 500 ml samples of the standard were run in multiples of three. The mean of these values was taken as peak area/ppb and this factor used to convert peak areas obtained from the chromatograms into mixing ratios. Ongoing calibration of the instrument was achieved using a working standard back calibrated to the certified standard. The working standard was produced in York and contained only isoprene at ~3 ppb. This standard was run in banks of three or five samples during periods of ambient air sampling. Running the working standard allows for the stability of the instrument, in terms of peak area/ppb, to be assessed without excessive use of the expensive NPL standard.

Occasionally, as discussed above, the system was unable to achieve the desired 500 ml sample volume so calibrations during periods where the sample volume was less than the target of 500 ml followed a similar procedure to that outline above. However, during these periods the working standard was run at the same volume as the ambient air samples and these areas/ppb values used to define a scaling factor so that all data was treated as 500 ml samples. The effect of scaling

the peak area/ppb values is seen in Figure 2.10. This figure shows all working standard samples run scaled to 500 ml volumes.

The instrument response for the first three months varies by a maximum of 200 pptv. Within successive standards half of this variability is seen suggesting that these differences are due to instrument noise. For the later periods there is more variability. The data in February has been scaled from 150 ml to 500 ml, although the instrument response should be linear, as shown in Figure 2.9, these values are consistently lower than the initial period. The final part of the data in March generally gives higher values than the initial measurement period. Given that the flame ionization detectors are not expected to show a significant drift and the changes in instrument response will be accounted for in the error calculations only two calibration factors will be used to calculate the VOC mixing ratios, one for the 500 ml samples and one for the 150 ml samples.

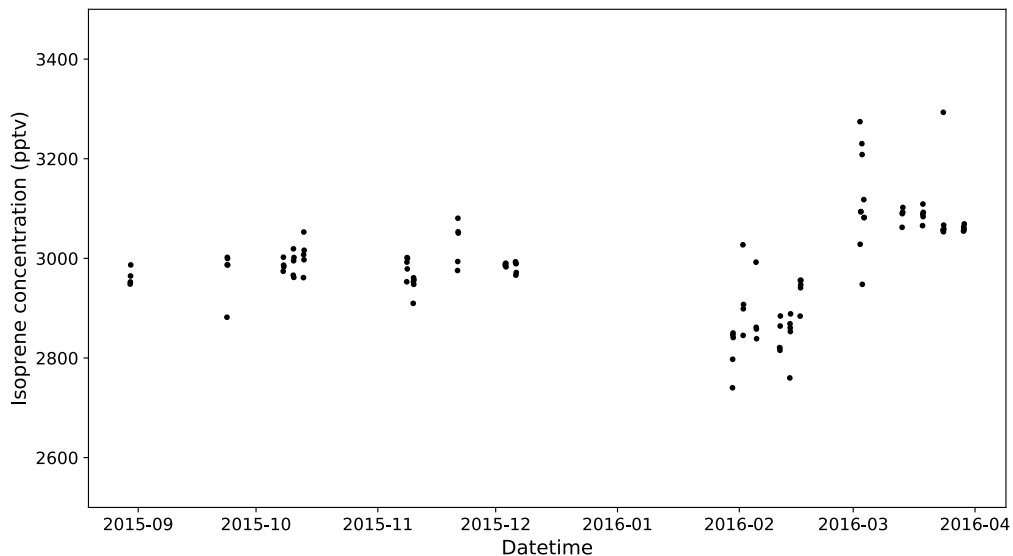


**Figure 2.10** Mixing ratios in ppb of the York working standard run across the measurement period. These mixing ratios are obtained using the peak areas/ppb values found from the National Physical Laboratory certified standard. The standards run throughout January and February were 150 ml sample volume but have been corrected to 500 ml.

Blank samples of N<sub>2</sub> gas and no flow blanks were run periodically in order to check for any possible contaminants that could affect measured VOC mixing ratios. Apart from when the instrument was initially set up or restarted after a long period (weeks or months) of being switched off the blank samples looked clean.

## 2.7 Limits of Detection

The limit of detection gives the minimum amount of a substance necessary for the sample to be differentiated from the baseline noise of the instrument and any quantity found in blank samples. These values were calculated using a method that follows the Aerosols, Clouds and Trace gases Research Infrastructure (ACTRIS) guidelines (ACTRIS, 2014). ACTRIS provide best practices for the measurement of VOCs and their subsequent analysis. A baseline signal was integrated over a time period similar to a typical peak width for the VOC species of interest. The integration was repeated ten times at a similar width by hand and the standard deviation of the integrated areas taken. This value was multiplied by three, with  $3\sigma$  representing the 99.7% confidence interval. This was then converted to a mixing ratio using a response factor calculated from the certified standard.

Table 2.1 shows limits of detection (LOD) calculated for the instrument used in this work. The numbers in brackets are for a similar instrument at the Cape Verde Atmospheric Observatory (Shalini Punjabi, personal communication May 2018) details of previous VOC measurements at the site can be found in the following paper (Read et al., 2009). Missing values are for species where a LOD was not previously calculated. For most species the LOD agree well with those from Cape Verde. Any differences could be due to differences in the detectors or columns or user error when integrating baseline noise.

**Table 2.1 Limits of detection for all VOC species measured in this work. The numbers in brackets represent the LOD values for the GC-FID at the Cape Verde Atmospheric Observatory.**

VOC species	Limit of Detection (pptv)
Ethane	4 (4)
Ethene	4 (4)
Propane	3 (6)
Propene	2 (1)
Iso-butane	2 (1)
N-butane	2 (1)
Acetylene	2 (1)
1-butene	4
Iso-pentane	2 (1)
Isoprene	2 (1)
N-heptane	1
Benzene	1 (1)
Toluene	1 (1)

The peak widths at the start of the run were generally greater than towards the end, hence the higher LOD for species such as ethane and ethene. The baseline was also noisier at the start of the run. 1-butene is much wider than surrounding peaks and so has a higher LOD than nearby peaks.

## 2.8 Error Analysis

Uncertainties for all measurements were calculated following ACTRIS VOC measurement guidelines (ACTRIS, 2014).

The overall uncertainty is determined from the root square sum of the precision and any systematic errors. Precision is calculated using the limits of detection for each species as listed above with a factor accounting for the stability of the working standard (equation 1).

$$\sigma_{prec} = \frac{1}{3}DL + C * \sigma_{working\ standard} \quad \text{Equation 10}$$

Where:

DL = limit of detection. This value is divided by three to give the standard deviation on the noise.

C = mixing ratio of the sample

$\sigma$  = standard deviation of the working standard over the measurement period.

Only isoprene is contained in the working standard and since the NPL standard was not run over the entire campaign period this value has been used for all species to account for any changes in sensitivity in the instrument.

The systematic uncertainty is calculated as follows (equation 10).

$$\sigma_{sys} = \frac{A_{sample} * V_{cal}}{A_{cal} * V_{sample}} * \delta_{cal} \quad \text{Equation 11}$$

Where:

$A_{sample}$  = peak area of sample

$A_{cal}$  = peak area of calibration

$V_{sample}$  = volume of sample

$V_{cal}$  = volume of calibration

$\delta_{cal}$  = quoted uncertainty for each VOC in the NPL certified standard

The precision and systematic uncertainties are then combined to produce the uncertainty for each measurement.

$$\sigma_{overall}^2 = \sigma_{prec}^2 + \sigma_{sys}^2 \quad \text{Equation 12}$$

For the purposes of data submission, any data at or below the limit of detection are reported as half the limit of detection, with an uncertainty of 100%. So for ethane any mixing ratios below 4 pptv are reported as  $2 \pm 2$  pptv.

## 2.9 Instrument Issues

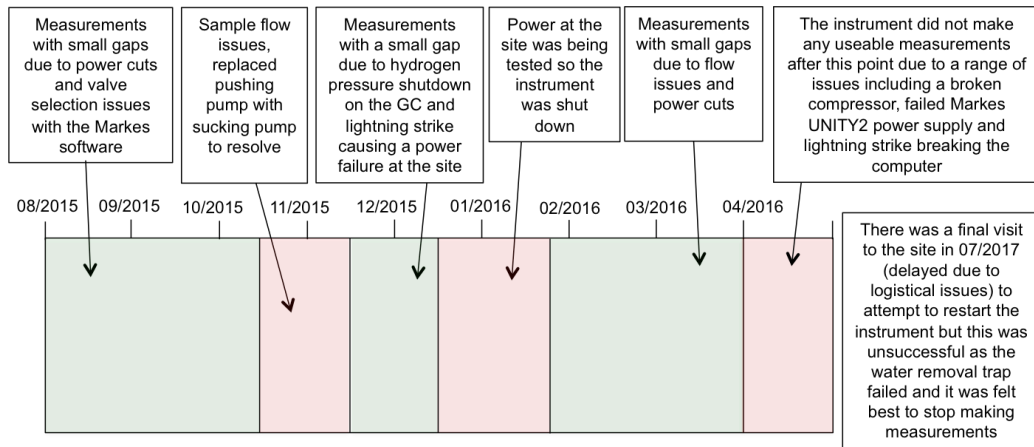


**Figure 2.11** Timeline showing periods with good measurement coverage (green boxes) and missing data periods (red boxes) for this work and a description of the instrument issues causing the gaps in data

The measurement site is surrounded by protected rainforest and is a two to three hour drive from the local office of our collaborators at the Malaysian Meteorology Department (MMD). The accessibility of the site caused logistical issues for maintenance and instrument repair. Staff only travelled to the site once a week, normally staying for one to two days at a time. Given the time difference with Malaysia (GMT+8), this made organising any work that needed to be done with the instrument difficult. In addition to this there were numerous issues with power at the site. There were several lightning strikes causing power outages and the power supply to the site was interrupted frequently. The lack of permanent personnel at the site meant that there were often long periods of time, ranging from several days to two or three weeks, without power before it was restored. These factors along with several instrument issues caused the gaps seen in the observational time series.

### 2.9.1 Power Issues

One of the major issues encountered was the lack of stability in the power at the site. Although a UPS system was installed for the most important equipment, remote connection to the instrument was lost on a regular basis. To be able to remotely access the instrument the computer at the site needed to be connected to

wi-fi. When power outages occurred wi-fi connection was lost and so the ability to remotely control the instrument was also lost. Moving the wireless router on to the UPS system helped improve the problem of loss of wi-fi connectivity. However, during the early part of the measurement period the UPS failed to charge from the mains due to the quality of the input power and despite being replaced with a new system the power supply to the UPS was not good enough to charge the batteries fully and so the UPS could not support the power needs of the instruments.

There was also a period where the power at the site was switched off for testing, this outage lasted for a few weeks from December 2015 into January 2016 and so no measurements were made during this period.

### **2.9.2 Flow Rate Variability**

A further problem was variability in the sample flow rate. This caused regular drops in flow and so a large proportion of samples were not at the expected sample volume (500 ml). Initially the software was set-up to sample by time (10 minutes at a flow rate of 50 ml min<sup>-1</sup>) this was changed to sample by volume (500 ml) to try and prevent drops in flow affecting the total sample volume. This change of method didn't solve this problem completely because the software was set to stop sampling if there is no flow for a set period of time. This was problematic because when there was a loss of power at the site the main sample pump turned off since it was not on the UPS, due to its high power requirements. When the pump was off the sample flow rate decreased and so many of the samples were still not reaching the expected volume.

Due to large variations in the sample flow rate, sampling was done by total volume not time from September 2015. These meant that the instrument would monitor the volume of sample acquired, regardless of flow rate and would continue to sample until the set sample volume was achieved. For several of the sampling periods the target flow rate of 50 ml min<sup>-1</sup> was not achieved. Replacement of the transfer line (at the beginning of March) between the GC and the Markes International UNITY-2 helped resolve this issue suggesting that there was probably a restriction in the sample line. This could have been due to some of the adsorbent material from the trap. The 500 ml sample volume was achieved for the majority of samples, although during January and February 2016 only a low

sample flow rate was achieved. During this period a target sample volume of 150 ml was used. The calibration process for these samples followed the same format as the 500 ml samples but with scaling the 150 ml sample volumes up to 500 ml and scaling the calibration factor. The instrument calibration procedure is given in section 2.4 of this chapter.

Ultimately the water removal unit failed to keep the glassware below the freezing point of water and this allowed water to pass through into the instrument. The instrument cannot run the chromatography properly with water in the samples, so the decision was made to finish making measurements and the instrument was packed up and shipped back to the UK in July 2017.

### **2.9.3 Chromatography Issues**

Specific issues were identified during measurements made in mid February and the very beginning of March. The top chromatogram in Figure 2.12 from late March, shows an expected chromatogram with no additional interference peaks. In the middle section, between 15 and 30 minutes, there is a large isoprene peak with a number of smaller peaks along the rest of the trace. The bottom chromatogram from early March shows a greater number of peaks, many of which have a large peak height and area. These peaks fall within the peak identification windows the software uses to identify which compound a peak is. This means that during these periods it is difficult to identify certain peaks and so this data has been removed from final analysis as individual VOCs could not be identified and quantified. The early March chromatograms were affected by a change in sampling height which is explained in the next section. The reason for the issues in mid-February are not clear but could be due to activity at the site such as cooking or vehicle emissions.



#### 2.9.4 Sampling Height

The height of the inlet for ambient air sampling was different during the OP3 campaign in 2008 compared with our work. For this work the inlet was run from the observation tower at ~30 m above ground level, whereas during OP3 the sampling height for the GC-FID was from ~5 m. As stated previously the reason for sampling from a greater height for our work was to sample from above the canopy top. During OP3 the inlet was co-located with the Fluorescence Assay by Gas Expansion (FAGE) inlet, which is at a fixed height, so that important supporting measurements could be made. To establish whether sampling height affected the observed mixing ratios the sample inlet was moved to a sampling height of ~2 m above ground level between 5<sup>th</sup> March 2016 – 7<sup>th</sup> March 2016. Isoprene observations over this time period showed no clear change in mixing ratio outside the range observed over the rest of the campaign period.

Data for other species over this time period was analysed after the field work period, this was because isoprene was the main focus of this work and so due to the lack of variation observed it was decided that sampling from 30 m would give a valid comparison to OP3 measurements. However, on analysis of hydrocarbon species other than isoprene an elevation in mixing ratios was seen for some compounds over the period of lower sampling height, most notably benzene, toluene, propane and ethene, see Figure 2.13. For this reason observations over this time period have been removed from the final analysis.

There is a strong possibility that OP3 measurements of certain compounds were affected by interferences due to the lower sampling height. This could be due to hydrocarbon emissions from the equipment at the site including a generator or due to canopy losses that remove certain species after ground level emissions. There were a number of different instruments and laboratory containers at the site during OP3 and so there may have been interferences from these. This may mean that the VOC measurements made during OP3 are not a true reflection of concentrations within the Danum Valley rainforest.

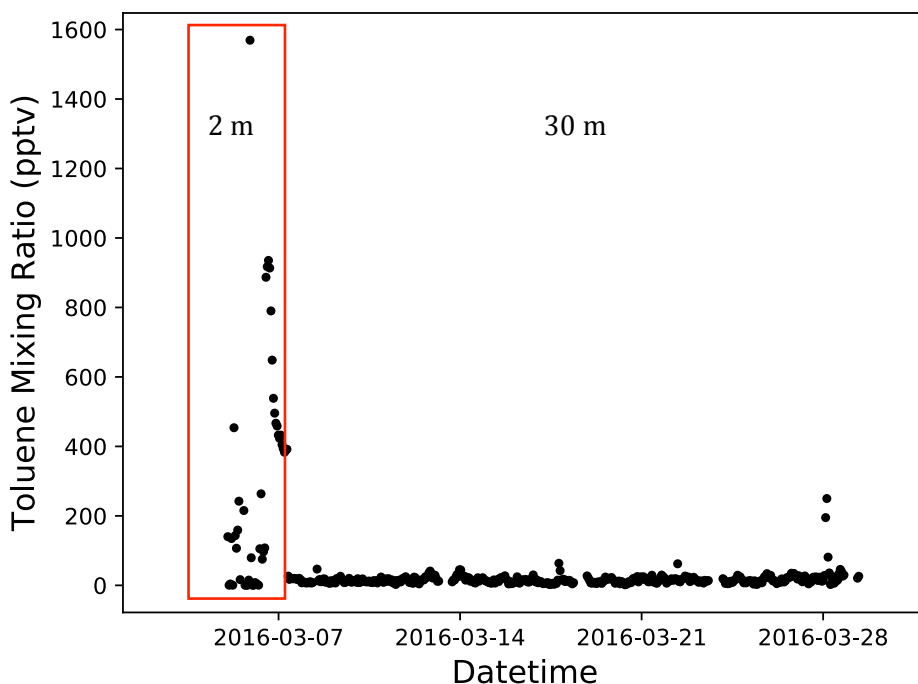


**Figure 2.13** Time series of toluene mixing ratios during March 2016. The early part of the series corresponds to measurements made with the sample inlet at lowered to ~2 m above ground level, a clear increase in mixing ratios is observed during this time

## 2.10 Conclusions

Gas chromatography with flame ionization detection under most circumstances provides a robust method of VOC analysis, requiring little manual input to produce automated, regular chromatograms. Over a period of 18 months this work collected and analysed around 1300 useable hourly air samples for thirteen VOCs. Measurements were made in five different months. Over the same period ~200 calibrations with the York working and NPL standards and ~200 blanks were run.

The problems encountered during this work were predominantly due to the logistics of working at a remote site. This affected the sampling and ability of the instrument to complete the analysis. The main issue was instability of power at the site; this caused multiple instrument parts to fail due to suspected surges in the power. The power problems were amplified by the UPS being unable to charge properly, this resulted in all equipment running straight from the mains. This meant equipment was not protected against variations in power and if power was lost all instrumentation shut down. Without UPS running any loss of power would

result in an instrument outage of between a few hours and several days depending on staff availability at the site to restore the power.

When the instrument was working the chromatography was clean and gave well defined peaks with minimal shifts in retention times. Looking at the working standard samples the instrument stability varied by about 10% over the whole measurement period.

Overall, working at this site proved challenging and future work at a remote site should consider how well the infrastructure at the proposed site is set up for this sort of project should issues arise . However, notwithstanding the numerous issues outlined above, a dataset has been collected for thirteen VOCs in a remote tropical rainforest. The measurements from this work have shown some interesting VOC behavior and effects on the rainforest site from local and longer range influences. The dataset is outlines in chapter 4, with a more detailed summary of biomass burning effects given in chapter5 and biogenic effects in chapter 6.



# Chapter 3

## 3 Model Description

### 3.1 Introduction

The GEOS-Chem model was used for all simulations in this work. GEOS-Chem is a three dimensional global chemistry transport model (<http://acmg.seas.harvard.edu/geos/>). The code is open source and is developed and supported by users, with code maintenance handled by the GEOS-Chem support team based at Harvard University.

The model is driven by meteorological reanalysis from the Goddard Earth Observing System (GEOS) of the NASA Data Assimilation Office (DAO). This reanalysis includes global time dependent fields such as the meteorological fields including temperature and wind speed and direction. In addition to the meteorological fields there are also variables that do not change with time, such as the fraction of different land types in each grid box. These fields are fed into the model and used to drive the emissions, chemistry and dynamics. There are several versions of the model code currently in use. Each version of the code contains updates, some of these are important for this work, particularly updates to the chemistry schemes and compatibility of different grids with new meteorological fields. Further details on the GEOS-Chem model can be found in a number of papers on model descriptions and developments (Bey et al., 2001, Wang et al., 2004, Philip et al., 2016, Zhang et al., 2015).

In this chapter a description for the model version used in this work is given at the start of section 3.5. Details on the important model inputs, such as meteorology are given after this. Key model components, including the biogenic emission algorithm and biomass burning inventories are explained in section 3.6.

## 3.2 User Selected Simulation Options

### 3.2.1 Horizontal Grid

The horizontal grid for each simulation determines the size of the grid boxes the area of interest is divided into. Simulations can be run on a global scale or over a smaller land area. There are a number of different horizontal grid resolutions that can be run with GEOS-Chem. The most coarse of these are the  $4^\circ \times 5^\circ$  and  $2^\circ \times 2.5^\circ$  global grids (all grid resolutions are given as degrees latitude x degrees longitude).

In addition to the global GEOS-Chem grids there is the option to run nested grids that cover a smaller area of the globe but at higher resolutions. The China/Asia grid covers an area around China and South East Asia, the exact area covered depends on which grid resolution is used (Chen et al., 2009). There are a number of different resolutions at which this grid can be run. The finest resolution grid is  $0.25^\circ \times 0.3125^\circ$  with coarser grids at  $0.5^\circ \times 0.625^\circ$  and  $0.5^\circ \times 0.666^\circ$  also available. The finer resolution grids generally cover a smaller area than more coarse nested grids.

Maps showing the surface isoprene mixing ratios for the  $4^\circ \times 5^\circ$  and  $0.5^\circ \times 0.625^\circ$  Asia nested grid simulations are shown in Figure 3.1 and Figure 3.2 respectively. The finer detail over Borneo, which is necessary for successful comparisons with the VOC observations from this work is clearly seen between the two plots.

The observational VOC dataset for this work was collected over a period from August 2015-March 2016. Therefore the model needed to run over these time periods to allow a comparison between the observations and simulated data. As well as needing this temporal coverage, the computational burden of the grid size needed to be considered. Finer resolution grids, despite their reduced size in the area covered, generally need a longer run time.

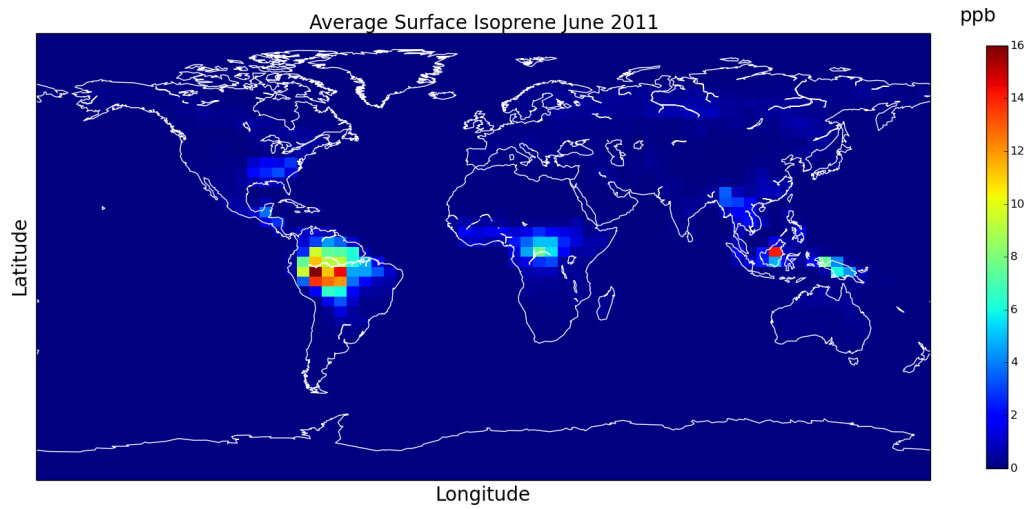


**Figure 3.1 Global  $4^\circ \times 5^\circ$  resolution plot of surface isoprene concentrations. The entire island of Borneo is covered by only two boxes**

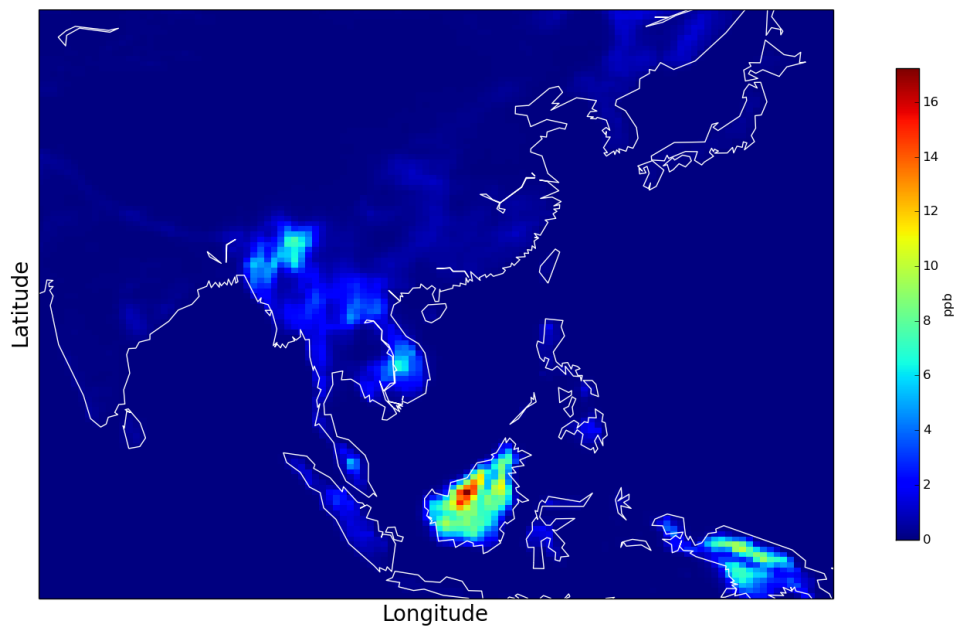


**Figure 3.2 Surface isoprene concentrations for the nested Asia grid at  $0.5^\circ \times 0.625^\circ$  resolution. There is much finer detail over Borneo than can be seen for the  $4^\circ \times 5^\circ$  global simulation**

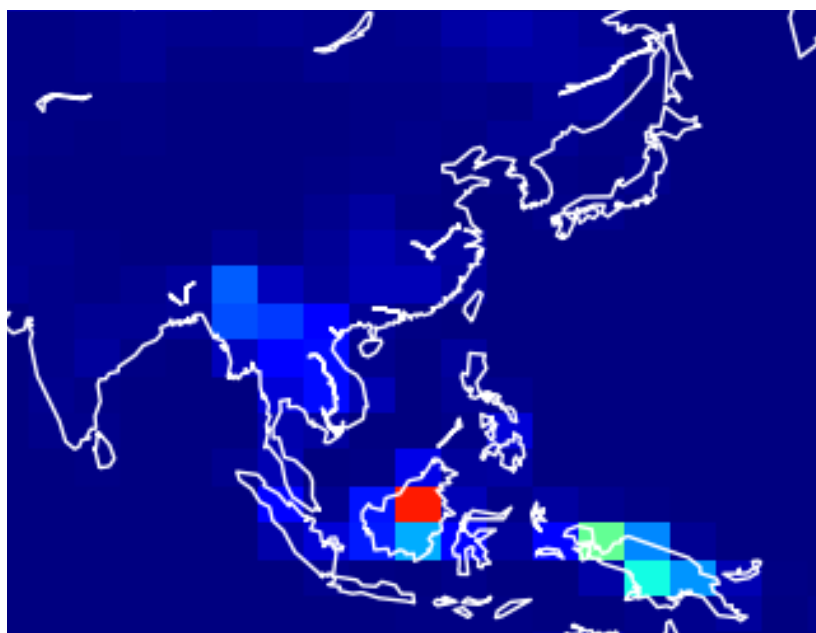


**Figure 3.3 Isoprene concentrations for the area covered by the Chinas grid at 4x5 resolution, on the same colour scale as Figure 3.1**

Figure 3.3 shows the resolution achieved over the China grid when using the 4° x 5°. For this work the model will be compared with measurements made at a single site situated in the rainforest. Comparison with the 4° x 5° grid would not be appropriate. The boxes are so large that the measurement site would be compared to a box containing coastal areas and the sea.

### **3.3 Meteorological Data**

There are two main options for running the China nested grid, 0.5° x 0.666° resolution with GEOS-FP meteorology and 0.5° x 0.625° with MERRA-2 meteorology (Gelaro et al., 2017, Todling, 2018).

The native resolution of the MERRA-2 fields is 0.5° x 0.625° and so no regridding of these files is necessary. The main advantage for this work of the MERRA-2 fields is that files are available from 1979 onwards and so there are files available to run simulations covering the dates of the Oxidant and Particle Photochemical Processes (OP3) campaign that made measurements at the same site as this work. This allows for a comparison of the model over the two time periods to investigate whether the model simulates any changes between these two time periods well. In

addition to this there are a large number of supporting measurements from the OP3 campaign, comparing these with simulated values will allow for a better understanding of any discrepancies with the model. This could lead to model problems or a lack of understanding of the low-NO<sub>x</sub> chemistry in this environment being identified.

From the available grid and meteorology options it was decided that the model would be run using the China nested grid, at a resolution of 0.5° x 0.625° using MERRA-2 meteorological fields. The higher resolution grid does not cover the area where measurements were made and the 0.5° x 0.666° grid is not compatible with meteorological fields that cover all measurement periods. The nested grid was decided on over a global simulation as a grid box more specific to the measurement can be used with a grid box size of ~50 x 60 km compared with a grid box of ~200 x 250 km for the global model. The global model grid box that contains the measurement site is likely to be influenced by coastal or possibly effects from the surrounding sea given that the site is located relatively near to the sea when the size of the grid box is accounted for. The China grid covers an area from 60° E-150° E and 11° S-55° N.

### **3.4 Vertical Grid**

In addition to a number of options for horizontal grid resolutions, there are two options for vertical grids in GEOS-Chem. There is the standard 72 layer or reduced 47 layer vertical grid. For this work the reduced 47 layer grid was used, which has fewer grid boxes in the stratosphere. This saves computational resources and as this work focuses on the surface layer it is an appropriate choice. The grid levels are divided into hybrid sigma pressures, where sigma is normalized by the pressure at the surface. At the surface the levels are pure sigma, moving up to pure pressure for the top levels in the atmosphere. Therefore this method removes topography effects that could cause physical disruptions and problems with exchange to the stratosphere in the higher levels of the atmosphere. The grid extends from a pressure of 1013.250 hPa at the surface up to 0.010 hPa.

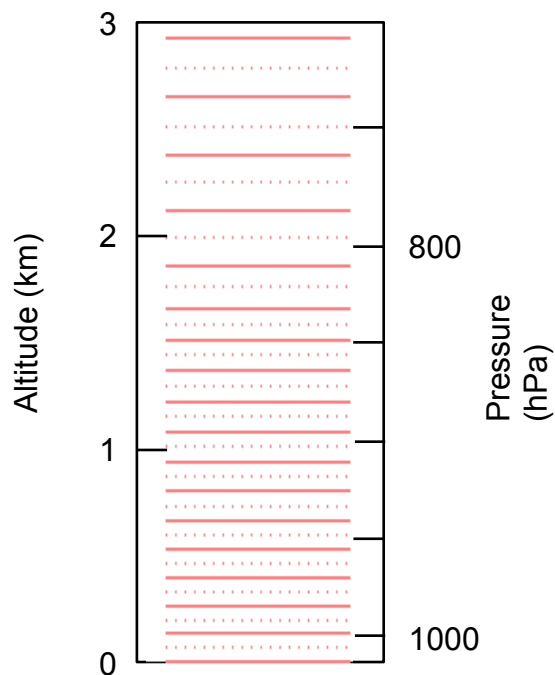


Figure 3.4 Vertical levels in GEOS-Chem with MERRA2 meteorology up to 3 km. Adapted from the GEOS-Chem wiki page [http://wiki.seas.harvard.edu/geos-chem/index.php/GEOS-Chem\\_vertical\\_grids#Vertical\\_grids\\_for\\_GEOS-5.2C\\_GEOS-FP.2C\\_MERRA.2C\\_and\\_MERRA-2](http://wiki.seas.harvard.edu/geos-chem/index.php/GEOS-Chem_vertical_grids#Vertical_grids_for_GEOS-5.2C_GEOS-FP.2C_MERRA.2C_and_MERRA-2)

## 3.5 Model Version

### 3.5.1 Version 11-02d

Version 11-02d of the GEOS-Chem model was used for most of this work due to an update in the code that enabled the China grid to run with MERRA-2 meteorology fields. This allowed the model to run over the entire observational period for this work and previous campaigns at the same site. Another advantage of using this model version was the additional advected tracers available. Benzene and toluene were both measured as part of this work and their chemistry was added in v11-02. Both of these species are emitted by biomass burning and so running v11-02 allowed for comparison of the biomass burning observations with additional model tracers. This allows for better validation of the model success at simulating biomass burning.

## **3.6 Model Inputs and Components**

Within the GEOS-Chem code there are several key components that perform tasks important to this work. The components that are most important for isoprene and other hydrocarbons include biogenic emissions and the chemistry schemes. These components are discussed in further detail below.

### **3.6.1 Restart Files**

GEOS-Chem simulations require a restart file input at the start of each simulation. This file contains initial conditions for all species in mixing ratio by volume. Standard restart files are available for each simulation type that can be used to begin a simulation. A new restart file can be generated during a model run, which will save the mixing ratios for all species as they are at the end of the requested period of the simulation. These new files with conditions suitable for the desired simulation can then be read in instead of the standard file. This allows for a more realistic atmosphere to be achieved by running a spin up period before the time of interest. This means the required simulations start with mixing ratios more appropriate for the simulation type than the standard restart file.

### **3.6.2 Boundary Conditions**

Running a GEOS-Chem nested grid requires boundary condition input files to be generated. These files contain the initial conditions to be fed into the nested model at the edges of the nested grid. The boundary conditions are output from a global simulation over the same time period as the nested grid will run over. For this work the boundary conditions used were at 4° x 5° resolution. The global simulation should use the same conditions that will be used for the nested simulation. For this reason MERRA-2 meteorological fields were used for the global simulation. The global simulations are run for a longer period of time (normally a year) before the period of interest to have a more realistic composition of the atmosphere. The box containing the measurement site is not near the edge of the grid so there should be minimal effects from boundary conditions.

### **3.6.3 Emissions in GEOS-Chem**

Versions 10 and onwards of GEOS-Chem include the Harvard-NASA Emissions Component (HEMCO) module (Keller et al., 2014). HEMCO is used to compute emissions in the model. The advantage of this module is that emissions can be calculated on a user-defined grid, thus saving the need for manual regridding of emissions for use on different resolution grids. The HEMCO module computes anthropogenic emissions including from ships and aircraft, lightning, biogenic and biomass burning emissions. The biogenic emissions are calculated using the Model of Emissions of Gases and Aerosols from Nature (MEGAN) emissions module. Biomass burning emissions are taken from the GFAS inventory. These are described further below.

#### ***3.6.3.1 MEGAN Biogenic Emissions***

For the emission of biogenic species including isoprene, propene and monoterpenes the MEGAN algorithm is used (Guenther et al., 2012). The emissions code is complex, with several factors being considered in the calculation of the final emission rate. To calculate the emissions for each species the base annual emission factor is scaled using an activity factors that account for the effects of radiation, temperature, leaf area index, soil moisture and leaf age. A normalization factor is also applied to give activity factors equal to one under standard conditions (303 K and 1000  $\mu\text{mol m}^{-2} \text{s}^{-1}$  of photosynthetically active radiation). The annual emission factors are defined using either pre-defined emission factor maps (isoprene, limonene) or using CLM4 plant functional type (PFT) distributions combined with specific emission factors for each PFT (ethene, formic acid). CLM4 is the Community Land Model (Oleson et al., 2010) and PFTs define the type of land cover, such as crops or broadleaf evergreen trees.

If the annual emission factor is read in not calculated then the code regrids the base emission files from their native  $1^\circ \times 1^\circ$  resolution and these values are then scaled to the meteorological conditions in each grid box at each time step, as outlined above. To scale the annual emission factors to the variables above, the code considers a range of meteorological parameters. These parameters account for values from previous days in addition to instantaneous values as these both affect future biogenic emissions (Sharkey et al., 1999). Average temperature values

are included from the previous 15 days and direct and diffuse radiation for the previous 10 days. The light and temperature dependent species algorithm is based upon electron transport and enzymatic activity respectively (Guenther et al., 1991). The calculated emissions are then fed into the model and chemistry and transport processed take effect.

The important species emitted through MEGAN for this work are isoprene and propene. Both of these species are included in the observational dataset and are discussed in more detail in chapter six. Isoprene emissions are calculated from a given emission factor. Propene emissions are calculated from the PFT map.

### ***3.6.3.2 Biomass Burning Emissions***

Biomass burning emissions in GEOS-Chem are important for this work as the non-negative matrix factorization analysis (discussed in chapter four) identified a component of the observational dataset that has been influenced by biomass burning.

The standard biomass burning emission inventory included in GEOS-Chem, the (GFED) Global Fire Emissions Database, is not suitable for use in this work (Field et al., 2016). GFED4, the most recent database version only has files available up to 2014. The 2015 biomass burning season was known to be one of the worst on record and so for understanding the effects of biomass burning on the measurement site during this period it is important that up to date emission values are used. It is also a good test of the model success in simulating biomass burning in South East Asia if the magnitude of this extreme burning season is well recreated.

### ***3.6.3.3 GFAS Emission Inventory***

The Global Fire Assimilation System (GFAS) uses satellite observations from the Moderate Resolution Imaging Spectroradiometer (MODIS) to calculate biomass burning emissions (Kaiser et al., 2009). Observations are made at wavelengths of 3.9 and 11  $\mu\text{m}$ . The satellite Fire Radiative Power (FRP) observations can be used to derive combustion rates for the burning. The conversion factor necessary to obtain combustion rates from FRP observations varies by land type and therefore

fuel type. Emission factors for each land type from a previous study (Andreae and Merlet, 2001) are multiplied by the calculated combustion rates to give the final emission rates. For species where emission factors have not been established scaling to other species such as CO is used.

Although not a standard biomass burning inventory in GEOS-Chem, the GFAS inventory has input files available over the measurement period of this work. The HEMCO emission component allowed for the GFAS biomass burning emission inventory to be easily added to GEOS-Chem. The input files were obtained courtesy of the MACC-II project (Inness et al., 2013).

The GFAS emissions input files are available at  $0.1^\circ \times 0.1^\circ$  resolution. The files contain fluxes in  $\text{kg m}^{-2} \text{s}^{-1}$  for all emitted species. There is a file for each month containing daily emission data. These emissions files are input to the model through the HEMCO emissions component. Species emitted from this inventory that are important for comparison with observations are: ethane, propane, benzene and toluene.

### 3.6.4 Chemistry

For the simulations in this work the GEOS-Chem 'tropchem' mechanism was used. This mechanism covers the surface up to the tropopause and includes  $\text{NO}_x$ ,  $\text{O}_x$ , hydrocarbon, aerosols species. V11-02d of the model contains 145 advected species. Advected species are those that are transported by the model, through winds or convective mass fluxes.

Reaction rates are calculated from experimentally determined rate constants, photolysis cross sections, quantum yields and actinic fluxes. Photolysis rates are calculated using the FAST-JX v6.2 photolysis mechanism (Wild et al., 2000). Kinetic reaction rates are calculated using JPL defined rate constants. The Kinetic PreProcessor (KPP) software is used to solve the differential equations required for the chemistry scheme in the versions of GEOS-Chem used in this work (Damian et al., 2002).

The most abundant of the measured hydrocarbons was isoprene. GEOS-Chem uses the Caltech isoprene scheme in v11-01 (Paulot et al., 2009b, Paulot et al., 2009a).

The isoprene reactions in GEOS-Chem depend on whether the environment is a high or low-NO<sub>x</sub> regime. For Borneo the relevant chemistry scheme is the low-NO<sub>x</sub> regime. In v11-02 there were several updates to the isoprene scheme, mainly affecting secondary organic aerosol formation (Marais et al., 2016). More information about isoprene chemistry is given in chapter 1.

### **3.7 Conclusions**

GEOS-Chem has proved a useful tool to help in the understanding of VOC observations made as part of this work. Some of the recent developments in the model have improved the ease with which the model can be edited to specific tasks. HEMCO is a good example of this development. Having a separate emissions module means that turning off or adding emission inventories was a simple task and this allowed detailed comparisons for the biomass burning and biogenic components of this work. These comparisons are given in chapters five and six respectively.

The GFAS emission inventory gave a good comparison with the observations for ethane and propane, suggesting that this inventory has successfully simulated the strong 2015 biomass burning season for some species. These comparisons are shown in chapter five. For other species, specifically propene the simulation was less successful with a large overestimation in mixing ratios. Propene has a significant biogenic component and the overestimation of these emissions likely contributed to the high model bias. This is discussed in detail in chapter six.



# Chapter 4

## 4 Data Overview and NMF analysis

### 4.1 Introduction

Volatile organic compounds (VOCs) are a group of organic atmospheric trace gases including light weight alkanes (ethane, propane) to heavier monoterpene species ( $\alpha$ -pinene, limonene) (Kesselmeier and Staudt, 1999). This family of compounds has biogenic (originating from vegetation), anthropogenic (originating from human activity), biomass burning (combustion of vegetation whether natural or human initiated) sources and other sources. Isoprene ( $C_5H_8$ ) is the VOC with the highest globally averaged emissions (Bracho-Nunez et al., 2013). It is emitted predominantly by the terrestrial biosphere, particularly tropical forests (Arneeth et al., 2011) with total emissions estimated to be around  $500 \pm 100$  Tg carbon per year. Compared with this anthropogenic sources are smaller and occur mainly from vehicle exhausts, solvent use, industrial activities and combustion processes (Chang et al., 2014, Theloke and Friedrich, 2007). At some locations biomass burning can have a strong influence over VOC emissions (Engling, 2014).

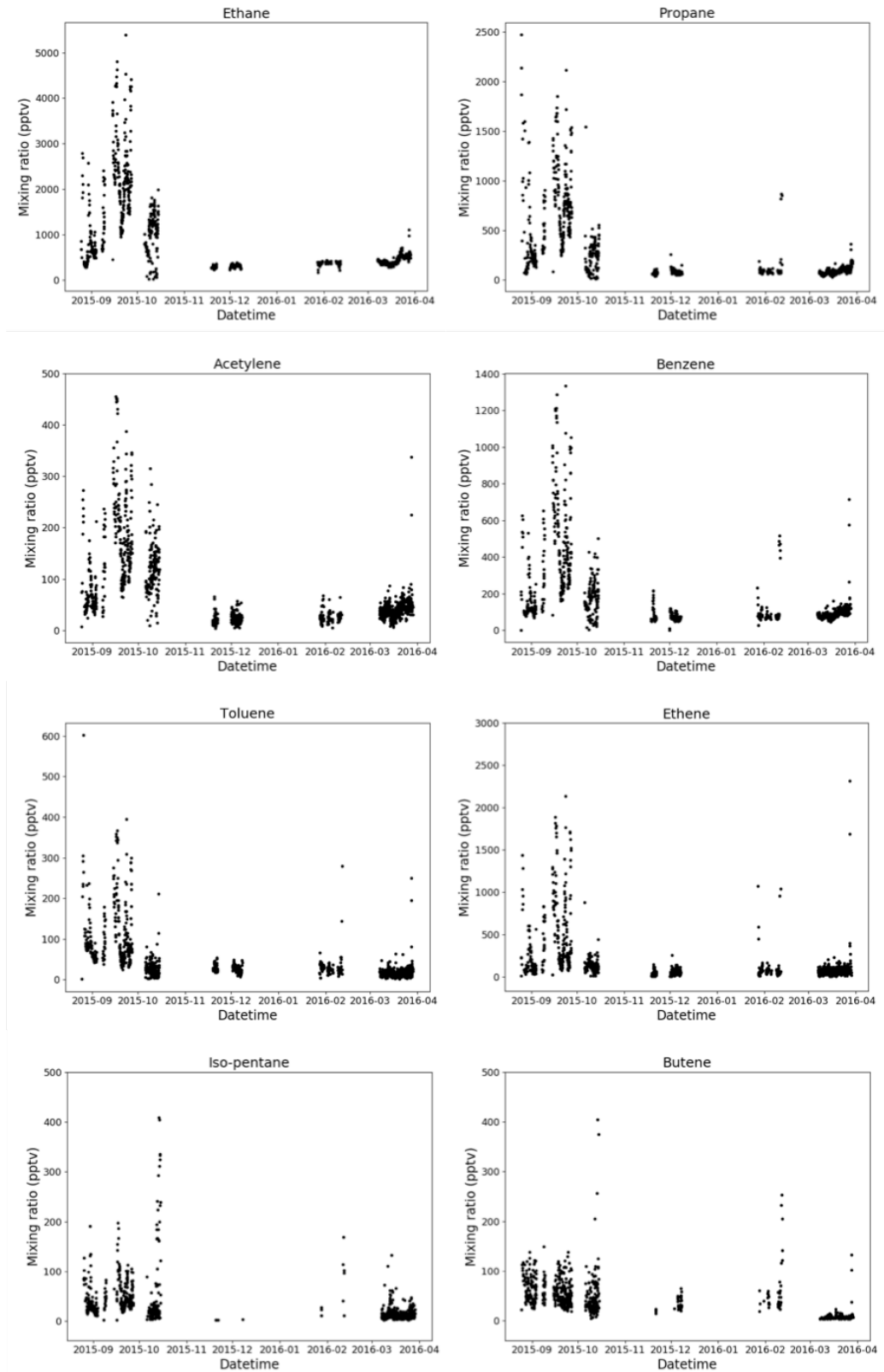
Some VOCs, predominantly aromatics, have adverse direct health effects (Duarte-Davidson et al., 2001, Bravo et al., 2002) but most interest in VOCs results from their secondary chemistry. The oxidation of VOCs in the presence of  $NO_x$  leads to the production of ozone, an important air pollutant and climate gas (Ebi and McGregor, 2008, Squire et al., 2014). However, in low  $NO_x$  environments VOCs can lead to enhanced ozone destruction. The oxidation of VOCs helps to determine the concentration of the OH radical and therefore the concentration of climate gases such as methane. Finally, VOCs can influence formation of secondary organic aerosol (SOA), (Kroll et al., 2006) which affects radiative forcing, climate and human health (Rich and Orimoloye, 2016, Jacobson, 2001).

For this thesis, a total of thirteen VOCs were measured and analysed between August 2015 and March 2016 in a tropical rainforest in Malaysian Borneo. Chapter 2 describes the measurement site and instrumentation used. In this chapter the observations are described and a statistical analysis performed to split the time

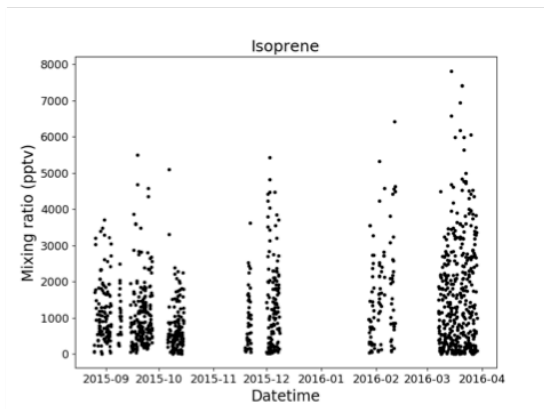
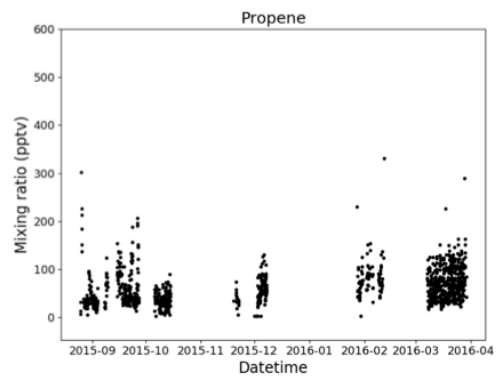
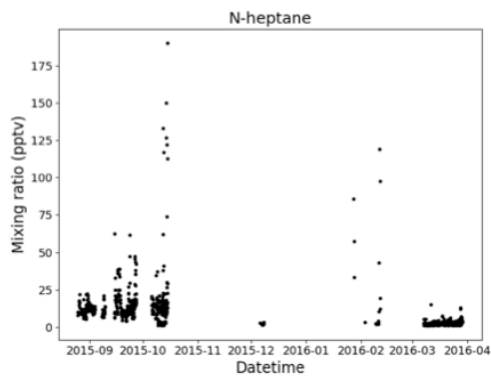
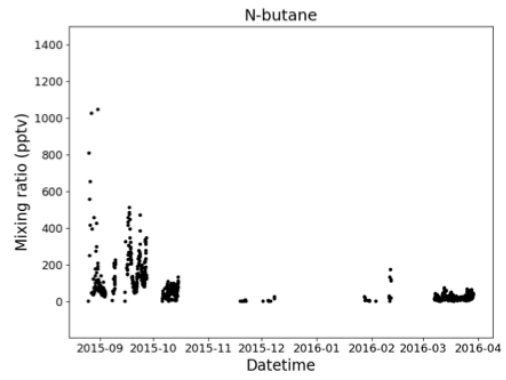
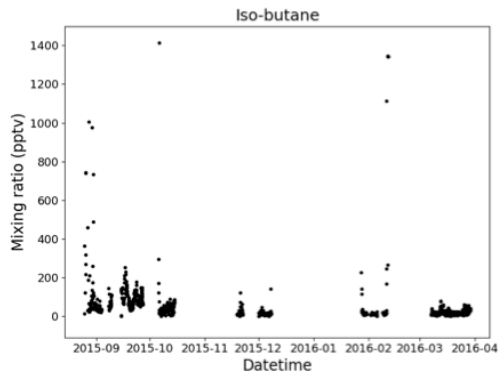
series into a number of periods. A comparison between the output of the GEOS-Chem model and the observations is then performed. Subsequent chapters analyse two of the periods in more detail.

## **4.2 Time series of observational data**

The time series for all measured species is shown in Figure 4.1. The same data is shown on a logarithmic scale in Figure 4.2. The measurements were made between August 2015 and March 2016, as discussed in chapter 2, there are several long time periods with no or limited data. The limit of detection values for each VOC are given in section 2.7 of chapter 2. Details of the error analysis is given in section 2.8 of chapter 2. Error values are approximately 10-15% of the measured values, with errors towards the higher end of the range for lower mixing ratios.



**Figure 4.1** Time series of VOCs species measured at the Bukit Atur observatory, Malaysian Borneo from August 2015 to March 2016. Gaps in the time series reflect site power failures and a number of instrument issues, which are described in chapter 2. Continued on next page.



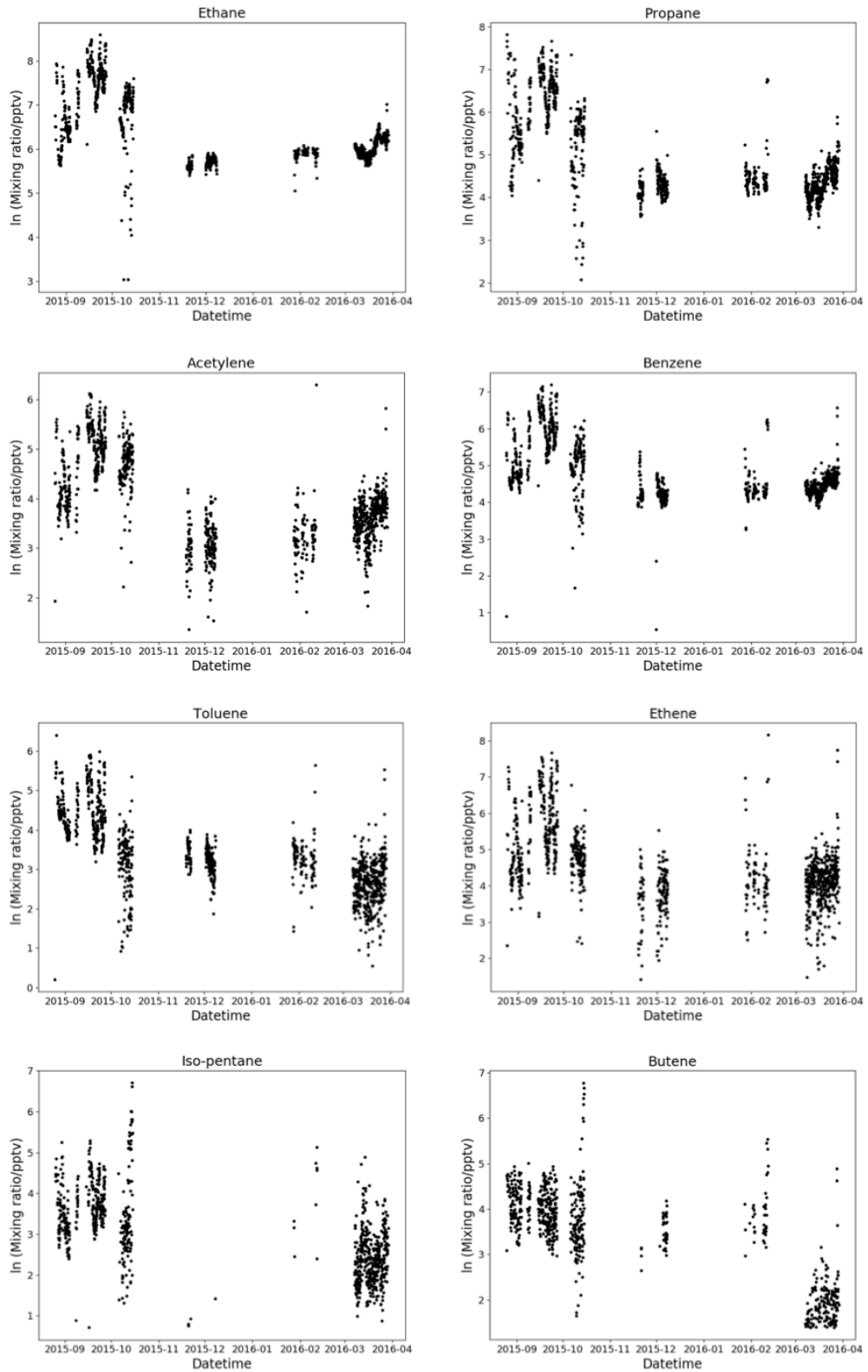
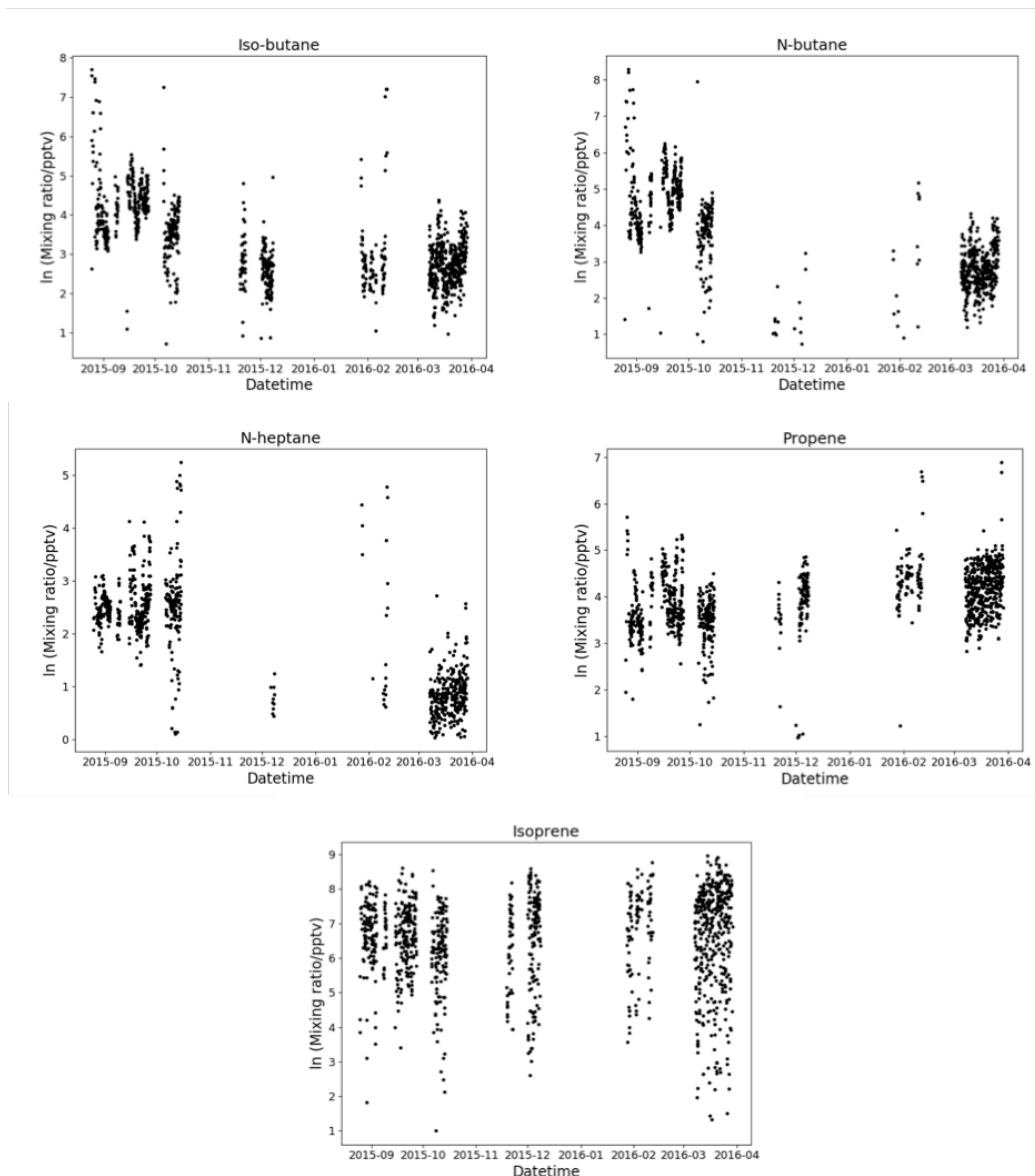


Figure 4.2 Same as Figure 4.1 but shown on a logarithmic scale. Continued on next page.



### 4.3 General Description of the Time Series

Over the time period shown, concentrations of VOCs vary considerably. In general the highest concentrations are at the start of the measurements (August – October 2015) with much lower concentrations over the rest of the measurement period. The exceptions to these trends are isoprene and propene, which are known to have predominately biogenic sources (Owen et al., 1997, He et al., 2000, Rhew, 2017, Goldstein et al., 1996), and show much less change over these timescales.

The dominant daytime VOC by concentration during the initial measurement period are ethane and isoprene. Isoprene is the dominant species for most of this

period but there are spikes with particularly high ethane mixing ratios, here ethane is the dominant species. For most of the rest of the dataset isoprene is the dominant VOC. This is in agreement with previous studies at tropical forest sites, including the Amazon (Saxton et al., 2007, Kesselmeier et al., 2000).

#### **4.4 Wider Dataset**

There has been one previous campaign at the same site where the current measurements were made. The OP3 campaign took place over two periods in 2008, April/May and June/July. During this campaign there were two instruments making measurements of VOCs at the Bukit Atur site. A GC-FID similar to the instrument used in this work and a proton transfer reaction mass spectrometry (PTR-MS); both made measurements during the campaign (Jones et al., 2011, Langford et al., 2010) A comparison between the current dataset and the PTR-MS measurements was only possible for isoprene as the other species, such as acetone, total monoterpenes and methanol measured in 2008 were not measured in this work. There is a greater overlap in species measured with the GC-FID measurements. A detailed comparison between biogenic species is found in chapter 6. The species measured in both campaigns were isoprene, ethane, propane, iso-pentane, iso-butane and n-butane. For these species the data collected from our work and the OP3 project are shown as a function of day of the year (Figure 4.3). The two OP3 isoprene datasets correspond to measurements made using the York gas chromatography with flame ionisation (GC-FID) and the Lancaster proton transfer reaction mass spectrometry (PTR-MS) instruments.

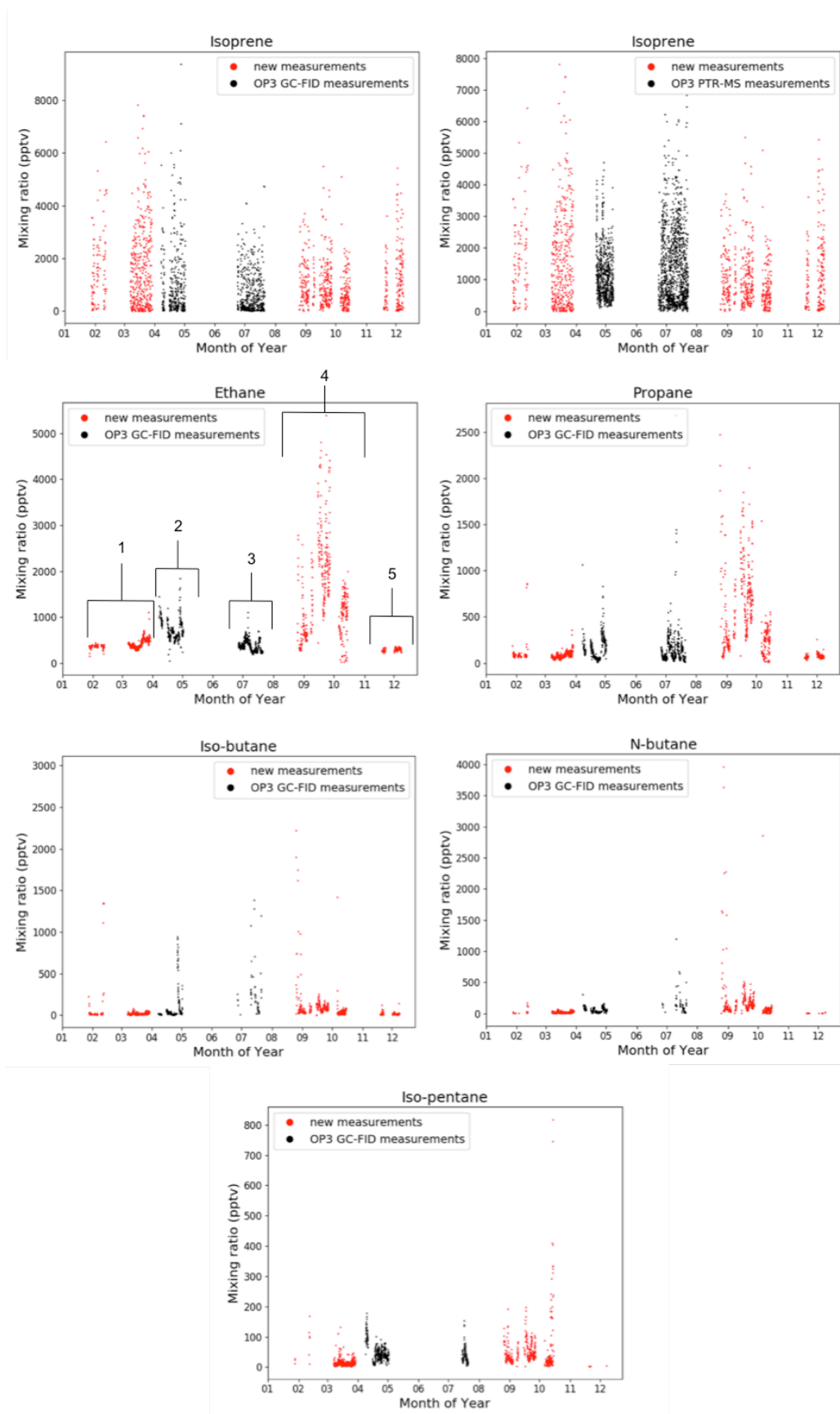
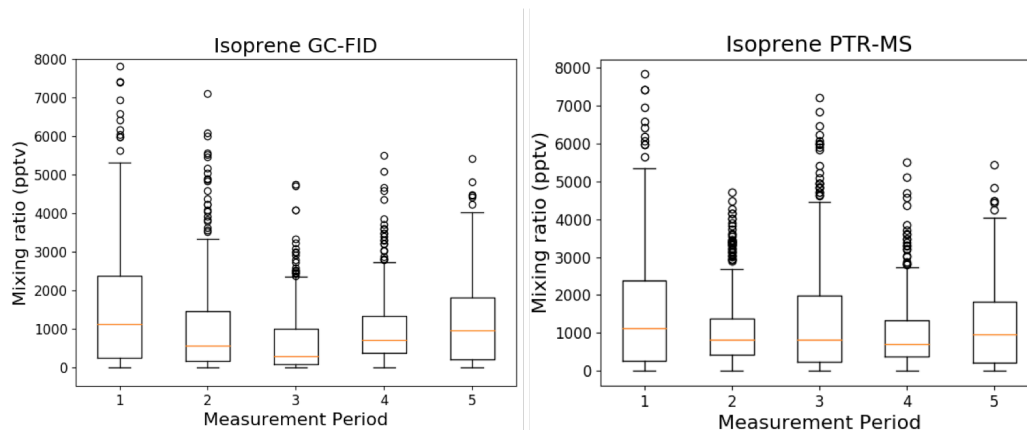


Figure 4.3 Measurements from this work (new measurements, red dots) and the OP3 project (black dots) presented by month. The year in which the measurements were made has been excluded for comparison purposes. All measurements were made using gas chromatography, with the exception of the second isoprene plot, which is PTR-MS data from the OP3 campaign.

#### 4.4.1 Isoprene



**Figure 4.4** Box and whisker plots for isoprene measured in this work and the OP3 campaign separated by the periods indicated in the ethane plot in Figure 4.3. Data from the two OP3 periods is within the black rectangles. The circles represent outliers. These are values that lie outside the nearest quartile  $\pm 1.5 * IQR$ . Periods 1, 4 and 5 include data from the BALI project, periods 2 and 3 are from the OP3 project.

**Table 4.1** Mean, median and inter-quartile range values for the periods identified in figure 4.3. The number in brackets identifies the measurement period, OP3 and BALI identify the project. The two OP3 instruments (GC and PTR-MS) are shown separately

	BALI GC (1)	OP3 GC (2)	OP3 GC (3)	BALI GC (4)	BALI GC (5)
<b>Mean</b>	1518	1077	648	980	1206
<b>Median</b>	1125	564	291	708	957
<b>IQR</b>	256-2383	172-1464	91-999	391-1338	211-1816

	OP3 PTR- MS (2)	OP3 PTR- MS (3)
<b>Mean</b>	1009	1219
<b>Median</b>	816	817
<b>IQR</b>	422-1393	249-1989

There is some variability between the measurement periods for the mean isoprene concentrations. The BALI period 1 mean is higher than the other periods by  $\sim 50\%$  and the OP3 GC (3) mean is around half of that for the other periods. However, looking at the other BALI periods, OP3 GC (2) and the two PTR-MS periods the variation in the mean is around 10%. Given there is a  $\sim 10\%$  error on the measurements it seems that isoprene concentrations at the site are fairly consistent. There is more variability in the median values between the datasets

and this is reflected in the upper range of the IQR being higher for some periods such as PTR-MS (3).

It should be noted that the PTR-MS measurements were made at 75 m above ground level (Langford et al., 2010) and the OP3 GC measurements were made at a sampling height of 5m (Jones et al., 2011). Measurements from our work were made at ~30 m above ground level. A sampling height of 75m is above the entire surrounding canopy, 30 m is above most of the canopy excluding some trees near the research tower and sampling at 5m is well within the canopy. The OP3 GC measurements were made at a sampling height of ~5 m above ground level.

(Jones et al., 2011) suggested that differences between the two instruments during the second OP3 measurement period were caused by localised ground level pollution events, leading to increased OH concentrations. Therefore, differences in the local chemistry, emissions and mixing within the column may well explain some of the differences seen between the measurements. (Nölscher et al., 2016) found significant differences between the concentrations of isoprene and other species at ground level and at heights of 40-80 m above ground measured from a tall tower in the Amazonian rain forest.

The range of isoprene mixing ratios observed in this work (~0.1-8 ppbv) gave a maximum value lower than the Kesselmeier study from the Amazon (4-10 ppbv) but higher than a previous study in a secondary forest in Benin (~0.01-3 ppbv).

Previous studies in the Amazon have shown isoprene to have a strong seasonal cycle, dependent on factors including biomass burning, meteorological conditions and new leaf growth (Kesselmeier et al., 2002, Barkley et al., 2008, Barkley et al., 2009). The (Kesselmeier et al., 2002) study showed that during the dry season mean isoprene concentrations increased by a factor of around four, from 4 ppb to almost 16 ppb. For the site in Borneo the mean isoprene values, across our work and the two OP3 datasets, vary by a factor of 1.5 if the low OP3 GC-FID period is excluded. It is difficult to say from this whether isoprene exhibits any seasonal behaviour and it seems that if there is any seasonal variability it is not as marked as in the Amazon. Previous studies at the site in Borneo have not reported any seasonal effects on the mixing ratio, although observations were only made for a total of two months (Langford et al., 2010, Jones et al., 2011). There is no evidence

for an increase in isoprene during the period (August – October) of enhanced concentrations for other species, with a mean of 980 ppt compared with 1518 ppt and 1206 ppt for the other BALI periods. If anything, isoprene concentrations were lower during this period. This work concludes that unlike the Amazon, isoprene concentrations do not show a strong seasonal cycle in the Danum Valley Rainforest.

#### 4.4.2 Small Alkanes

The major sources of atmospheric ethane are anthropogenic in origin. Fossil fuels, including natural gas production and transport are the main source with contributions from biofuel use and biomass burning (Hausmann et al., 2016). Sources of propane are similar to ethane, with fossil fuel production and biomass burning as major sources (Zhou et al., 2017). Natural gas leakage is also a source of propane (Chen et al., 2001).

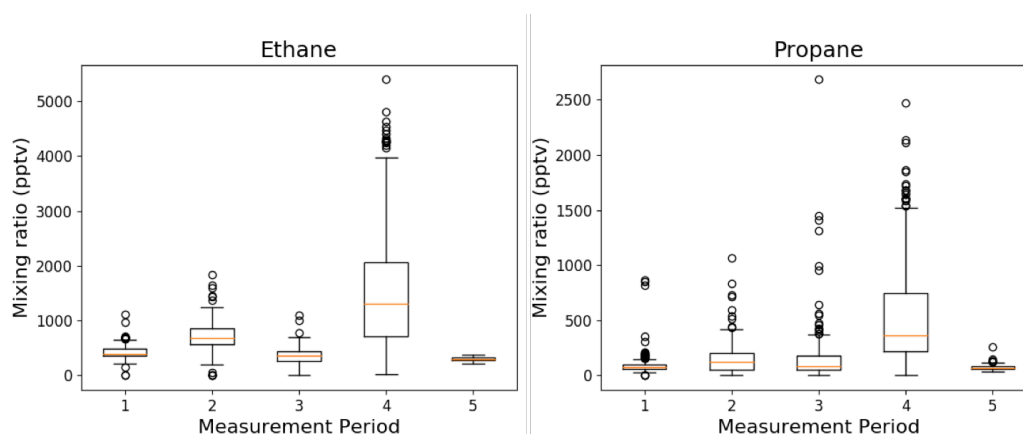


**Figure 4.5** Same as figure 4.4 for ethane and propane

Ethane shows sustained high mixing ratios during the initial measurement period, with a mean value of  $1500 \pm 200$  ppt but concentrations of  $390 \pm 40$  ppt during the rest of the year. Propane shows similar patterns in mixing ratios to ethane, with a mean concentration of  $520 \pm 50$  ppt during the initial measurement period and dropping to  $1300 \pm 10$  ppt in the later periods.

Figure 4.6 shows the correlation between ethane and propane over the entire BALI measurement period. The high degree of correlation ( $R^2 = 0.76$ ) suggests that there are common sources for these species. The correlation is reduced by a small

number of observations where ethane mixing ratios are much lower when compared with propane. Much of the source for these VOCs is known to be anthropogenic with large biomass burning sources (Franco, 2016, Pozzer et al., 2010). This is discussed in chapter 5.

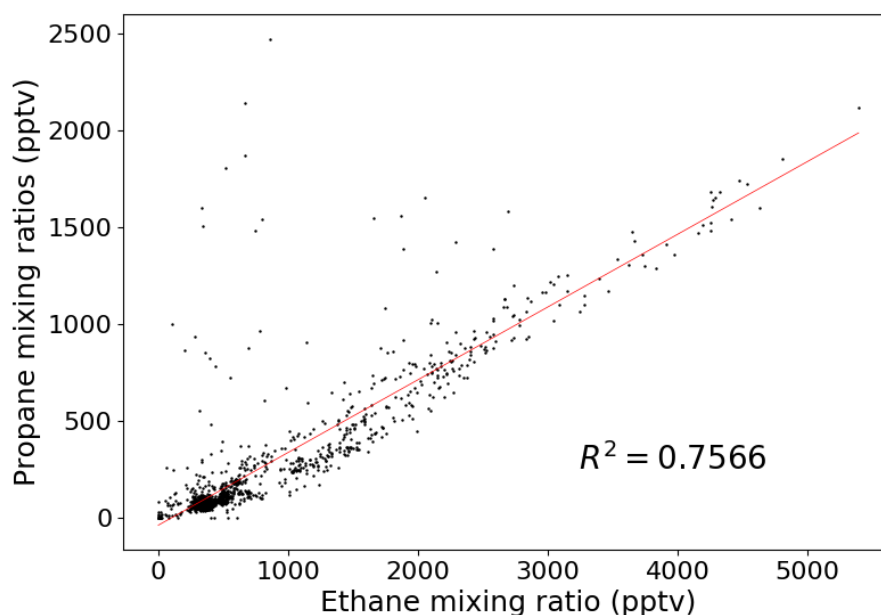


**Figure 4.6 Correlation plot for ethane and propane mixing ratios for all observations made during this work**

The ethane time series Figure 4.3 shows a large amount of variability both within and between the BALI and OP3 datasets. There is a sustained increase in mixing ratios observed during period 4 in the new observations due to biomass burning. Excluding this period, the two datasets combined seem to show the expected global mean seasonal cycle for ethane. This cycle shows a peak around March/April with a minimum around August, although there are variations in this dependent on location (Rudolph, 1995, Helmig et al., 2015). However, the April/May data was measured in 2008 and our data in 2015/16. There was a 21% decrease in ethane, between 1984 and 2010 (Simpson et al., 2012), but this trend has since reversed (Helmig et al., 2016). This makes ethane concentrations over different years difficult to compare.

Excluding the biomass burning period, the background concentrations for propane are similar for both studies ( $130 \pm 10$  and  $140 \pm 10$  ppt for BALI and OP3

respectively) but the OP3 data shows more outliers and a larger inter-quartile range than this work (50-190 ppt for OP3 compared with 60-100 ppt for our work). The biomass burning season in Indonesia, particularly Sumatra can begin in July so it may be that the spike in propane and some other species seen during OP3 is due to this (Field et al., 2016). However, analysis of air mass origin for this work discussed in chapter 5, showed that the air mass origin does not generally originate from this area, so it is unlikely.

An alternative explanation is that the low sampling height for OP3 makes it possible that local effects from nearby containers and work activity could have influenced measured VOC mixing ratios. This would explain why an increase was seen in measurement period 2. This was discussed in chapter 2, section 2.9.4.

#### 4.4.3 Other Alkanes (i-pentane, i-butane & n-butane)

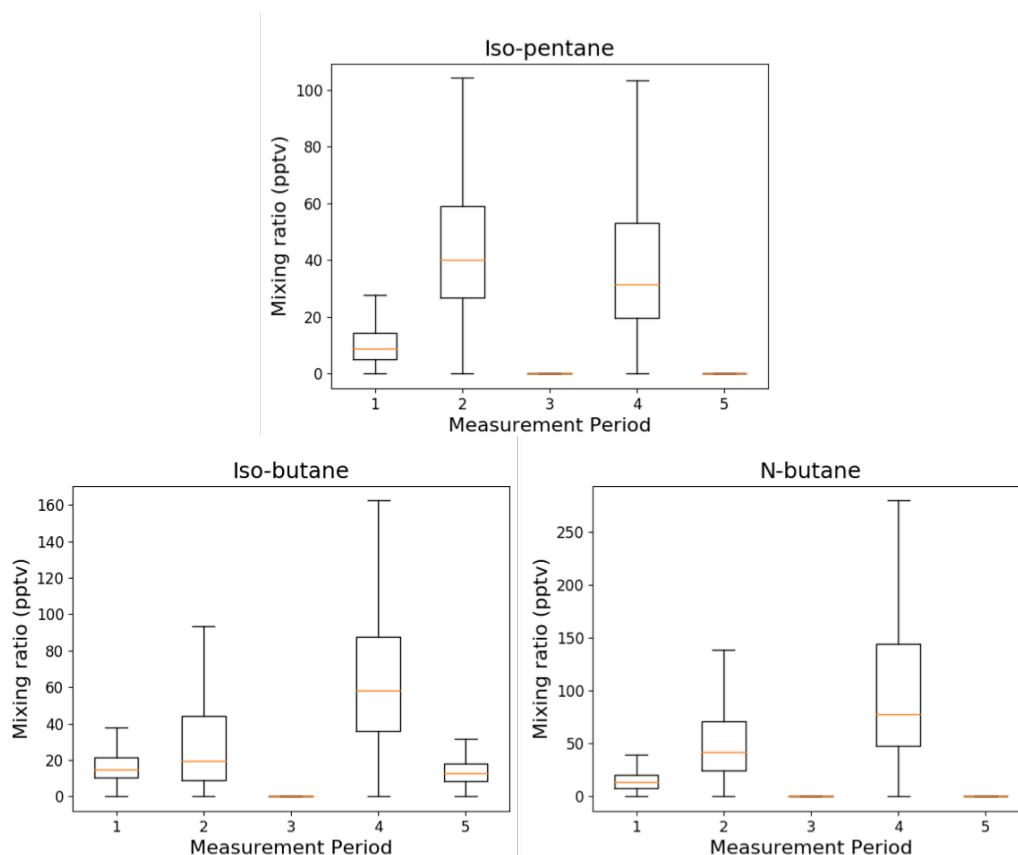


Figure 4.7 Same as figure 4.4 for iso-pentane, iso-butane and n-butane

The sources of iso-pentane and iso- and n-butane include biomass burning and natural gas emissions (Umukoro and Ismail, 2017). Another important source is evaporative fuel emissions from vehicle use (Yue et al., 2017).

Iso-pentane shows a strong enhancement during the initial measurement period (August – October 2015) with a mean mixing ratio of 56 ppt compared with 14 ppt for most of the rest of the measurements. Some measurements have been excluded from this analysis due to being much greater than the mean values. Iso-butane (100 ppt, 10 ppt) and n-butane (197 ppt, 18 ppt) show similar strong enhancements in mixing ratio during the initial period, numbers in brackets show the mean mixing ratio for the initial period followed by the mean for the majority of the rest of the data. N-heptane shows a very low mean mixing ratio for most of the measurement period of only 3 ppt, near the limit of detection for this compound. There is an enhancement in the mean during the initial measurement period to 16 ppt, but this is not as marked as for the other VOCs. The main increase in n-heptane is seen during three main events, where a sharp spike is seen in the mixing ratio. The cause of these spikes is not known but it is assumed a short lived, local event must have been the source. This feature is also present in the majority of VOC time series. Unlike the enhanced mixing ratios seen during the initial measurement period these are not sustained high levels but normally occur over a period of a few hours. The source of these increased VOC mixing ratios is not known. It may be that there is a local influence at the site causing short-lived increases in VOC mixing ratio but these have not been quantified.

For most samples iso-pentane mixing ratios were below the limit of detection, hence there is little data for this VOC during periods 1 and 5. Measureable concentrations of iso-pentane were only observed at the site during the biomass burning period (August – October 2015). Period 2 from OP3 data shows an increase in iso-pentane over the BALI data (even including the biomass burning period) and the other OP3 measurement period. As discussed for propane, it may be that due to the lower sampling height and presence of other activity at the site there may have been local influences that were not an issue for this work.

It is difficult to get a clear picture of the variability in iso-pentane due to the lack of measurements above the detection limit for this work. The box and whisker plot (figure 4.6) also shows that most of the data points are outliers, this occurs

because so most of the measurements are at or near the limit of detection. This would support the argument that spikes in data caused by biomass burning and possible local interferences are responsible for detectable mixing ratios for isopentane, with very low if any present in the background.

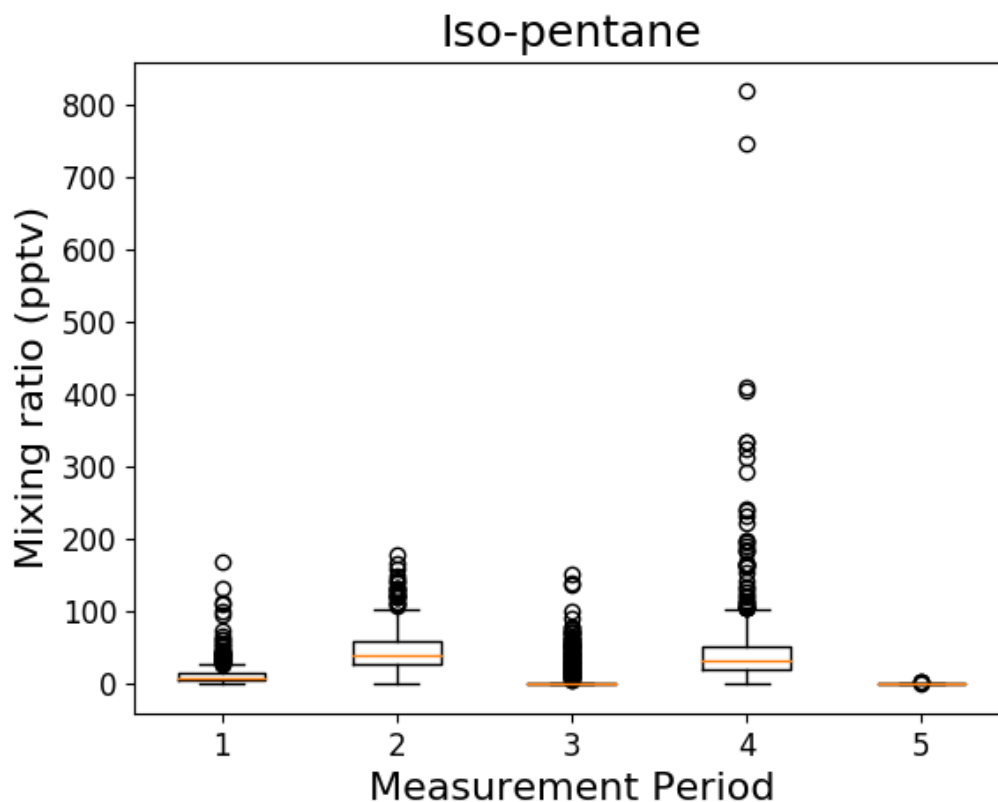
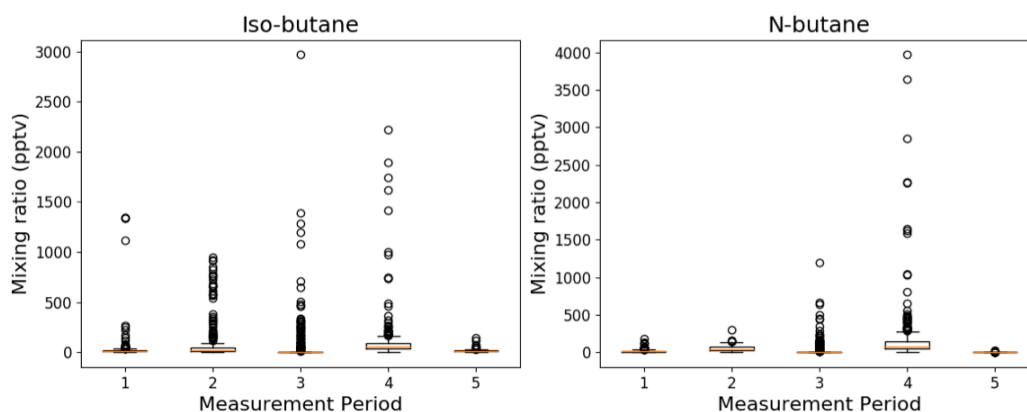


Figure 4.8 Box and whisker plot for iso-pentane including outliers

Both the BALI and OP3 datasets show sharp spikes in the iso-butane concentrations. Other than these events background mixing ratios were generally low during all months, in the tens of ppts. There is the same consistent increase observed in September/October due to biomass burning emissions. N-butane shows a similar pattern of behaviour; with generally low mixing ratios (tens of ppts or less) throughout the year apart from the increase due to biomass burning in period 4.

The median values for period 3 for both iso- and n-butane are very low, this is due to the large spikes in mixing ratio leading to the data being mainly outliers. Overall the data suggests that background mixing ratio of the butanes is low, with biomass burning and possible local influences during OP3 dominating.



**Figure 4.9** Box and whisker plots for the butanes including outliers

#### 4.4.4 Alkenes

Ethene, propene and 1-butene have multiple sources including a biogenic source (Goldstein et al., 1996). The major ethene source is thought to be biogenic, with almost three quarters of global ethene emissions from natural sources (Sawada, 1967). This is dominated by terrestrial emissions with a smaller contribution from oceanic sources. There is also a major source from biomass burning (Yokelson et al., 1997).

1-butene and propene also have biogenic sources but globally emissions of these species are dominated by ocean or anthropogenic sources (Kansal, 2009), including biomass burning (Liu et al., 2017). The mean ethene mixing ratio measured in this thesis over the whole measurement period (66 ppt) is similar to that found during the OP3 campaign at the same site (77 ppt daytime mean). Although measurements of the fluxes of propene have been measured previously (Khalil and Rasmussen, 1992, Goldstein et al., 1996) finding ambient concentration measurements over a comparable environment has proved challenging.

Ethene and 1-butene on the other hand do not show a clear diurnal cycle. For 1-butene the mixing ratios are low, near to the limit of detection for the instrument so this may contribute to the lack of diurnal cycle. Propene does not show the enhancement in mixing ratio during the initial measurement period (August – October 2015) seen for most of the other VOCs and there is actually a lowering of the mean from 65 to 50 ppt during the initial measurement period.

#### 4.4.5 Acetylene

While biofuel burning is the dominant global source of acetylene, there is also a source from biomass burning (Xiao et al., 2007). Enhancements in acetylene are seen during the biomass burning period (August – October 2015) in our work. Emission rates for acetylene are smaller than ethane and propane and the rate constant for acetylene + OH is larger than the other species so lower mixing ratios are observed (Xiao et al., 2007).

#### 4.4.6 Aromatics

Benzene and toluene atmospheric sources are mainly anthropogenic in origin, with the burning and evaporation of petrol being the dominant source (Clarkson, 1996). There is also a smaller source from biomass burning (Lewis et al., 2013). Given that the main source of these VOCs are anthropogenic fuel use and the distance of the site from extensive anthropogenic activity and the short lifetime of these species (10 and 2 days respectively, assuming an OH concentration of  $1 \times 10^6$  molecules  $\text{cm}^{-3}$ ), it would be expected that mixing ratios of benzene and toluene would be low. A previous study conducted at a remote site in the Amazon found maximum benzene and toluene mixing ratios of  $\sim 0.1$  and 0.8 ppb respectively (Kesselmeier et al., 2000). The mixing ratios varied strongly with sampling height. The majority of observations from our work give values in a similar range, although the maximum toluene mixing ratio found was lower than the Amazon study value, even during the initial measurement period where mixing ratios were strongly enhanced. The authors of that study concluded that the low benzene and toluene mixing ratios indicated that the site could be considered remote, with the air mass having travelled largely over pristine forest. The same is likely true of most of this work, excluding the initial measurement period given that benzene and toluene are most often tracers of anthropogenic activity.

A comparison for all measured species between OP3 and the BALI project is shown in Table 4.2.

**Table 4.2 Mean, median and interquartile range concentrations for all measured hydrocarbons from this work and the OP3 campaign**

	Ethane	Ethene	Propane	Propene	Iso-butane	N-butane	Acetylene	1-butene	Iso-pentane	Isoprene	N-heptane	Benzene	Toluene	
All new data	mean	812	324	293	97	116	93	93	64	44	1431	33	198	59
	median	443	88	100	57	25	36	46	21	21	952	10	102	27
	inter-quartile range	336-1044	54-185	70-318	35-88	12-64	15-93	28-105	18-69	11-41	366-2008	3-15	74-230	15-57
All OP3 GC-FID data	mean	524	/	145	/	107	68	/	/	45	830	/	/	/
	median	485	/	104	/	26	52	/	/	40	394	/	/	/
	inter-quartile range	341-656	/	54-189	/	11-62	25-84	/	/	24-58	117-1183	/	/	/

## **4.5 Non Negative Matrix Factorisation (NMF) analysis**

Given the number of observations collected, a method is needed to synthesise the observations down to a number of different periods where the observations are impacted by a number of different factors. A range of approaches could be adopted for this: for example by eye, cluster analysis (Omar et al., 2005, Scott and Knott, 1974), or principal components analysis (Wold et al., 1987, Abdul-Wahab et al., 2005). In this case Non-negative Matrix Factorization has been used. Here the technique is described and then the results of applying the factorization to the BALI dataset outlined.

### **4.5.1 Non-negative vs Positive Matrix Factorisation and other source analyses**

Positive matrix factorisation (PMF) analysis is a numerical tool used within the atmospheric science field for the identification and interpretation of observational data (Chueinta et al., 2000, Lee et al., 1999). This technique has been used most frequently with aerosol data. More specifically PMF has been used with Aerosol Mass Spectrometer (AMS) data for studies including the identification and interpretation of different organic aerosol sources (Ulbrich et al., 2009, Paglione et al., 2014). It has also been used for assigning the sources of polycyclic aromatic hydrocarbons (PAHs), using gas and particle phase data (Gao et al., 2015). A similar method to PMF analysis but used less often in the atmospheric science field is non-negative matrix factorisation (NMF) analysis. Whereas PMF assumes all numbers are positive, NMF assumes all numbers are non-negative, but also includes zero values, unlike PMF analysis. For this work there are no zeroes within the data as values below the limit of detection for the instrument have been removed.

NMF is less computationally demanding than commercial PMF analysis (Liang and Fairley, 2006). There is also a free to access, relatively user friendly package for NMF analysis using python from the skilearn decomposition package (Pedregosa, 2011). Other techniques such as principal component analysis (PCA) have been used for source analysis (Song et al., 2006). However, whereas PCA looks for

strong correlation only in variables whether this is positive or negative correlation, NMF analysis, because it forces the product matrices to be positive, means only correlations with the same signs are grouped together.

#### 4.5.2 Non-Negative Matrix Factorisation Theory

The basis of NMF analysis is to calculate two matrices whose product is representative of the input matrix (Hoyer, 2004).

$$K = B \times C \quad \text{Equation 13}$$

where  $K$  is the input matrix; matrix  $B$  is a component or base matrix where each vectors in matrix  $K$  can be found through addition of the vectors in  $B$  and matrix  $C$  contains the coefficients that approximate the input matrix  $K$  when multiplied by the matrix  $B$ .

For this work the input matrix is the observational dataset, giving a matrix with column number equal to the number of VOCs and rows equal to the number of datetimes. The NMF analysis is run for the observational dataset and produces two matrices. Matrix  $B$  has a number of columns the same size as the number of components selected for the analysis and rows equal to the number of times from the observational dataset. Matrix  $C$  has a number of columns equal to the number of measured VOCs and rows equal to the number of components selected for the analysis.

The matrices  $B$  and  $C$  are found using a squared Frobenius norm algorithm (<http://mathworld.wolfram.com/FrobeniusNorm.html>). This algorithm minimizes the distance between the input matrix and the product of matrices  $B$  and  $C$ . It does this by taking the square root of the sum of the squares of the matrix elements.

NMF analysis therefore takes the observed data matrix and decomposes it into two model matrices, by minimizing the divergence between the data matrix and the matrix product of the two model matrices. This algorithm requires the selection of several parameters (Kitamura, 2016). For this work the parameters that were set are number of components, the initialization method and random state. The number of components gives how many non-observed variables will be used in the analysis to account for the variability in the data, with each additional component

accounting for a smaller amount of the total variability. The initialisation method is used to assign initial values to the two model matrices before the iterative process can begin. This work uses random initialisation, where the initial matrix values are scaled using equation 13.

$$\sqrt{\frac{\text{observations.mean}}{\text{number of components}}} \quad \text{Equation 14}$$

The random state parameter sets the seed number for the random number generator, in this case the value has been set to zero. This seed values ensures that the set of numbers generated by the random number generator is the same each time the analysis is run.

## 4.6 Results

NMF analysis was run for the available observational data (the OP3 data were not included in this analysis) using four different treatments of the measured mixing ratios. The first approach used the mixing ratio data with no further processing. The second normalized the data by dividing each species by its maximum observed value, putting all data on a 0 to 1 scale. The third and fourth approaches divided all data for each species by the mean and median for each species. Although these methods do not normalise on a 0 to 1 scale, it was thought that scaling the data in this way would remove some of the bias towards the species that have high concentrations dominating the analysis.

Figure 4.10-4.11 show the relative contribution of each hydrocarbon to the different components used in NMF analysis for the four data analysis methods. An arbitrary number of five components were used to run this analysis. A final choice for the number of components is made later in this chapter.

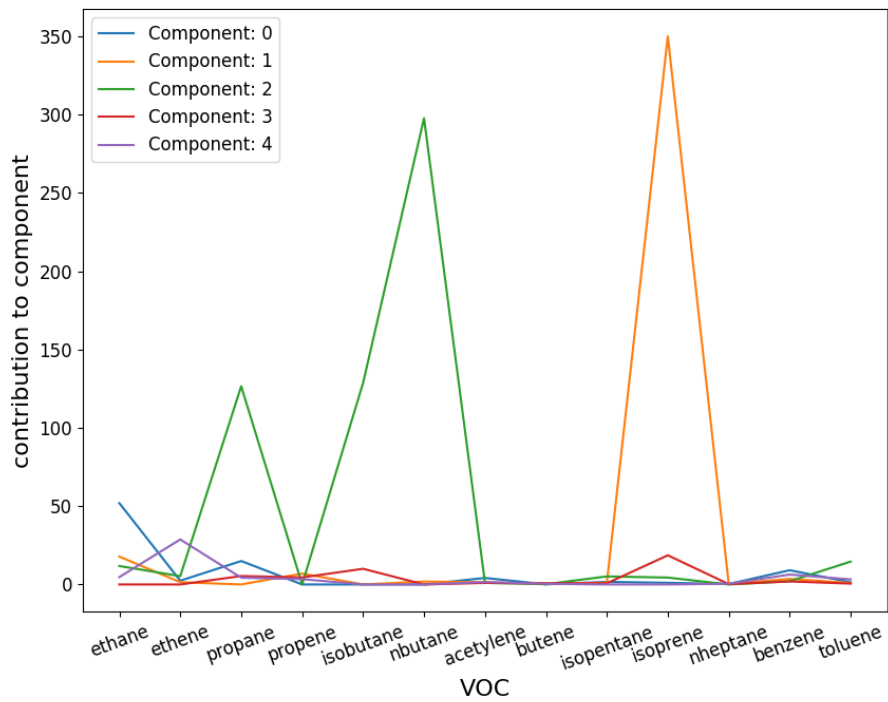


**Figure 4.10** The contribution of all VOCs to each component of the five components from the NMF analysis. This analysis used un-normalized measured mixing ratio VOC data.

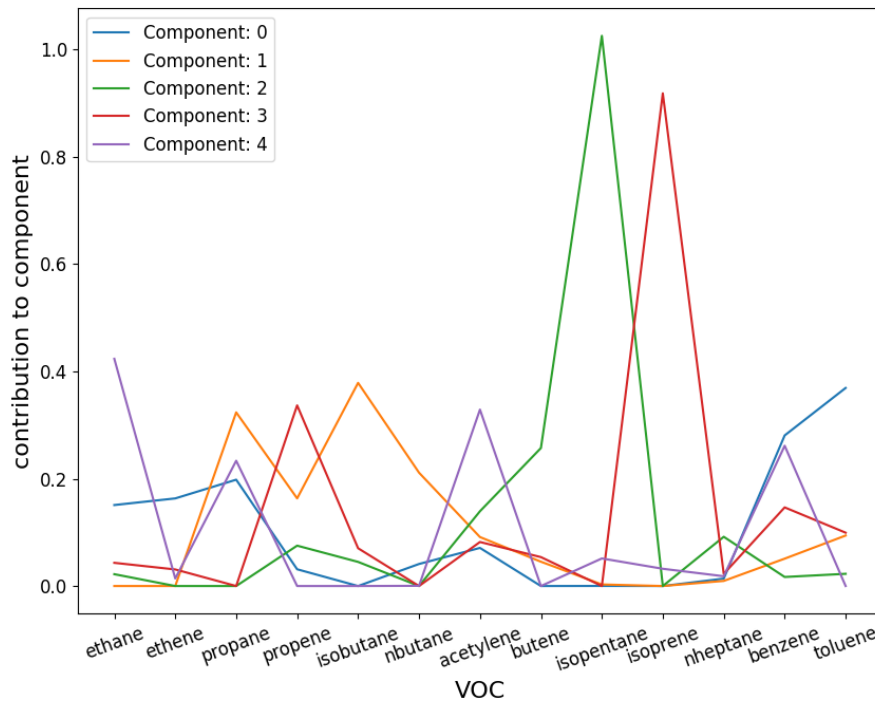


**Figure 4.11** The relative contribution of all VOCs to each of the five component from the NMF analysis. This analysis used data normalized by dividing the measured mixing ratios by the maximum value for each VOC

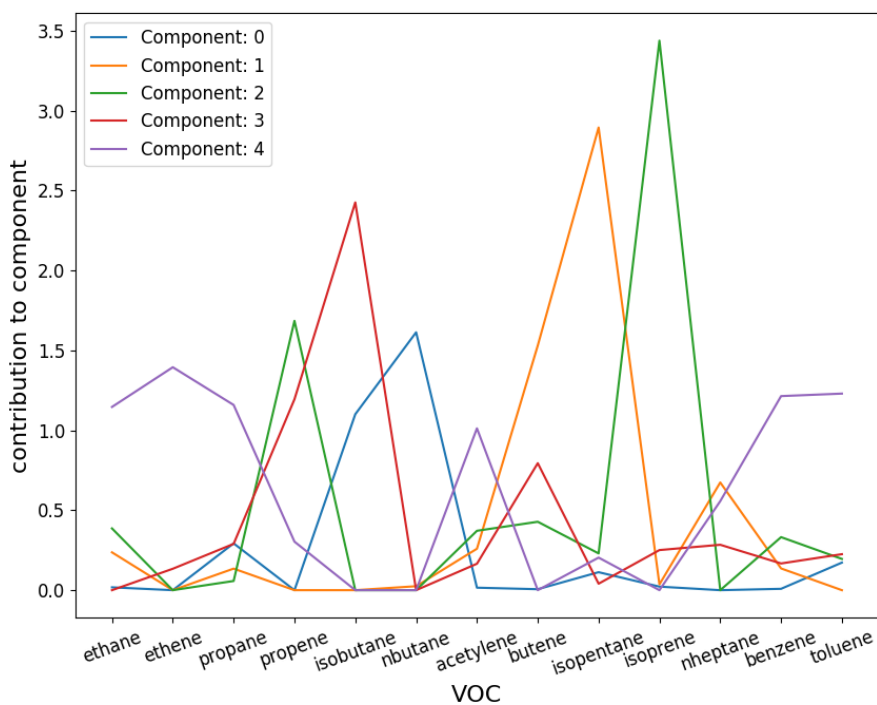


**Figure 4.12** The relative contribution of all VOCs to each of the five component from the NMF analysis. This analysis used data normalized by dividing the measured mixing ratios by the mean value for each VOC

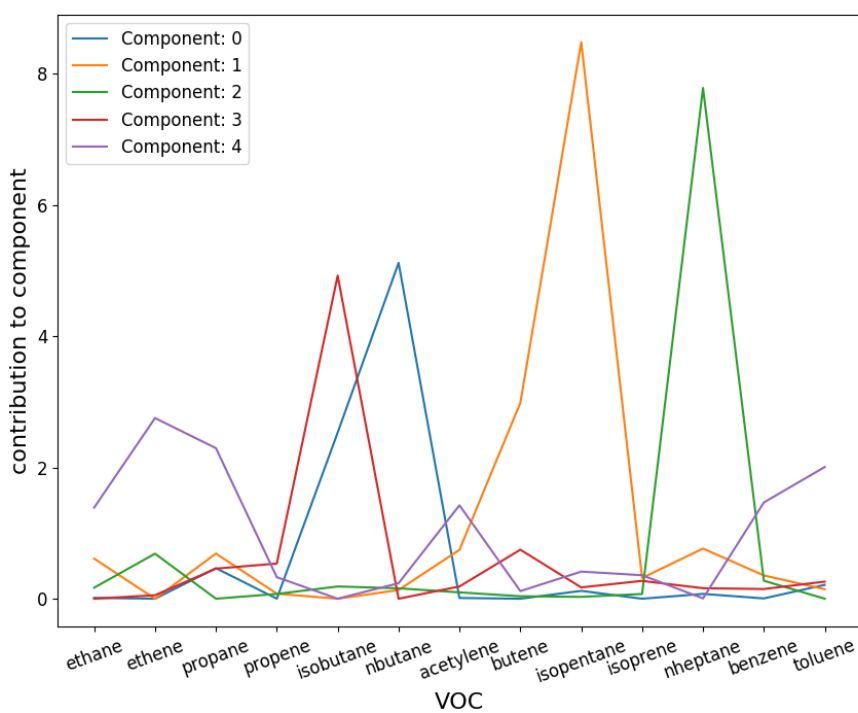


**Figure 4.13** The relative contribution of all VOCs to each of the five component from the NMF analysis. This analysis used data normalized by dividing the measured mixing ratios by the median value for each VOC

## 4.7 NMF Analysis Evaluation and Method Selection

### 4.7.1 Normalisation Method Selection

For NMF analysis using the measured mixing ratios, shown in Figure 4.10, isoprene dominates component one and propane and n-butane dominate component two. When the same analysis was run using the normalised data other species made a greater relative contribution to each component. For example when the concentrations were divided by the maximum value (Figure 4.11) the component dominated by isoprene (now component 3) is joined by propene and acetylene and to a lesser extent benzene.

To help decide which method of data analysis would be best the four different methods of data analysis were used for NMF analysis with a number of components between one and ten. For each number of components the  $R^2$  values were found from plotting the model output against observations. The  $R^2$  values found from plotting the observed hydrocarbon values and those from the NMF analysis are shown Figure 4.14.

The NMF prediction of concentration values were calculated by multiplying together the two matrices found from the NMF analysis. These were the component number, hydrocarbon matrix and the time, component number matrix. Multiplying these matrices gives a matrix of time and hydrocarbon number, giving effectively a time series that can be compared with the observational matrix of the same format. The different data analysis methods: using measured mixing ratios, dividing all values by the mean, maximum and median values are shown in red, blue, green and purple respectively.

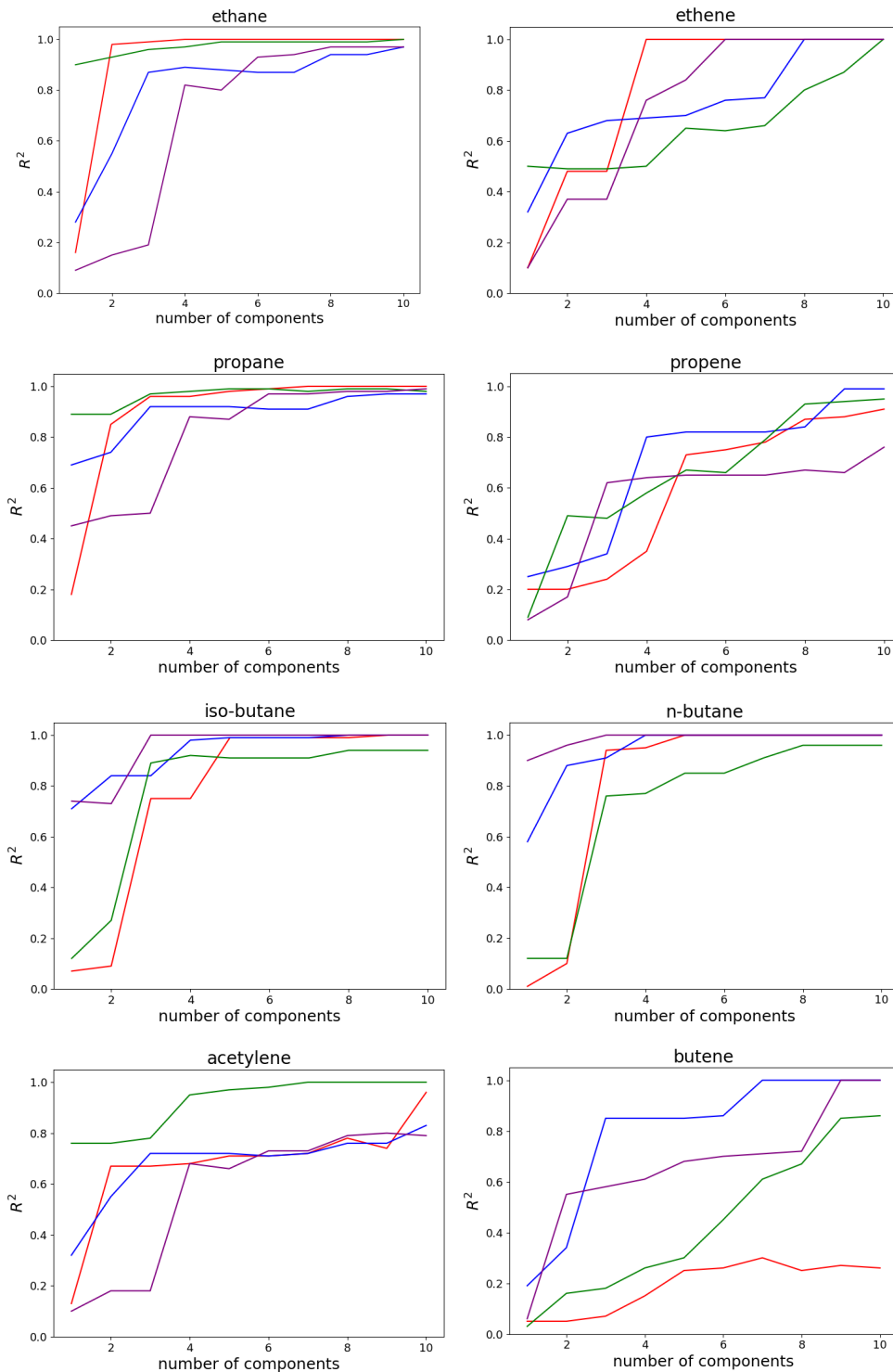
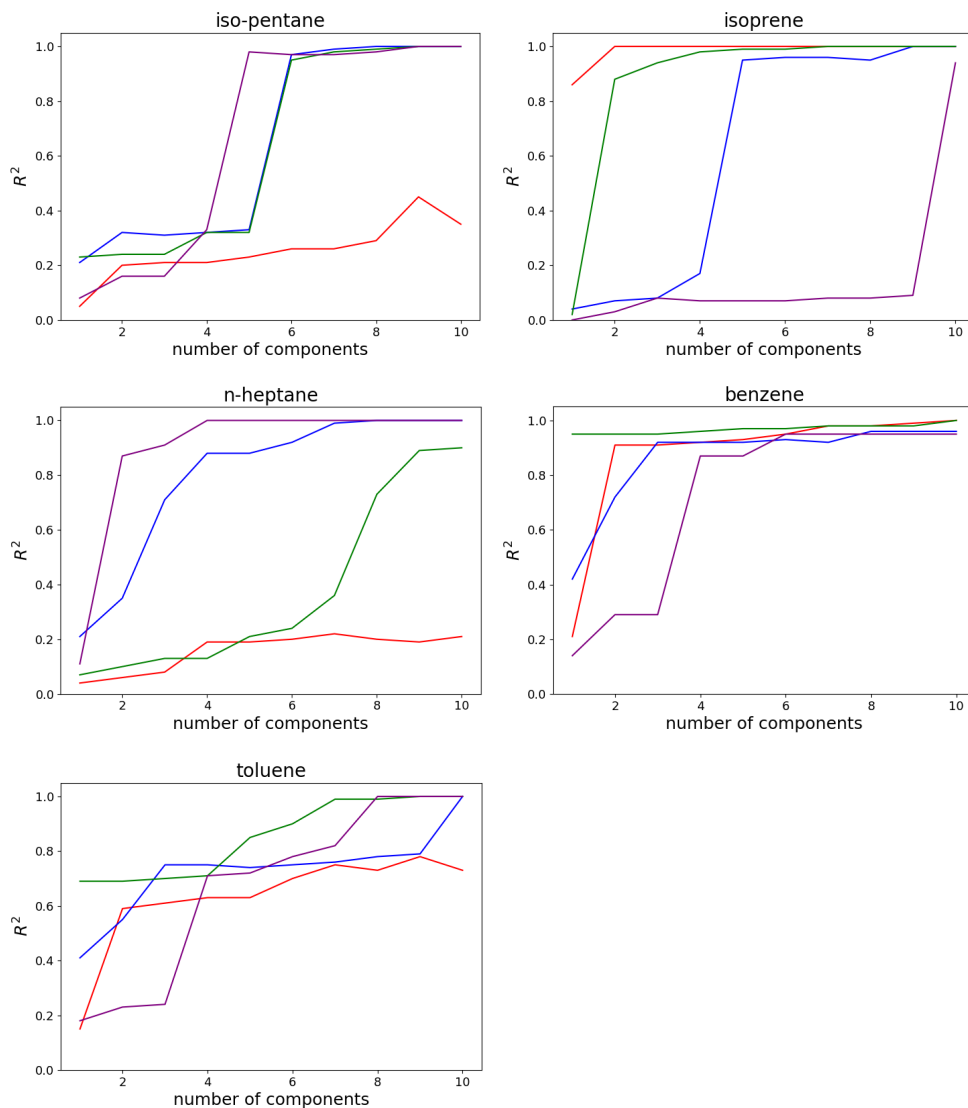


**Figure 4.14**  $R^2$  values, found from correlation of VOC observations with those predicted by the NMF analysis for differing numbers of components. The modelled values are the product of the two matrices produced by the analysis. For each VOC the  $R^2$  values is calculated for NMF analysis using one to ten components. The analysis was run using four different data analysis methods: measured mixing ratios (red), division by the mean (blue), maximum (green) and median (purple) mixing ratios. Continued on next page.



By the time ten components were used nearly all species showed high correlation coefficients between the observations and the prediction made by the NMF analysis, regardless of the normalization method. Overall the least successful approach was using the un-normalized data, where some VOCs showed low regressions coefficients even when using 10 components. However, all methods of NMF analysis capture the variability in ethane, propane, benzene and iso- and n-butane well with a small number of components. Completing the analysis with four or fewer components gave an  $R^2$  value of above 0.7 for all of these species.

Looking at the time series for these species they all show a large increase during the initial measurement phase. From the NMF analysis this period accounts for the largest amount of variability within the data for all methods and so this could

explain why these hydrocarbons are well captured. Most of these species are also relatively long lived. Approximate lifetimes assuming  $[\text{OH}]$  of  $1 \times 10^6$  molecules  $\text{cm}^{-3}$  and temperature of 298K are 1.5 months for ethane, 11 days for propane and 10 days for benzene. This is likely to lead to less variability on a small timescale, making it easier for the NMF analysis to capture the larger scale variability observed. Isoprene is also well captured by the NMF analysis for all data analysis methods apart from division by the median. For this reason the median normalization method will not be used for further analysis. Unlike the previously mentioned species, isoprene has a short atmospheric lifetime of  $\sim 1.4$  hours in the troposphere at 298 K, with respect to OH (Atkinson and Arey, 2003). The likely reason for most of the NMF analysis methods capturing the variability in isoprene well is that it has a strongly defined diurnal cycle, with only a small amount of variability over a longer time period.

For other species there are clear differences in the level of success for each data analysis method. For ethene only the analysis with observed mixing ratios gives a high  $R^2$  value with less than eight components. Ethene has a shorter lifetime than the ethane and propane (species for which the NMF analysis gives good agreement with a small number of components), with a lifetime ranging from hours to a couple of days depending on conditions (Solberg et al., 1996). This shorter lifetime combined with relatively low observed mixing ratios could explain the difficulties in the NMF analysis of simulating ethane.

From the  $R^2$  analysis above it was seen that normalising the data using any method generally gave higher  $R^2$  values with fewer components than using the measured mixing ratio data. Therefore it was decided that a normalisation method would be used on the data. Dividing by the median has already been dismissed as it fails to capture the variability in isoprene mixing ratios. For the two remaining normalisation methods there were hydrocarbons where both methods gave equally high  $R^2$  values, but there were also hydrocarbons where one method was better than the other. On balance, it was decided that division by the maximum was the normalisation method that would be used. Overall both methods gave a similar level of success but for isoprene, the most abundant hydrocarbon measured during this work, division by the maximum gave much higher  $R^2$  values with fewer components and so this is the method that will be used for further analysis. Isoprene has a strong diurnal cycle and this shorter scale variability is of

interest in addition to the larger scale variations, which is only captured through division with the maximum.

#### **4.7.2 Selection of Number of Components for Analysis**

The next decision to be made regarding the NMF analysis was the number of components to use. Using nine components and the division by maximum normalisation method gave an  $R^2$  value of greater than 0.8 for all species. However, given that there were only 13 hydrocarbons measured this seemed a large number of factors to attribute the observed variability to. For most components using four or five factors gave a good  $R^2$  and adding another two or three components gave little improvement in the  $R^2$  when the complexity of the NMF output was considered.

It was found that running with three components characterized the main features of the dataset. Additional components focused on spikes in individual VOCs that were not of interest for this work. Therefore it was decided to run the analysis with three components.

### 4.7.3 Three Component Analysis

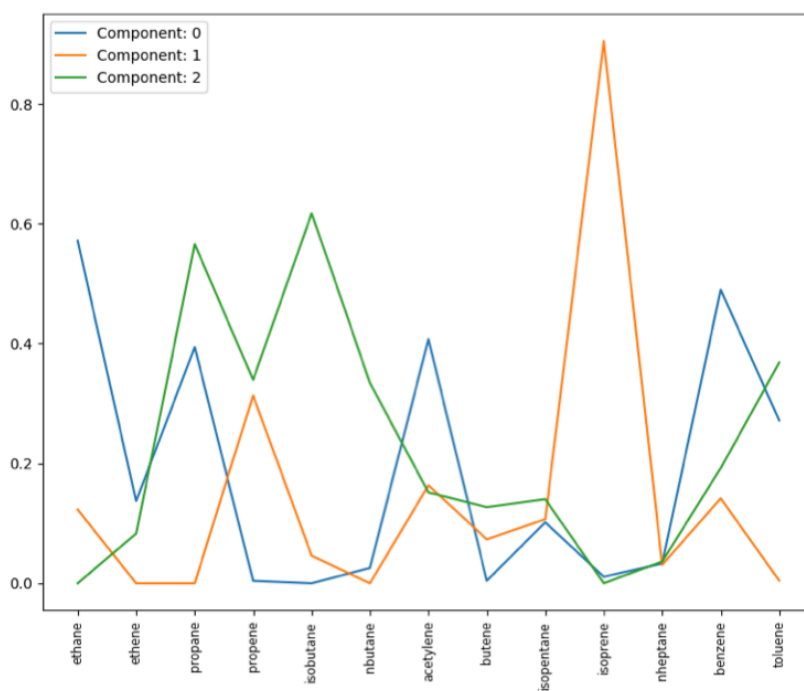


**Figure 4.15 Contributions of all VOCs to each component from three component NMF analysis using mixing ratio data normalised through division by the maximum values.**

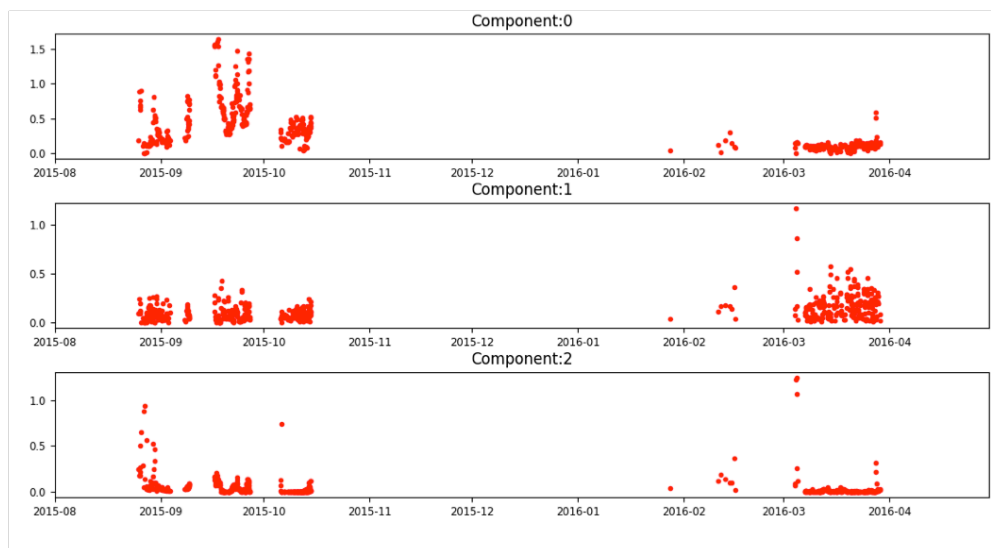


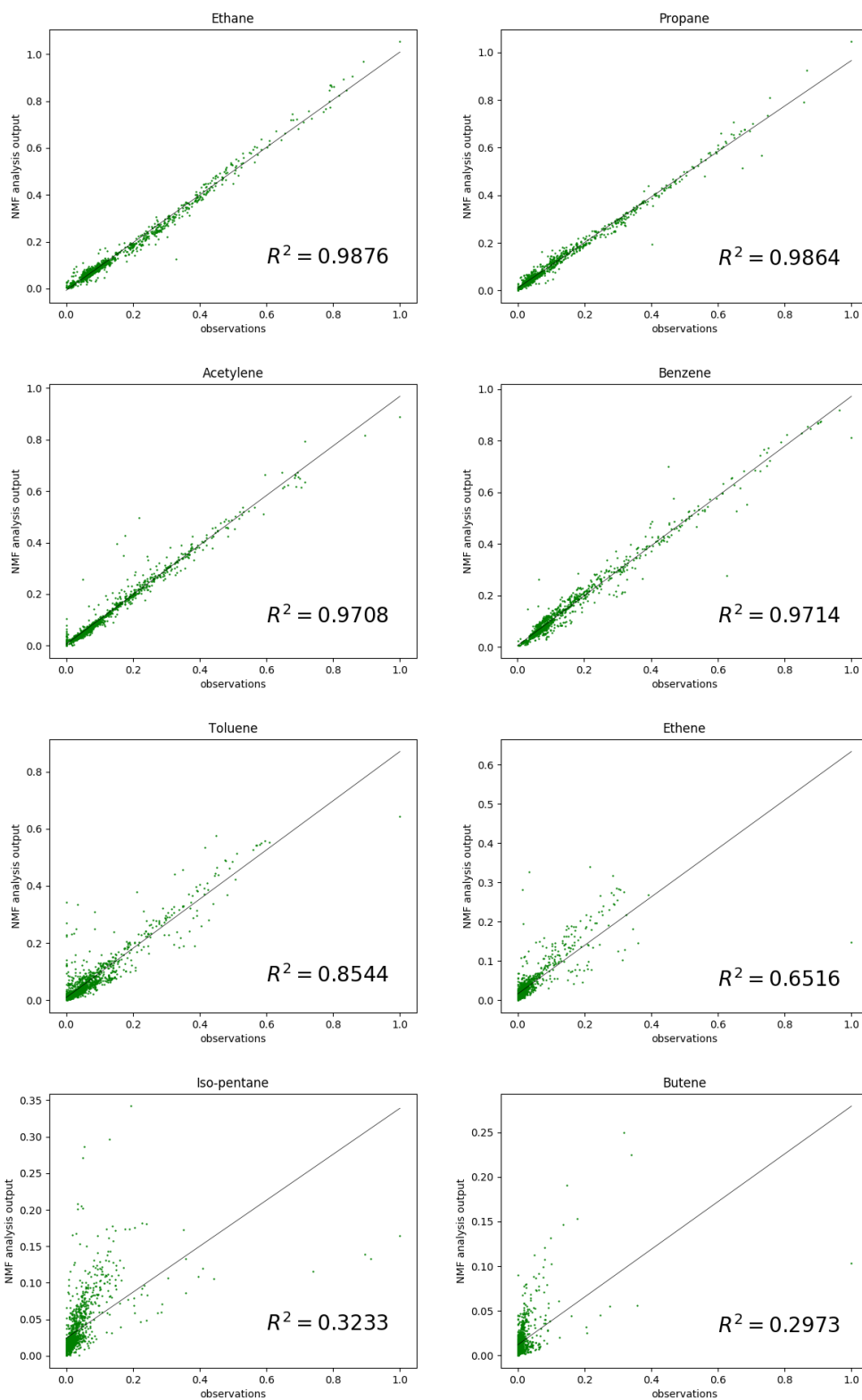
**Figure 4.16 Time series for the NMF analysis using three components with data normalised by division with the maximum mixing ratio. Component zero is high during the initial measurement period, when most of the measured VOCs are high and likely reflects biomass burning influence. Component one shows less variability over the time series. This corresponds to high influence from isoprene and propene. Component two is dominated by sharp spikes in the mixing ratio, which occur at several time periods.**

Component zero shows a time series that with a large enhancement in mixing ratio at the beginning of the measurement period. Component one shows little variability over the measurement period aside from one spike in March. Component two is characterized by sharp spikes in the data with a small amount of variability at other times.

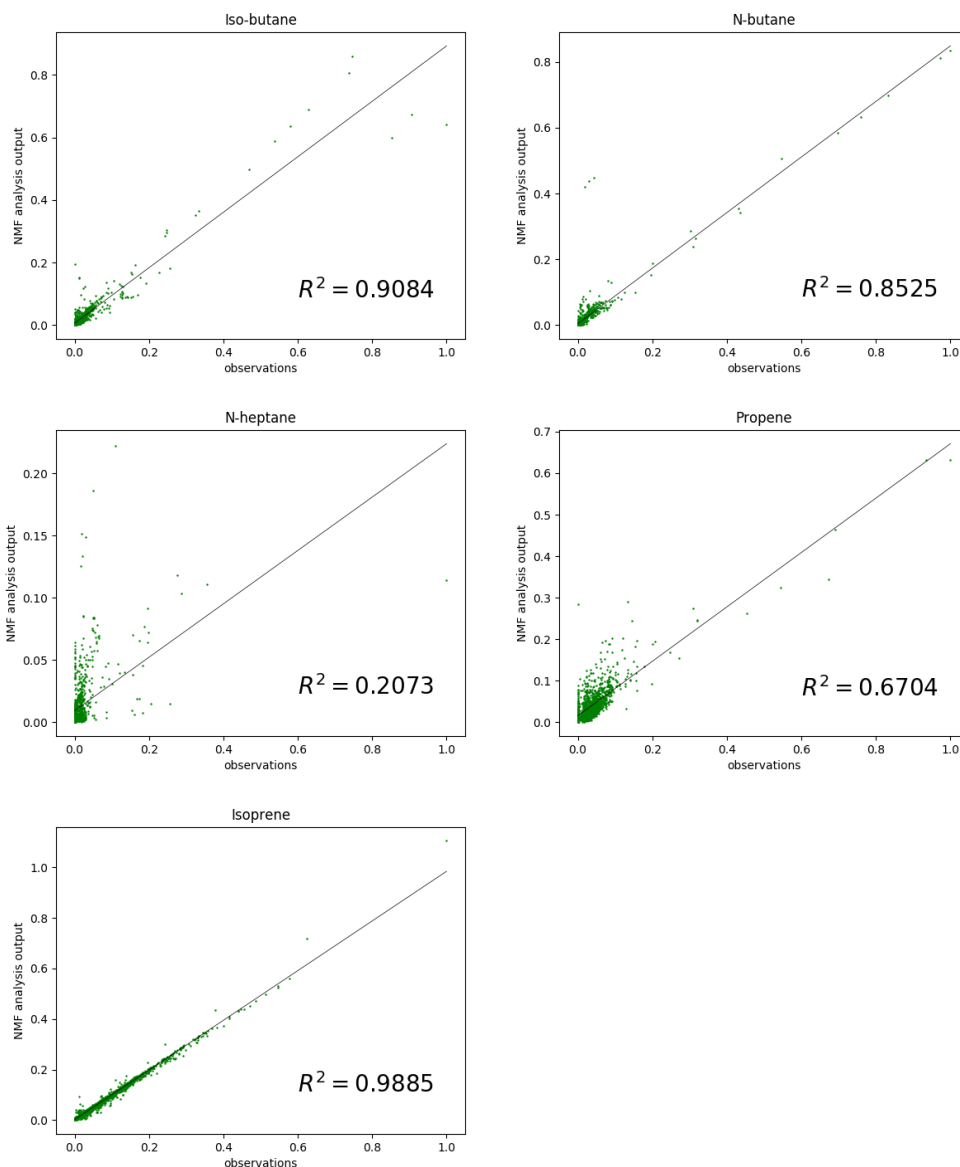
#### **4.7.3.1 Correlation Plots for Three Factor NMF Analysis**

Figure 4.17 shows the comparison between the observed VOC mixing ratios and those calculated from the three factor NMF analysis. The calculated NMF values were found using the three factor NMF analysis. For the majority of species this gave  $R^2$  values of above 0.8. For iso-pentane, butene and n-heptane the  $R^2$  values were substantially lower, 0.32, 0.29 and 0.20 respectively. Looking at the correlation plots for these species it can be seen that the observed values were generally very low, this is particularly the case for butene and n-heptane. This could be the reason that the analysis doesn't simulate the observations well. The observations were so low that there is variability caused by noise within the instrument and the analysis is trying to fit to this noise. Both of these species also showed a smaller increase during the first measurement period when compared with the majority of species, this could be one reason why the NMF analysis generally overestimates these values. For iso-pentane there was a marked increase in mixing ratio observed during the initial measurement period but in addition to this there is a large spike in mixing ratios at the end of this period. Looking at the  $R^2$  plot for iso-pentane there are two distinct sections to the plot, one of which shows a large increase in observations not simulated by the NMF analysis. This explains why the  $R^2$  value is so low, without this spike the agreement between the two data sets would be much improved. Propene and ethene both show an  $R^2$  value of  $\sim 0.6$ . For propene there is a large spike in mixing ratios that is not captured by the NMF analysis, this biases the best fit line downwards, hence the lower  $R^2$  value. For ethene there is also a number of points where the NMF analysis underestimates the observed mixing ratios, this has the same effect on the  $R^2$  values as seen for propene.

Despite the issues in simulating the mixing ratios for some species, NMF analysis of data normalised through division by the maximum value for each hydrocarbon using three factors will be used for further analysis.



**Figure 4.17 Correlation plots of the mixing ratio values obtained through the NMF analysis, calculated from the product of the two output matrices (component number, hydrocarbon and component number, time). This gives a simulated time series for each VOC that was then plotted against the observation time series. The  $R^2$  value is also given. For most VOCs a high  $R^2$  value  $>0.8$  was calculated. The reasons for the low  $R^2$  values has been discussed above. Continued on next page.**



## 4.8 Events within the dataset

Using the ethane time series as an example the different components found from NMF analysis have been used to assign different periods within our dataset (Figure 4.18). Component 0 has been used to assign a period at the start of the project, which has been interpreted as being influenced by biomass burning. Component 1 is interpreted as periods influenced by local influences. Other periods are interpreted as being background periods. Table 4.3 shows the mean, median and 25<sup>th</sup> and 75<sup>th</sup> percentile values for all three periods.

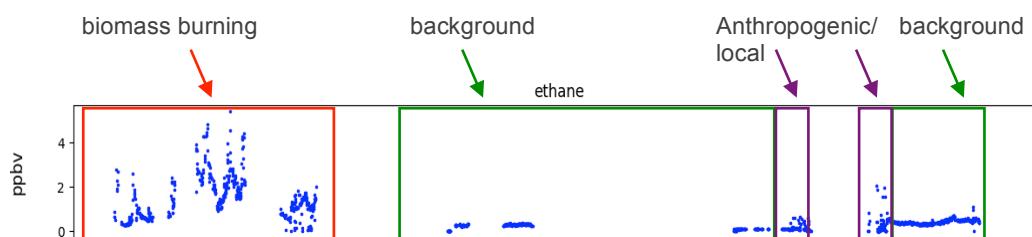


**Figure 4.18 Ethane time series overlaid with the three regimes affecting the VOC mixing ratios. Biomass burning, increase in many VOC seen as a result of air masses travelling over active fires in the surrounding regions (see chapter 5). Biogenic, VOC mixing ratios are affected mainly by local events with little influence from surrounding regions. Isoprene dominated the VOC composition during these periods. Anthropogenic/local, increases were seen for some VOC during these periods, often these events were short lived. These periods have been assigned to a change in local conditions but no specific source as been identified, equally there have been no instrument issues found to justify the exclusion of this data.**

#### **4.8.1 Biomass burning period**

The first component identified by the NMF analysis shows a clear sustained increase in most hydrocarbon mixing ratios (Figure 4.1) during the initial measurement period (August – October 2015) when compared with the rest of the timeseries. The majority of the VOCs measured contribute towards this component, with large increases seen in both the mean and median values for most VOCs when compared to the biogenic periods. Previous measurements at the site did not observe such high mixing ratios of these VOCs, but this likely reflects the lack of overlap in the time periods over which measurements were made between this work and the OP3 project (Jones et al., 2011, Langford et al., 2010). It is therefore likely that a specific event was the source of these increased VOC mixing ratios. To identify the source of the VOC events within the local environment and further afield were investigated. The time of year that these measurements were made coincides with the Indonesian biomass burning season (Lestari et al., 2014, Engling, 2014).

Further details on the influence of regional biomass burning at the measurement site will be given in chapter 5.

#### **4.8.2 Background periods**

The background periods were assigned to periods where the observations were dominated by isoprene with lower levels of all other hydrocarbons. During these periods it was thought that hydrocarbon mixing ratios were driven by the local environment rather than dominated by regional influences. The prevailing wind direction during these time periods brought air from the North East, over the South China Sea and the Phillipines.

Isoprene and propene both show a strong diurnal cycle, suggesting they are biogenic in origin and therefore influenced by local meteorological conditions. The biogenic species are discussed further in chapter six, with a particular focus on isoprene.

#### **4.8.3 Local/Anthropogenic time periods**

These periods were characterized by short live spikes in concentrations of some VOCs including propane and toluene. For some species during these periods, notably benzene and toluene, there was interference from additional unidentified peaks falling within the peak identification window. This has been discussed in chapter two. The air mass during this period was coming from the same direction as the surrounding dates, when mixing ratios were substantially lower. Therefore, it would seem either there was a localized event or change in local conditions that caused the observed enhancement such as an anthropogenic interference at the site itself.

Unless an identifiable issue was found with the data, such as those discussed regarding the height of the sampling inlet and interference from unknown peaks in chapter two, the data has not been discarded from the dataset. This is because there is no justifiable reason for doing so and the results are thought to be real measurements. However, given the lack of explanation for the observed VOC mixing ratio increases further analysis will not be carried out on any data falling within the local/anthropogenic periods. The mean, median and 25<sup>th</sup> and 75<sup>th</sup> percentile values for all three periods are summarized in table 4.3.

**Table 4.3 : Mean, median and interquartile range values for all measured hydrocarbons by each of the periods identified**

	Ethane	Ethene	Propane	Propene	Iso-butane	N-butane	Acetylene	1-butene	Iso-pentane	Isoprene	N-heptane	Benzene	Toluene	
Biomass burning	mean	1492	336	519	50	100	197	138	12	56	1015	16	308	81
	median	1315	163	363	39	60	87	122	7	35	737	12	231	56
	inter-quartile range	716-2043	99-357	225-745	29-60	36-88	53-172	77-178	5-12	22-60	407-1385	9-15	132-406	35-94
Background period	mean	351	66	72	65	16	18	33	10	14	1298	3	77	18
	median	345	55	68	59	13	15	31	6	10	831	2	75	15
	inter-quartile range	290-432	30-79	53-88	34-83	9-20	10-22	21-43	4-10	7-16	218-2016	2-3	61-93	9-24
Local period	mean	206	614	220	191	360	36	174	57	34	1455	55	192	60
	median	129	431	109	96	242	30	83	36	29	985	30	143	31
	inter-quartile range	87-288	174-1021	50-243	50-204	86-385	11-38	18-356	19-61	10-38	422-1637	10-60	100-214	10-80

## 4.9 Model VOC Time Series

In order to place the observational data into another context the GEOS-Chem model (see chapter 3) was run for the whole time period (August 2015 – April 2016). The model performance is now discussed by grouping the species into a number of groups: isoprene, small alkanes, aromatics, alkenes and other alkanes.

Comparison plots between the model and measurements are shown in each subsection below. Not all species measured are available to output from GEOS-Chem so are not included here. For species where model output contains a large amount of noise a 24 hour running average has been plotted ( $\geq C_3$  alkenes,  $\geq C_4$  alkanes and toluene). For isoprene an 8 hour moving average is shown in an attempt to include the diurnal variability but minimise the large amount of model noise from the plot.

### 4.9.1 Isoprene

Isoprene concentrations are highly variable in both the model and measurements, but overall there is some agreement between the two datasets as shown in Figure 4.19. There is a detailed discussion of the observations and concentrations in GEOS-Chem in chapter 6.

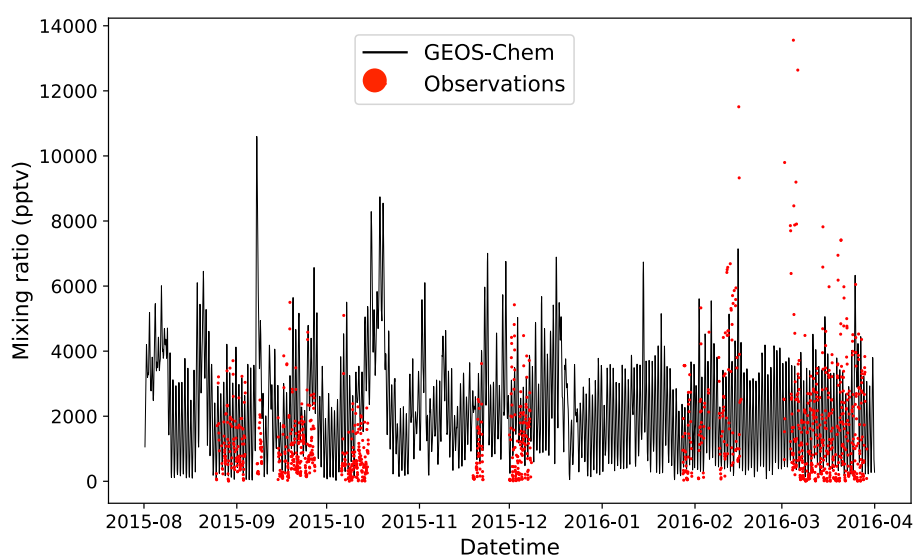


**Figure 4.19 Comparison between isoprene observations and GEOS-Chem**

#### 4.9.2 Small Alkanes

Figure 4.20 and Figure 4.21 show the comparison between the model and measured ethane and propane concentrations respectively. The high ethane and propane concentrations due to biomass burning are simulated by the model and discussed in chapter 5. The model predicts a significant biomass burning event in mid-August 2015, days before our observations start. Agreement during the background periods is good for ethane, with an observed mean concentration of 350 ppt. There is a small overestimation in the model for propane (mean observed background concentration 70 ppt) during these periods. This is discussed in chapter 5.

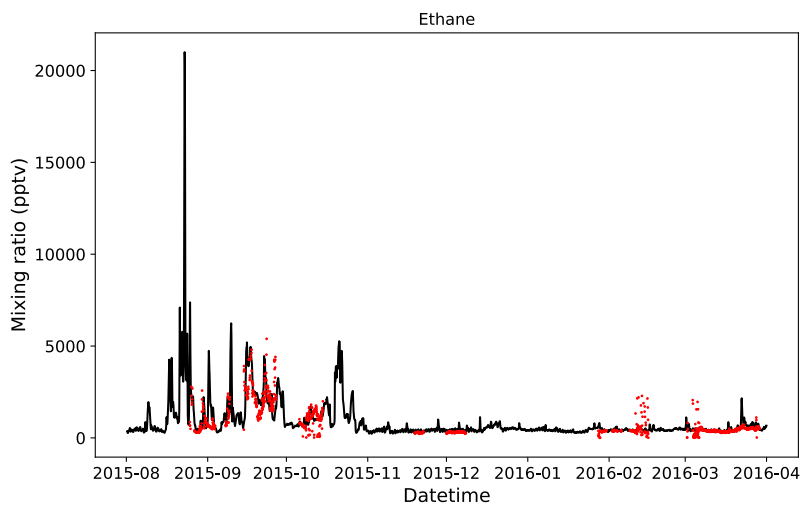


Figure 4.20 Same as Figure 4.19 but for ethane

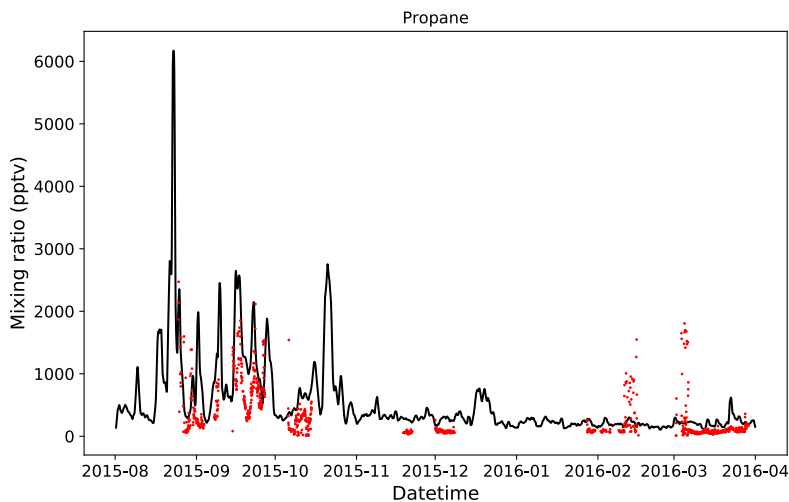
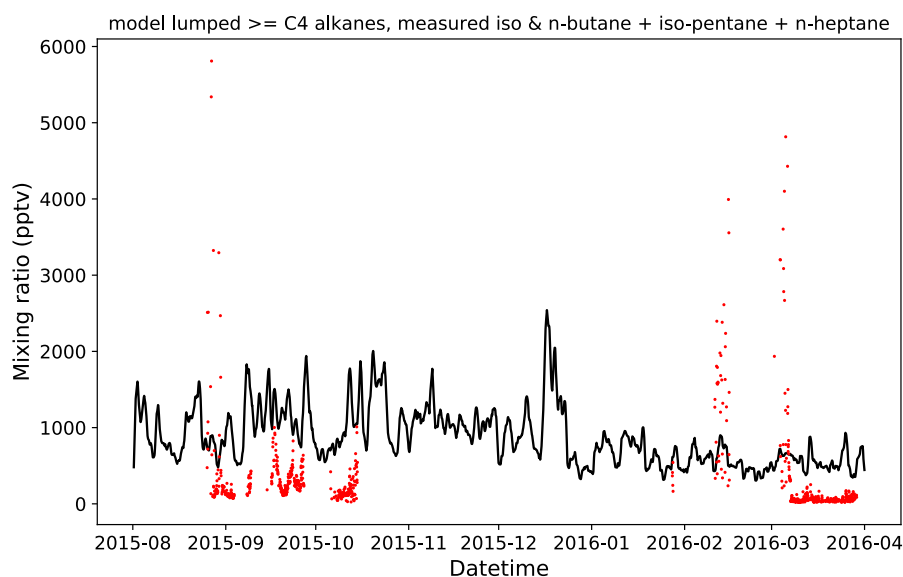


Figure 4.21 Same as Figure 4.19 but for propane

The model does not simulate enhanced concentrations in February and March when the NMF shows the importance of component 2. This suggests that the source of these enhanced observations is likely fairly localised in scale.

### 4.9.3 Other Alkanes

GEOS-Chem does not simulate the larger alkanes well. The model includes a tracer, which is all alkanes with 4 or more carbons lumped together. Therefore the sum of observed (iso- and n-butane, iso-pentane and n-heptane) is used for comparison. Given the poor agreement between the model and observations this group of compounds will not be discussed in later chapters.



**Figure 4.22** Same as Figure 4.19 but for the other alkanes. For the model this is alkanes with 4 carbons or more, the observations are iso & n-butane, iso-pentane and n-heptane

### 4.9.4 Alkenes

Figure 4.23 shows the comparison between model and measured alkene tracer. In the model PRPE is the lumped alkenes with 3 or more carbons, so this is compared to the observed propene and 1-butene. There is poor agreement between the observations and GEOS-Chem for the alkenes. With the model almost always overestimating the observations. Chapter 6 discusses this in more detail and

describes problems with the anthropogenic emissions in the grid box containing the measurement site and the biogenic emissions of propene.

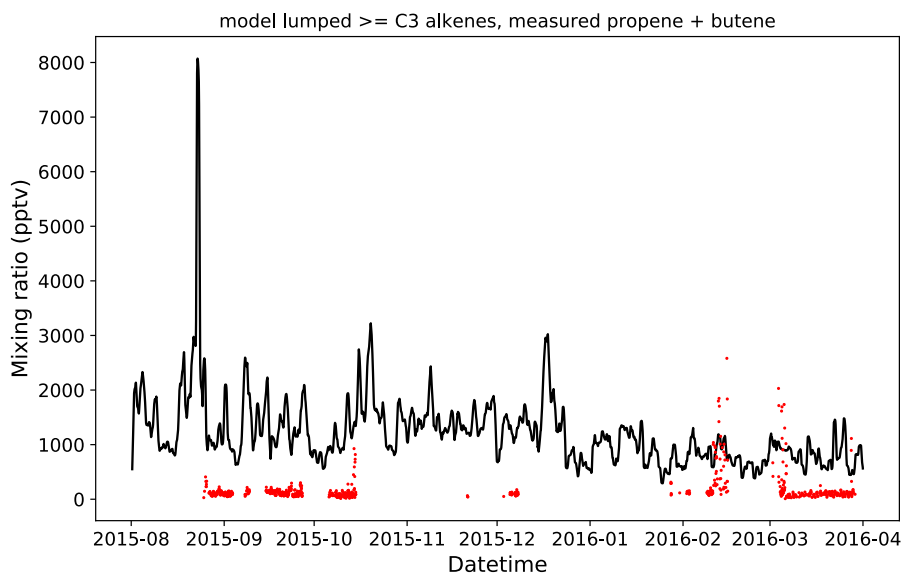


**Figure 4.23** Same as Figure 4.19 but for the alkenes. For the model this is alkenes with 3 carbons or more, the observations are propene and butene

#### 4.9.5 Aromatics

The model simulates well the observed background benzene concentrations ~80 ppt. The model does underestimate the concentrations during the biomass burning period, this is discussed in chapter 5. For toluene the model underestimates the observed concentrations for the background and biomass burning periods. This is discussed in chapter 5.

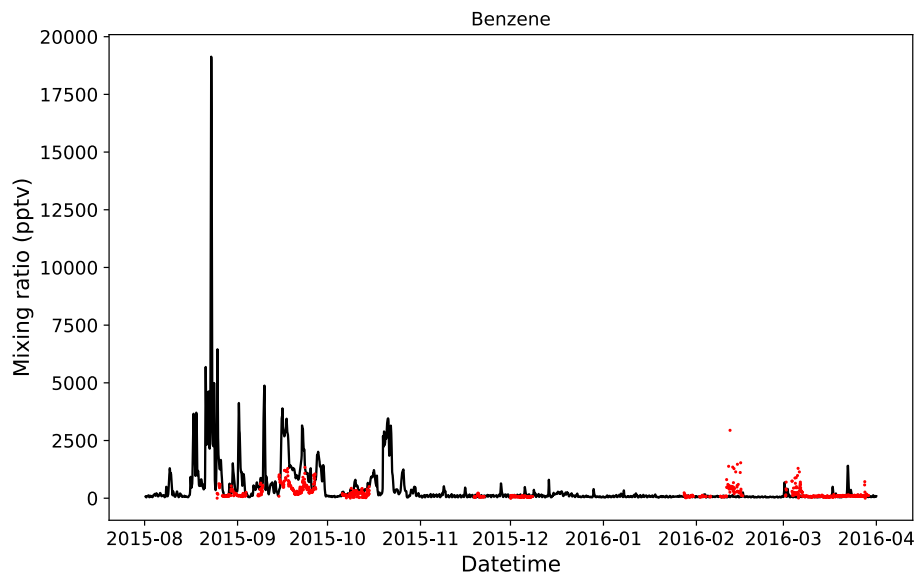


**Figure 4.24** Same as Figure 4.19 but for benzene

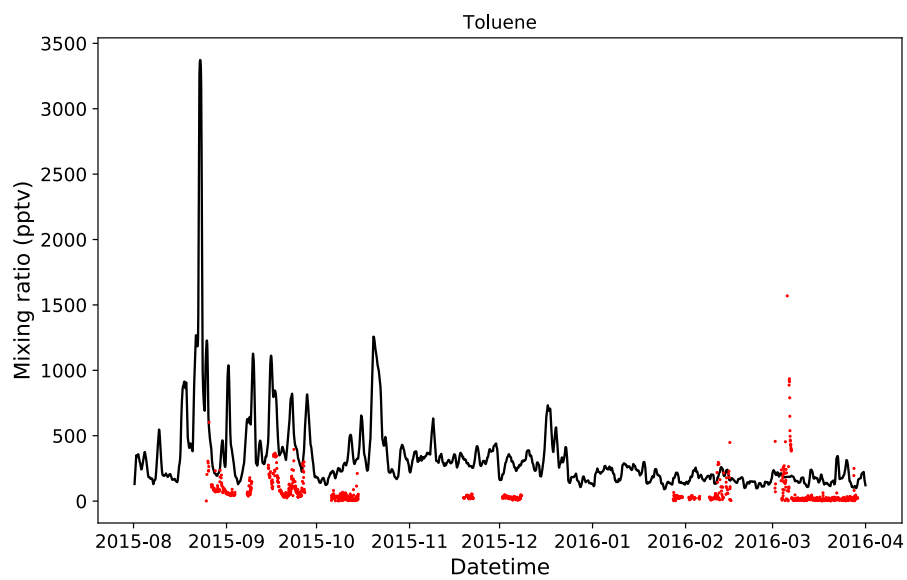


**Figure 4.25** Same as Figure 4.19 but for toluene

## 4.10 Summary of Model Observation Comparisons

To summarize, the model seems to simulate ethane well, it overestimates propane in the background periods. For alkenes and the larger alkanes the model overestimates compared with observations. The model overestimates benzene during the biomass burning periods and for toluene the model overestimates throughout the measurement period.

Although the model resolution used in this work is comparatively fine ( $0.5^\circ \times 0.625^\circ$ ) each model grid box represents a large area (300 million square meters) and the measurements were made at a single site. Given the location of the measurement site it seems reasonable to assume the measurements are representative of a remote tropical rainforest. However, due to the size of the model grid box it may be that it includes areas affected by anthropogenic emissions that would influence VOC mixing ratios within the box that is used for comparison with observations.

To demonstrate this, Figure 4.26 shows the box within which the coordinates of the measurement site fall (red line) and an adjacent box (blue line). The agreement with observations for ethane is better for the adjacent box but this agreement varies by species. One box does not consistently give better agreement with observations than the other. It appears that there is a possible overestimation of anthropogenic emissions in the area, leading to a higher than expected background value for some VOCs.

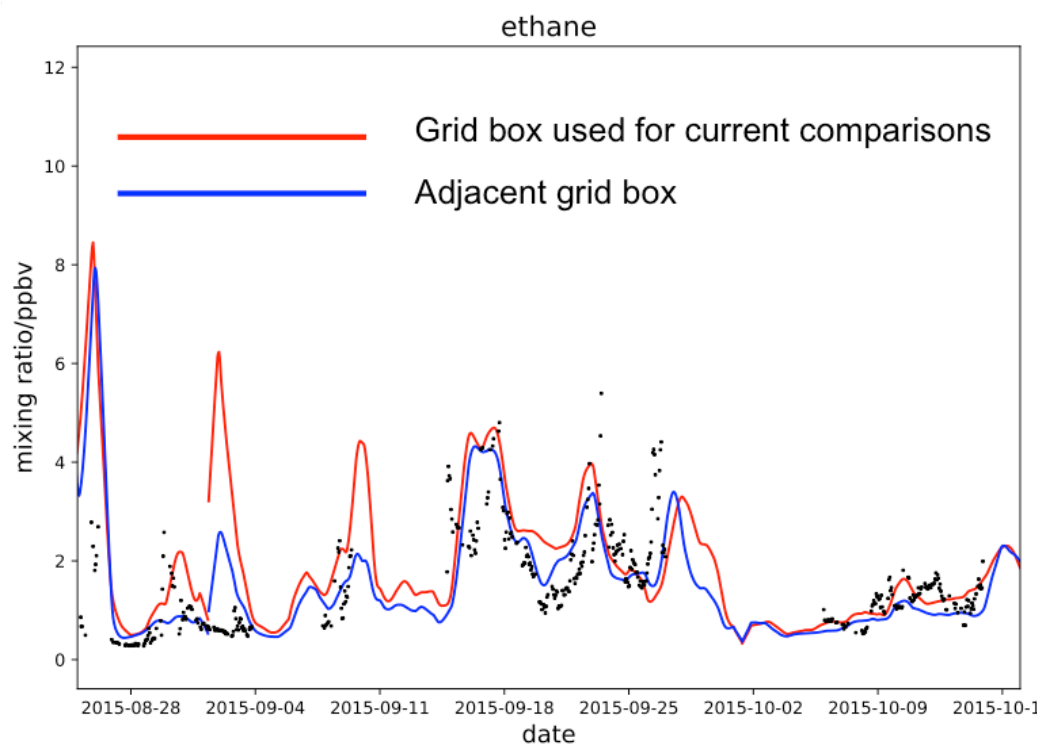


**Figure 4.26** Ethane mixing ratios for two grid boxes in the  $0.5^\circ \times 0.625^\circ$  Asia simulation. The line in red includes the coordinates for the measurement site. The line in blue is an adjacent grid box.

Scale factors to give better agreement between background observations and GEOS-Chem are calculated in chapter 5 to allow a fair evaluation of biomass burning emissions. A discussion of the relative effects of biogenic and anthropogenic sources in the measurement site grid box is given in chapter 6.

## 4.11 Conclusions

The mixing ratios of thirteen VOCs were measured between August 2015 and March 2016 at the Bukit Atur observatory, Malaysian Borneo. There are several periods of time with no observations due to instrumental difficulties. The mixing ratios generally agreed well with observations made in 2008 during the OP3 campaign using a similar instrument, giving confidence in the measurement technique despite the instrumental issues encountered.

Non-negative matrix factorisation analysis was used to identify the factors influencing the VOC mixing ratios. The optimum variables found for the analysis in

this work were a three component analysis using data normalised through division by the maximum value for each measured VOC. From this analysis the three components assigned to the data were a biomass burning period, background periods and periods influenced by a local, probably anthropogenic event. This analysis technique provided a useful approach for separating the dataset into different periods and in combination with an understanding of local chemistry and larger scale events within the tropics provides a useful technique for VOC source appointment.

GEOS-Chem was found to have mixed success in simulating the observations. For some species, including ethane and isoprene the model gave good agreement.

An unexpected result was the observation of increased mixing ratios for the majority of measured VOCs during the Indonesian biomass burning season. This has not been observed previously at this location. There also appears to be a series of short lived local events where a sharp increase in the mixing ratio of some VOCs is observed. This occurrence was also seen in the observations from the OP3 campaign. This is something that should be noted and investigated if possible in any future work in this area. Supporting meteorological measurement that were not available for this work may provide a clearer picture of conditions during these events. During most of the measurement periods isoprene was the dominant VOC and showed a strong diurnal cycle, as expected due to its biogenic origin and therefore being driven by meteorological conditions. The biomass burning and biogenic time periods will be discussed in the following two chapters.



## Chapter 5

### 5 Biomass Burning

#### 5.1 Introduction

The positive matrix factorization analysis in chapter 4 gave a component that was characterized by a large increase in the majority of hydrocarbon mixing ratios early in the dataset (September/October 2015) with lower values later in the time series. This is shown in Figure 5.1 for ethane, with the enhanced period shown in the red box. In this period ethane mixing ratios were  $1500 \pm 200$  compared with  $400 \pm 40$  ppt in the other periods. This component accounted for the highest fraction of the variability in the data with all hydrocarbons other than isoprene, propene and 1-butene showing significantly enhanced concentrations during this period.

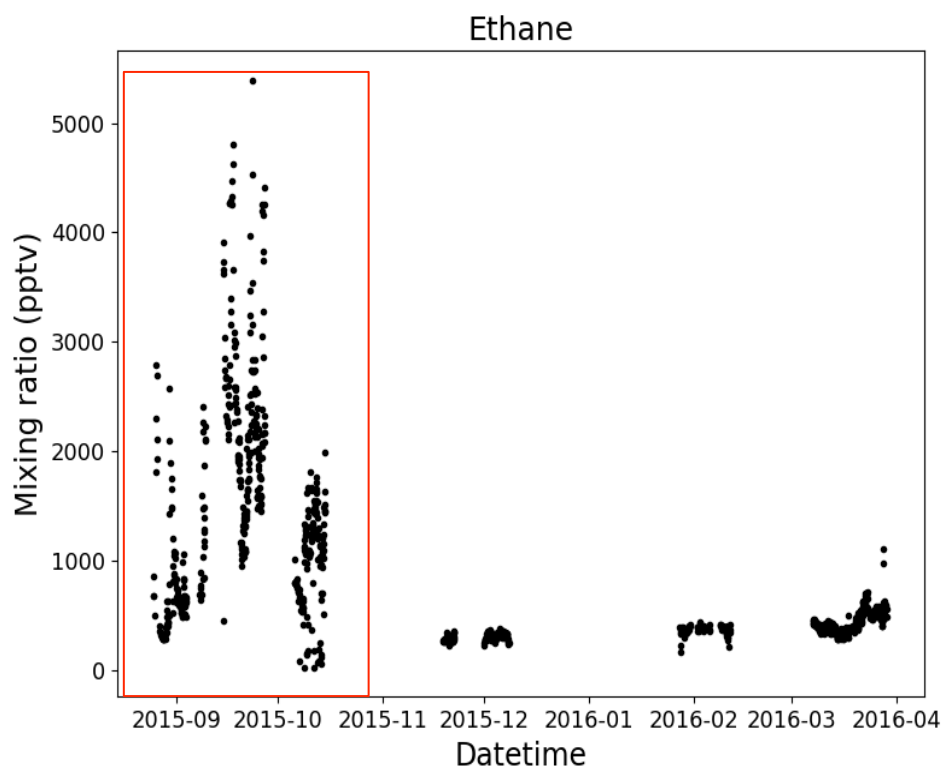
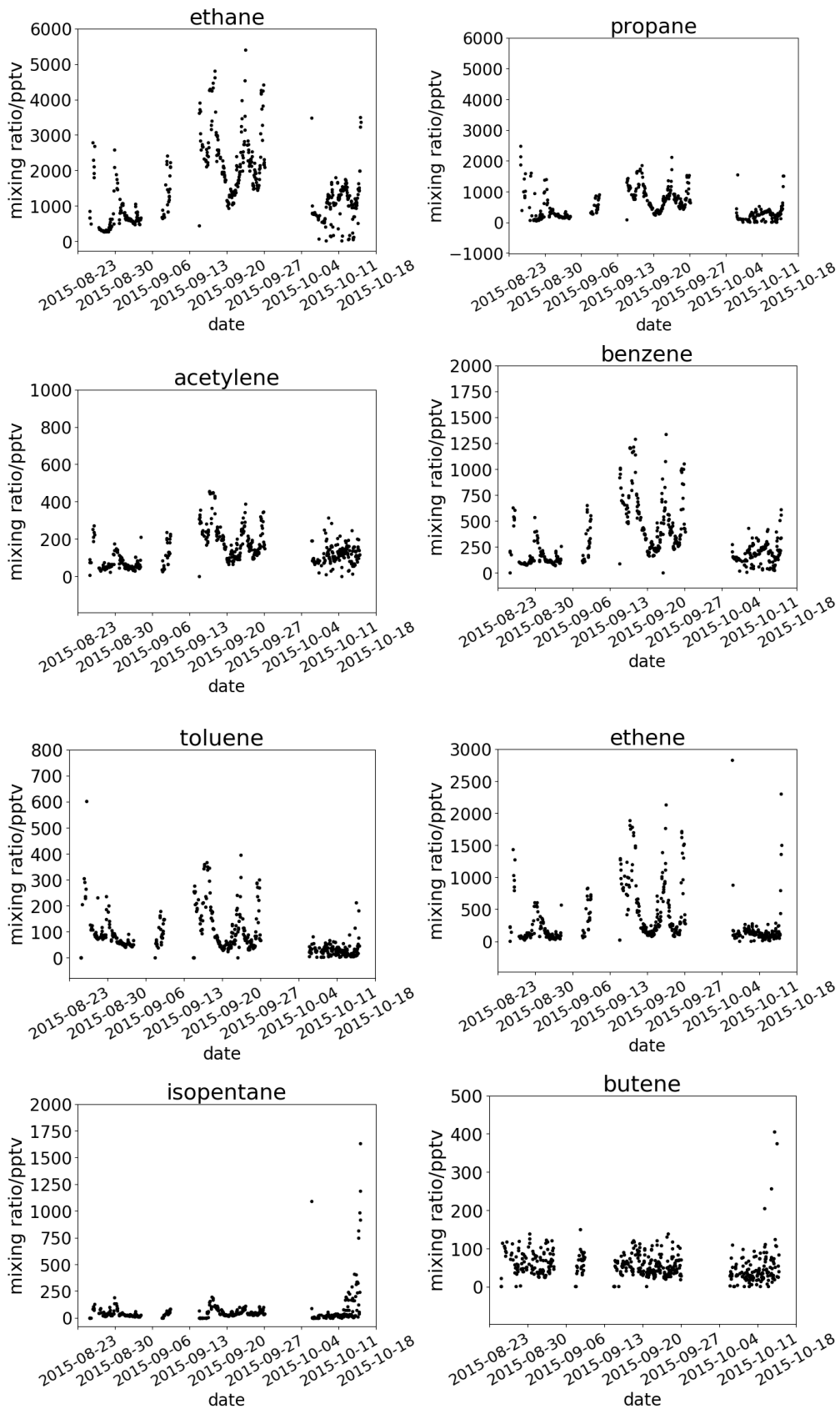
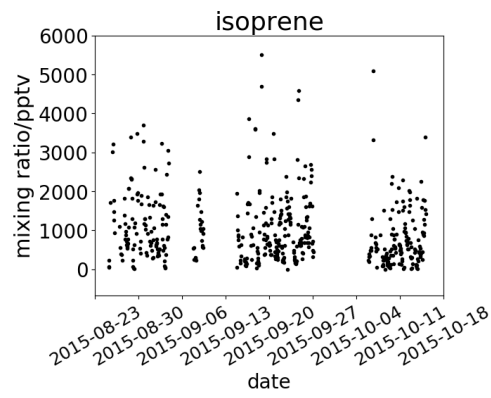
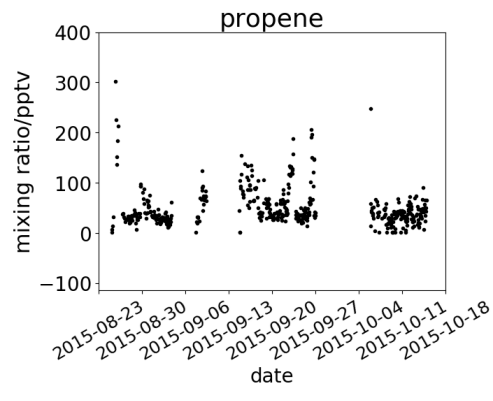
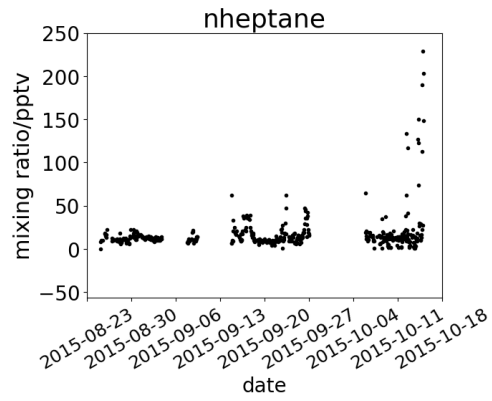
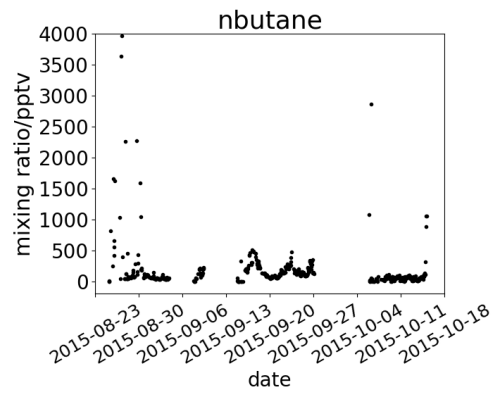
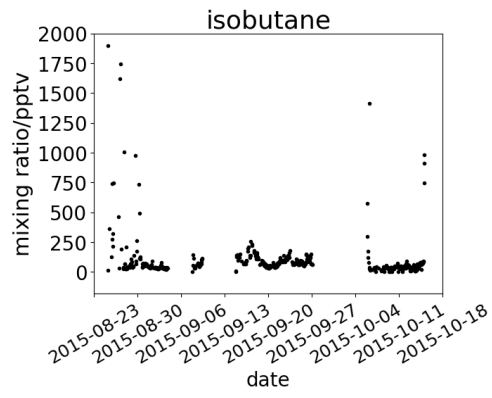


Figure 5.1 Time series for ethane measurements made as part of this work. This chapter focuses on measurements between August and October, where an enhancement in most VOCs was seen

Figure 5.2 shows the measurements for only the period associated with biomass burning (28<sup>th</sup> August - 14<sup>th</sup> October 2015), data in the red box above. Within this time period there is a high level of variability in the mixing ratios for individual VOCs. Table 5.1 shows the mean, median and inter-quartile range values for the biomass burning and background periods.



**Figure 5.2** Time series of all VOC observations over the period defined as being affected by biomass burning in the surrounding region. Continued on next page.



**Table 5.1 VOC mean, median and inter-quartile range mixing ratios during the background and biomass burning periods**

	Ethane	Ethene	Propane	Propene	Iso-butane	N-butane	Acetylene	1-butene	Iso-pentane	Isoprene	N-heptane	Benzene	Toluene	
Biomass burning	mean	1492	336	519	50	100	197	138	12	56	1015	16	308	81
	median	1315	163	363	39	60	87	122	7	35	737	12	231	56
	inter-quartile range	716-2043	99-357	225-745	29-60	36-88	53-172	77-178	5-12	22-60	407-1385	9-15	132-406	35-94
Background period	mean	351	66	72	65	16	18	33	10	14	1298	3	77	18
	median	345	55	68	59	13	15	31	6	10	831	2	75	15
	inter-quartile range	290-432	30-79	53-88	34-83	9-20	10-22	21-43	4-10	7-16	218-2016	2-3	61-93	9-24

In chapter 4 the increase in hydrocarbons was attributed to regional biomass burning. This was because a large increase was seen for ethane, benzene and toluene. These species are all known to be emitted by biomass burning, along with a wide range of other VOCs (Andreae and Merlet, 2001). In addition to this the 2015 biomass burning season was one of the worst on record and this coincided with the initial measurement period for this work (Field et al., 2016).

Biomass burning in Borneo and the surrounding areas occurs on a seasonal cycle. These burning events are most prevalent during the dry season, between June and November (Lestari et al., 2014). One of the most intense Indonesian biomass burning events in on record took place during the initial measurement period for this work, from late August to October 2015 (Koplitz et al., 2016) with the worst of this burning occurring during September and October. This event resulted in severe haze over many parts of South East Asia, primarily effecting Malayisa, Indonesia and Singapore (BBC news article (Porter, 2016)). During this time increased mixing ratios of most VOCs were observed in this work as shown in Figure 5.2.

Excluding isoprene, propene and 1-butene all VOCs show a similar pattern in the magnitude of the mixing ratios throughout this period. There are several periods where a sharp increase in VOC mixing ratio is observed followed by a return to lower values. During these periods the lowest mixing ratios are still generally higher then during the background measurement periods (November 2015 – March 2016).

In the next sections the sources and impact of the enhanced VOC concentrations are explored. Sections 2 and 3 use fire maps and trajectory frequencies to show that biomass burning over Indonesia has influenced the mixing ratios of VOCs observed at the Bukit Atur measurement site. Section 4 uses results from the GEOS-Chem model and the ECMWF's GFAS emissions to quantitatively evaluate understanding of VOC emissions from these burning events. Emission ratios from previous campaigns are then compared with those from this work and the GEOS-Chem biomass burning emissions inventory. Finally the effects of biomass burning emissions on ozone in GEOS-Chem are investigated, both for the measurement site and the wider region.

## 5.2 Fire Maps

To investigate whether biomass burning in Indonesia had an effect on observed VOC mixing ratios at the measurement site satellite based fire maps for times both with and without suspected biomass burning effects were generated. Fire maps were obtained using data from the moderate-resolution imaging spectroradiometer (MODIS) instrument on board the NASA Terra satellite (Giglio et al., 2003). Fire maps were accessed via the global forest watch website (2014).

Comparison of global forest watch fire maps for two differing periods in the time series (biomass burning and background, October and March 2015 respectively) showed a significant increase in the level of fires in the region during the biomass burning season are shown in Figure 5.3.

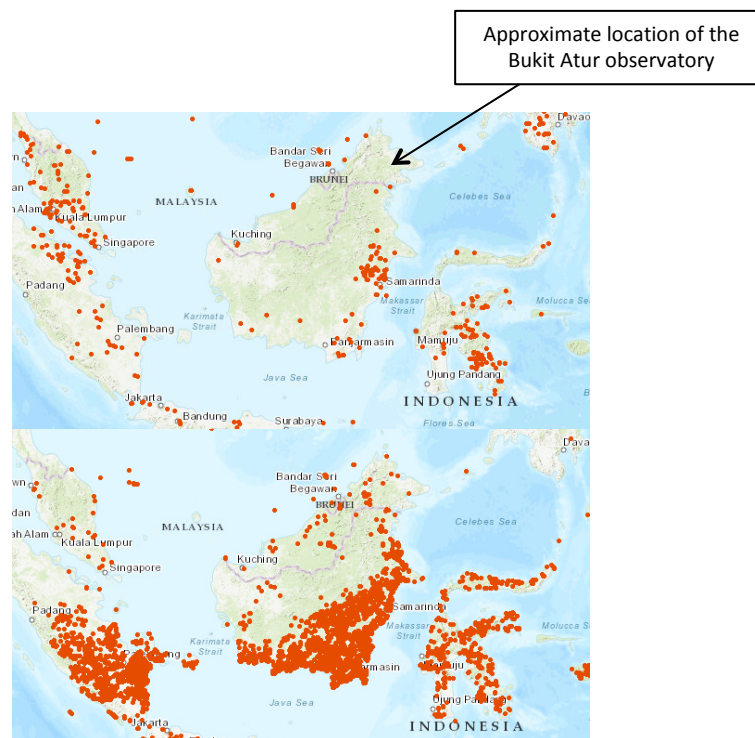


**Figure 5.3** A map of the area surrounding the measurement site showing fire events. The top panel shows a background period during the first week of January 2016. The bottom panel shows biomass burning occurring in the first week of October 2015 (bottom).

Throughout the periods identified as being dominated by biomass burning (August – October 2015) the active fire maps in the areas surrounding the measurement site showed a consistently high numbers of active fires. This is a strong indicator

that biomass burning was the cause of the observed increase in mixing ratios for most VOCs.

To better understand the biomass burning this period has been split into a number of shorter periods. Figure 5.4 shows the ethane observations divided into six individual periods. Figure 5.5 shows the satellite derived fire maps for each of these periods.

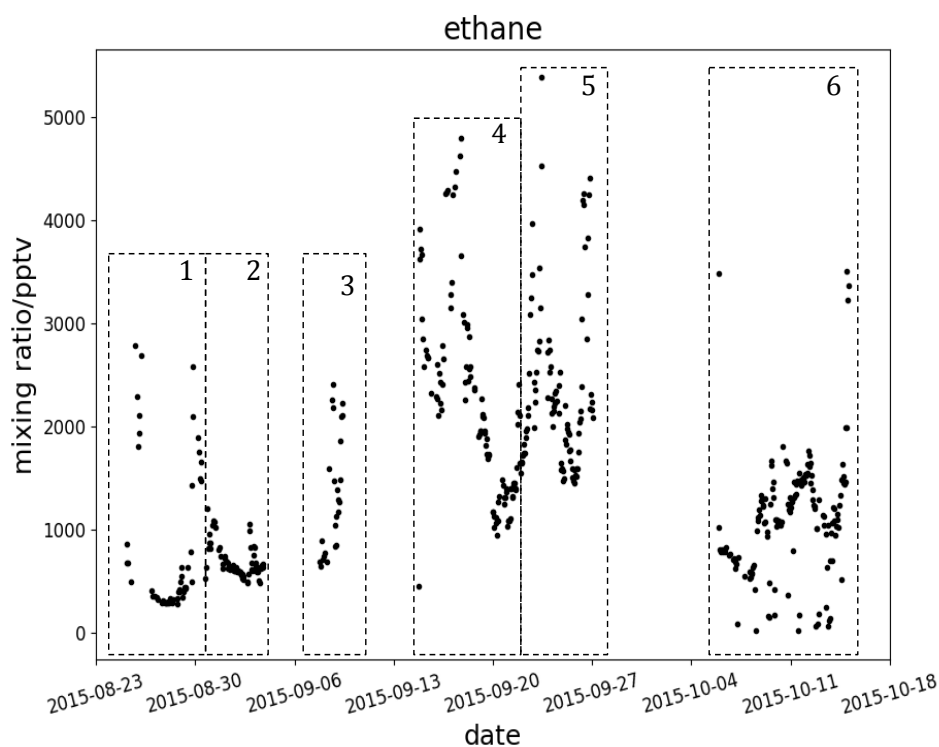


**Figure 5.4 Ethane time series over the biomass burning period, divided into sections by distinct changes in VOC mixing ratios**

It appears that during periods five and six the density of active fires on the more southerly side of the island of Borneo is lower than in previous periods. The trajectories shown in section 5.3 show that the air is generally not travelling over this area and so this should not substantially affect mixing ratios observed at the site. Period six also shows a greater number of fires localized to the measurement site than most of the other periods. The lack of distinct changes in the burning maps does not help to explain the variability observed in VOCs during this period. This suggests that variability in VOC concentrations is being driven by changes in the meteorology. For this, air mass frequency trajectories will be used to determine the origins of the air mass arriving at the during these periods.

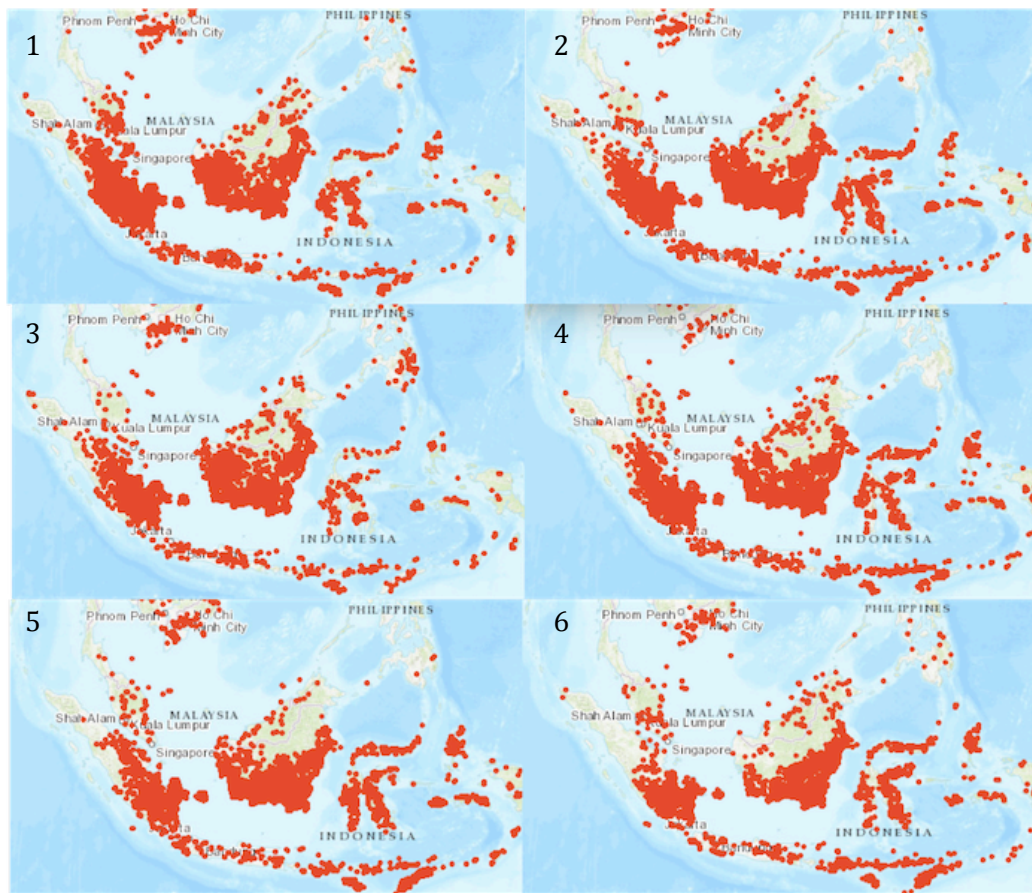


**Figure 5.5** Fire maps for the periods shown in Figure 5.4. For periods shorter than one week fire maps for seven days are shown so as not to give a downward bias to the number of active fires by the smaller number of days.

### 5.3 Air Mass Trajectories

Back trajectories calculate the origin of an air mass arriving at a chosen site from wind vectors (Stein et al., 2015). In this work the HYSPLIT model was run for trajectory frequencies using Global Data Assimilation System (GDAS) global meteorological data at 0.5° resolution. For the trajectory frequency method used in this work, a starting location was selected and trajectories were run every three hours over a total model run time of 48 hours. The trajectory starting height was 250 m above ground level. Once all trajectories are calculated trajectory densities were calculated from the number of trajectory endpoints per grid cell as a percentage of the total number of trajectories. The trajectories were run online using the HYSPLIT archive model (Stein et al., 2015, Rolph et al., 2017). The periods referred to here are those shown in Figure 5.4.

Trajectory frequencies for the periods shown in Figure 5.4 are discussed below.

### **5.3.1 Period 1**

The first measurement period showed initial high VOC concentrations, followed by a sharp decrease to similar concentrations as the background periods and then another sharp increase. Figure 5.6 shows the trajectories for each day during this period. Initially the air mass is coming from the South of Borneo, an area with a high number of fires, Figure 5.5. Then the direction of the air mass changes direction coming from the East mainly over the sea so there is little burning. Towards the end of the period the air mass returns to travelling from the South. The variability of VOC concentrations over this period seems to correlate with the changing direction of the air mass.

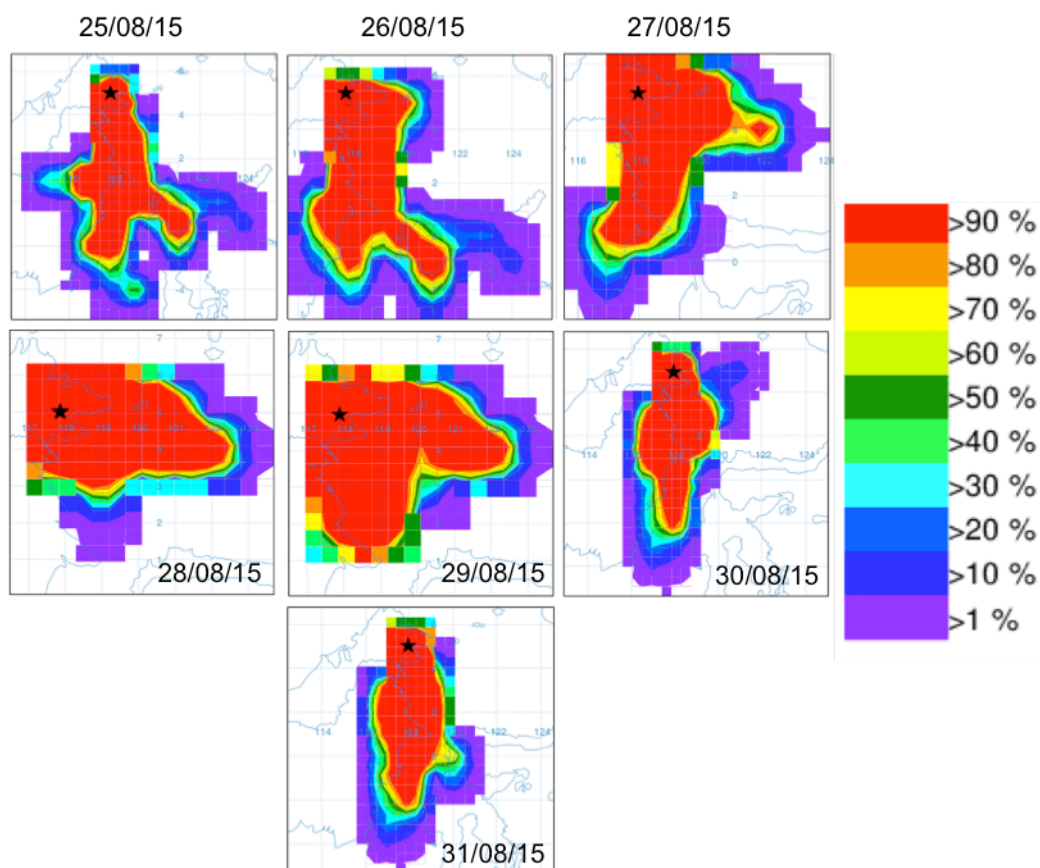


**Figure 5.6 Trajectories for period one. From left to right are trajectories ending on each day between 25<sup>th</sup> and 31<sup>st</sup> August. The black star represents the approximate location of the Bukit Atur observatory, where measurements were made for this work.**

### 5.3.2 Period 2

During this period the VOC mixing ratios were relatively low and stable. Trajectories over this week (Figure 5.7) show that the air masses were generally coming from the same southerly direction and covering a similar area. The area includes the edge of the Indonesian Borneo biomass burning zone. There was a small increase in concentrations on the 2<sup>nd</sup> September, although no strong change was seen in the direction of the trajectory.

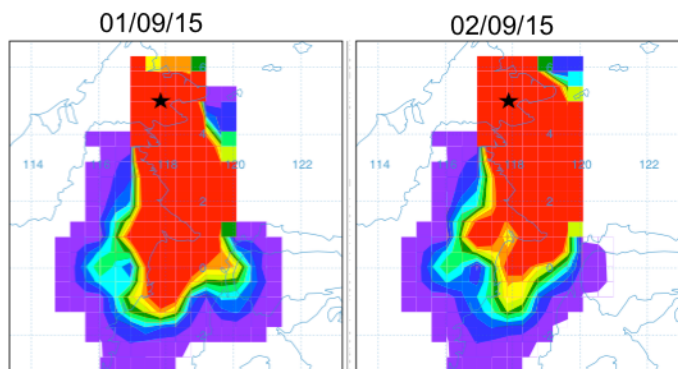


**Figure 5.7** Back trajectories run under the same conditions as described previously, finishing on 01/09/2015, 02/09/2015. These plots show that over this period the air mass is travelling over a similar area.

### 5.3.3 Period 3

A sharp increase in VOC mixing ratios compared to the previous weeks was seen on 8<sup>th</sup> and 9<sup>th</sup> of September. This increase coincides with a change of area over which the air mass travels. On the 8<sup>th</sup> September the air has travelled from further inland in Indonesian Borneo, so travels over a greater area of burning. The following day the area covered by the back trajectory covers more inland area than previous weeks but in addition to this there is also air travelling from the Indonesian islands, an area with active fires. These two factors combined likely lead to the observed increase in VOC concentrations.

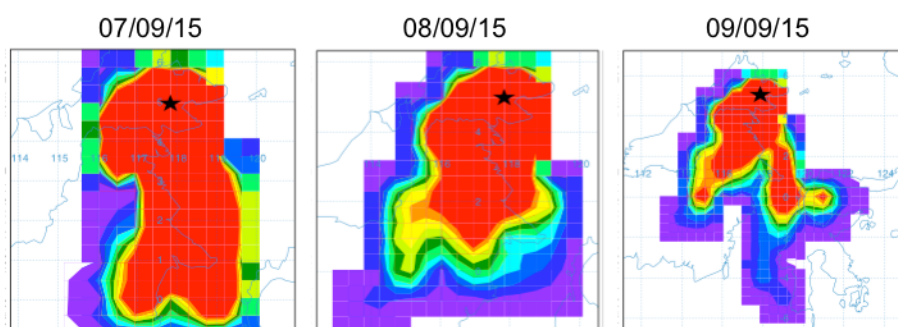


**Figure 5.8** Back trajectories, under the same conditions as the previous two figures but finishing on 7<sup>th</sup>, 8<sup>th</sup> and 9<sup>th</sup> of September

### 5.3.4 Period 4

This period showed a high level of variability, with VOC mixing ratios near to the maximum observed values during this work but also included days where the mixing ratios were much lower.

From the back trajectories in Figure 5.10 it can be seen that there is a large difference in the areas covered by the air mass on different days. Initially an area South of the measurement site covering some of the areas of biomass burning in Indonesian Borneo is shown. As the week progresses the source of the air mass becomes much more localised, covering a smaller area that covers Malaysian Borneo and the Celebes Sea. At either end of the week the VOC concentrations are high due to the incoming air travelling over areas of biomass burning. Whereas during the days where a smaller more localised back trajectory is calculated, a sharp drop in observed VOC concentrations is seen. During these periods the observed mixing ratios for most species remain higher than throughout the background periods. This could be the result of such high mixing ratios in the previous days, especially for the longer lived species.



Figure 5.9 Map showing the areas surrounding Borneo, highlighting the Celebes sea where the air mass travels over during this period

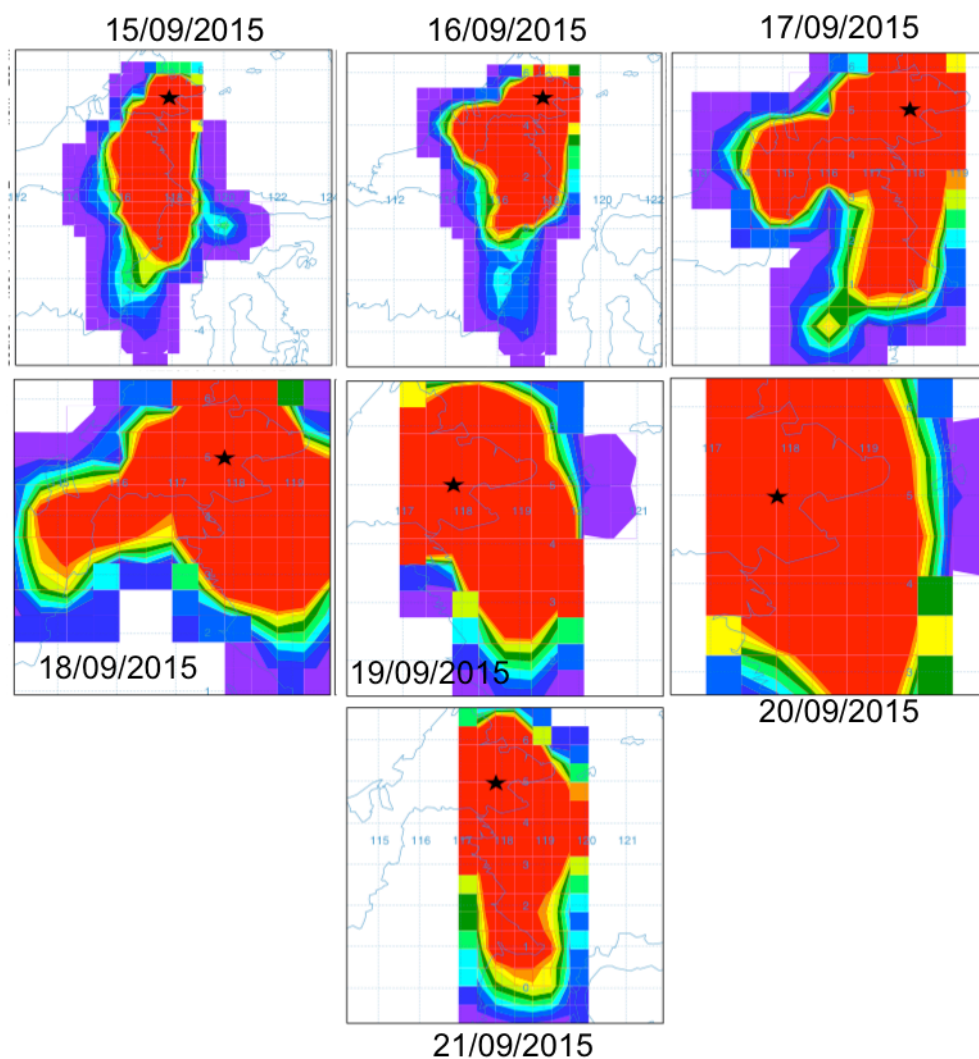


**Figure 5.10 Back trajectories run daily between 15<sup>th</sup> and 21<sup>st</sup> September**

### 5.3.5 Period 5

The early part of this week showed a strong increase in VOC mixing ratios with the maximum values over the entire dataset observed on 23<sup>rd</sup> September. In the following days the VOC mixing ratios fall, although values remain greater than during the background periods. The change is probably due to the air mass travelling over a more localized area covering less of the biomass burning area. During these days the air mass travels from the West over some active fires that are in closer proximity to the measurement site than the fires in Indonesian Borneo. This, combined with the more stagnant air mass not removing VOC from

the previous days at the site, may explain why increased mixing ratios were still observed.

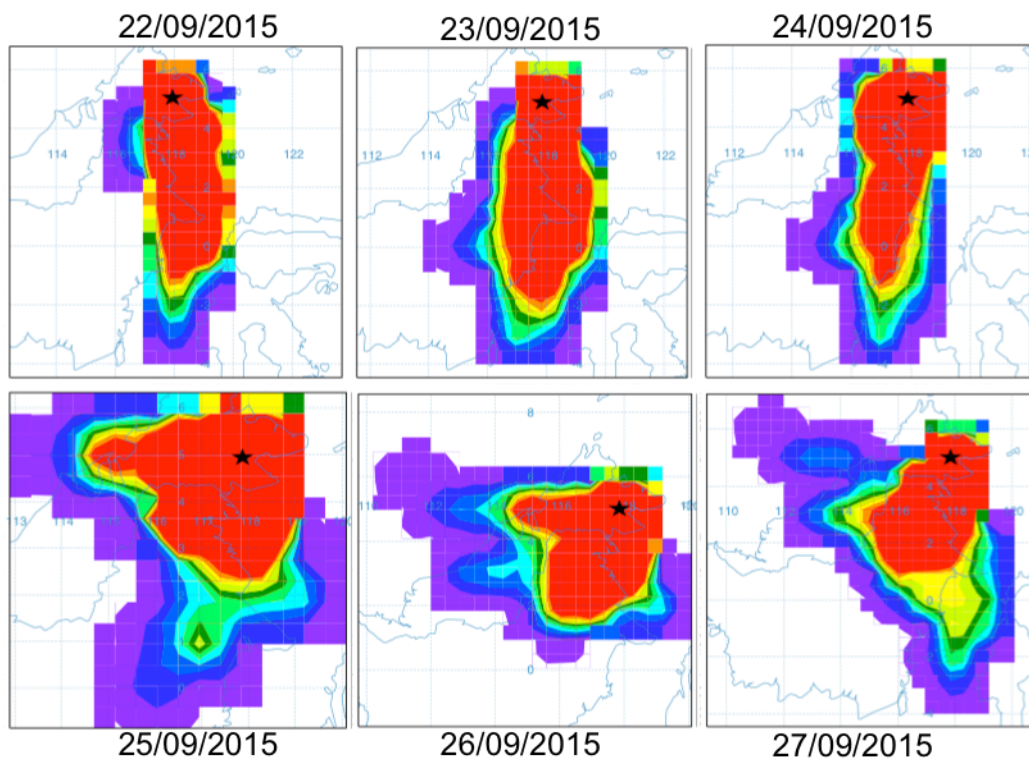


Figure 5.11 Back trajectories between the 22<sup>nd</sup> and 27<sup>th</sup> September

### 5.3.6 Period 6

This period covers the final observations in the biomass burning period. During this period VOC mixing ratios are lower than the peak observations with a large amount of variability, including some very low readings. The back trajectories show that the origins of the air masses over this time are more localized than during previous periods. Mixing ratios were generally higher than during the background periods. Unlike the other biomass burning periods the air mass does not pass over the main biomass burning regions in Indonesian Borneo. There are however active fires in Malaysian Borneo, closer to the measurement site. This may be the cause of increased VOC mixing ratios. The air masses have not travelled as far as in earlier periods, this suggests that the surrounding air is more stagnant during this time. This may have led to the sustained higher VOC mixing ratios observed as the biomass burning VOC were not transported out of the area as quickly. During this time the enhancement in VOC mixing ratio is more prominent for the longer lived VOC such as ethane propane and benzene. This supports the

idea that a lack of mixing and transport out of the area combined with more local burning is the cause of increase VOC mixing ratios.

When combined, the fire maps and back trajectories indicate that biomass burning was the source of increased concentrations of most VOCs during this period. It also shows that the meteorology rather than the density of fires drives variability in VOCs over this time period.

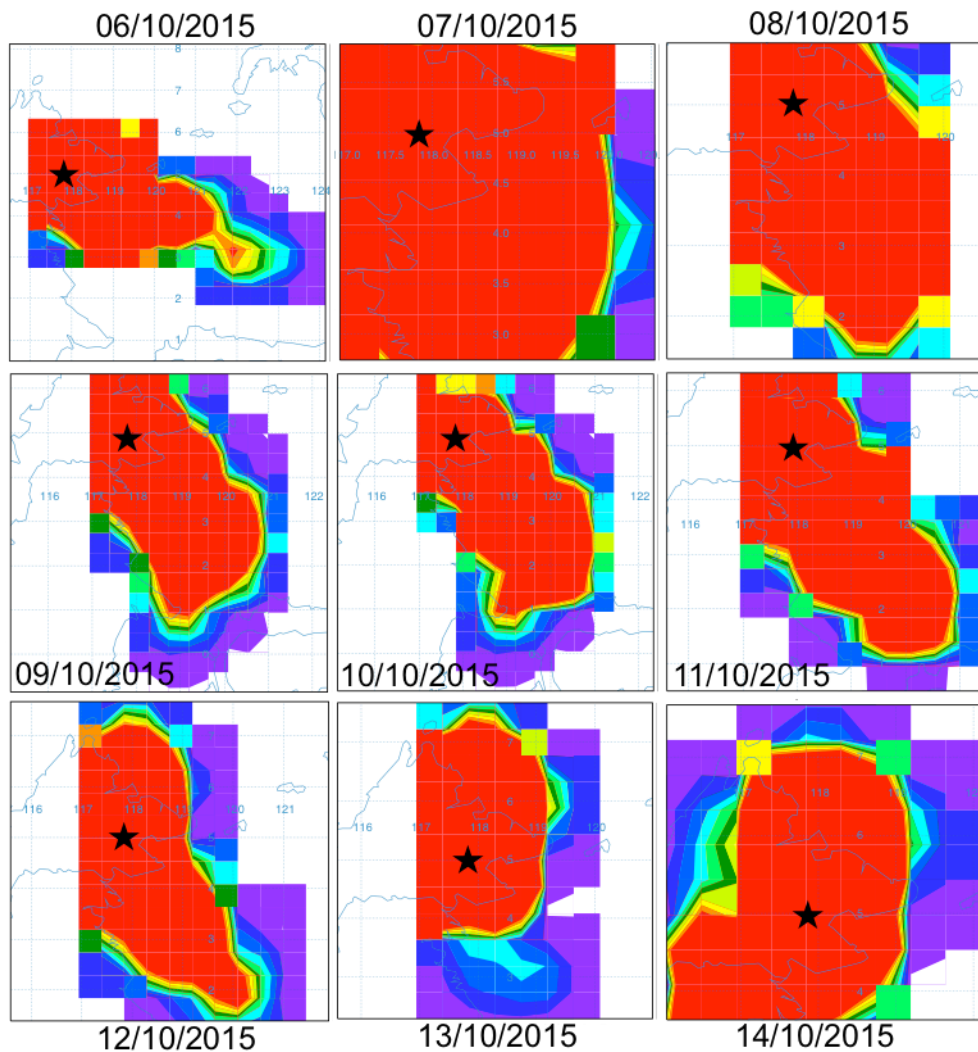


**Figure 5.12** Back trajectories for the final period of the biomass burning period. Trajectories were run daily between the 6<sup>th</sup> and 14<sup>th</sup> of October

## **5.4 Comparison with known biomass burning events**

A difficulty for this work in linking the observed increase in VOCs with biomass burning events is a lack of co-measurements. For most biomass burning studies elevated CO/CO<sub>2</sub> levels identify specific plumes from the burning events and emission ratios are scaled to CO. Unfortunately there are no CO/CO<sub>2</sub> measurements supporting this work. In addition to this typical biomass burning tracers such as furan and furfural are not measured using gas chromatography with flame ionization detection (Lewis et al., 2013). However, previous studies of biomass burning events in South East Asia and other locations allow for an understanding of which VOC species are emitted by biomass burning and whether these are the VOCs that show an enhancement in this work. The ratios of different VOCs to each other released by burning events will be compared in different studies to understand key chemical signatures for biomass burning events.

## **5.5 Kalimantan Peat Fires**

During the 2015 biomass burning season a study in central Kalimantan, Indonesian Borneo measured emissions from peat fires (Stockwell et al., 2016). The peat fires can occur deep underground and are often slow burning and difficult to extinguish. These fires can have large impacts on both local and regional air quality.

Trace gas measurements of a wide range of VOCs, including all those measured in this work were made during September and October 2015. VOCs were measured using a Fourier transform infrared spectrometer and whole air canister sampling. The canister samples were analysed using gas chromatography with a range of detectors.

Most of the VOCs that showed an enhancement in this work were one of the twenty trace gases with the highest emission factors in the peat fire plumes. This includes ethane, benzene and acetylene. Stockwell et al, (2016) showed that many VOCs show an enhancement compared with background levels during the peat fires. All VOCs that showed an enhancement in this thesis were also reported as having elevated levels from the peat burning. Isoprene and propene showed an enhancement in the Stockwell et al, (2016) peat burning study but in this thesis

showed no significant enhancement during this period. This may be due to their high reactivity and short lifetimes compared with ethane or benzene that do show sustained increases in the observed mixing ratios. Given that the major source of biomass burning VOCs at the Bukit Atur measurement site seems to be from Kalimantan observing increased mixing ratios of the most prominent peat burning VOCs is a good indicator that these raised levels are the result of biomass burning.

## 5.6 Emission ratios

In 2008 as part of the Arctic Research of the Composition of the Troposphere from Aircraft and Satellites (ARCTAS-B) project measurements of a number of VOCs in addition to other important trace gases such as CO and NO<sub>2</sub> were made in boreal fire smoke plumes. Samples were collected using canisters and analysis done using gas chromatography with a number of detectors including flame ionization detectors and a quadrupole mass spectrometer detector.

Another project made measurements of a number of VOCs over Eastern Canada in 2010 as part of the BOREal forest fires on Tropospheric oxidants over the Atlantic using Aircraft and Satellites (BORTAS) campaign (Lewis et al., 2013, Palmer et al., 2013). Canister samples collected from a whole air sampling (WAS) system were analysed using a gas chromatogram with flame ionization detection.

Both of the studies above reported emission factors of VOCs to CO (pptv/ppbv). Emission factors to CO could not be calculated for this work due to the lack of availability of CO observations. The VOC to CO (pptv/ppbv) emission factors reported were used to give a VOC to propane (pptv/pptv) emission factor to allow comparison between the work from this thesis and previous studies. This value was obtained from the ratio of each VOC to CO emission factor to the propane VOC to CO emission factor. The emission ratios for this work were calculated as VOC mixing ratio to propane mixing ratio all in pptv.

For the peat fire study (Stockwell et al., 2016) emission factors were given in units of grams of species emitted per kg of biomass burnt. Emission ratios from this thesis were calculated relative to propane.

The studies chosen for this comparison both made measurements of boreal forest fires, this is not the most desired comparison since this work focuses on biomass burning in a tropical forest. However, there is a lack of reported emission factors in units of mixing ratio to mixing ratio from other forest types.

### **5.6.1 Comparison of Emission Ratios**

Emission ratios to propane for several VOCs in pptv/pptv are shown in Figure 5.13. Values are shown for the Lewis et al., (2013) and Simpson et al., (2011) studies both conducted in boreal forest burning in Canada. These values are reported with an error bar showing the range of possible values for the emission ratio to propane. This range was calculated from the ratio of the minimum and maximum values for each VOC and the propane emission ratio to CO from the reported uncertainty in individual emission ratios.

Emission factors from the (Stockwell et al., 2016) study conducted on peat burning are given with the error bar representing the reported standard deviations propagated as the square root of the sum of the squares for each VOC and propane. The (Andreae and Merlet, 2001) report gives some emission factors as single values and others as a range of possible values. The values used are for tropical burning. The bar represents either the single or minimum reported value with the bar representing the maximum value if reported as a range. The GFAS values are taken from the emission files used in GEOS-Chem. Details of how the values are calculated are given in section 5.7.

There are two emission ratios reported for this work, the first is calculated from the measured mixing ratios of each VOC to propane. The error bars represent the range of possible values calculated as the ratio of the minimum and maximum values for each VOC and propane. The second emission ratio shows the same data but corrected by accounting for the loss of each VOC by OH over the estimated three day period it takes for the air mass to be transported from the area of burning to the measurement site. The three day loss period was used due to the back trajectories showing air travelling over the active fires and to the site over ~three days.

Not all measured VOCs are shown here. For some species emission ratios are not available from other studies. In the case of propene the emission ratio calculated from the new measurements was much greater compared with previous measurements. It is thought that this was due to a strong biogenic propene source at the measurement site. When a correction factor for loss by OH was applied to the ratio the emission ratio was larger than expected. This is likely due to the measured propene mixing ratio being dominated by biogenic sources with little biomass burning influence. Thus, when the correction factor was applied an artificially high emission factor was calculated, particularly given the rapid removal of propene by OH.

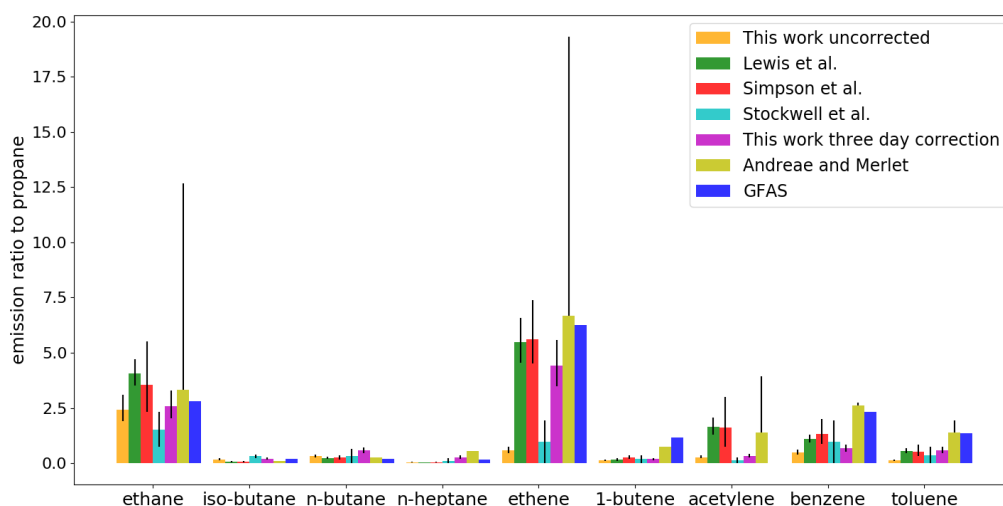


**Figure 5.13 Emission ratios of different VOCs to propane calculated for this work and previous studies by Lewis *et al.* (2013) and Simpson *et al.* (2011), both in Canada. Stockwell *et al.* results from peat burning in Indonesian Borneo and Andreae and Merlet, which reports values from a number of studies in tropical rainforests. A value for this work but corrected for three days of loss via OH has also been included.**

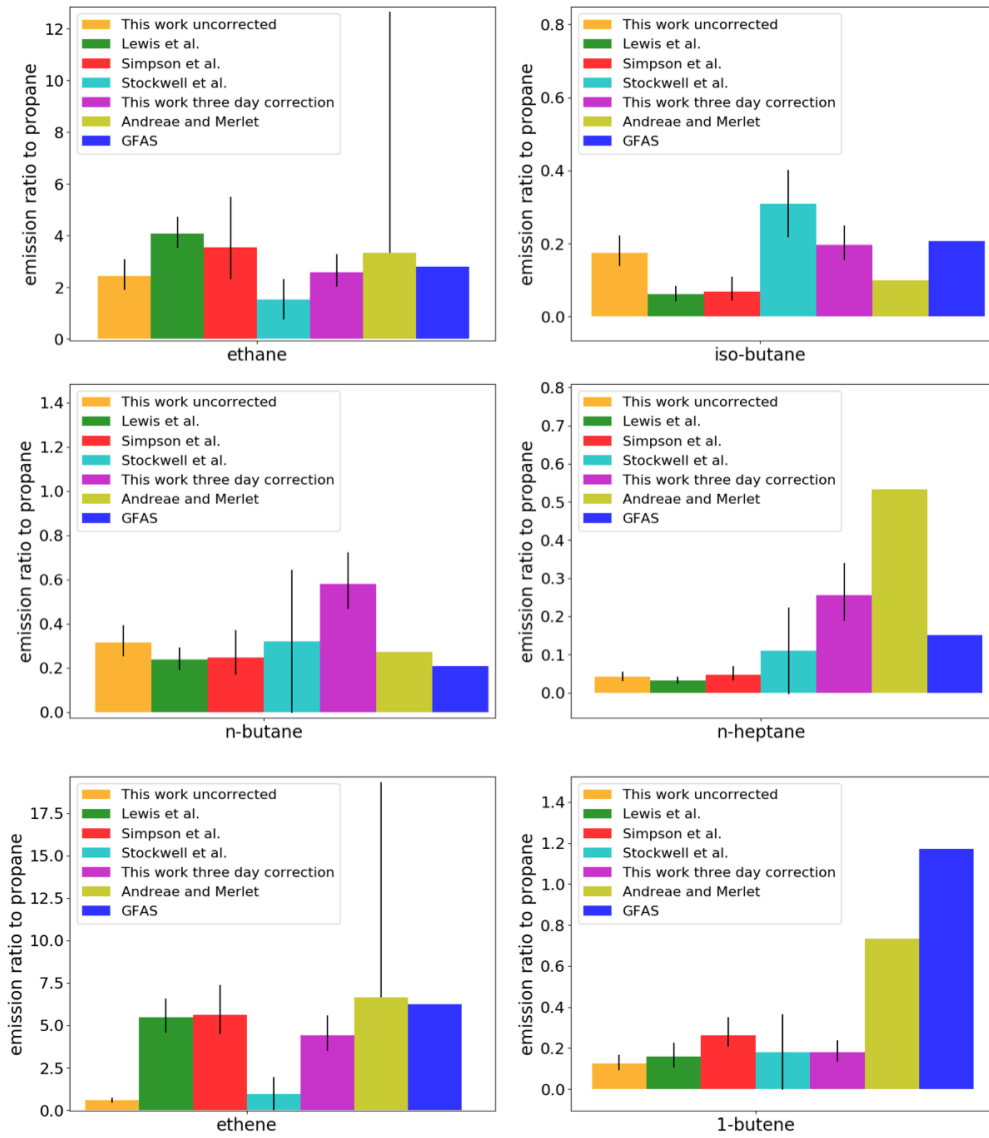
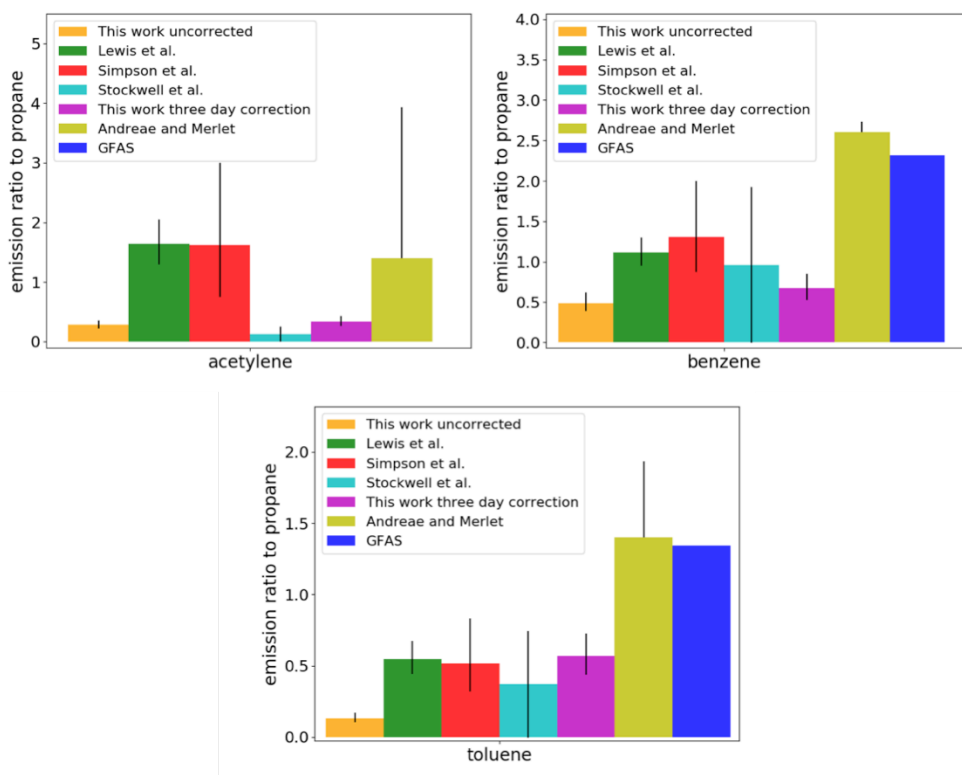


**Figure 5.14 Emission ratios for each VOC in Figure 5.13, shown at a greater zoom level for individual VOC. Continues on net page.**



For most VOCs there is fairly good agreement in the emission ratios from all observational studies. This is particularly true for ethane, although the maximum reported value for Andreae and Merlet (2001) is over double the highest values of the other studies. This may be because the Andreae and Merlet (2001) work reports values from all types of tropical burning.

For iso-butane the peat burning showed a higher emission ratio than the boreal or tropical burning. This value is in better agreement with the value calculated from this work, indicating that the measurement site is influenced by peat burning.

The emission ratio from this work for n-butane is higher than reported in all other studies. However, the uncertainty on the peat burning ratio is large and the value from this work falls within the upper uncertainty of the Stockwell study.

For n-heptane the emission ratio from this work is higher than either of the boreal studies but falls between the peat and tropical burning values. Again the value from this work falls within the uncertainty of the peat burning study.

The ethene value from this work shows good agreement with the boreal and tropical burning studies but is much higher than is observed from peat burning.

1-butene shows good agreement with all studies excluding the tropical burning which reports a much higher value.

The acetylene emission ratio for this work is substantially lower than reported for the boreal or tropical burning. However, it shows good agreement with the peat burning study. This is a strong indicator that peat burning is influencing the site.

Benzene and toluene both show fairly good agreement with the boreal and peat burning studies. The values from the tropical burning are much greater.

Overall comparison of emission ratios would suggest that the measurement site is influenced, at least in part by peat burning. The back trajectories show that the air mass arriving at the site has travelled on some days over Kalimantan (Indonesian Borneo) and this is an area known for peat burning. Some agreement of emission ratios with the boreal and tropical burning studies would suggest that both peat burning and forest fires influence the measurement site.

## **5.7 GFAS Emission Ratios**

Emission ratios were calculated for the Global Fire Assimilation System (GFAS) emission input files, which was used in the GEOS-Chem simulations for this work. The files for August – October 2015 were used as these months were found to be the peak of the biomass burning season in South East Asia. The final emission ratios were calculated from the average of a single day from each of the months. Emission ratios for several other days in each month were calculated to ensure a fair representation of model values. This included days where the biomass burning emissions peaked and where the influence was minimal, the variability within these values was small so it was felt this method gave a fair representation of model emission ratios. It should be noted that the input files are at  $1^\circ \times 1^\circ$  resolution on a global scale. Therefore calculated model emission ratios are averaged over the whole globe. During these months the burning was most prominent in the tropics with generally the highest emission ratios found in Indonesia.

The blue bars in Figure 5.14 show that for most species model emission ratios were higher than the observations from this work and the Stockwell peat burning study. The exception to this is the butanes, where all observations are higher than the model. This work and the peat burning study found emission ratios, particularly for iso-butane that were higher than the boreal burning. The emission ratios for butanes in Indonesia were calculated for a couple of days during August and this gave an emission ratio of  $\sim 0.05$ , it would appear that GFAS strongly underestimates the butane emissions, particularly from peat burning.

For ethane there is good agreement between GFAS and observations for this work and the Andreae and Merlet study. This suggests that emissions of ethane from biomass burning are well characterized from observations for implementation in to the model. The model mixing ratio for ethane also shows good agreement with observations suggesting this VOC is well understood. Given its long lifetime and global distribution this is probably expected.

The ethene GFAS mixing ratio shows good agreement with the Andreae and Merlet study and agrees with the values from this work within  $\sim 25\%$ . These values are all much greater than is observed from the peat burning. Given that it is expected that the burning emissions affecting the measurement site are a combination of peat and forest burning, the model emission ratio for ethene seems appropriate, although possibly too high depending on how large an influence peat burning has on the air mass arriving at the measurement site.

For benzene and toluene there is fairly good agreement between the peat burning and observations from this work; however GFAS and Andreae and Merlet values are much greater. The latter two emission ratio values show good agreement. This suggests that the emission ratios for these species globally in the model are appropriate but too high for the region of interest for this work. This is reflected in the model overestimating the mixing ratios for both of these species.

There is a similar pattern for the butenes, although butene is not a tracer in GEOS-Chem so a comparison of observational and model mixing ratios is not possible. All observations emission ratios excluding the Andreae and Merlet study, show good

agreement with each other. This strongly indicates that the model emission ratio for butenes is too high.

The model emission ratio for heptanes shows good agreement with both the observations from this work and the peat burning study. The Andreae and Merlet study gives a higher emission ratio. Considering uncertainties the GFAS emission ratios for the heptanes is likely appropriate.

The model emission ratio for the butanes is lower than any of the observations. Comparing the peat burning and observations from this work with the boreal studies in it can be seen that the former emission ratios were higher than the latter. It may be that given the model values is a global average that a more temperate type of burning lowers the average compared to the this work and peat burning observations. The Andreae and Merlet study is also higher than the model and this value is representative of all tropical burning not just a regional effect. Even though the model value is a global average of the burning over these months was dominated by tropical burning, so it is likely that the model emission ratio for the butanes is too low.

## **5.8 Model Biomass Burning Simulations**

To provide a quantitative assessment of biomass burning emissions of VOCs, the GEOS-Chem model (described in chapter 3) was run over the biomass burning period. V11-02d of the GEOS-Chem 3D chemical transport model was used to perform all simulations in this chapter. The biomass burning emissions are important for the analysis in this chapter. There are a number of biomass burning inventories that can be used in the model, including the Global Fire Emissions Dataset and the Fire Inventory from NCAR (GFED and FINN).

For this work the Global Fire Assimilation System (GFAS) biomass burning emissions were used (Kaiser et al., 2009). This inventory was selected as the file resolution is higher than FINN and has files processed for 2015/16 unlike GFED. The emission data is at  $0.1^\circ \times 0.1^\circ$  horizontal resolution. Important VOCs for this work, emitted by GFAS are: ethane, propane, benzene and toluene. Full details of the model, including the biomass burning emissions are given in chapter 3.

The model was run from August to November 2015 to cover the observations during the biomass burning period. Comparisons for the main species that were both measured and available to output from the model are shown in

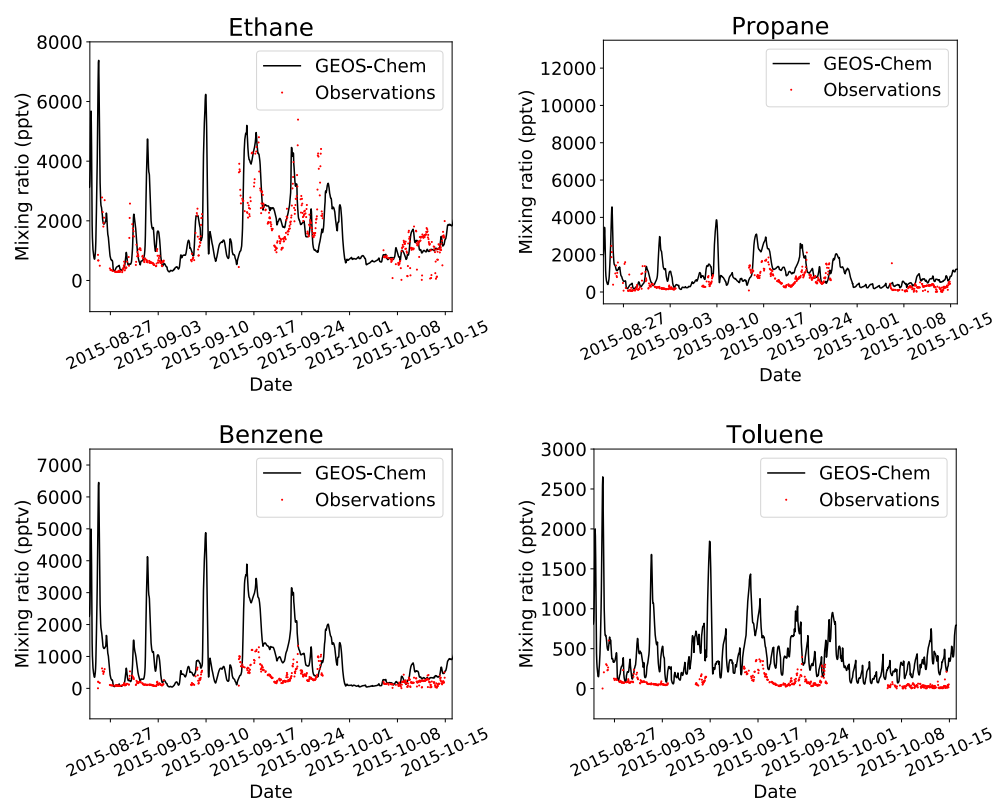


**Figure 5.15 Comparison between GEOS-Chem (black line) and observations (red dots) during the biomass burning periods**

## 5.9 Model Scale Factors

Given that chapter 4 identified that there is a model bias for most species, the reasons for which may not be easily explained, a scaling factor was applied to the model data to give better agreement during the background periods with observations. This allowed the biomass burning emissions to be evaluated independently of any intrinsic model bias.

For analysis of the influence of biomass burning on the measurement site the following scale factors listed in Table 5.2 were applied to model output. These scaling factors give model and observation values with better agreement during

the background periods, so the correlation plots show a more even spread of values around the 1:1 line. Any spikes in model or observational data are excluded when deciding on scaling factors.

**Table 5.2 Scaling factors for each VOC to be applied to model output (model will be multiplied by these values) to give better agreement with observations during background periods**

<b>VOC (model grouping)</b>	<b>Scaling Factor</b>
<b>Ethane</b>	1
<b>Propane</b>	1.5
<b>Benzene</b>	1
<b>Toluene</b>	6

## **5.10 Evaluation of Biomass Burning Emission**

Time series of observations and model data are shown in Figure 5.16. This data covers only the biomass burning period and the data is scaled using the scale factors calculated in section 5.9.

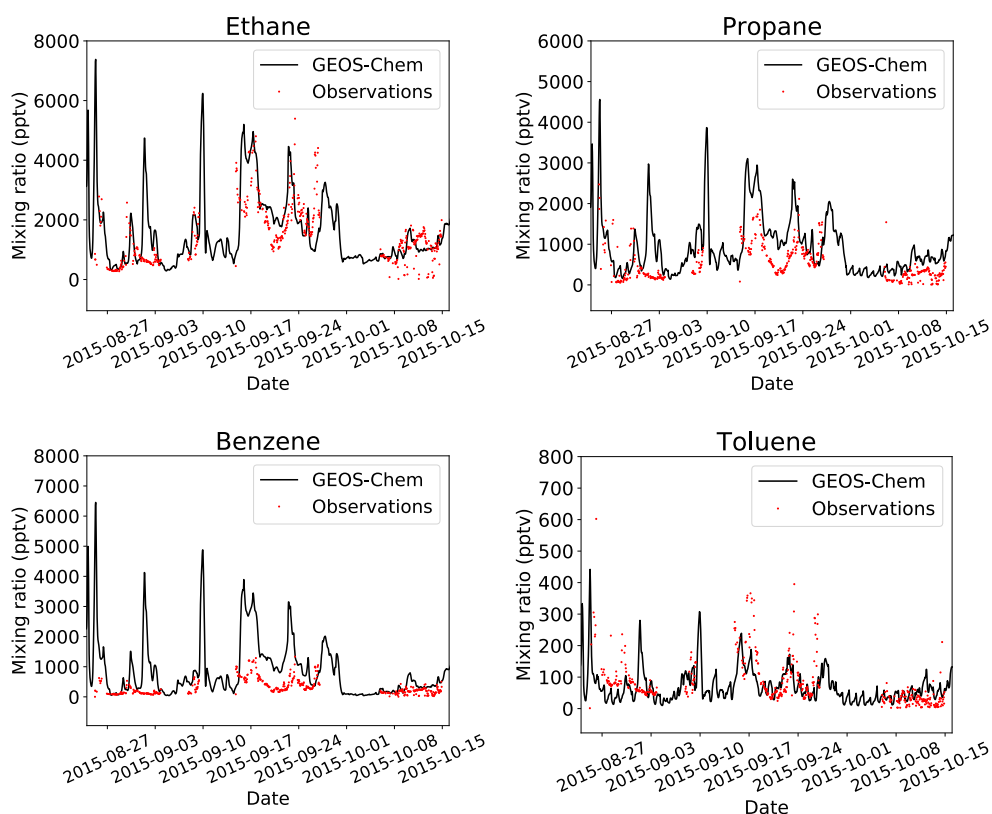


**Figure 5.16 Comparison between GEOS-Chem scaled using the factors in Table 5.2 (black line) and observations (red dots) during the biomass burning periods**

For ethane and propane (with the scaling factor applied) the model simulates well the observed mixing ratios. The timing of the main peaks generally shows good agreement, although one of the large model peaks at the start of September was not seen in the observations.

For the lumped alkanes the increase in mixing ratios, both model and observations is not as large as for other VOCs. Overall the model simulates well the magnitude of the mixing ratio, although there are spikes seen in the observations that are not in the model.

The model underestimates benzene during the peak of the biomass burning by a factor of  $\sim 4$ , agreement for the 'base' values is better. This suggests that there is an issue with the biomass burning emissions for benzene being too large, or the model underestimates the removal of benzene after it is emitted.

With the scaling factor applied agreement for toluene observations with the model is overall good. The shape and magnitude of the lower mixing ratios and the peaks show good agreement, although at the peaks the observations are higher than the model. This may be due to an overestimation of the scale factor in some circumstances and suggests that the biomass burning emissions simulate toluene well.

Overall the Global Fire Assimilation System (GFAS) inventory gives good agreement with the observations from this work for most species. The scale factors calculated in chapter four are needed to give this agreement. This again suggests that there is an issue with the base mixing ratios for most species being too high for this grid box as a representation of the measurement site. However, accounting for this the GFAS inventory gives good agreement for all species apart from benzene. The reason for this is not clear especially given that for toluene, another aromatic species agreement is much better.

In addition to this the model was run with biomass burning emissions both on and off. This should show how significant a contribution to VOC mixing ratios biomass burning makes. The influence of these emissions on the local chemistry can also be quantified, including OH and O<sub>3</sub> mixing ratios.

This section focuses on model output over the dates where VOC observations are available. Table 5.3 gives the mean, median and inter-quartile range for all VOCs emitted by biomass burning in the model. The non biomass burning values were calculated over three months between May and July, the biomass burning period covers August to October.

As would be expected, there is an increase in the mean mixing ratio at the measurement site grid box for most species during the biomass burning period. This increase is more pronounced in some species than others. Isoprene shows a similar mean, median and inter-quartile range in both periods. The isoprene observations also show no noticeable increase in mixing ratios during the biomass burning period. It could be that emissions of isoprene from biomass burning are not particularly high and combined with the short lifetime of isoprene most of the emissions are removed before the air mass reaches the measurement site. Alternatively, given the high mixing ratios of isoprene observed at the

measurement site it may be that the biogenic emissions dominate the local area at the measurement site and so any additional isoprene from biomass burning falls within the natural variation observed.

Longer lived species including ethane and carbon monoxide show mixing ratios that are more than double the non biomass burning periods. The measurement site is not directly surrounded by areas with burning. Back trajectories showed that it took air masses around two to three days to arrive from the burning to the measurement site. The maps for biomass burning emissions show that the pattern of burning is similar for the model and so it would be expected that the enhancement is generally less significant for shorter lived species due to their more rapid removal in the air mass during transport to the measurement site.

**Table 5.3 Mean, median and inter-quartile range values for the observations and GEOS-Chem during non biomass burning (No BB: 05, 06, 07/2015) and biomass burning (BB: 08, 09 & 10/2015) time periods. All values are given in pptv.**

<b>Model (scaled)</b>	<b>Non</b>			<b>BB</b>		
<b>Species</b>	Mean	Median	IQR	Mean	Median	IQR
<b>Ethane</b>	482	452	405-508	1715	1271	863-1937
<b>Propane</b>	196	184	127-240	711	525	354-828
<b>Benzene</b>	102	89	67-111	983	547	278-1160
<b>Toluene</b>	46	44	28-61	86	66	46-97
<b>Observations</b>	<b>Non</b>			<b>BB</b>		
<b>Species</b>	Mean	Median	IQR	Mean	Median	IQR
<b>Ethane</b>	351	345	290-432	1492	1315	716-2043
<b>Propane</b>	72	68	53-88	519	363	225-745
<b>Benzene</b>	77	75	61-93	308	231	132-406
<b>Toluene</b>	18	15	9-24	81	56	35-94

## 5.11 Modelled Influence of Biomass Burning Emissions

The GEOS-Chem China nested grid was run between 1<sup>st</sup> August 2015 – 1<sup>st</sup> November 2015. For the non biomass burning period the model was run for one month before the start date without biomass burning emissions to generate a new

restart file. The impact of biomass burning on ethane, isoprene, OH and ozone is discussed below.

### 5.11.1 Ethane

Figure 5.17 shows the ethane concentrations at the Bukit Atur site with and without biomass burning. This shows that biomass burning has a substantial impact on the ethane concentrations at the measurement site, with mean concentrations four times higher. During certain events such as around the 22<sup>nd</sup> August mixing ratios peaked around 20 ppbv, around 50 times higher than the mean without biomass burning.

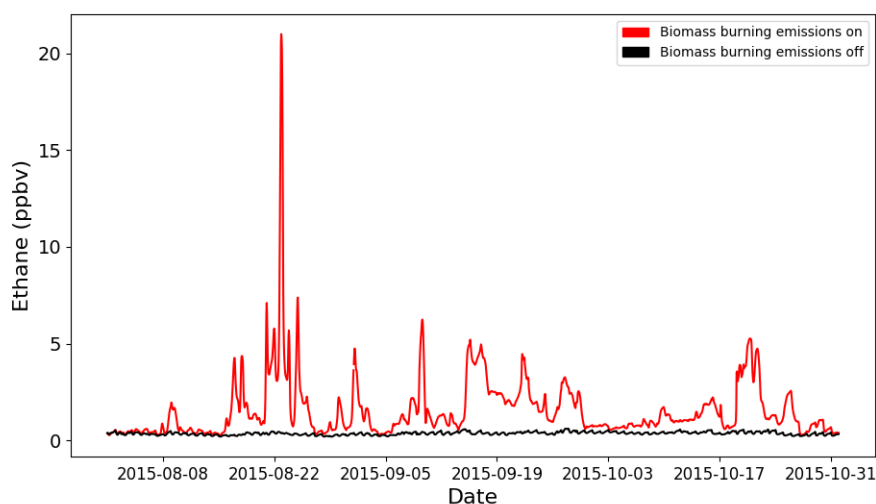
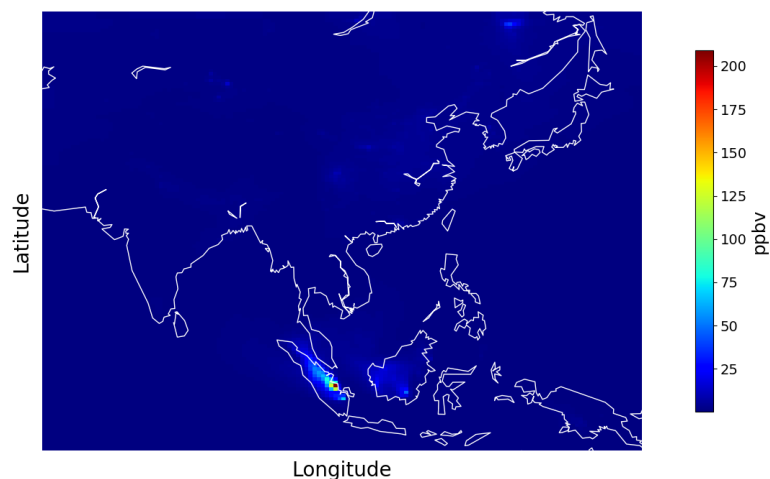


**Figure 5.17 Ethane mixing ratios for the box containing the measurement site in GEOS-Chem, with biomass burning emissions turned on and off**

**Table 5.4 Mean, median and inter-quartile range values for GEOS-Chem ethane with and without biomass burning emissions turned on**

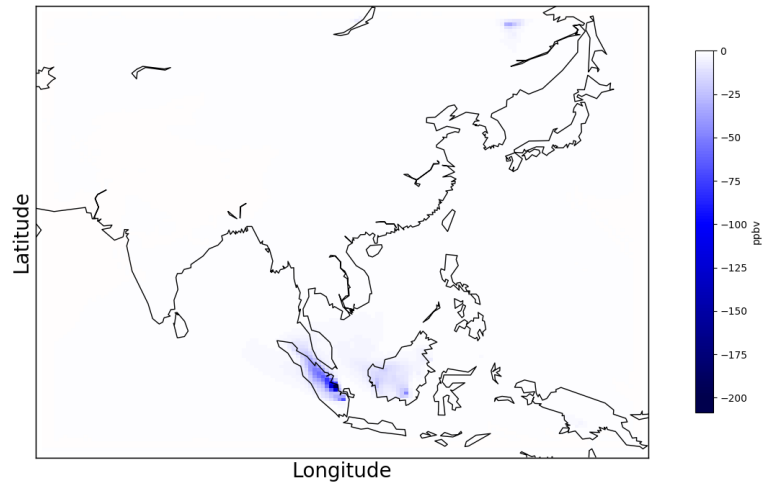
<b>Ethane</b>	<b>Mean (ppbv)</b>	<b>Median(ppbv)</b>	<b>Inter-quartile range (ppbv)</b>
<b>BB on</b>	1.6	1.0	0.6-2
<b>BB off</b>	0.4	0.4	0.3-0.4

Figure 5.18 shows the spatial distribution of surface ethane for the GEOS-Chem China nested grid. Ethane concentrations are generally low for most areas (<10 ppbv) but around the areas of biomass burning concentrations are much higher, peaking around 200 ppbv.



**Figure 5.18 Ethane mixing ratios with biomass burning emissions turned on for September 2015**

Figure 5.19 and Figure 5.20 show the absolute and percentage changes in ethane concentration when biomass burning emissions were switched off. This shows that there are the largest absolute changes at the sources of the biomass burning emissions, where ethane concentrations were highest. However, looking at the percentage change this shows that ethane concentrations decrease by up to 60-70% for large parts of South East Asia.



**Figure 5.19** The absolute change in ethane when biomass burning emissions were turned off in GEOS-Chem. The model was run over September 2015.

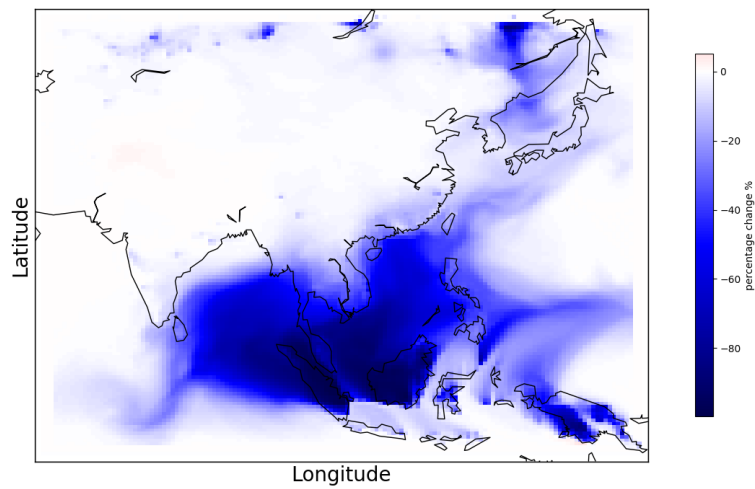


**Figure 5.20** The percentage change in ethane when biomass burning emissions were turned off in GEOS-Chem. The model was run over September 2015.

### 5.11.2 Isoprene

Figure 5.21 shows the isoprene concentrations at the Bukit Atur site with and without biomass burning. Apart from the initial week (this appears to be an issue with using different restart files) there is very little impact on isoprene concentrations from biomass burning at the measurement site. This agrees with the observations from this project. Table 5.5 shows the statistics including the mean and median for isoprene with biomass burning emissions on and off.

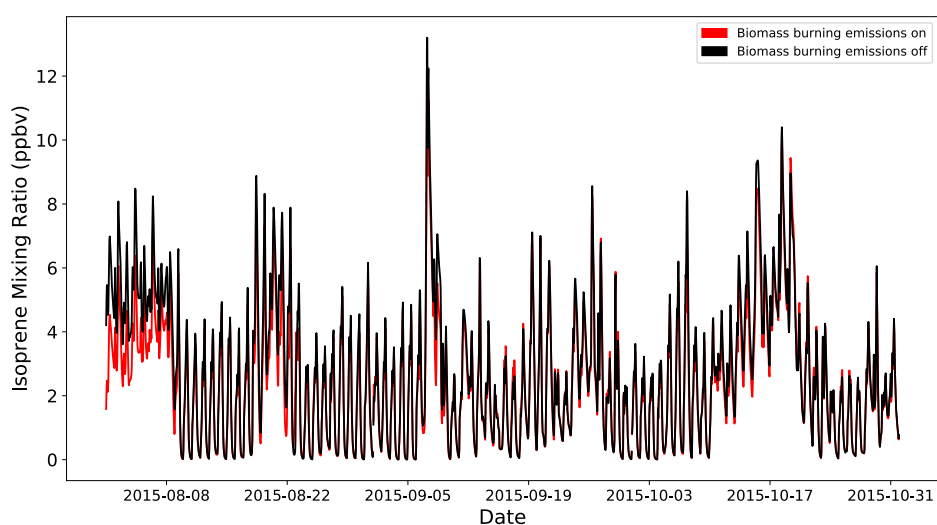


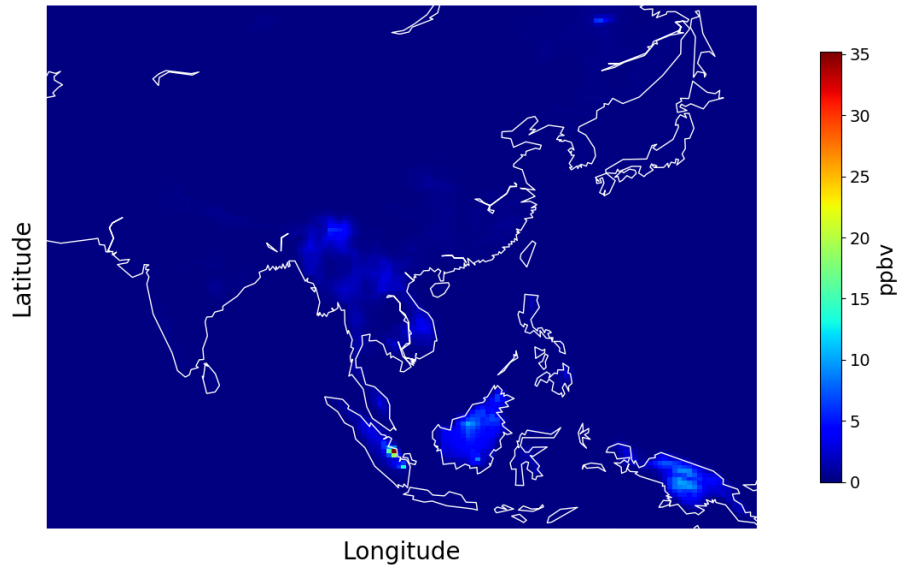
**Figure 5.21 Isoprene mixing ratios for the box containing the measurement site in GEOS-Chem, with biomass burning emissions turned on and off**

**Table 5.5 Mean, median and inter-quartile range values for GEOS-Chem isoprene with and without biomass burning emissions turned on**

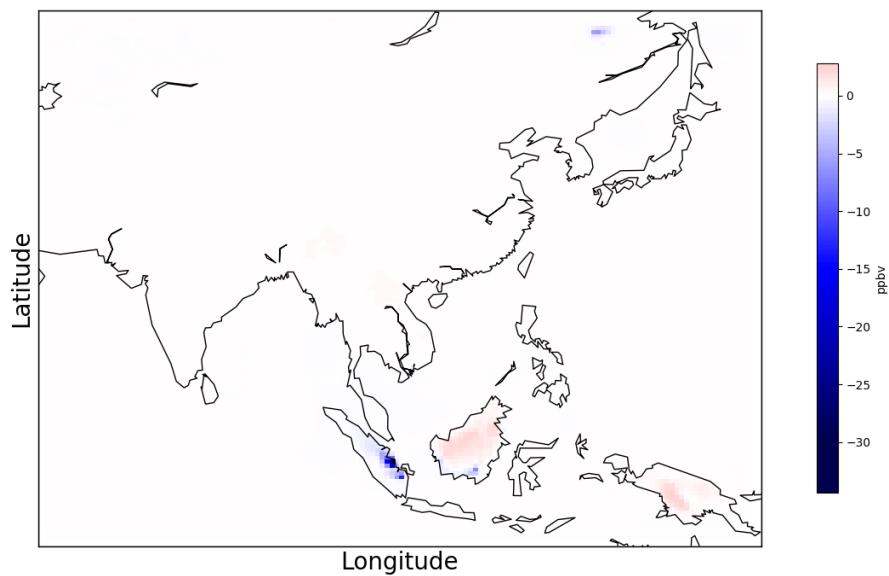
<b>Isoprene</b>	<b>Mean (ppbv)</b>	<b>Median(ppbv)</b>	<b>Inter-quartile range (ppbv)</b>
<b>BB on</b>	2.5	2.3	0.9-3.6
<b>BB off</b>	2.7	2.4	0.9-4.1

Figure 5.22 shows the spatial distribution of surface isoprene concentrations for the GEOS-Chem China nested grid with biomass burning emissions turned on for September 2015. This shows that isoprene concentrations over more industrialized areas are generally low, with higher concentrations over the

forested region of Malaysia and Borneo. Very high isoprene concentrations are seen for a couple of grid boxes. These values correlate with the main site of the biomass burning and so the high concentrations seen are from burning emissions.



**Figure 5.22 Isoprene mixing ratios with biomass burning emissions turned on for September 2015**



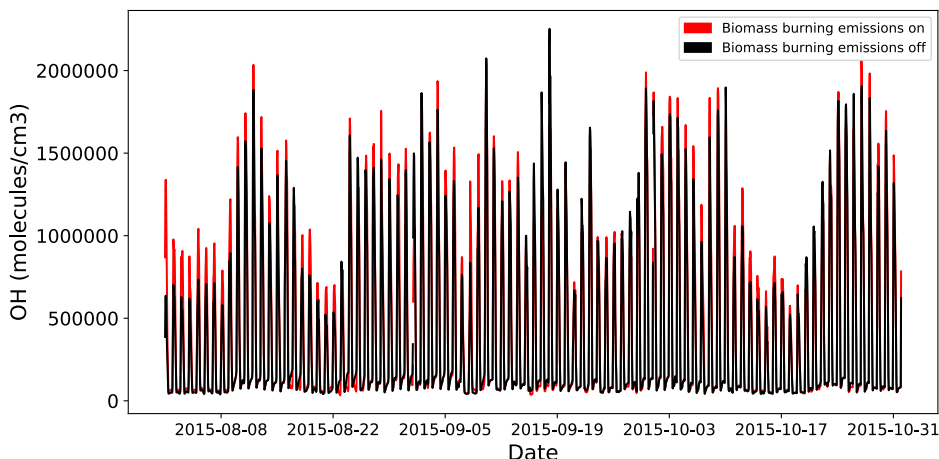
**Figure 5.23 The absolute change in isoprene when biomass burning emissions were turned off in GEOS-Chem. The model was run over September 2015.**

Figure 5.23 shows the absolute change in ppbv for isoprene as a result of turning off biomass burning emissions. This shows a large increase where isoprene concentrations were highest due to direct emission from biomass burning. Over some of Borneo and Indonesia isoprene concentrations show a small increase. Turning off biomass burning emissions results in lower ozone and slightly lower OH concentrations (discussed below). These species are the main removal routes for VOCs and so lower concentrations likely explains the increase in isoprene concentrations.

These changes show a different pattern to ethane as described above. Ethane shows a large decrease across most parts of South East Asia when biomass burning emissions were turned off. Isoprene shows both increases and decreases only over small parts of Borneo and Indonesia. This can be explained by the much shorter lifetime of isoprene (hours) against ethane (months). Although isoprene is also directly emitted from biomass burning it reacts quickly, mainly with OH and so burning emissions of isoprene are not transported any real distance. Hence why decreases in isoprene are seen around the areas of burning but an increase is seen over Borneo because there is less sink for biogenic isoprene emissions which dominate in this area. Ethane is much longer lived and so the emissions from the burning are able to be transported larger distances, explaining the large decrease over South East Asia when biomass burning emissions are switched off.

### **5.11.3 OH**

Figure 5.24 shows the OH concentrations at the Bukit Atur site with and without biomass burning. This shows that turning off biomass burning emissions leads to a small decrease in OH concentrations. Biomass burning emissions result in an increase in model ozone and since ozone photolysis is the main production route for OH this would explain the decrease in model OH when the emissions were turned off.



**Figure 5.24 OH mixing ratios for the box containing the measurement site in GEOS-Chem, with biomass burning emissions turned on and off**

**Table 5.6 Mean, median and inter-quartile range values for GEOS-Chem OH with and without biomass burning emissions turned on**

OH	Mean ( $10^5$ molecules/cm <sup>3</sup> )	Median ( $10^5$ molecules/cm <sup>3</sup> )	Inter-quartile range ( $10^5$ molecules/cm <sup>3</sup> )
<b>BB on</b>	4.3	1.2	0.8-7.4
<b>BB off</b>	4.0	1.2	0.8-6.4

#### 5.11.4 Ozone

Biomass burning emissions can cause changes to atmospheric composition beyond the species directly emitted. One important species influenced by biomass burning is ozone. VOC and NO are important for ozone production and both are emitted by biomass burning (Crutzen et al., 1979). VOCs are oxidized and the radical intermediates formed react with NO to produce NO<sub>2</sub>, which is then photolysed giving ozone.

Therefore biomass burning in the tropics tends to result in an increase in tropospheric ozone and this has been shown in previous observational and model studies for example (Ziemke et al., 2009) showed that there was a global increase of 8-10 ppb on mean values of 35-55 ppb during the main biomass burning season (August-November 2006). GEOS-Chem showed an increase of 3 ppb on a mean of 17 ppb (August to October) for the grid box containing the measurement site

(Figure 5.25). For August the increase was slightly higher of 5 ppb on a mean of 16 ppb. Although these changes are relatively small it can be seen that during events such as that around the 22<sup>nd</sup> August, biomass burning can have a profound impact on ozone, more than doubling the ozone concentration.

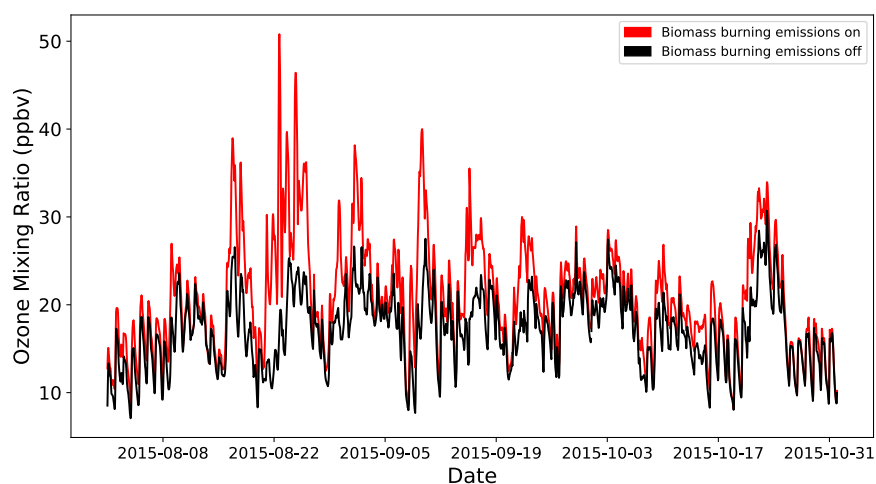
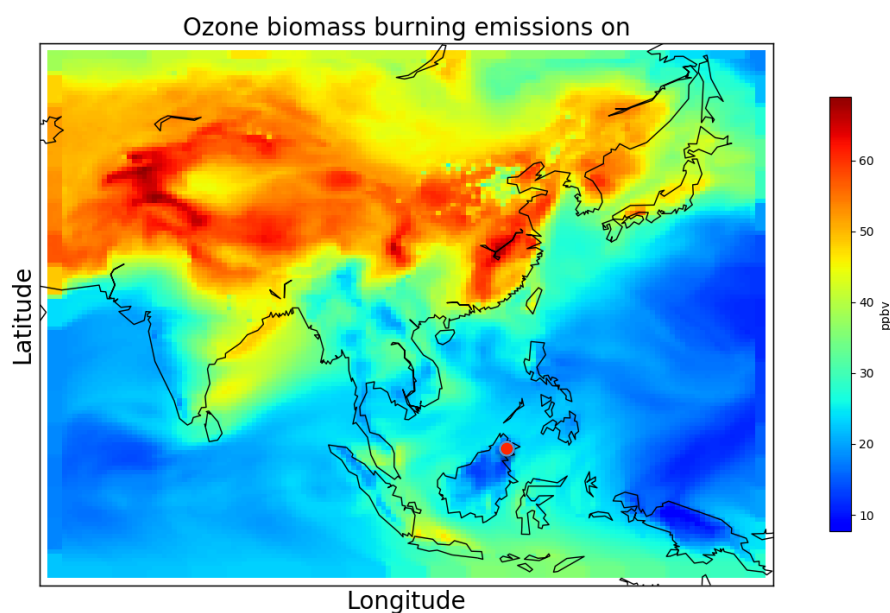


**Figure 5.25 Ozone mixing ratios for the box containing the measurement site in GEOS-Chem, with biomass burning emissions turned on and off**

**Table 5.7 Mean, median and inter-quartile range values for GEOS-Chem OH with and without biomass burning emissions turned on**

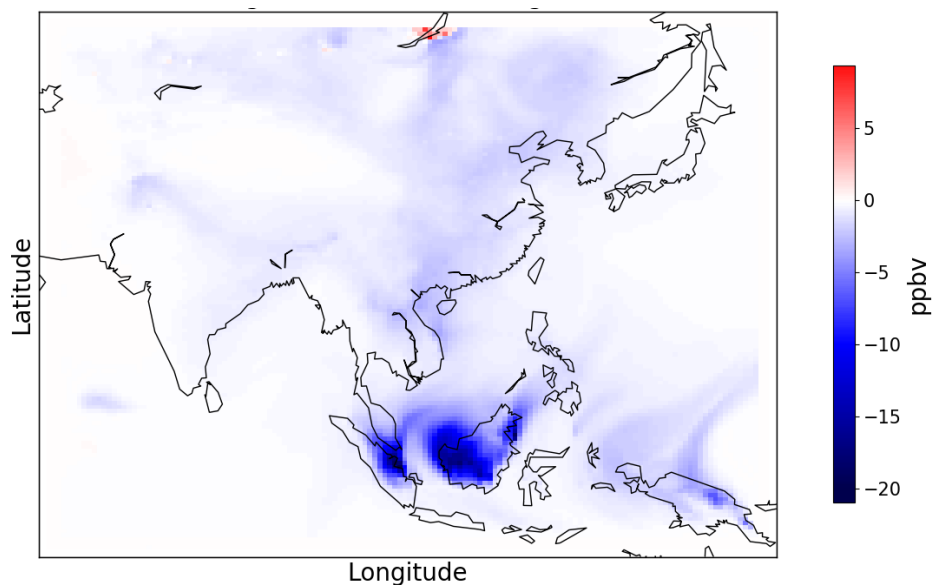
Ozone	Mean (ppbv)	Median(ppbv)	Inter-quartile range (ppbv)
<b>BB on</b>	21	20	16-24
<b>BB off</b>	17	17	14-20

Figure 5.26 shows the spatial distribution of surface ozone in the GEOS-Chem China nested grid with biomass burning emissions turned on for September 2015. This shows high ozone concentrations over more industrialized areas including China and parts of India. Much lower concentrations are seen over most of Malaysia and Indonesia.



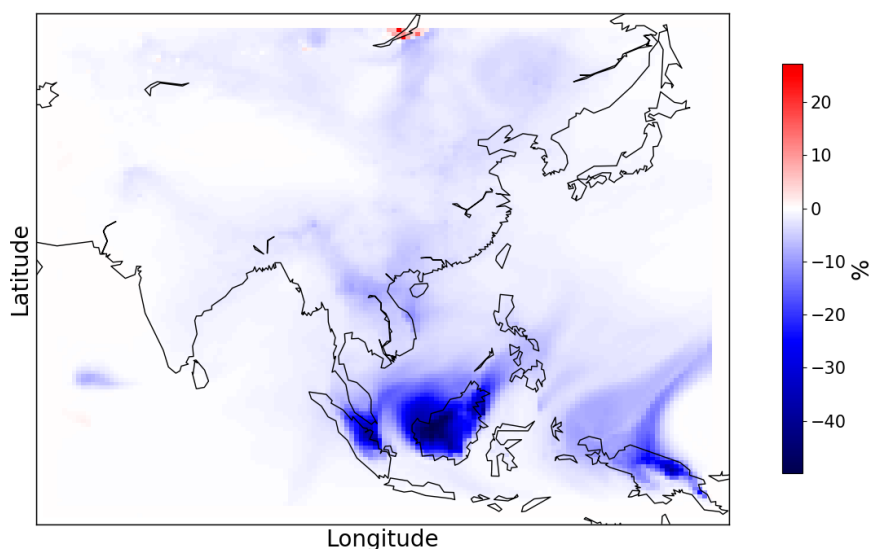
**Figure 5.26 Ozone mixing ratios with biomass burning emissions turned on for September 2015.**

Figure 5.27 shows the absolute change (ppb) in ozone as a result of turning off biomass burning emissions for the China regional grid. There is an increase in ozone at the top of the grid, the reason for this is not clear but it is likely influenced by the boundary conditions that are read in by the model. The areas around the main biomass burning events in Sumatra and Southern Borneo show the strongest decrease in ozone when biomass burning was turned off, with up to 20 ppb less at the centre of the burning. This is to be expected as the emission source is where mixing ratios of VOCs and  $\text{NO}_x$  will be highest. This map shows that the influence of biomass burning emissions on ozone is not limited just to the source of the biomass burning. Increases in ozone resulting from emissions occur as far as India, China and other parts of South East Asia.



**Figure 5.27 The absolute change in ozone when biomass burning emissions were turned off in GEOS-Chem. The model was run over September 2015.**

Figure 5.28 shows the same change as above but this time as a percentage change from values when biomass burning emissions were switched on. This shows that without biomass burning ozone mixing ratios would be up to 50% lower in the areas immediately surrounding the burning. For the top part of Borneo these changes result in ozone levels that are still below  $\sim 20$  ppb. However for parts of Indonesia, ozone reached levels of almost 50 ppb. This is approaching the world health organization guidelines for 8 hour average ozone exposure ( $100 \mu\text{g}/\text{m}^3$ , approximately 50ppb) (WHO, 2006). Global warming is predicted to worsen El Nino events in South East Asia (Thirumalai et al., 2017). Given that these events cause droughts and therefore result in conditions that increase the likelihood for biomass burning it is likely that going forward even higher levels of ozone will be seen in these areas. This is in addition to with an expected increase in oil palm plantations which contribute to an increase in background ozone levels of up to 4.5 ppbv (Silva et al., 2016).



**Figure 5.28** The percentage change in ozone when biomass burning emissions were turned off in GEOS-Chem. The model was run over September 2015.

## 5.12 Conclusions

This chapter has shown that biomass burning in South East Asia causes a substantial increase in most VOC concentrations at the Bukit Atur measurement site. Fire maps and trajectories showed that much of the variability during this period can be explained by changes in meteorology.

Emission ratios against propane were calculated from the observational dataset from this project and compared with previous studies. Agreement for ethane, ethene and toluene was good when compared with boreal burning studies. For other species, however, comparison with a study on peat burning gave much better agreement, particularly for acetylene. This is indicative that burning in this area was due to a combination of forest and peat burning. The GFAS model emission factors were also compared with the observations. These showed good agreement with (Andreae and Merlet, 2001) a study that combined various datasets of emission factors. The model however overestimated compared with the peat burning emissions, which is known to be an important source of burning in Indonesia (Page et al., 2002).

Scaling factors were applied to the model data to bring the background values into better agreement with the observations. These corrected mixing ratios were then compared with the observations during the biomass burning period to evaluate the Global Fire Assimilation System (GFAS) biomass burning inventory. Overall this inventory simulated well the observed VOC concentrations, particularly for ethane and toluene. The model did not simulate benzene as successfully.

Finally the effect of biomass burning emissions in GEOS-Chem was investigated. Ethane concentrations showed a substantial decrease across large parts of South East Asia when biomass burning emissions were switched off, the same trend was seen for other VOCs including propane. Isoprene concentrations decreased substantially at the site of burning but showed a small increase across some forested areas due to decreases in ozone and OH when emissions were turned off. OH showed a small decrease in concentration at the measurement site when biomass burning emissions were turned off, this was likely due to the decrease in ozone leading to less OH production. At the measurement site there was an increase in ozone comparable as a percentage to a previous model study. Turning off biomass burning emissions gave a decrease in ozone over large parts of the China grid. Near the site of the fires biomass contributes an increase in ozone of up to 50%, pushing values over some parts of Indonesia to around 50 ppbv.

# Chapter 6

## 6 Biogenic VOCs

### 6.1 Introduction

Biogenic volatile organic compounds (BVOCs) emitted by vegetation are thought to contribute 90% of total global annual VOC emissions (Sindelarova et al., 2014), with the tropics responsible for 70% of these BVOC emissions (Karl et al., 2007). Isoprene is the dominant BVOC, accounting for ~50% of emissions (Guenther et al., 2012). A wide range of other species including monoterpenes, sesquiterpenes, alcohols, alkanes and alkenes make up the remaining fraction. The Model of Emissions of Gases and Aerosols from Nature (MEGAN) (Guenther et al., 2012) contains ~150 species and this does not include all species reported to be emitted by vegetation

The species measured in Bukit Atur as part of this project that are predominately biogenic in origin are thought to be propene and isoprene. Measurements for both species are discussed in this chapter together with those made previously as part of the OP3 project. Initially the propene observations are discussed and compared to a GEOS-Chem model simulation. This is followed by the same analysis for isoprene. Finally the influence of biogenic emissions in GEOS-Chem on ozone, OH and PM<sub>2.5</sub> for the measurement site and wider region are explored.

### 6.2 Propene

#### 6.2.1 Propene Observations

A time series of the propene measurements made as part of this project is shown in Figure 6.1. The graph is plotted from January to January, so data from February and March 2016 is shown before the measurements made in 2015 (September – December). This is to allow a clearer comparison on a monthly basis with the OP3 measurements that were made in 2008 for isoprene later in this chapter.

Mean propene concentrations over the year were 90 ppt, with a median value of 56 ppt and range (5<sup>th</sup> to 95<sup>th</sup> percentiles) of 21-183 ppt. The highest concentrations were seen in February and March, but propene over the measurement period was generally below 200 ppt. During OP3 a mean value of 47 ppt, median of 31 ppt and range (5<sup>th</sup> to 95<sup>th</sup> percentile) of 19-56 ppt was observed (Jones et al., 2011). This compared with a mean of 90 ppt, median of 56 ppt and range of 21-183 ppt from our work. Concentrations measured from our work were thus generally higher than those collected during OP3, with the mean twice what was observed during OP3. The lower end of the range was similar for both projects but concentrations were consistently higher for this work than the upper end of the OP3 range.

Between August and October the other VOC species showed a large increase in concentration (around 5-10 times larger depending on VOC) due to biomass burning emissions (see chapter 5). Apart from a few readings during this period the propene mixing ratios were consistent with, or even lower than other times of the year (mean value during biomass burning period  $50 \pm 30$  ppt, other periods  $80 \pm 60$  ppt). This suggests that propene emitted from biomass burning plumes does not reach the measurement site at an appreciable mixing ratio. This may be expected given the short lifetime of propene  $\sim 8$  hours (Donoso et al., 1996) and that the site is  $\sim 700$  km from the centre of the biomass burning on Borneo. Assuming a mean horizontal wind speed of  $10 \text{ m s}^{-1}$  this gives at least two half lives of propene between emissions and the air reaching the GAW site.

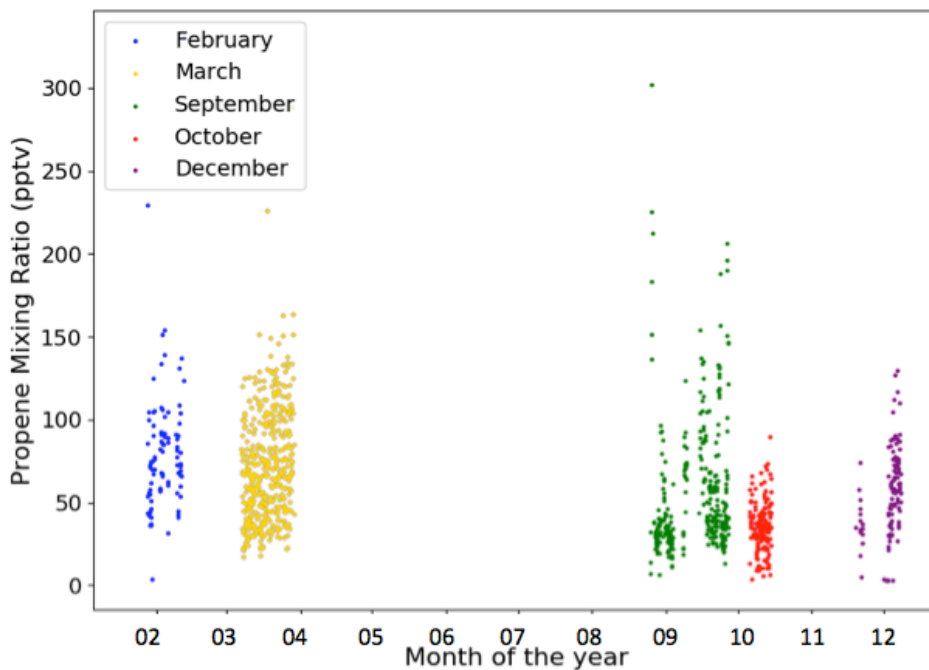


**Figure 6.1 Time resolved propene measurements made during this work. The data is separated into five periods labeled as the nearest month**

Figure 6.2 shows the measured diurnal average profiles for the five months sampled by this work. The observations in general show a nighttime mixing ratio of around 40-60 ppt with increasing concentrations in the morning. This is followed by a peak in concentration from noon to late afternoon. There is, however, variability between the months.

September and October show an early peak of ~90 and 60 ppt respectively. This is followed by a rapid depletion of propene during the day with concentrations decreasing to 40 and 15 ppt respectively. Since these measurements were made during the biomass burning period (chapter 5) it is possible that biomass burning is the cause of the change in diurnal cycle. This pattern would be consistent with an increase in OH during this period, which increased propene destruction around noon. Increased ozone concentrations are expected during biomass burning periods and this could lead to an increase in OH concentrations (Crutzen and Andreae, 1990, Baylon et al., 2018). Without supporting measurements to provide further information this seems to provide a reasonable explanation for the change in the diurnal cycle of propene.

For the other months the diurnal cycle peaks between midday and 3pm, with concentrations ranging from 90 to 115 ppt. concentrations fall during the afternoon and into the evening.

To investigate the consistency between these observations and our understanding of the processes controlling propene concentrations we can compare the observations to the output of the GEOS-Chem model.

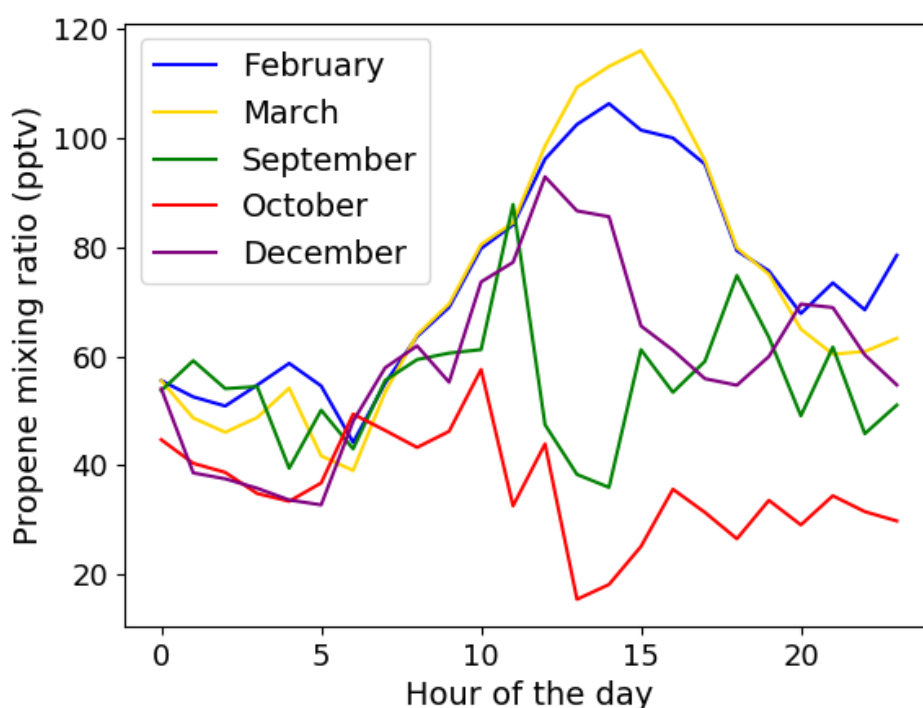


Figure 6.2 Diurnal average profiles for the measurement months identified in figure 1. Times shown are local time (GMT+8)

### 6.3 Modelled Propene

The China nested grid version of the GEOS-Chem model, described in chapter 3, was run over three months from November 2015 – January 2016 during a background period. That is a period predominantly influenced by local conditions and not, for example, biomass burning emissions. This was to focus on the observations independently of the effects of any biomass burning emissions. The model was also run over the same period with biogenic emissions turned off. The magnitude of the concentrations will be evaluated against the observations, followed by the diurnal cycle.

### 6.3.1 Magnitude of Modelled Propene

Figure 6.3 shows model propene concentrations with and without biogenic emissions, the observations over the same time period are shown in red. The mean model propene was 1200 ppt, which is higher than the 90 ppt that was observed. The difference was a factor of around 10.

Switching off biogenic emissions (Figure 6.3) still gave propene concentrations higher than the observations. Without biogenic emissions the mean propene concentration was half of that simulated with biogenics on but concentrations were still significantly higher than the observations (580 ppt against observed 90 ppt).

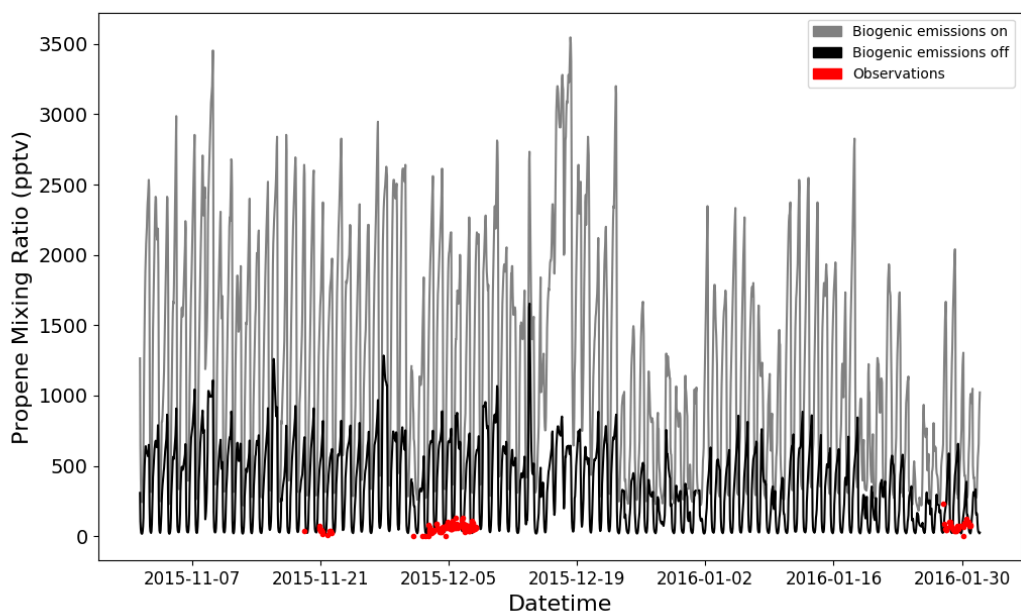


**Figure 6.3 Model propene mixing ratios with biogenic emissions switched on (grey) and off (black), with observations over the same time period (red circles)**

**Table 6.1 Mean, median and range (5<sup>th</sup> to 95<sup>th</sup> percentiles) for propene from this work, OP3 and GEOS-Chem**

	MEAN (PPTV)	MEDIAN (PPTV)	RANGE 5 <sup>TH</sup> - 95 <sup>TH</sup> PERCENTILES (PPTV)
THIS WORK	90	56	21-183
OP3 CAMPAIGN	47	31	19-56
GEOS-CHEM (BIOGENICS ON)	1200	1100	280-2600
GEOS-CHEM (BIOGENICS OFF)	580	569	0-1300

Propene in GEOS-Chem is lumped with other >C3 alkenes (PRPE) and this includes butene, which was also measured as part of this work. However, even adding butene into calculation doesn't resolve the issue. Mean observed propene + butene is 130 ppt which is still substantially less than modeled propene.

The model shows that there is a substantial anthropogenic component of about 50% of the final propene mixing ratio in this grid box. This includes contributions from industrial and residential sources. Figure 6.4 shows a map of the anthropogenic emissions over the island of Borneo together with the location of the field site. It can be seen that there are anthropogenic emissions within that grid box. However, the field site is remote from any of these influences. Therefore the model resolution is causing it to appear that there is a background anthropogenic signal at the site, whereas in reality there is none.

However, even if this background anthropogenic propene signal is removed the biogenic source of propene is significantly higher than that observed ( $900 \pm 600$ ) ppt. It would appear that the MEGAN inventory used to calculate the emissions of propene are significant higher than those found in this region. Reducing the flux of propene by a factor of 10 would likely bring the model and measurements into better agreement.

The MEGAN 2.1 emissions for propene are based on measurements made by (Goldstein et al., 1996) over a midlatitude forest. From the measurements made at Danum Valley it would appear that the current emissions are not suitable for use in some tropical rainforest environments.

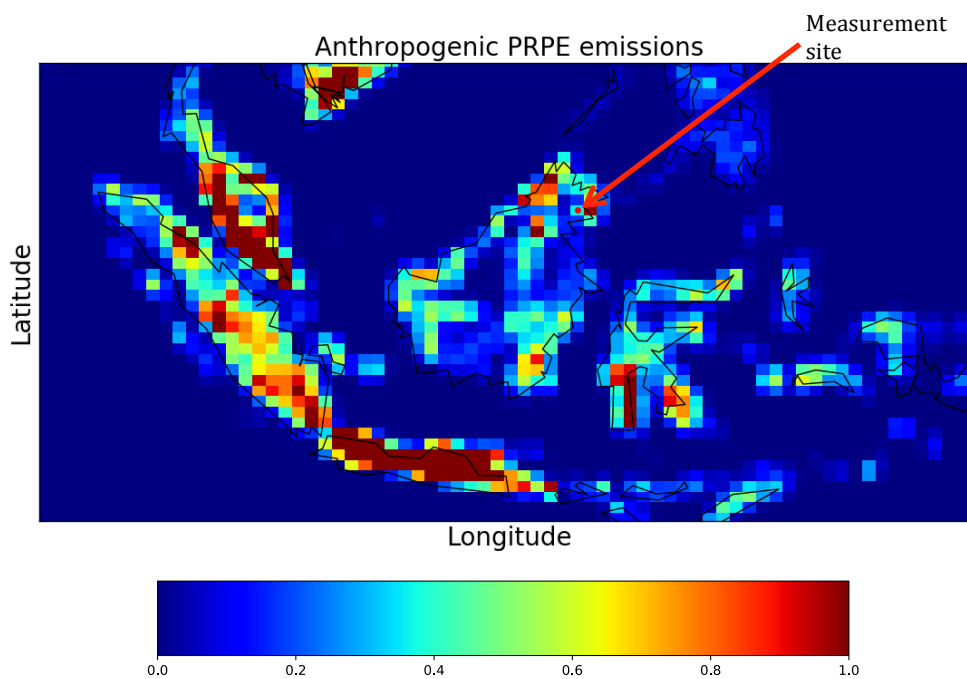


**Figure 6.4** Map of anthropogenic propene emissions over Borneo and the surrounding areas. Colour scale is in  $\times 10^{11}$  atomsC  $\text{cm}^{-2}$   $\text{s}^{-1}$ . Values above  $1 \times 10^{11}$  atomsC  $\text{cm}^{-2}$   $\text{s}^{-1}$ , have been masked as dark red to remove bias on the colour scale caused by very large anthropogenic emission sources such as major cities.

## 6.4 Propene Diurnal Cycle

Although the model does not simulate the magnitude of the propene concentrations well, the diurnal cycle in the model and measurements is evaluated next. Figure 6.5 shows the normalized (data is divided through by the maximum

value) diurnal cycles for both the measured and modelled propene mixing ratios for the periods shown in Figure 6.1. This normalized data was then grouped by hour to give the diurnal profile. The model and measurements have very different diurnal cycles. As shown earlier the measurements show either a daytime maximum or a flat diurnal cycle, whereas the model a daytime minimum around midday.

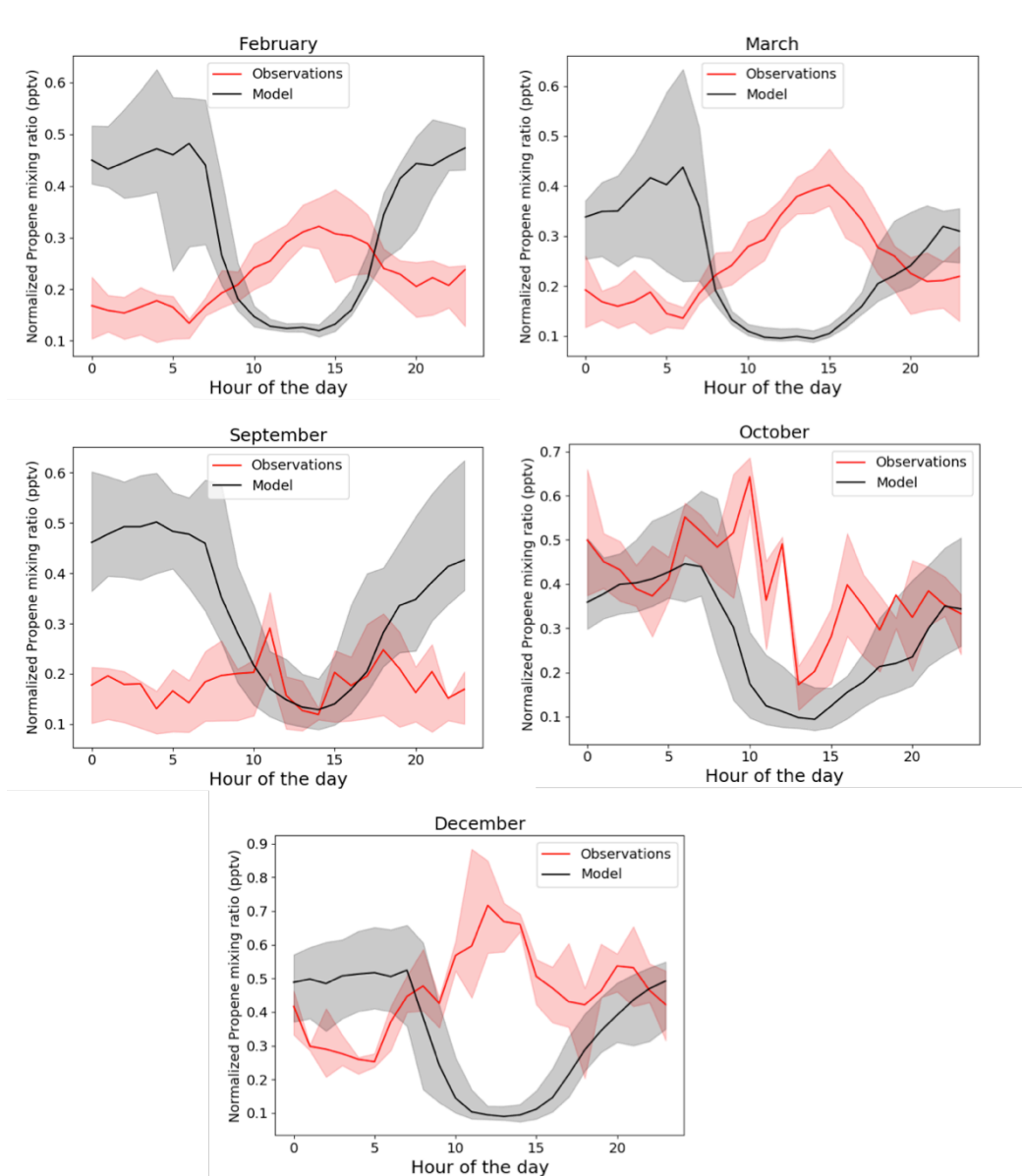


**Figure 6.5 Model (black) and Observations (red) diurnal medians by month. The shaded areas represent the 25<sup>th</sup> to 75<sup>th</sup> percentiles**

The decrease in the modeled propene in the morning corresponds to an increase in OH concentrations (Figure 6.6). In the observations it appears that the increase in emissions due to increasing sunlight occurs faster than the increase in the OH sink, which generally leads to maximum concentrations during the day. Assuming that the boundary layer mixing is consistent throughout the day, there are two possible reasons for the model failure: 1) the increase in propene emissions likely driven by increasing photosynthetically active radiation (Guenther et al., 2012) may not be large enough, or 2) there is too much OH in the model. Measurements made during the OP3 campaign gave mean peak OH as  $2.5 \times 10^6$  molecules  $\text{cm}^{-3}$  (Whalley et al., 2011). The modeled mean is  $\sim 1.8 \times 10^6$  molecules  $\text{cm}^{-3}$ . The available evidence suggests that the model underestimates the OH at the site in agreement with the long term underestimation of OH in forested regions (Lelieveld et al., 2008, Pugh et al., 2010, Lu et al., 2012). It therefore seems unlikely that the model overestimates OH concentration. The other possibility is that the model does not simulate the diurnal pattern for propene emissions correctly. There may be too high emissions in the morning and not enough around midday.

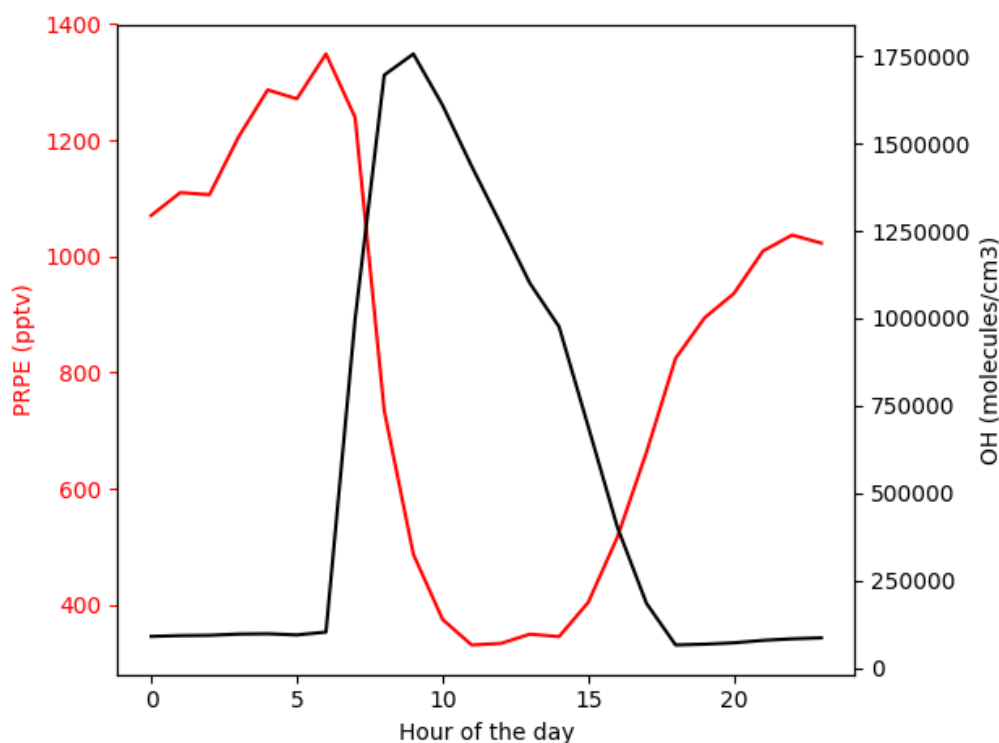


Figure 6.6 Average model diurnal over one year for propene (red) and OH (black)

Overall, GEOS-Chem does not simulate propene in this environment well. There is a significant impact of anthropogenic emissions on the grid box containing the Danum Valley site, whereas there is no evidence for this in the observations. However, even without the anthropogenic emissions there is still a significant overestimation of propene concentrations in the model. This is likely due to the emissions algorithm based upon observations in a North American mid-latitude forest not being suitable for the tropical forest found in Borneo.

However given that isoprene emissions in this grid box are ~100 times greater than propene, in terms of the wider chemistry such as ozone, OH and particulate matter formation the ability of the model to simulate propene is not a key issue.

## **6.5 Isoprene**

Isoprene is the dominant VOC measured at the field site (see chapter 4). These observations will be discussed along with previous observations made at the site and those made in other forested locations.

### **6.5.1 Isoprene Observations**

A time series of all the isoprene measurements from this project and from GC-FID measurements made during the OP3 campaign is shown in Figure 6.7 (Jones et al., 2011). The OP3 GC-FID (as opposed to the PTR-MS (Langford et al., 2010)) measurements have been shown here as measurements were made with similar instrumentation. This time series shows that overall the magnitude of observed mixing ratios is similar for both campaigns, even though they took place in different years (2015/16 for this work and 2008 for OP3).

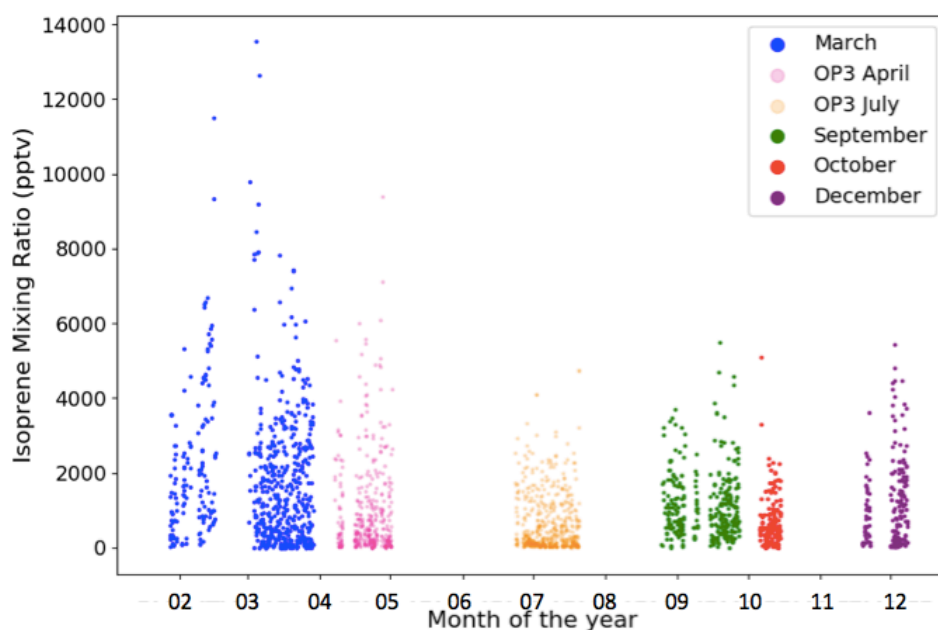


**Figure 6.7** An isoprene time series showing measurements from this work (solid circles) and measurements made using GC-FID during the OP3 campaign (faded circles)

A more detailed comparison between each of the OP3 datasets (GC-FID and PTR-MS) and measurements from this project is given in chapter 4. The box and whisker diagrams are also shown below in Figure 6.8 and Figure 6.9. Chapter 4 concluded that concentrations were more consistent with the PTR-MS measurements than the GC-FID. However, given the disagreement between the two OP3 datasets and that measurements were made in different years at different heights it was not possible to firmly assess whether there was any seasonality in isoprene at the measurement. The median isoprene values could be argued as being higher at the start and end of the year (measurement periods 1 and 5), but when looking at the range of values this is not consistent.

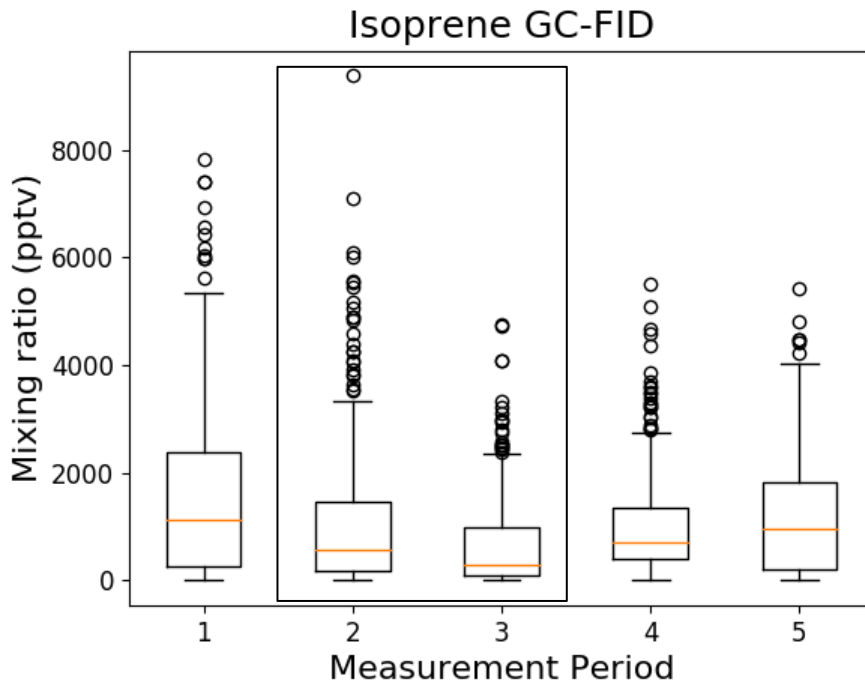


Figure 6.8 Box and whisker plots for isoprene measurements from this project and the OP3 GC-FID measurements. OP3 measurements are shown in the black box

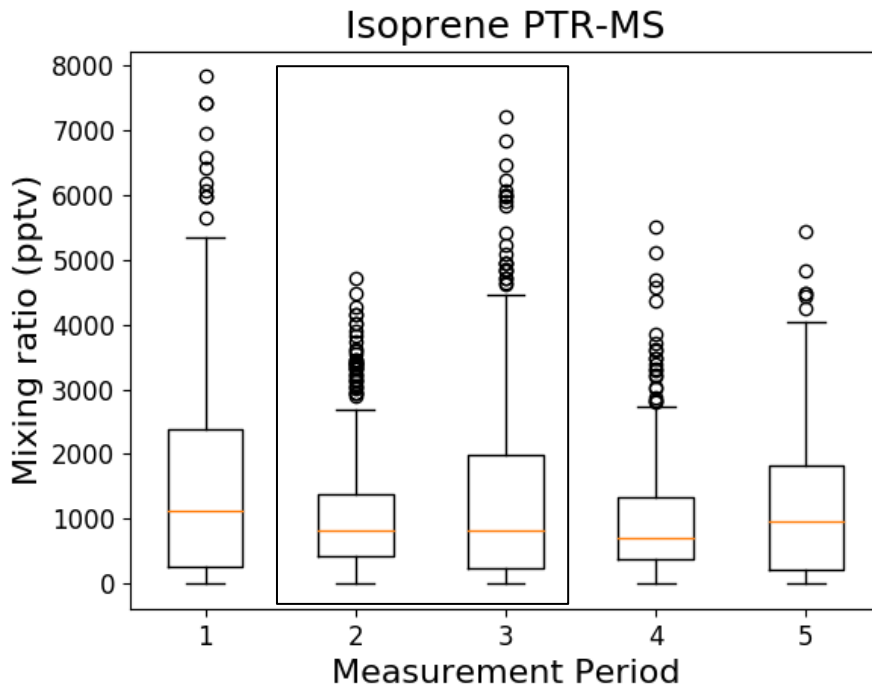


Figure 6.9 Same as Figure 6.8 but with OP3 PTR-MS measurements

Figure 6.10 shows OP3 data from April for both the GC-FID (Jones et al., 2011) and PTR-MS (Langford et al., 2010). For comparison the data from this work is from March as this is the nearest month available. Figure 6.11 shows the OP3 data from July with data from this work from the end of August and September.

The OP3 GC-FID data sampled from 5 m above ground level and the PTR-MS from 75m above ground level. The sampling height for this work was ~30 m above ground level.

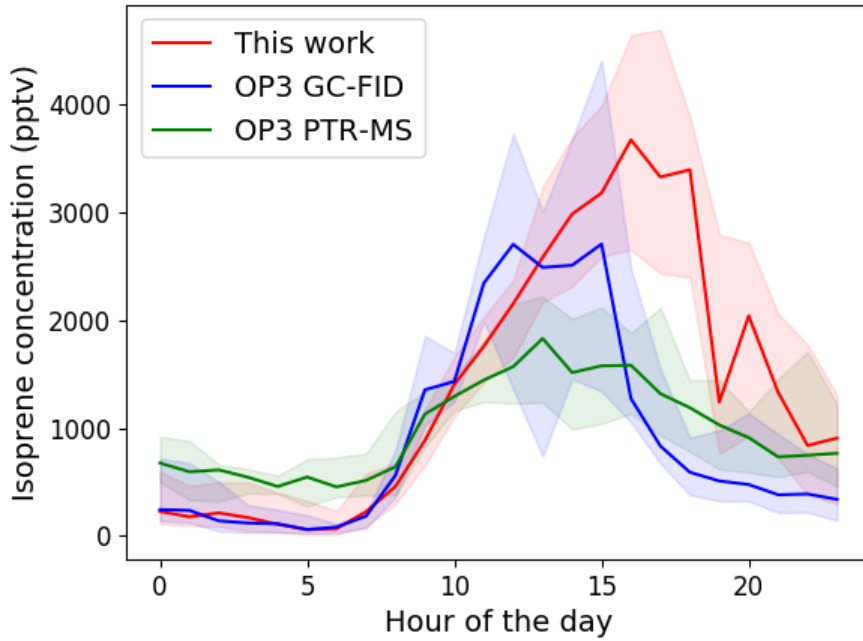


Figure 6.10 Isoprene diurnal profiles for March from our work and the April OP3 campaign. The line is the median value, with shaded areas representing the 25<sup>th</sup> and 75<sup>th</sup> percentiles. The OP3 data from April is compared to the March data from our work as this is the nearest available month for comparison

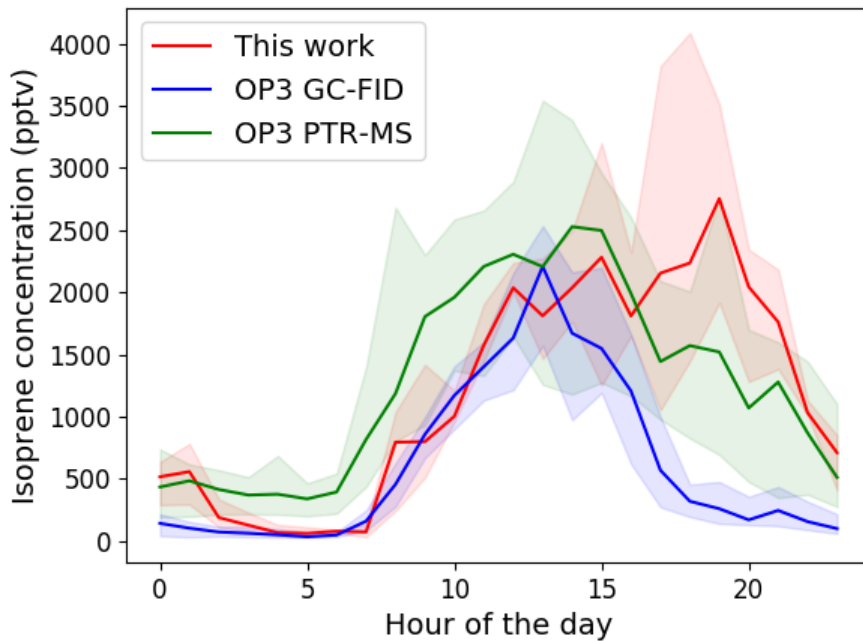


Figure 6.11 Isoprene diurnal profiles for September from our work and the July OP3 campaign. The line is the median value, with shaded areas representing the 25<sup>th</sup> and 75<sup>th</sup> percentiles. The OP3 data from July is compared to the September data from our work as this is the nearest

The data from this work shows a peak later in the day (4-8pm) than was seen in either of the OP3 datasets. There is good agreement between the two GC-FID datasets for the early morning isoprene mixing ratios, with low mixing ratios approaching zero. The morning PTR-MS data is ~500 ppt higher than both of the GC datasets.

The PTR-MS data shows mixing ratios sustained through the night into the early morning. In the afternoon agreement is better between this work and the PTR-MS data, with mixing ratios for these two datasets being sustained into the late evening. The differences between the OP3 datasets and this work may be in part due to the measurements being made in different years and months. (Jones et al., 2011) attributed the differences between the two OP3 GC datasets to variations in local NO conditions. It is highly likely that there were difference conditions when the measurements were made for this work compared with the OP3 campaigns. Particularly knowing that the September measurements from this work were influenced by a strong biomass burning season. In addition to this the different sampling heights will influence the observations. Sampling from 5 m (OP3 GC-FID) is within the canopy and so the isoprene mixing ratios here will be influenced by nearby emissions as well as canopy losses. 75 m (OP3 PTR-MS) and to a lesser extent 30 m (our measurements) is above all surrounding canopy and so influences from canopy losses will not have as high an influence on these measurements. It may also be that the higher sampling height is representative of a wider geographical area and thus this data is subject to influences from a wider area.

Overall given the variations in condition between the three datasets the magnitude of the three datasets generally show good agreement in the magnitude of the isoprene mixing ratios. This suggests that inter-annual variability in isoprene at this site is not large.

### 6.5.2 Diurnal Cycles

Monthly diurnal isoprene concentrations for the data collected as part of this work and the OP3 GC-FID measurements are shown in Figure 6.12. All profiles show lower concentrations at night (100-1500 pptv) with increasing concentrations (peaks 1500-3500 pptv) during the day that decrease again in the evening. However the timings of the peak concentration vary. The March, December and OP3 July data for this work show a single midday or late afternoon peak (midday to 7pm). The September, October and OP3 April data show two peaks, one before and one after midday. The differences in diurnal cycles must result from changes in isoprene sources and sinks at different times of the year.

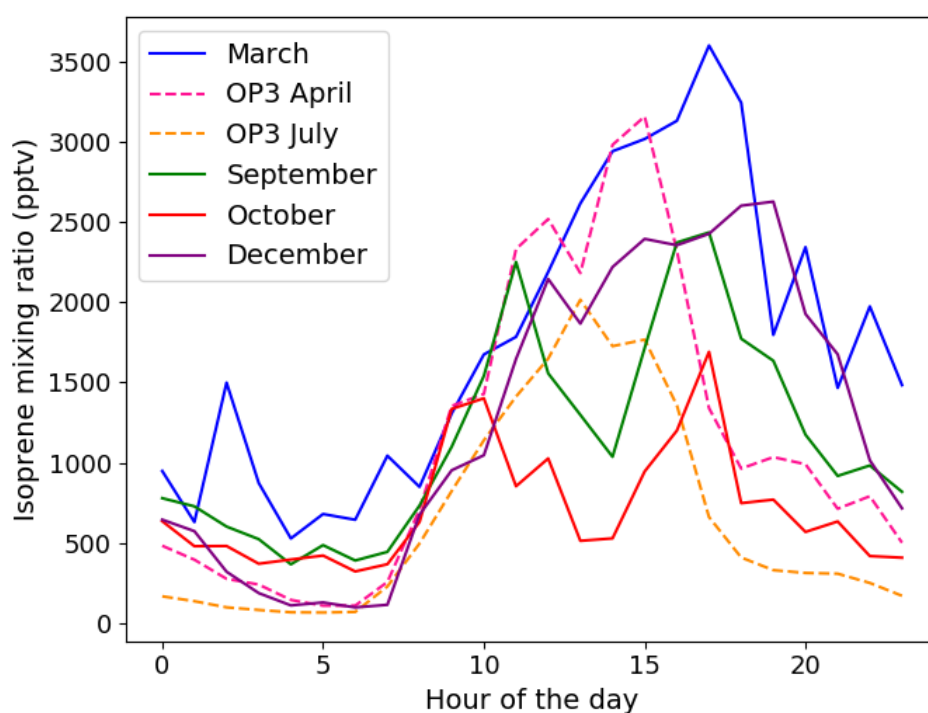


Figure 6.12 Diurnal average profiles for the periods identified in figure 6.1. The OP3 data is shown with dashes lines

Variations in OH concentrations alone may explain these differences. Changes in the timing or magnitude of the OH peak could lead to changes in the diurnal profile that shows a build up in isoprene during the day followed by a decrease at night if OH concentrations are relatively low and spread out over the day, such as in March. If OH concentrations are high and concentrated around noon then a double peak can be seen like in October due to strong daytime removal of isoprene. The relationship between isoprene and OH is complex (Edwards et al., 2013). Understanding these profiles fully would require additional supporting measurements (such as those made during OP3) that are not available for this work or alternatively a significant box modeling effort.

The ability of the model to simulate the observed isoprene concentrations is explored next.

### **6.5.3 Modelled Isoprene**

Chapter 3 describes the GEOS-Chem chemical transport model and MEGAN biogenic emissions inventory. Figure 6.13 shows one year of isoprene mixing ratios for GEOS-Chem.

The annual mean isoprene concentration in the model is  $2200 \pm 1800$  ppt, which compares with the observed mean of  $1300 \pm 1200$  pptv (mean $\pm$ SD). The large bias seen for propene (section 6.3.1), with model concentrations being ~70% higher than the observations, is not present for isoprene. This would be consistent with the model calculating the correct isoprene emissions but having too little OH. The model simulates an annual mean OH concentration for the measurement site grid box of  $1.9 \times 10^6$  molecules  $\text{cm}^{-3}$  compared with the OP3 measured mean of  $2.5 \times 10^6$  molecules  $\text{cm}^{-3}$  (Whalley et al., 2011).

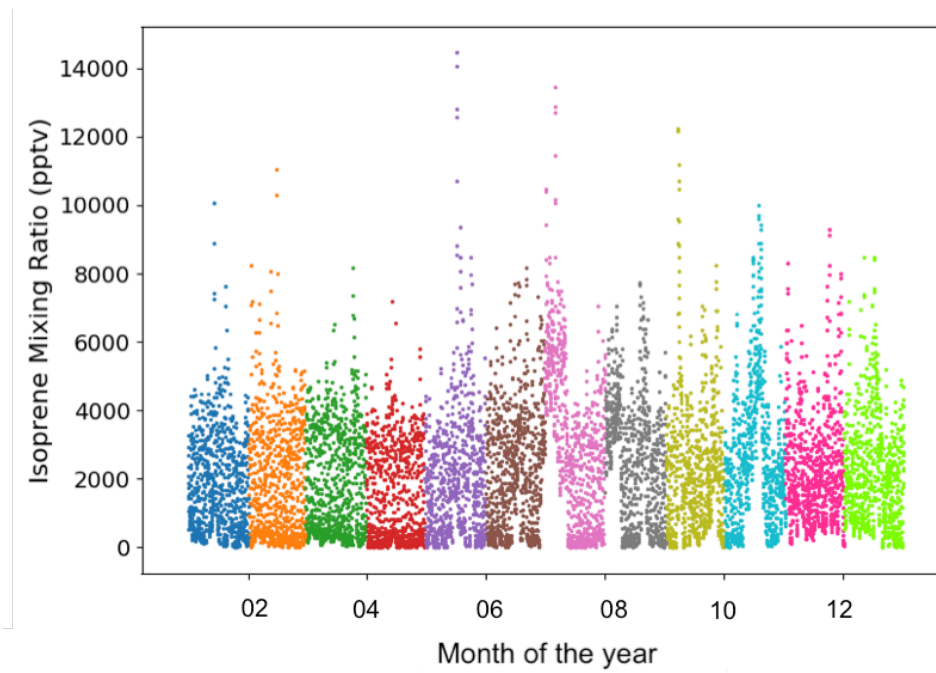


**Figure 6.13 Time series for one year of GEOS-Chem isoprene concentrations, coloured by month**

### 6.5.4 Diurnal Cycles

The monthly mean diurnal cycle of isoprene in the model is shown in Figure 6.14. Similar to the observations the model shows a characteristic morning time increase in isoprene concentrations leading to a late afternoon peak. Most months show a smaller peak around noon followed by a larger late afternoon peak. November shows an earlier first peak and July does not show a strong double peak. The changes in peak shape show some similarity to the observations from this work Figure 6.12.

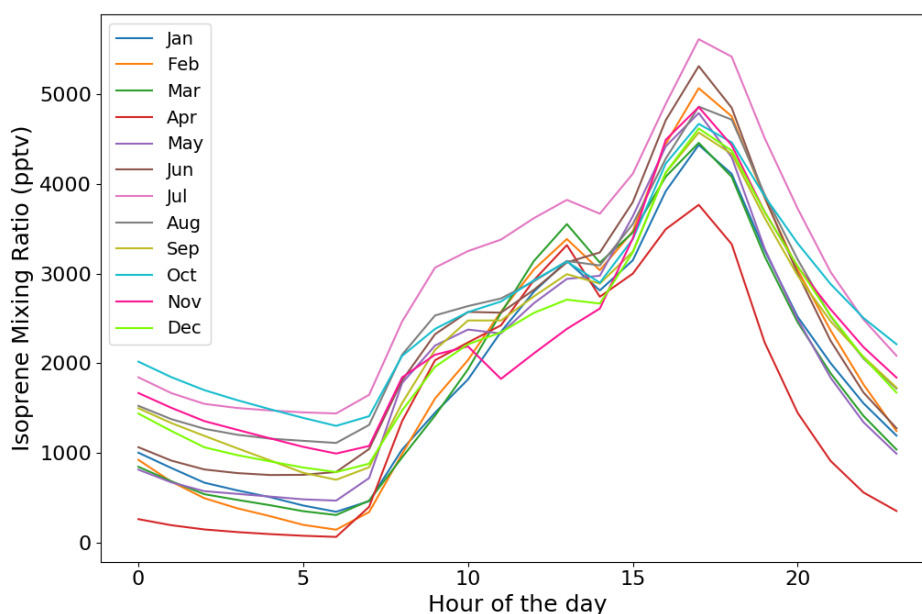


**Figure 6.14 Average diurnal profiles for isoprene concentrations from GEOS-Chem**

The isoprene diurnal profiles for observations from this project and GEOS-Chem are shown in Figure 6.15. Mean, median and inter-quartile range values for the model and observations are shown in Table 6.2 and Table 6.3.

**Table 6.2 Mean, median and inter-quartile range (25<sup>th</sup> – 75<sup>th</sup> percentiles) values for both the observations and model by month**

MONTH	Observations			Model		
	MEAN	MEDIAN	IQR	MEAN	MEDIAN	IQR
MARCH	1800	1300	330-2600	1950	1600	510-3200
SEPTEMBER	1100	820	480-820	2300	2000	840-3200
OCTOBER	720	520	280-900	2600	2300	1100-3700
DECEMBER	1200	960	210-1800	2240	2000	1000-3000

**Table 6.3 Mean, median and inter-quartile range (25<sup>th</sup> – 75<sup>th</sup> percentiles) values for the peak isoprene (11:00-18:00) for both the observations and model by month**

MONTH	Observations			Model		
	MEAN	MEDIAN	IQR	MEAN	MEDIAN	IQR
MARCH	2900	2600	1900-3500	3600	3500	2900-4000
SEPTEMBER	2100	1800	1100-2800	3400	2900	2300-3900
OCTOBER	1000	600	300-1800	3600	3200	2300-4400
DECEMBER	2200	2000	1400-2400	3300	3000	2200-4100

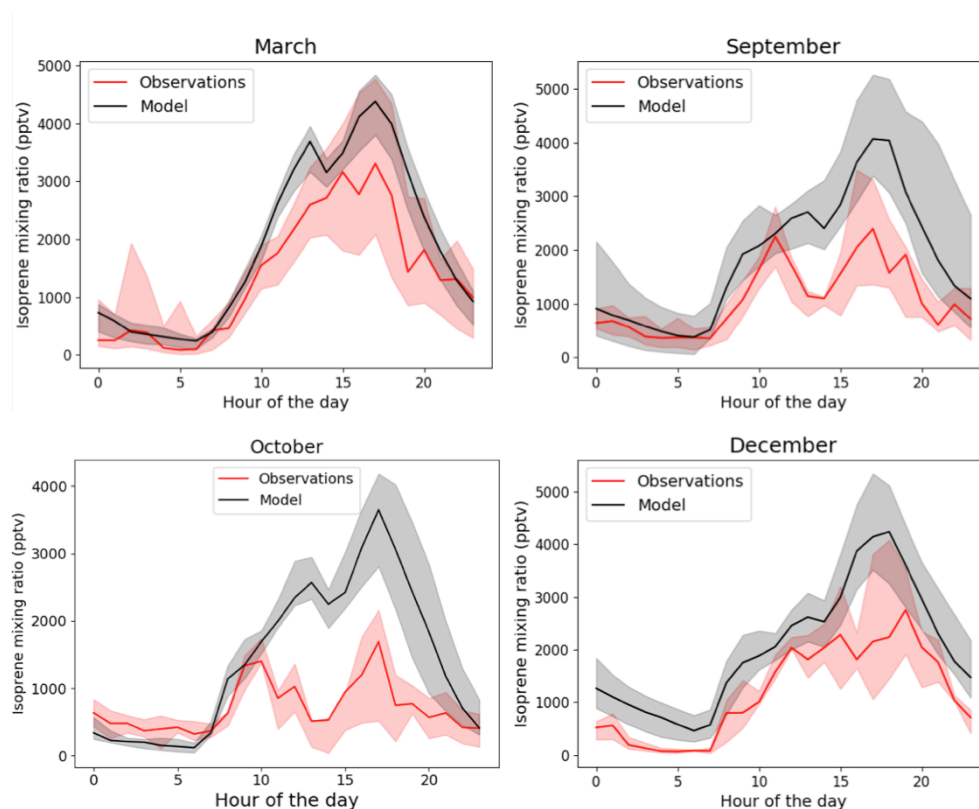


**Figure 6.15 Diurnal isoprene profiles for this work and the GEOS-Chem model. The line represents the median values, with the shaded areas showing the 25<sup>th</sup> and 75<sup>th</sup> percentiles.**

The March data shows good agreement between model and observations both for the shape and magnitude of the isoprene diurnal. The agreement for December, which is also a ‘background’ period, is fairly good for the profile although the model does overestimate the magnitude of the mixing ratios. This suggests that the model does a good job of simulating the background isoprene mixing ratios, when local conditions dominate (away from the biomass burning period).

The observations for September and October show a more distinct double peak than the other data, with suppression of isoprene around midday. Although the model data does show a strong afternoon peak the distinct double peak is there but not as strong as the observations. The model also overestimates the magnitude of the mixing ratios. There is a factor of two difference between the average values at peak isoprene. This suggests that GEOS-Chem underestimates the depletion effects of biomass burning emissions on VOC. This could be because the increase in VOC emissions is larger than any increase in OH due to an increase in ozone.

## **6.6 Discussion of High Isoprene Periods**

To understand what drives the variability in isoprene concentrations in the model the sources and sinks of isoprene are investigated in more detail. There are a number of periods where high mixing ratios of isoprene are sustained, these are highlighted in Figure 6.13. During these periods isoprene concentrations stay high throughout the day without approaching zero at night. To understand whether there is a variation in the removal rate of isoprene in the model during these periods time series for a number of species relevant to isoprene chemistry are shown below.

Firstly, the emissions during a period with sustained high isoprene concentrations will be compared with surrounding months where concentrations are lower. Figure 6.16 shows maps of isoprene emissions for October, November and December. The red circle shows the area that the measurement site falls within. These maps show that emissions of isoprene are similar in October and November but higher in December. However, mid-October shows sustained high isoprene concentrations and concentrations in December are not generally 50% higher than the other months as the emissions are. This suggests that emissions alone do not determine isoprene concentrations in the model.

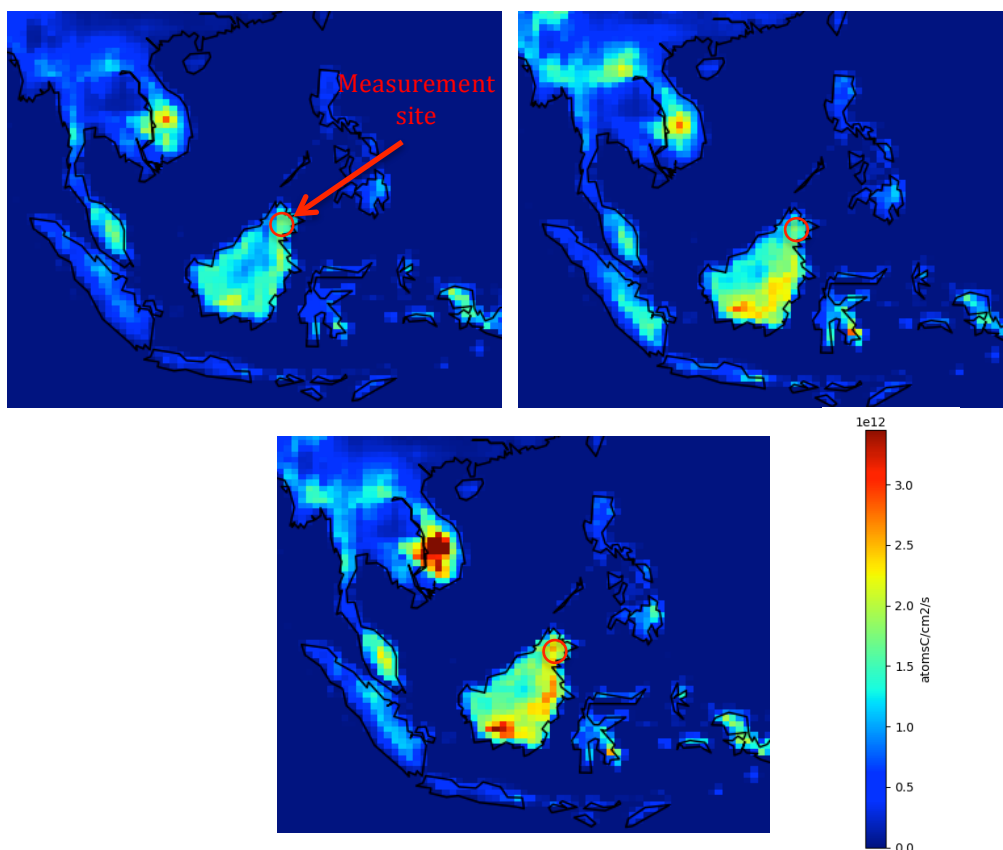


**Figure 6.16** Maps showing isoprene emissions in South East Asia for clockwise October, November and December)

During the periods highlighted in Figure 6.13 there is decrease in OH concentrations. Reaction with OH is the main removal pathway for isoprene and other VOCs. During these periods there is an increase in CO and some VOC species including ethane the timing of these events coincide with the biomass burning period. These species all react with OH and this is their main removal pathway and this may explain why there are lower OH concentrations. There is also an increase in black carbon during these periods and this will scatter more sunlight and likely decrease OH production. These factors together possibly explain the sustained high mixing ratios of propene and isoprene, where the mixing ratios stay high even in the night when there is the absence of biogenic emission. One issue with this explanation is that there are periods of increased CO and black carbon during other times, such as September but an increase in isoprene is not seen. During late August and early September there is an increase in ozone concentrations, probably due to biomass burning. Since photolysis of ozone is the main pathway for OH formation it may be that even though the increase in CO and some VOCs act to deplete OH concentrations, the additional OH formed due to increased ozone

offsets this effect and so isoprene concentrations do not show the same sustained increases seen in July and October. This suggests that biomass burning emissions impact upon isoprene concentrations at the measurement site by removal of OH and that OH concentrations are the controlling factor for isoprene concentrations over emissions. There seems to be a competing effect between increased ozone increasing OH concentrations and increased CO and VOCs acting to decrease OH concentrations.

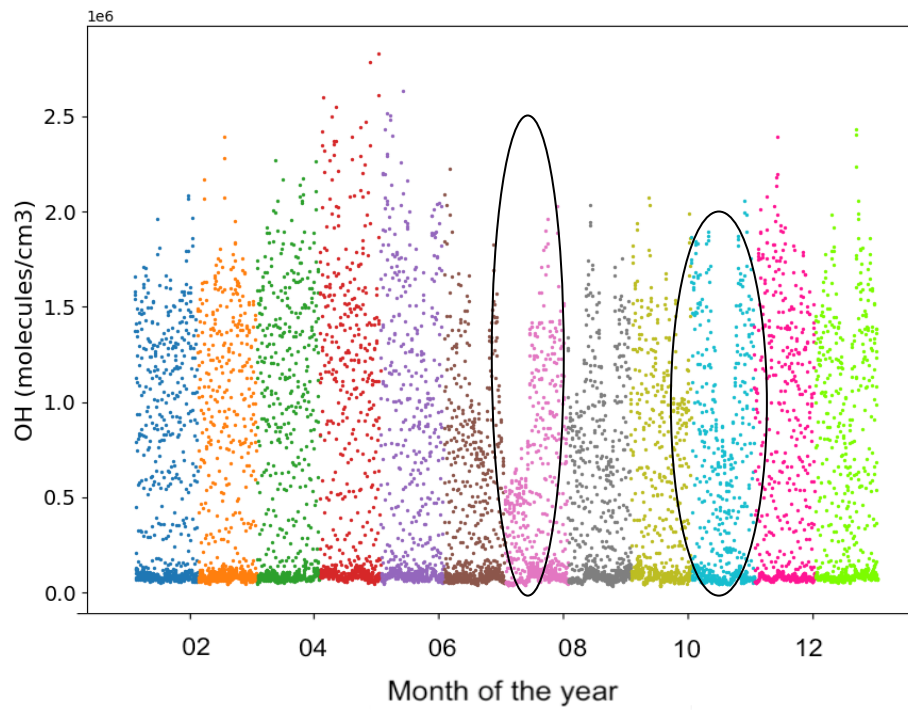


Figure 6.17 Same as Figure 6.13 for OH

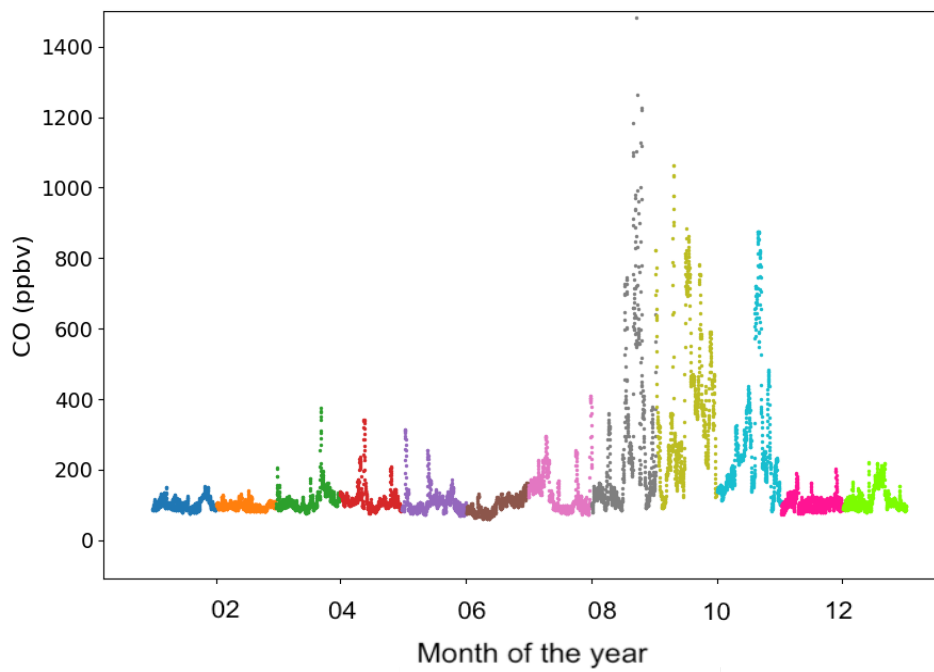


Figure 6.18 Same as Figure 6.13 for CO

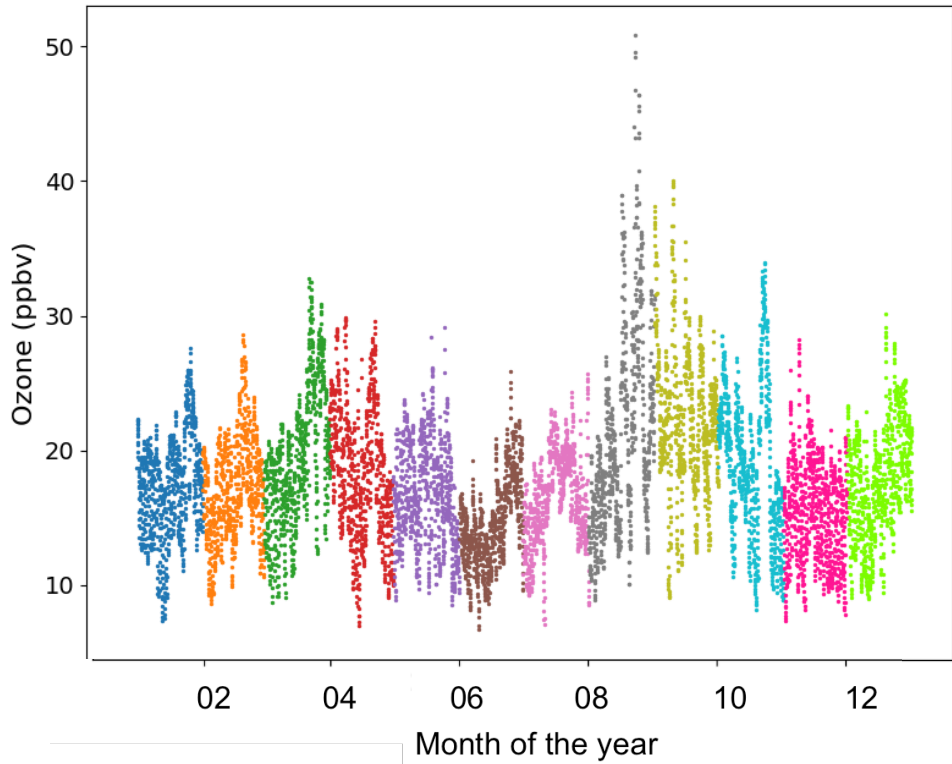


Figure 6.20 Same as Figure 6.13 for ozone

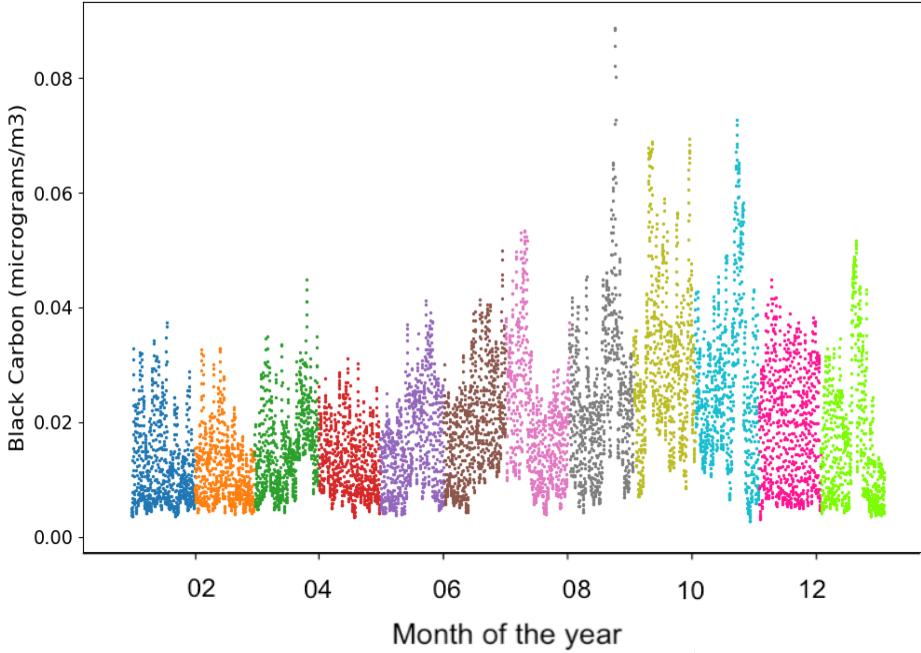


Figure 6.19 Same as Figure 6.13 for black carbon

## 6.7 Effect of Biogenic Emissions in GEOS-Chem

Biogenic emissions have large impacts on the composition, oxidizing capacity and aerosol and ozone concentrations in the atmosphere. The GEOS-Chem China grid (see chapter 3) was run with and without biogenic emissions from 1<sup>st</sup> November 2015 – 1<sup>st</sup> January 2016. These dates were chosen as this is a period where local effects should be dominant as the biomass burning season would have been finished. This should allow the effects of biogenic emissions to be studied independently of anthropogenic influences. The impact of biogenic emissions on a number of important atmospheric tracers is now described.

### 6.7.1 Isoprene

Figure 6.21 shows isoprene concentrations in GEOS-Chem with biogenic emissions turned on and off. This shows that isoprene at the measurement site is essentially all from biogenic sources. Considering the remote location of the site this would be expected. Figure 6.22 shows the surface concentrations of isoprene in the GEOS-Chem China nested grid.

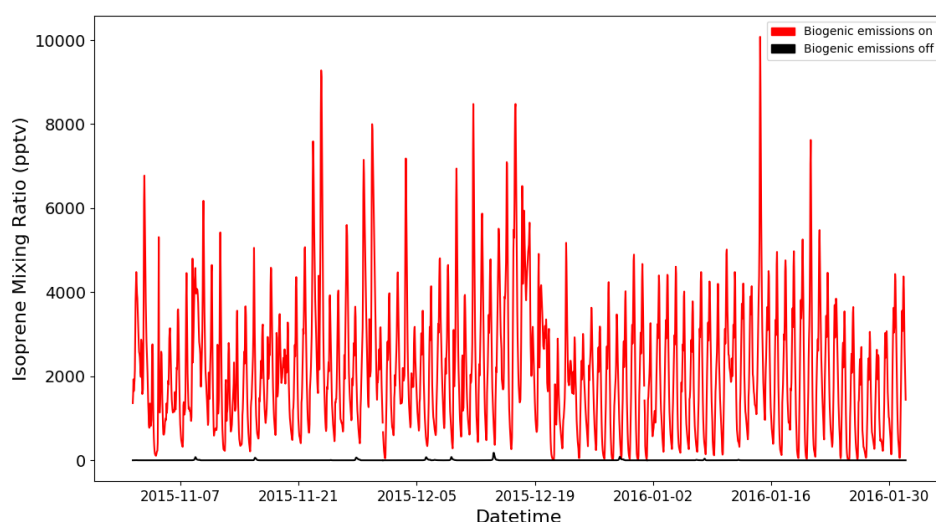


**Figure 6.21 Isoprene concentrations at the measurement site from GEOS-Chem with biogenic emissions turned on (red line) and off (black line)**

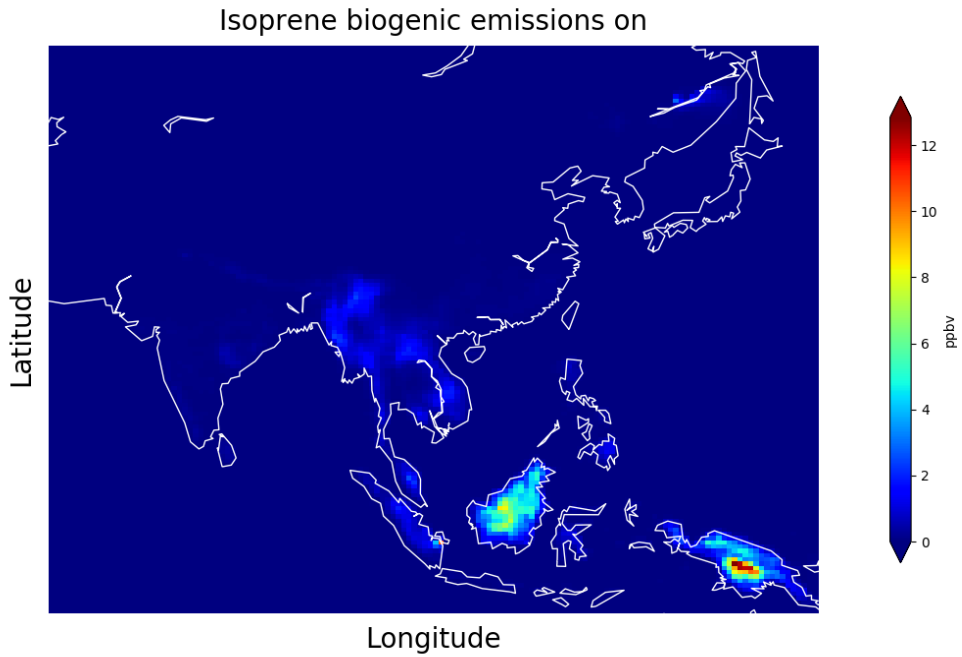


**Figure 6.22 Surface isoprene concentrations for the GEOS-Chem China nested grid with biogenic emissions on**

The change in isoprene concentrations when biogenic emissions were turned off is shown in. As expected this shows isoprene concentrations become essentially zero in forested remote regions when biogenic emissions are turned off.

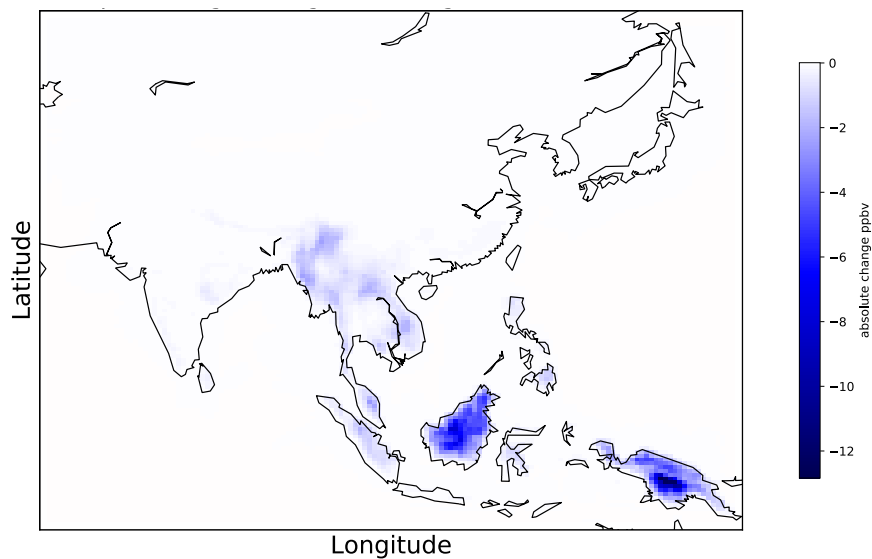


**Figure 6.23 The absolute change in isoprene (ppbv) when biogenic emissions were turned off in the GEOS-Chem China nested grid for November 2015**

## 6.8 OH

Figure 6.24 shows the differences in OH concentration at the measurement site with biogenic emissions turned on and off. This shows that mean OH concentrations increased by a factor of around five when biogenic emissions were turned off. BVOCs (mainly isoprene) and their oxidation products contribute the major sink (calculated to be >90% at noontime) to OH in a tropical rainforest environment (Edwards et al., 2013). Without this sink the OH removal rate is decreased and so OH concentrations are significantly greater than with biogenic emissions turned on.

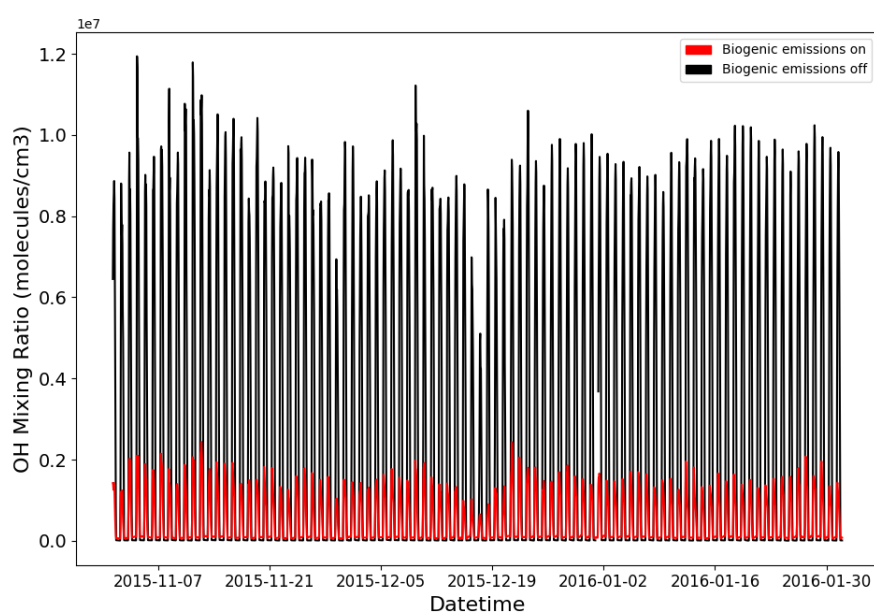


**Figure 6.24 OH concentrations at the measurement site from the GEOS-Chem China nested grid with biogenic emissions turned on (red line) and off (black line)**

**Table 6.4 Mean, median and inter-quartile range values for the measurement site in GEOS-Chem with and without biogenic emissions turned on**

OH	MEAN ( $10^6$ MOLEC/CM <sup>3</sup> )	MEDIAN ( $10^6$ MOLEC/CM <sup>3</sup> )	INTER QUARTILE RANGE ( $10^6$ MOLEC/CM <sup>3</sup> )
BIOGENICS ON	0.5	0.1	0.06-1.6
BIOGENICS OFF	2.7	0.02	0.008-9

## 6.9 Ozone

Turning off biogenic emissions in the model did not have a large impact on ozone mixing ratios for the measurement site. Although the peak ozone mixing ratios were sometimes higher, all statistics showed very little change (Table 6.5).

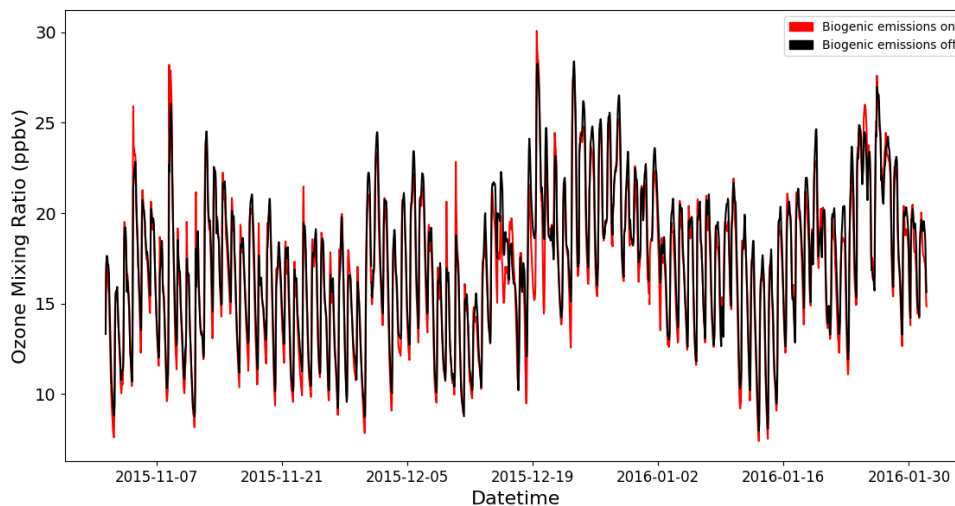


**Figure 6.25** Surface ozone concentrations from GEOS-Chem for the measurement site, with (red line) and without (black line) biogenic emissions turned on

**Table 6.5** Mean, median and inter-quartile range values for the measurement site in GEOS-Chem with and without biogenic emissions turned on

OZONE	MEAN (PPBV)	MEDIAN (PPBV)	INTER-QUARTILE RANGE (PPBV)
BIOGENICS ON	17.0	17.1	14.2-19.5
BIOGENICS OFF	17.3	17.5	14.7-20.0

Figure 6.26 shows surface ozone concentrations for the China nested grid run with biogenic emissions on. Ozone concentrations at the measurement site and the nearby areas are fairly low, less than 30 ppbv.

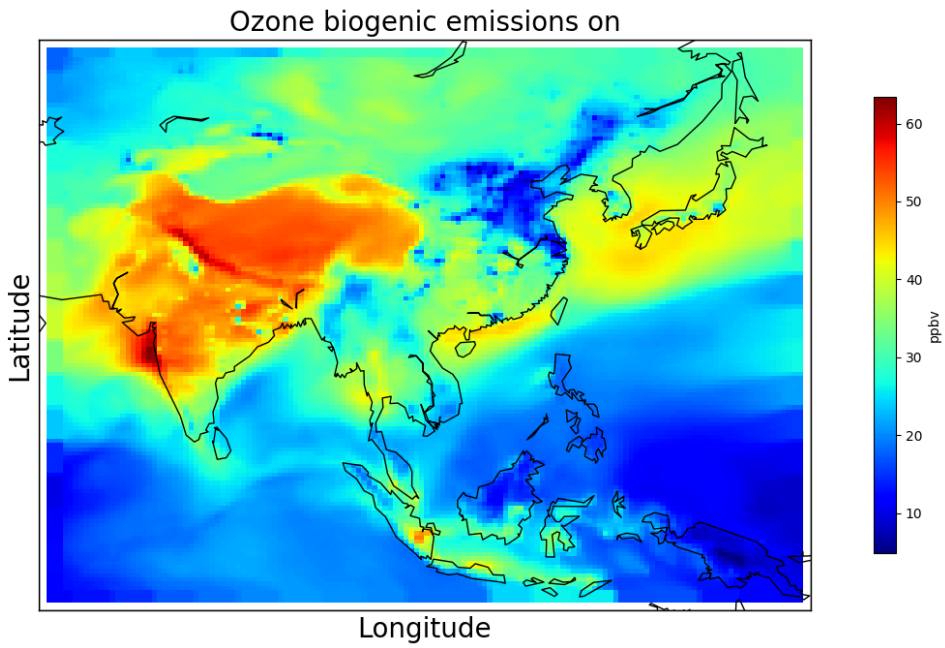


Figure 6.26 Surface ozone concentrations for the China nested grid with biogenic emissions on for November 2015

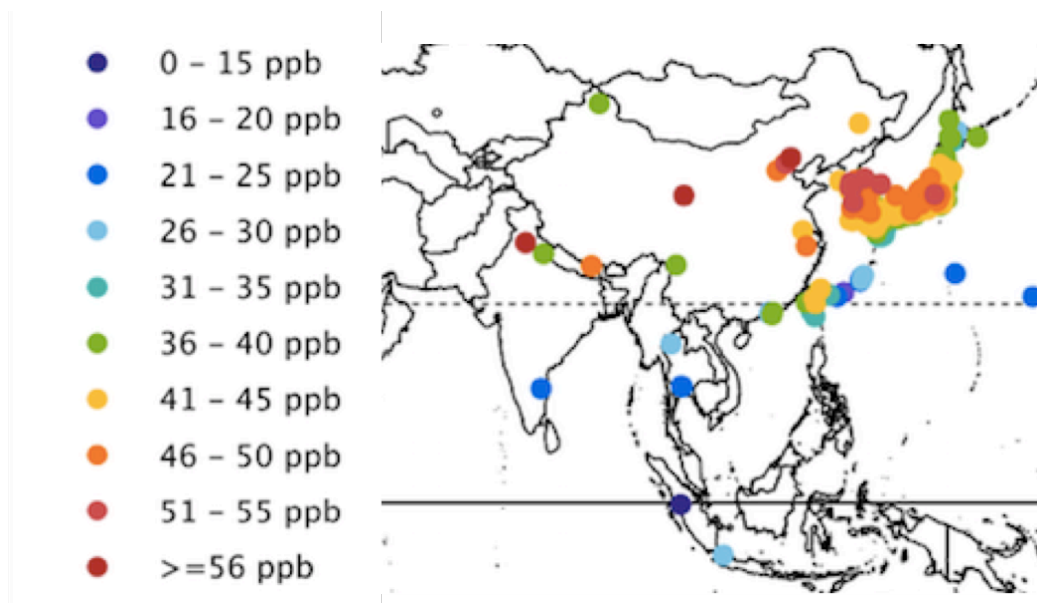
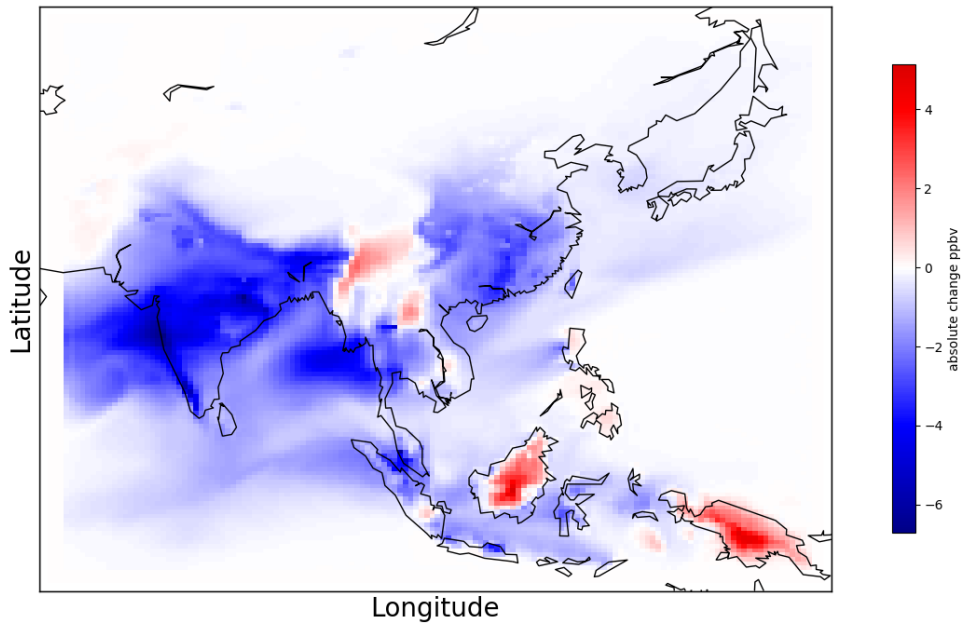


Figure 6.27 Daytime average surface ozone concentrations over Asia between 2010-2014. Data is from the TOAR database (Schultz et al. 2017). The map is adapted from the original downloaded from the PANGAEA website (<https://doi.pangaea.de/10.1594/PANGAEA.876109>).

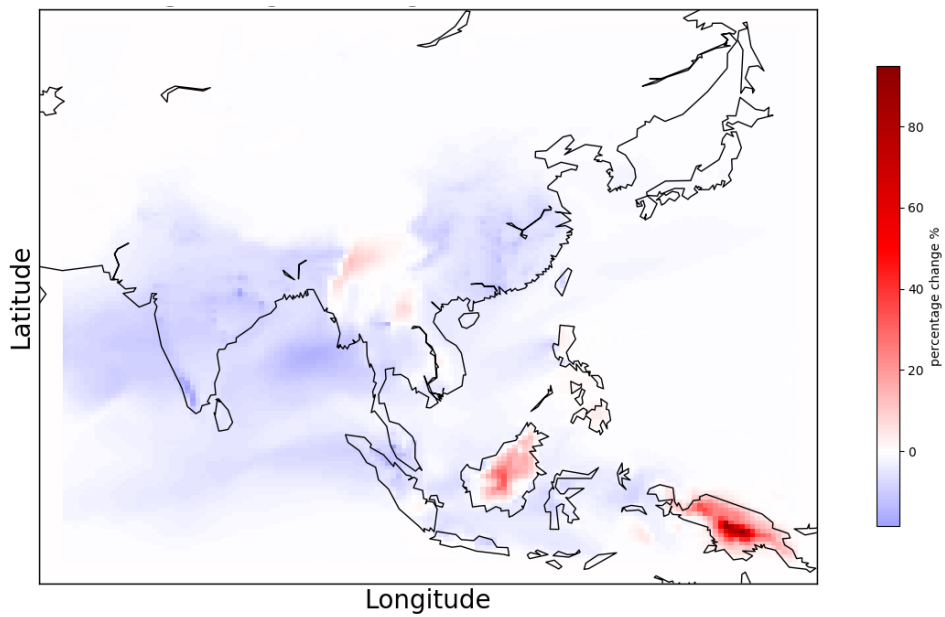
Figures 6.26 and 6.27 show surface ozone concentrations over Asia for GEOS-Chem in November 2015 and from the TOAR dataset (Schultz et al. 2017), daytime average between 2010-2014. There is a lack of observations surrounding the measurement site. The observations show higher concentrations over India, China and Japan, which is reflected in the model concentrations. Much lower concentrations are seen over most of the Southern parts of Asia, again this is reflected in the model.

Figure 6.28 shows the absolute change in ozone mixing ratios when biogenic emissions are turned off for the China nested grid. The change in mixing ratio varies between about -6 and +4 ppbv. As a percentage this accounts for an increase in ozone by as much as 80% for some regions, particularly over Borneo and some parts of Indonesia. The reason for an increase in ozone over these areas is that the reaction of ozone with VOCs (mainly isoprene) is an important removal process for ozone at the surface in the tropics. Several studies have shown that increased VOC emissions can lead to a decrease in ozone concentrations and this agrees with the changes in ozone simulated in this work (Brewer and Levine, 1985, Sanderson et al., 2003).

The opposite trend is seen over more polluted areas such as India and China. The decrease in ozone when biogenic emissions are turned off, is observed because VOC oxidation plays a key role in the formation of ozone under high  $\text{NO}_x$  conditions (Bowman and Seinfeld, 1994). Isoprene oxidation forms  $\text{RO}_2$  and  $\text{HO}_2$  radicals. These radicals can then react with  $\text{NO}$  to form  $\text{NO}_2$ . Subsequent photolysis of  $\text{NO}_2$  then leads to the formation of ozone (da Silva et al., 2018). Previous studies have shown that a decrease in VOCs can lead to a decrease in tropospheric ozone production and in some places reducing VOC emissions has been implemented as an air quality improvement strategy (Shao et al., 2009, Warneke et al., 2012)



**Figure 6.28** The mean absolute change in surface ozone (ppbv) when biogenic emissions were turned off in the GEOS-Chem China nested grid for November 2015



**Figure 6.29** The mean percentage change in surface ozone (ppbv) when biogenic emissions were turned off in the GEOS-Chem China nested grid for November 2015

## 6.10 PM<sub>2.5</sub>

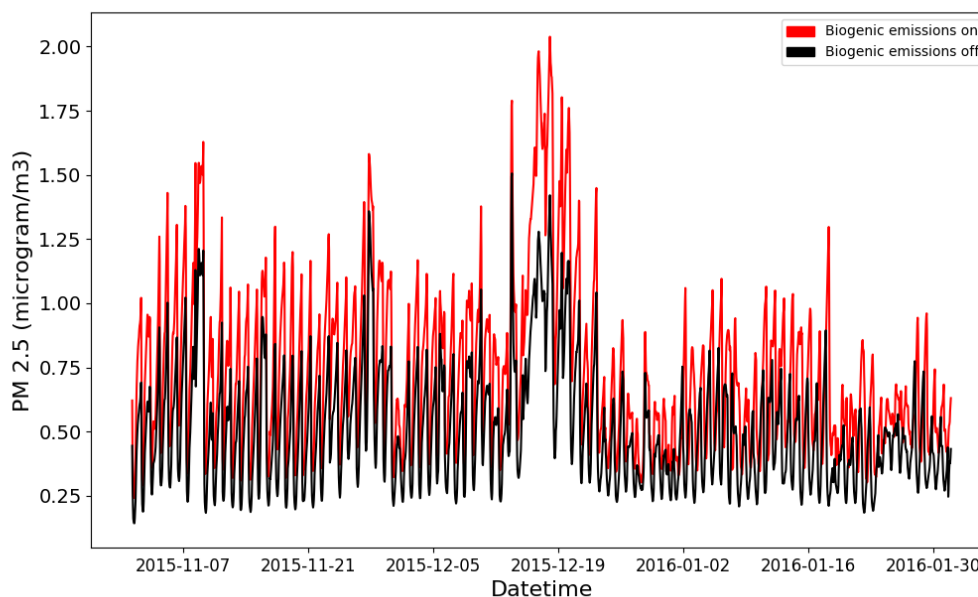


**Figure 6.30 Change in PM<sub>2.5</sub> for GEOS-Chem at the measurement site with biogenic emissions turned on off**

The effect of turning off biogenic emissions on surface PM<sub>2.5</sub> in GEOS-Chem is shown in Figure 6.30. The decrease in PM<sub>2.5</sub> is due to a decrease in SOA formation from biogenic VOCs. Other contributors to PM such as sulfates and nitrates do not change over this period.

**Table 6.6 Mean, median and inter-quartile range values for the measurement site in GEOS-Chem with and without biogenic emissions turned on**

PM 2.5	MEAN (MG/M <sup>3</sup> )	MEDIAN (MG/M <sup>3</sup> )	INTER-QUARTILE RANGE (MG/M <sup>3</sup> )
BIOGENICS ON	0.7	0.6	0.5-0.9
BIOGENICS OFF	0.5	0.5	0.3-0.6

Figure 6.31 shows the mean PM<sub>2.5</sub> concentrations for the China grid in November 2015 with biogenic emissions on. This shows that concentrations of PM<sub>2.5</sub> are comparatively low in the areas surrounding the measurement site, less than 2 µg/m<sup>3</sup>.

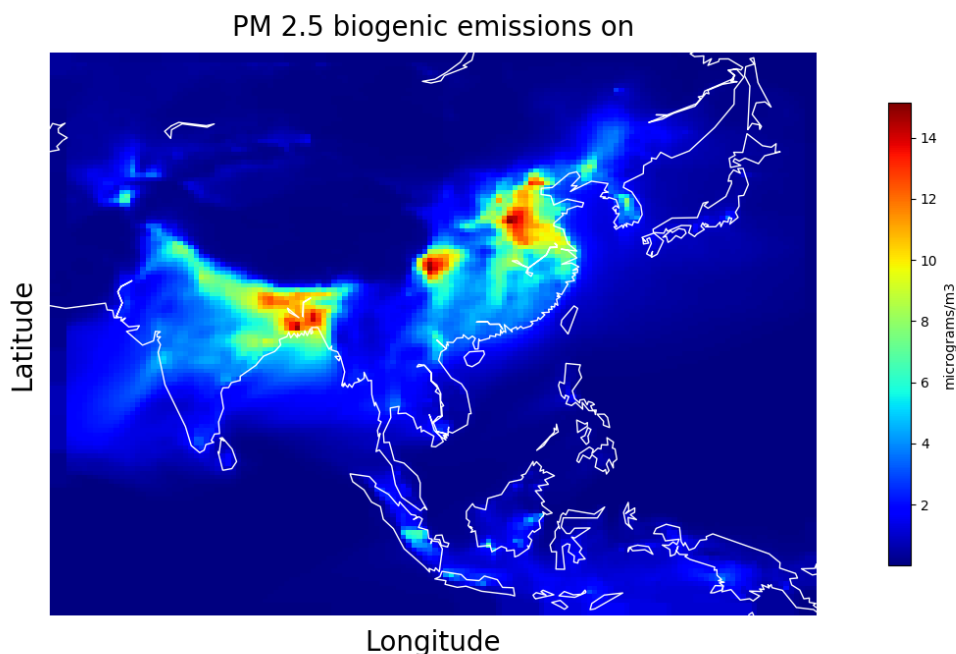


**Figure 6.31 Surface concentrations of PM<sub>2.5</sub> for the GEOS-Chem China nested grid with biogenic emissions on**

The absolute change in PM<sub>2.5</sub> when biogenic emissions were turned off is shown below in Figure 6.32. These maps show a decrease in PM<sub>2.5</sub> for large areas of the China grid. The decrease is due to a reduction in SOA formation due to the lack of biogenic emissions. Previous studies have shown that SOA contributes a substantial fraction of PM<sub>2.5</sub> formation. (Gelencsér et al., 2007) found that SOA contributes ~70% of PM<sub>2.5</sub> at several remote or rural European sites. (Carlton et al., 2009) report that in the tropics the contribution can be as high as 90%. A decrease in PM<sub>2.5</sub> would thus be expected when biogenic emissions are turned off. Over certain areas including large parts of Indonesia PM<sub>2.5</sub> decreases by 80% when biogenic emissions were switched off.

Given the substantial impact of biogenic emissions on PM<sub>2.5</sub> considering the impacts of potential changes is important. It has been shown that oil palm emits more isoprene than the native tropical rainforest and that VOC emissions could increase by a factor of three due to the expansion of oil palm (Misztal et al., 2011). This is something that should be considered when assessing future PM<sub>2.5</sub> in this region, as biogenic SOA for some areas is the dominant contributor to PM<sub>2.5</sub>. In addition to changes to VOC emissions from oil palm NO<sub>x</sub> emissions can also

increase (MacKenzie et al., 2011). This is likely to change the oxidative environment significantly and so understanding changes in land use is important.

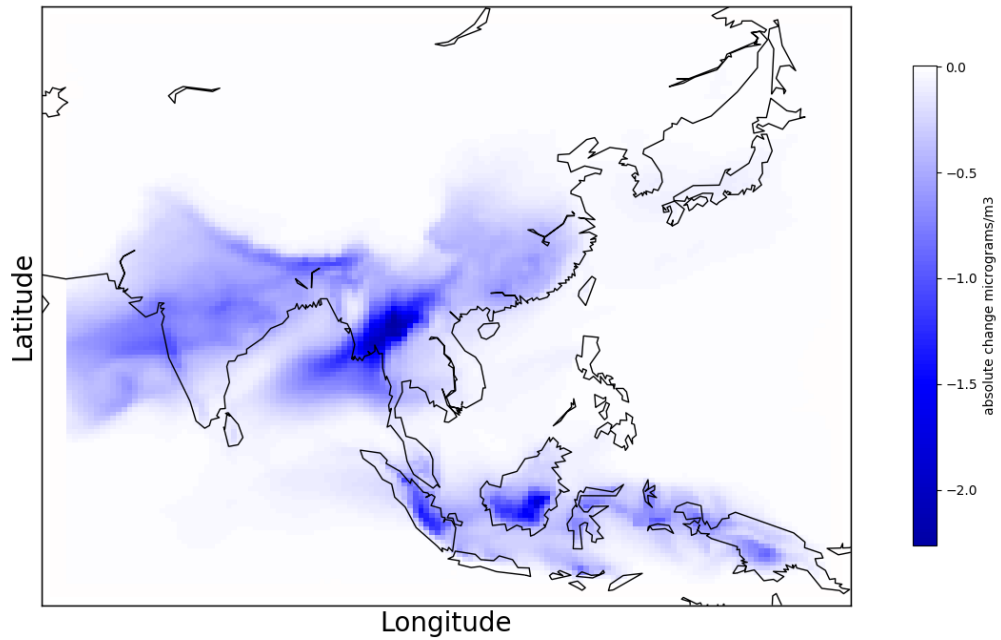


**Figure 6.32** The absolute change in PM<sub>2.5</sub> (µg/m<sup>3</sup>) when biogenic emissions were turned off in the GEOS-Chem China nested grid

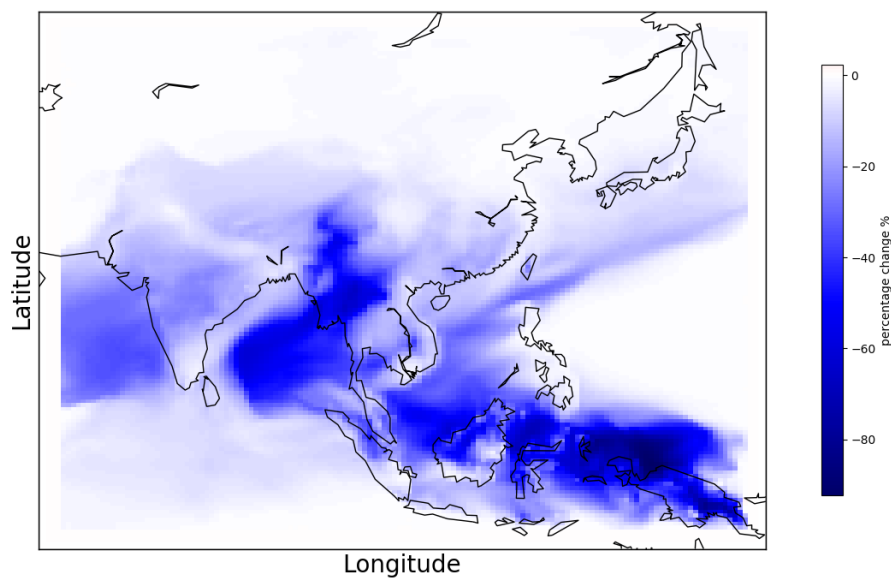


**Figure 6.33** The percentage change in PM<sub>2.5</sub> (µg/m<sup>3</sup>) when biogenic emissions were turned off in the GEOS-Chem China nested grid

## 6.11 Conclusions

This chapter focused on the background periods identified by NMF analysis. These periods were dominated by biogenic emissions with isoprene the dominant VOC.

Observations of propene made as part of this work showed propene mixing ratios in the tens to low hundreds of ppts. The GEOS-Chem model was run over the same time period but overestimated propene, giving mixing ratios in the thousands of ppts. The diurnal profiles from the observations showed a peak in the early afternoon for background periods, with daytime depletion during the biomass burning periods. The model showed a strong daytime depletion for all months. There was a strong anthropogenic contribution to the propene mixing ratios. When this component was removed model propene was still ten times greater than the observations. This is likely because MEGAN emission of propene are based upon observations in mid-latitude forests of the United States. Overall the model does not simulate well propene in the rainforest environment. However, given that isoprene emissions are 100 times greater than total model PRPE the impact of this problem is minimal. Where total PRPE is the sum of greater than three carbon alkenes.

GEOS-Chem does a better job overall in simulating the observed isoprene mixing ratios. The shape and magnitude of the mixing ratios during the background periods showed fairly good agreement. However, during the biomass burning months the model overestimated isoprene by a factor of around two. Whether this is due to a change in emissions (potentially from aerosol scattering affecting the distribution of leaves receiving light) or a change in the primary sink (OH) is difficult to know given the observational constraints available.

The effects of turning off biogenic emissions in GEOS-Chem on surface OH were large, with ~5 times as much OH when biogenic emissions were turned off. However, the impacts on ozone and PM<sub>2.5</sub> at the measurement site were relatively small. The mean concentration of ozone did not really change and a decrease in mean concentration of around 50% was seen for PM<sub>2.5</sub> when biogenic emissions were turned off. Given that the starting value of PM<sub>2.5</sub> was low, only ~1 (µg/m<sup>3</sup>), this is unlikely to have a significant impact. Large areas of the China nested grid showed a decrease in PM<sub>2.5</sub> when biogenic emissions were turned off. This was due

to the decrease in SOA production from biogenic VOCs. Changes in ozone were more varied across the region. Some areas with low  $\text{NO}_x$  concentrations showed an increase in ozone when biogenic emissions were turned off. This was due to no direct reaction of isoprene with ozone. Other areas with higher  $\text{NO}_x$  showed a decrease in ozone. This occurred because there was no reaction between VOCs and  $\text{NO}$ , which eventually leads to ozone production.

As expected isoprene concentrations at the site were due exclusively due to biogenic emissions. This was also true for large parts of the more remote regions of the China nested grid. Turning off biogenic emissions resulted in an increase in  $\text{OH}$  at the measurements site by a factor of around 5. This was due to the lack of VOC sink.



## Chapter 7

### 7 Conclusions and Future Work

This work made surface measurements of the mixing ratios of thirteen VOCs at the Bukit Atur measurement site in Malaysian Borneo between August 2015 and March 2016. The measurements were made using gas chromatography with flame ionisation detection (GC-FID). Non-negative matrix factorization (NMF) analysis identified three components in the dataset. These were indicative of biomass burning, background and local anthropogenic influences. The GEOS-Chem model was run over the measurement period to evaluate its success in simulating VOC concentrations during the different periods. The observations from this work were compared with those made using GC-FID and proton transfer reaction mass spectrometry (PTR-MS) during the oxidant and particle photochemical processes (OP3) campaign.

GC-FID is a well-established technique for the measurement of atmospheric VOCs and has previously been used for both short and long-term projects. When the instrument was working well the quality of data was generally good. However, this project showed that the instrument is reliant on a good quality, continuous power supply. Without this, regular manual intervention is needed. Overall, running an instrument at the Bukit Atur site involved a number of challenges and any future work either at this site or somewhere similar would benefit from considering and addressing the issues raised by this work before deployment. The issues with power, both quality and reliability, staff availability and working with a large time difference of 7-8 hours from UK time interfered with the aim of recording continuous hourly data. It may be that sampling with canisters and analysis away from the measurement site could offer an alternative method to on-line sampling at a remote site (Wang and Hao, 2012). However this comes at a cost to the temporal resolution of measurements and still requires manual input at the measurement site. Canister sampling has been used for long term VOC measurements but sampling was done on a weekly basis (Ochiai et al., 2003). For biogenic processes understanding the diurnal variations is key and so significant changes in canister technology would be needed for canisters to compete with in-situ measurements.

The OP3 PTR-MS measurements and those from this work generally showed good agreement, as did those from the first OP3 measurement period using the GC-FID. This is despite measurements being made in two different years across different months and the BALI project measurements were made during a strong El-Nino year, causing droughts within the region unlike the OP3 measurements. This suggests that there is not a large inter-annual or seasonal change in isoprene at this site. This is in contrast to the Amazon where strong seasonality in isoprene has been observed.

There were however differences in isoprene concentrations for the second OP3 measurement period between the GC-FID and PTR-MS datasets even though these were made at the same time at the same location. These measurements were made from 5 m (GC-FID) and 75 m (PTR-MS) above ground level. So although sampling height itself does not appear to affect isoprene measurements at this location, given the agreement during the first OP3 measurement period, possible localised events mean that it should be considered in the future when making measurements. This is especially important if measurements are intended to be representative of a wider region.

For other species there was more variability across the measurements from this project and OP3 during the background periods. Tests from this work showed that sampling at a lower height similar to the OP3 GC-FID measurements gave an increase in most VOCs, including propane, toluene and ethene. Isoprene did not show any increase during the lower sampling period (consistent with the agreements between the GC-FID and PTR-MS during the first OP3 measurement period). This suggests a local interference, possibly from vehicles, generators or emissions from other human activity such as cooking at the site.

The observations were separated into three periods using non-negative matrix factorisation analysis. This proved to be a relatively easy to use, useful technique for providing a statistical separation of the dataset into distinct components. The different components identified from the analysis fit well with our understanding and consideration of local and regional conditions and events in the wider region. This analysis could easily be applied to other atmospheric datasets.

The different periods identified by the non-negative matrix factorisation analysis were then compared with output from the GEOS-Chem model. The HEMCO emissions module enabled the Global Fire Assimilation System (GFAS) biomass burning inventory to be added into GEOS-Chem with relative ease, enabling comparison between the model and observations with temporally appropriate biomass burning emissions. Being able to turn off specific inventories allowed the effects of biomass burning and biogenic emissions on the atmospheric composition both at the measurement site and the wider region. This can be a useful indicator of what events have the biggest impacts on air quality and human health at individual sites and in the region more generally. This can be used to help decide what policies could have the biggest impacts on air quality in the region. Future work with GEOS-Chem could implement predictions of changes in biomass burning due to changes in climate or changes in VOC emissions due to land use changes to understand the impact on important species such as ozone and particulate matter. Comparison of the model calculations with World Health Organisation vegetation exposure guidelines could be used to link any changes in atmospheric composition to impacts on health.

Scaling factors for most VOCs were applied to the data in order to better assess the biomass burning and biogenic emissions independently of any overall model bias. Generally the model overestimated the concentration of most VOCs including propane, toluene and propene during the background periods. For some species (notably short lived species such as propene and the >C<sub>4</sub> alkanes) this was attributed to the emissions inventory having anthropogenic emissions in the measurement site grid box that were not realistic. This is likely a problem with grid resolution. The 0.5° x 0.625° simulated used here has a grid resolution of ~50 x 60 km. The measurement site grid box overlaps with anthropogenic activity leading to anthropogenic emissions becoming significant for the whole grid box. The spatial resolution contributes to this issue and the higher resolution a simulation the less likely it is that these sorts of issues will occur. When comparing with measurements at a single site it may be more appropriate to run simulations at a finer resolution, such as the 0.25° x 0.3125° Asia grid in GEOS-Chem. This relies on the assumption that suitably high resolution emissions data is available. An alternative to this would be to select a grid box other than the one that contains the actual latitude and longitude of the measurement site. In this work the grid box of interest was influenced by anthropogenic emissions. However nearby grid

boxes were not or were to a lesser extent. For future work it may be appropriate to look at whether adjacent grid boxes may better simulate the measurement site. However this may be problematic because the model may give better agreement with the observations but this could be for the wrong reasons.

During the biomass burning period, fire maps and back trajectories showed that air masses arriving at the measurement site travelled over areas of burning, predominantly in Indonesian Borneo. This period showed strong enhancements in most VOCs. Ethane and propane concentrations were up to ten times higher during this period compared with background concentrations. A similar enhancement was seen for other alkanes including iso and n-butane. Benzene and toluene both increased by a factor of around 5. Enhancements over this period were also seen in the GEOS-Chem simulations. The model seemed to simulate the timing of the biomass burning season and some of the variability during this period well. Once any intrinsic model bias was removed, the model generally simulated well ethane, propane, lumped >C4 alkanes and toluene during the biomass burning period. There was however an underestimation for benzene. This suggests that the GFAS emission inventory generally simulates well the magnitude of emissions during the Indonesian biomass burning season. Although not a default inventory in GEOS-Chem this work suggests that, at least for the Indonesian burning season, this inventory is a good choice. Especially given that data files are available in near real time.

The fire maps and trajectories combined show that variations in the concentration of different VOCs, resulting from biomass burning emissions, depend upon the meteorological conditions. Fire activity was near consistent over the measurement period and any variability in the VOCs concentrations was due to changes in wind directions.

Biomass burning emission ratios to propane calculated from the Danum Valley observations generally agreed better with previously determined values for peat burning rather than tree burning. Peat burning is known to contribute significantly to the overall burning emissions in Indonesia. The GFAS emission ratios generally showed better agreement with tree burning rather than peat burning. Comparison of our observed emission ratios with both forest and peat burning show that the

burning emissions at the measurement site resulted from a combination of peat and forest burning.

The background periods were primarily influenced by local, predominately biogenic emissions and VOC concentrations were dominated by isoprene. For other compounds, concentrations were determined by the large-scale regional background. The dominant biogenically sourced VOC of interest during these periods were propene and isoprene. GEOS-Chem substantially overestimated the propene mixing ratios at the site, by a factor of around ten. Even when the biogenic emissions were separated from any other emissions the propene mixing ratios were still too high. This suggests a problem with the biogenic emissions algorithm. The base propene emission is calculated from the relevant plant functional type (PFT). There is a single PFT that represents tropical broadleaf rainforests. For this PFT there is an emission factor for each type of VOC and propene is calculated as a percentage of the “other” VOC species. This base emission factor is then scaled to the meteorological data. The base emissions values are however based upon observations made at a temperate forest site in the United States because there is a lack of propene observations in the tropics. This thesis concludes that the current propene emission values are not appropriate for a tropical rainforest site.

An additional issue with this approach is an assumption that the tree type and therefore emission quantities are the same for all tropical broadleaf forests. To improve this more studies of tree types and their individual emissions factors are needed so that different areas of tropical rainforest can have emissions simulated more accurately. The isoprene emissions are 100 times greater than propene and so for the OH reactivity and SOA formation isoprene is the main concern.

The GEOS-Chem model generally simulated the isoprene mixing ratios well during the background periods, including the late afternoon peak that was observed for the BALI project but not during the OP3 campaign. GEOS-Chem isoprene emissions use the MEGAN emissions algorithm. Previous studies have found that MEGAN overestimates isoprene emissions in the tropics, however, this thesis shows that for the rainforest in Danum Valley the MEGAN isoprene emission values are appropriate.

Turning off the biogenic emissions in GEOS-Chem results in a decrease of up to 2  $\mu\text{g m}^{-3}$   $\text{PM}_{2.5}$  over forested areas of Borneo and Indonesia due to the lack of biogenic SOA formation. Changes in ozone were not consistent over the region. Large parts of Borneo, Indonesia and Papua New Guinea showed an increase in ozone when biogenic emissions were turned off. More polluted areas including China and India showed a decrease in ozone when biogenic emissions were turned off. This was dependant on local  $\text{NO}_x$  concentrations. In regions with low  $\text{NO}_x$  the direct reaction between isoprene and ozone means a likely reduction in ozone concentrations. In higher  $\text{NO}_x$  regions isoprene oxidation leads to the production of radicals that lead to ozone formation. The strongest effect from turning off biogenic emissions was seen for OH. At the measurements site OH concentrations increased by a factor of five. Although it is difficult to draw firm conclusions from this given the uncertainty about the response of OH concentrations to changes in VOCs (Lelieveld et al., 2008). However, this does show how important VOCs are in determining the oxidation capacity of the atmosphere and highlights the need for an improved understanding of the effects of VOC chemistry on OH concentrations.

Initially, the expectation of this project was that observations at this site would show an influence only from biogenic processes. However, this work has shown that VOCs at this remote tropical rainforest site are subject to localised anthropogenic conditions, regional scale biomass burning as well as biogenic emissions. Biomass burning emissions had a large seasonal impact increasing most measured VOCs. The observations made as part of the BALI project between August and October 2015, which showed an influence from biomass burning, coincided with the Indonesian biomass burning season. The fires during the 2015 burning season were on a larger scale than is experienced on an average year.

Model simulations showed that increases in ozone were seen as a result of biomass burning emissions across large parts of South East Asia. This may impact upon human and plant health and shows the importance of managing the burning and understanding how future changes in climate might affect burning in this region and therefore wider air quality. Given the success of GEOS-Chem in simulating the biomass burning period this would be a useful tool in understanding the impacts of future changes. Biogenic emissions dominated the background periods of this work. Model simulations showed that biogenic VOCs are important for understanding the oxidation capacity of the atmosphere. There

were also small impacts upon ozone and PM<sub>2.5</sub> concentrations when biogenic emissions were turned off. Given the large land use changes already happening in parts of South East Asia (such as the clearing of rainforest for agriculture) understanding the impacts of future changes is important for climate and air quality.



## 8 References

- Global Forest Watch* 2014 [Online]. <http://www.globalforestwatch.org>: World Resources Institute. [Accessed 2018].
- ABDUL-WAHAB, S. A., BAKHEIT, C. S. & AL-ALAWI, S. M. 2005. Principal component and multiple regression analysis in modelling of ground-level ozone and factors affecting its concentrations. *Environmental Modelling & Software*, 20, 1263-1271.
- ACTRIS 2014. WP4-NA4: Trace gases networking: Volatile organic carbon and nitrogen oxides. Deliverable D4.9: Final SOPs for VOC measurements. Accessed from <http://www.actris.net/>
- AINSWORTH, E. A. 2008. Rice production in a changing climate: a meta - analysis of responses to elevated carbon dioxide and elevated ozone concentration. *Global Change Biology*, 14, 1642-1650.
- AINSWORTH, E. A., YENDREK, C. R., SITCH, S., COLLINS, W. J. & EMBERSON, L. D. 2012. The effects of tropospheric ozone on net primary productivity and implications for climate change. *Annual Review of Plant Biology*, 63, 637-661.
- ANDREAE, M. O. & MERLET, P. 2001. Emission of trace gases and aerosols from biomass burning. *Global Biogeochemical Cycles*, 15, 955-966.
- ARCHIBALD, S., ROY DAVID, P., VAN, W. B. W. & SCHOLES ROBERT, J. 2009. What limits fire? An examination of drivers of burnt area in Southern Africa. *Global Change Biology*, 15, 613-630.
- ARNETH, A., SCHURGERS, G., LATHIERE, J., DUHL, T., BEERLING, D. J., HEWITT, C. N., MARTIN, M. & GUENTHER, A. 2011. Global terrestrial isoprene emission models: sensitivity to variability in climate and vegetation. *Atmospheric Chemistry and Physics*, 11, 8037-8052.
- ATKINSON, R. 2000. Atmospheric chemistry of VOCs and NOx. *Atmospheric Environment*, 34, 2063-2101.
- ATKINSON, R. 2007. Gas-phase tropospheric chemistry of organic compounds: a review. *Atmospheric Environment*, 41, 200-240.
- ATKINSON, R. & AREY, J. 2003. Atmospheric Degradation of Volatile Organic Compounds. *Chemical Reviews*, 103, 4605-4638.
- ATKINSON, R. W., KANG, S., ANDERSON, H. R., MILLS, I. C. & WALTON, H. A. 2014. Epidemiological time series studies of PM<sub>2.5</sub>; and daily mortality and hospital admissions: a systematic review and meta-analysis. *Thorax*.

- AVNER, S., MAUZERALL, D. L., LIU, J. & HOROWITZ, L. W. 2011. Global crop yield reductions due to surface ozone exposure: 1. Year 2000 crop production losses and economic damage. *Atmospheric Environment*, 45, 2284-2296.
- B. NGUYEN, T., D. CROUNSE, J., H. SCHWANTES, R., TENG, A., BATES, K., ZHANG, X., M. ST. CLAIR, J., H. BRUNE, W., S. TYNDALL, G., N. KEUTSCH, F., H. SEINFELD, J. & WENNERBERG, P. 2014. *Overview of the Focused Isoprene eXperiment at the California Institute of Technology (FIXCIT): mechanistic chamber studies on the oxidation of biogenic compounds. Atmospheric Chemistry and Physics*, 14, 13531-13549.
- BAEK, K. H., KIM, J. H., PARK, R. J., CHANCE, K. & KUROSU, T. P. 2014. Validation of OMI HCHO data and its analysis over Asia. *Science of The Total Environment*, 490, 93-105.
- BAKER, A. K., SLEMR, F. & BRENNINKMEIJER, C. A. M. 2010. Analysis of non-methane hydrocarbons in air samples collected aboard the CARIBIC passenger aircraft. *Atmospheric Measurement Techniques*, 3, 311-321.
- BARKLEY, M. P., PALMER, P. I., DE SMEDT, I., KARL, T., GUENTHER, A. & VAN ROOZENDAEL, M. 2009. Regulated large-scale annual shutdown of Amazonian isoprene emissions? *Geophysical Research Letters*, 36(4).
- BARKLEY, M. P., PALMER, P. I., KUHN, U., KESSELMEIER, J., CHANCE, K., KUROSU, T. P., MARTIN, R. V., HELMIG, D. & GUENTHER, A. 2008. Net ecosystem fluxes of isoprene over tropical South America inferred from Global Ozone Monitoring Experiment (GOME) observations of HCHO columns. *Journal of Geophysical Research: Atmospheres*, 113(D20).
- BARTENBACH, S., WILLIAMS, J., PLASS-DÜLMER, C., BERRESHEIM, H. & LELIEVELD, J. 2006. *In-situ measurement of reactive hydrocarbons at Hohenpeissenberg with comprehensive two-dimensional gas chromatography (GC×GC-FID): Use in estimating HO and NO<sub>3</sub>. Atmospheric Chemistry and Physics*, 7, 1-14.
- BAUWENS, M., STAVRAKOU, T., MÜLLER, J. F., DE SMEDT, I., VAN ROOZENDAEL, M., VAN DER WERF, G. R., WIEDINMYER, C., KAISER, J. W., SINDELAROVA, K. & GUENTHER, A. 2016. Nine years of global hydrocarbon emissions based on source inversion of OMI formaldehyde observations. *Atmospheric Chemistry and Physics*, 16, 10133-10158.
- BAYLON, P., JAFFE, D. A., HALL, S. R., ULLMANN, K., ALVARADO, M. J. & LEFER, B. L. 2018. Impact of Biomass Burning Plumes on Photolysis Rates and Ozone

- Formation at the Mount Bachelor Observatory. *Journal of Geophysical Research: Atmospheres*, 123, 2272-2284.
- BEIG, G. & BRASSEUR, G. P. 2006. Influence of anthropogenic emissions on tropospheric ozone and its precursors over the Indian tropical region during a monsoon. *Geophysical Research Letters*, 33(7).
- BELL, M. L., GOLDBERG, R., HOGREFE, C., KINNEY, P. L., KNOWLTON, K., LYNN, B., ROSENTHAL, J., ROSENZWEIG, C. & PATZ, J. A. 2007. Climate change, ambient ozone, and health in 50 US cities. *Climatic Change*, 82, 61-76.
- BELL, M. L., MCDERMOTT, A., ZEGER, S. L., SAMET, J. M. & DOMINICI, F. 2004. Ozone and short-term mortality in 95 us urban communities, 1987-2000. *JAMA*, 292, 2372-2378.
- BEY, I., JACOB, D. J., YANTOSCA, R. M., LOGAN, J. A., FIELD, B. D., FIORE, A. M., LI, Q., LIU, H. Y., MICKLEY, L. J. & SCHULTZ, M. G. 2001. Global modeling of tropospheric chemistry with assimilated meteorology: Model description and evaluation. *Journal of Geophysical Research: Atmospheres (1984-2012)*, 106, 23073-23095.
- BLOSS, C., WAGNER, V., JENKIN, M. E., VOLKAMER, R., BLOSS, W. J., LEE, J. D., HEARD, D. E., WIRTZ, K., MARTIN-REVIEJO, M., REA, G., WENGER, J. C. & PILLING, M. J. 2005. Development of a detailed chemical mechanism (MCMv3.1) for the atmospheric oxidation of aromatic hydrocarbons. *Atmospheric Chemistry and Physics*, 5, 641-664.
- BOUSQUET, P., CIAIS, P., MILLER, J. B., DLUGOKENCKY, E. J., HAUGLUSTAINE, D. A., PRIGENT, C., VAN DER WERF, G. R., PEYLIN, P., BRUNKE, E. G., CAROUGE, C., LANGENFELDS, R. L., LATHIÈRE, J., PAPA, F., RAMONET, M., SCHMIDT, M., STEELE, L. P., TYLER, S. C. & WHITE, J. 2006. Contribution of anthropogenic and natural sources to atmospheric methane variability. *Nature*, 443, 439-443.
- BOUVIER-BROWN, N. C., HOLZINGER, R., PALITZSCH, K. & GOLDSTEIN, A. H. 2009. Large emissions of sesquiterpenes and methyl chavicol quantified from branch enclosure measurements. *Atmospheric Environment*, 43, 389-401.
- BOWMAN, F. M. & SEINFELD, J. H. 1994. Fundamental basis of incremental reactivities of organics in ozone formation in VOC/NO<sub>x</sub> mixtures. *Atmospheric Environment*, 28, 3359-3368.
- BRACHO-NUNEZ, A., KNOTHE, N. M., WELTER, S., STAUDT, M., COSTA, W. R., LIBERATO, M. A. R., PIEDADE, M. T. F. & KESSELMEIER, J. 2013. Leaf level

- emissions of volatile organic compounds (VOC) from some Amazonian and Mediterranean plants. *Biogeosciences*, 10, 5855-5873.
- BRAVO, H., SOSA, R., SÁNCHEZ, P., BUENO, E. & GONZÁLEZ, L. 2002. Concentrations of benzene and toluene in the atmosphere of the southwestern area at the Mexico City Metropolitan Zone. *Atmospheric Environment*, 36, 3843-3849.
- BREWER, D. A. & LEVINE, J. S. The Role of Isoprene Oxidation in the Tropospheric Ozone Budget in the Tropics. *Atmospheric Ozone*, 1985 Dordrecht. Springer Netherlands, 715-719.
- BROWN, N. 1993. The Implications of Climate and Gap Microclimate for Seedling Growth Conditions in a Bornean Lowland Rain Forest. *Journal of Tropical Ecology*, 9, 153-168.
- BRUNEKREEF, B. & FORSBERG, B. 2005. Epidemiological evidence of effects of coarse airborne particles on health. *European Respiratory Journal*, 26, 309-318.
- BYUN, D. W. 1990. On the Analytical Solutions of Flux-Profile Relationships for the Atmospheric Surface Layer. *Journal of Applied Meteorology*, 29, 652-657.
- CAHOON JR, D. R., STOCKS, B. J., LEVINE, J. S., COFER III, W. R. & O'NEILL, K. P. 1992. Seasonal distribution of African savanna fires. *Nature*, 359, 812-815.
- CARLTON, A., WIEDINMYER, C. & KROLL, J. 2009. A review of Secondary Organic Aerosol (SOA) formation from isoprene. *Atmospheric Chemistry and Physics*, 9, 4987-5005.
- CARSLAW, D. C., BEEVERS, S. D., TATE, J. E., WESTMORELAND, E. J. & WILLIAMS, M. L. 2011. Recent evidence concerning higher NO<sub>x</sub> emissions from passenger cars and light duty vehicles. *Atmospheric Environment*, 45, 7053-7063.
- CHAI, M. & PAWLISZYN, J. 1995. Analysis of Environmental Air Samples by Solid-Phase Microextraction and Gas Chromatography/Ion Trap Mass Spectrometry. *Environmental Science & Technology*, 29, 693-701.
- CHAMEIDES, W. L., YU, H., LIU, S. C., BERGIN, M., ZHOU, X., MEARN, L., WANG, G., KIANG, C. S., SAYLOR, R. D., LUO, C., HUANG, Y., STEINER, A. & GIORGI, F. 1999. Case study of the effects of atmospheric aerosols and regional haze on agriculture: An opportunity to enhance crop yields in China through emission controls? *Proceedings of the National Academy of Sciences*, 96, 13626-13633.

- CHAN, L., LIU, H., LAM, K., WANG, T., OLTMANS, S. & HARRIS, J. 1998. Analysis of the seasonal behavior of tropospheric ozone at Hong Kong. *Atmospheric Environment*, 32, 159-168.
- CHANG, C.-C., WANG, J.-L., LUNG, S.-C. C., CHANG, C.-Y., LEE, P.-J., CHEW, C., LIAO, W.-C., CHEN, W.-N. & OU-YANG, C.-F. 2014. Seasonal characteristics of biogenic and anthropogenic isoprene in tropical-subtropical urban environments. *Atmospheric Environment*, 99, 298-308.
- CHEN, D., WANG, Y., MCELROY, M., HE, K., YANTOSCA, R. & SAGER, P. L. 2009. Regional CO pollution and export in China simulated by the high-resolution nested-grid GEOS-Chem model. *Atmospheric Chemistry and Physics*, 9, 3825-3839.
- CHIN, J.-Y. & BATTERMAN, S. A. 2012. VOC composition of current motor vehicle fuels and vapors, and collinearity analyses for receptor modeling. *Chemosphere*, 86, 951-958.
- CHEN, T.-Y., SIMPSON, I. J., BLAKE, D. R. & ROWLAND, F. S. 2001. Impact of the leakage of liquefied petroleum gas (LPG) on Santiago Air Quality. *Geophysical Research Letters*, 28, 2193-2196.
- CHUEINTA, W., HOPKE, P. K. & PAATERO, P. 2000. Investigation of sources of atmospheric aerosol at urban and suburban residential areas in Thailand by positive matrix factorization. *Atmospheric Environment*, 34, 3319-3329.
- CLARKSON, T. S., MARTIN, R.J., RUDOLPH, J., GRAHAM, B.W.L., 1996. Benzene and toluene in New Zealand air. *Atmospheric Environment*, 30, 569-577.
- COLMAN, J. J., SWANSON, A. L., MEINARDI, S., SIVE, B. C., BLAKE, D. R. & ROWLAND, F. S. 2001. Description of the Analysis of a Wide Range of Volatile Organic Compounds in Whole Air Samples Collected during PEM-Tropics A and B. *Analytical Chemistry*, 73, 3723-3731.
- CROUNSE, J. D., PAULOT, F., KJAERGAARD, H. G. & WENNERBERG, P. O. 2011. Peroxy radical isomerization in the oxidation of isoprene. *Physical Chemistry Chemical Physics*, 13, 13607-13613.
- CRUTZEN, P. J. & ANDREAE, M. O. 1990. Biomass Burning in the Tropics: Impact on Atmospheric Chemistry and Biogeochemical Cycles. *Science*, 250, 1669-1678.
- CRUTZEN, P. J., HEIDT, L. E., KRASNEC, J. P., POLLOCK, W. H. & SEILER, W. 1979. Biomass burning as a source of atmospheric gases CO, H<sub>2</sub>, N<sub>2</sub>O, NO, CH<sub>3</sub>Cl and COS. *Nature*, 282, 253-256.

- DA SILVA, C. M., CORRÊA, S. M. & ARBILLA, G. 2018. Isoprene Emissions and Ozone Formation in Urban Conditions: A Case Study in the City of Rio de Janeiro. *Bulletin of environmental contamination and toxicology*, 100, 184-188.
- DAMIAN, V., SANDU, A., DAMIAN, M., POTRA, F. & CARMICHAEL, G. R. 2002. The kinetic preprocessor KPP-a software environment for solving chemical kinetics. *Computers & Chemical Engineering*, 26, 1567-1579.
- DELMAS, R., SERÇA, D. & JAMBERT, C. 1997. Global inventory of NO<sub>x</sub> sources. *Nutrient Cycling in Agroecosystems*, 48, 51-60.
- DERWENT, R. G., MIDDLETON, D. R., FIELD, R. A., GOLDSTONE, M. E., LESTER, J. N. & PERRY, R. 1995. Analysis and interpretation of air quality data from an urban roadside location in Central London over the period from July 1991 to July 1992. *Atmospheric Environment*, 29, 923-946.
- DERWENT, R. G., SIMMONDS, P. G., SEURING, S. & DIMMER, C. 1998. Observation and interpretation of the seasonal cycles in the surface concentrations of ozone and carbon monoxide at mace head, Ireland from 1990 to 1994. *Atmospheric Environment*, 32, 145-157.
- DIMITRIADES, B. 1972. Effects of hydrocarbon and nitrogen oxides on photochemical smog formation. *Environmental Science & Technology*, 6, 253-260.
- DING, A. & WANG, T. 2006. Influence of stratosphere - to - troposphere exchange on the seasonal cycle of surface ozone at Mount Waliguan in western China. *Geophysical Research Letters*, 33(3).
- DONOSO, L., ROMERO, R., RONDÓN, A., FERNANDEZ, E., OYOLA, P. & SANHUEZA, E. 1996. Natural and anthropogenic C<sub>2</sub> to C<sub>6</sub> hydrocarbons in the central-eastern Venezuelan atmosphere during the rainy season. *Journal of Atmospheric Chemistry*, 25, 201-214.
- DUARTE-DAVIDSON, R., COURAGE, C., RUSHTON, L. & LEVY, L. 2001. Benzene in the environment: an assessment of the potential risks to the health of the population. *Occupational and Environmental Medicine*, 58, 2-13.
- DUNCAN, B. N., MARTIN, R. V., STAUDT, A. C., YEVICH, R. & LOGAN, J. A. 2003. Interannual and seasonal variability of biomass burning emissions constrained by satellite observations. *Journal of Geophysical Research: Atmospheres*, 108(D2).
- EBI, K. L. & MCGREGOR, G. 2008. Climate Change, Tropospheric Ozone and Particulate Matter, and Health Impacts. *Environmental Health Perspectives*, 116, 1449-1455.

- EDWARDS, D. P., EMMONS, L. K., GILLE, J. C., CHU, A., ATTIÉ, J. L., GIGLIO, L., WOOD, S. W., HAYWOOD, J., DEETER, M. N., MASSIE, S. T., ZISKIN, D. C. & DRUMMOND, J. R. 2006. Satellite - observed pollution from Southern Hemisphere biomass burning. *Journal of Geophysical Research: Atmospheres*, 111(D14).
- EDWARDS, P. M., EVANS, M. J., FURNEAUX, K. L., HOPKINS, J., INGHAM, T., JONES, C., LEE, J. D., LEWIS, A. C., MOLLER, S. J., STONE, D., WHALLEY, L. K. & HEARD, D. E. 2013. OH reactivity in a South East Asian tropical rainforest during the Oxidant and Particle Photochemical Processes (OP3) project. *Atmospheric Chemistry and Physics*, 13, 9497-9514.
- EMMANUEL, S. C. 2001. Impact to lung health of haze from forest fires: The Singapore experience. *Respirology*, 5, 175-182.
- ENGLING, G., HE, J., BETHA, R. & BALASUBRAMANIAN, R. 2014. Assessing the regional impact of Indonesian biomass burning emissions based on organic molecular tracers and chemical mass balance modeling. *Atmospheric Chemistry and Physics*, 14, 8043-8054.
- ERVENS, B., CARLTON ANNMARIE, G., TURPIN BARBARA, J., ALTIERI KATY, E., KREIDENWEIS SONIA, M. & FEINGOLD, G. 2008. Secondary organic aerosol yields from cloud - processing of isoprene oxidation products. *Geophysical Research Letters*, 35(2).
- FALL, R., KARL, T., HANSEL, A., JORDAN, A. & LINDINGER, W. 1999. Volatile organic compounds emitted after leaf wounding: On - line analysis by proton - transfer - reaction mass spectrometry. *Journal of Geophysical Research: Atmospheres*, 104, 15963-15974.
- FARES, S., SCHNITZHOFFER, R., JIANG, X., GUENTHER, A., HANSEL, A. & LORETO, F. 2013. Observations of Diurnal to Weekly Variations of Monoterpene-Dominated Fluxes of Volatile Organic Compounds from Mediterranean Forests: Implications for Regional Modeling. *Environmental Science & Technology*, 47, 11073-11082.
- FEREK, R., REID, J., HOBBS, P. V., BLAKE, D. R. & LIOUSSE, C. 1998. *Emission factors of hydrocarbons, halocarbons, trace gases and particles from biomass burning in Brazil*. *Journal of Geophysical Research: Atmospheres*, 103(D24).
- FIELD, R. D., VAN DER WERF, G. R., FANIN, T., FETZER, E. J., FULLER, R., JETHVA, H., LEVY, R., LIVESEY, N. J., LUO, M. & TORRES, O. 2016. Indonesian fire activity and smoke pollution in 2015 show persistent nonlinear sensitivity

- to El Niño-induced drought. *Proceedings of the National Academy of Sciences*, 113, 9204-9209.
- FIELD, R. D., VAN DER WERF, G. R. & SHEN, S. S. P. 2009. Human amplification of drought-induced biomass burning in Indonesia since 1960. *Nature Geoscience*, 2, 185-188.
- FILLEUL, L., CASSADOU, S., MÉDINA, S., FABRES, P., LEFRANC, A., EILSTEIN, D., LE TERTRE, A., PASCAL, L., CHARDON, B., BLANCHARD, M., DECLERCQ, C., JUSOT, J.-F., PROUVOST, H. & LEDRANS, M. 2006. The Relation Between Temperature, Ozone, and Mortality in Nine French Cities During the Heat Wave of 2003. *Environmental Health Perspectives*, 114, 1344-1347.
- FINLAYSON-PITTS, B. J. & PITTS, J. N. 1993. Atmospheric Chemistry of Tropospheric Ozone Formation: Scientific and Regulatory Implications. *Air & Waste*, 43, 1091-1100.
- FIOLETOV, V. E., BODEKER, G. E., MILLER, A. J., MCPETERS, R. D. & STOLARSKI, R. 2002. Global and zonal total ozone variations estimated from ground - based and satellite measurements: 1964–2000. *Journal of Geophysical Research: Atmospheres*, 107(D22).
- FISHMAN, J., RAMANATHAN, V., CRUTZEN, P. J. & LIU, S. C. 1979. Tropospheric ozone and climate. *Nature*, 282, 818-820.
- FISHMAN, J., WOZNIAK, A. & CREILSON, J. 2003. Global distribution of tropospheric ozone from satellite measurements using the empirically corrected tropospheric ozone residual technique: Identification of the regional aspects of air pollution. *Atmospheric Chemistry and Physics*, 3, 893-907.
- FOWLER, D., NEMITZ, E., MISZTAL, P., DI MARCO, C., SKIBA, U., RYDER, J., HELFTER, C., CAPE, J. N., OWEN, S. & DORSEY, J. 2011. Effects of land use on surface–atmosphere exchanges of trace gases and energy in Borneo: comparing fluxes over oil palm plantations and a rainforest. *Philosophical Transactions of the Royal Society B: Biological Sciences*, 366, 3196-3209.
- FRANCO, B., MAHIEU, E., EMMONS, LK., TZOMPA-SOSA, ZA., FISCHER, EV., SUDO, K., BOVY, B., CONWAY, S., GRIFFIN, D., HANNIGAN, JW., STRONG, K., WALKER, KA. 2016. Evaluating ethane and methane emissions associated with the development of oil and natural gas extraction in North America. *Environmental Research Letters*, 11(4).
- FRANKENBERG, E., MCKEE, D. & THOMAS, D. 2005. Health consequences of forest fires in Indonesia. *Demography*, 42, 109-129.

- GALLOWAY, J. N. 1995. Acid deposition: Perspectives in time and space. *Water, Air, and Soil Pollution*, 85, 15-24.
- GAO, B., WANG, X.-M., ZHAO, X.-Y., DING, X., FU, X.-X., ZHANG, Y.-L., HE, Q.-F., ZHANG, Z., LIU, T.-Y., HUANG, Z.-Z., CHEN, L.-G., PENG, Y. & GUO, H. 2015. Source apportionment of atmospheric PAHs and their toxicity using PMF: Impact of gas/particle partitioning. *Atmospheric Environment*, 103, 114-120.
- GELARO, R., MCCARTY, W., SUÁREZ, M. J., TODLING, R., MOLOD, A., TAKACS, L., RANGLES, C. A., DARMENOV, A., BOSILOVICH, M. G., REICHLER, R., WARGAN, K., COY, L., CULLATHER, R., DRAPER, C., AKELLA, S., BUCHARD, V., CONATY, A., DA SILVA, A. M., GU, W., KIM, G.-K., KOSTER, R., LUCCHESI, R., MERKOVA, D., NIELSEN, J. E., PARTYKA, G., PAWSON, S., PUTMAN, W., RIENECKER, M., SCHUBERT, S. D., SIENKIEWICZ, M. & ZHAO, B. 2017. The Modern-Era Retrospective Analysis for Research and Applications, Version 2 (MERRA-2). *Journal of Climate*, 30, 5419-5454.
- GELENCSE, A., MAY, B., SIMPSON, D., SÁNCHEZ - OCHOA, A., KASPER - GIEBL, A., PUXBAUM, H., CASEIRO, A., PIO, C. & LEGRAND, M. 2007. Source apportionment of PM<sub>2.5</sub> organic aerosol over Europe: Primary/secondary, natural/anthropogenic, and fossil/biogenic origin. *Journal of Geophysical Research: Atmospheres*, 112(D23).
- GIGLIO, L., DESCLOITRES, J., JUSTICE, C. O. & KAUFMAN, Y. J. 2003. An Enhanced Contextual Fire Detection Algorithm for MODIS. *Remote Sensing of Environment*, 87, 273-282.
- GOLDSTEIN, A. H., FAN, S. M., GOULDEN, M. L., MUNGER, J. W. & WOFSY, S. C. 1996. Emissions of ethene, propene, and 1-butene by a midlatitude forest. *Journal of Geophysical Research: Atmospheres*, 101, 9149-9157.
- GONZÁLEZ ABAD, G., LIU, X., CHANCE, K., WANG, H., KUROSU, T. P. & SULEIMAN, R. 2015. Updated Smithsonian Astrophysical Observatory Ozone Monitoring Instrument (SAO OMI) formaldehyde retrieval. *Atmospheric Measurement Techniques*, 8, 19-32.
- GREENBERG, J. P., GUENTHER, A. B., PÉTRON, G., WIEDINMYER, C., VEGA, O., GATTI LUCIANA, V., TOTA, J. & FISCH, G. 2004. Biogenic VOC emissions from forested Amazonian landscapes. *Global Change Biology*, 10, 651-662.
- GREENBERG, J. P., ZIMMERMAN, P. R., HEIDT, L. & POLLOCK, W. 1984. Hydrocarbon and carbon monoxide emissions from biomass burning in

- Brazil. *Journal of Geophysical Research: Atmospheres* (1984–2012), 89, 1350-1354.
- GRENFELL, R. J. P., MILTON, M. J. T., HARLING, A. M., VARGHA, G. M., BROOKES, C., QUINCEY, P. G. & WOODS, P. T. 2010. Standard mixtures of ambient volatile organic compounds in synthetic and whole air with stable reference values. *Journal of Geophysical Research*, 115(D14).
- GUENTHER, A., GREENBERG, J., HARLEY, P., HELMIG, D., KLINGER, L., VIERLING, L., ZIMMERMAN, P. & GERON, C. 1996. Leaf, branch, stand and landscape scale measurements of volatile organic compound fluxes from U.S. woodlands. *Tree Physiology*, 16, 17-24.
- GUENTHER, A., KARL, T., HARLEY, P., WIEDINMYER, C., PALMER, P. & GERON, C. 2006. Estimates of global terrestrial isoprene emissions using MEGAN (Model of Emissions of Gases and Aerosols from Nature). *Atmospheric Chemistry and Physics Discussions*, 6, 107-173.
- GUENTHER, A. B., JIANG, X., HEALD, C. L., SAKULYANONTVITTAYA, T., DUHL, T., EMMONS, L. K. & WANG, X. 2012. The Model of Emissions of Gases and Aerosols from Nature version 2.1 (MEGAN2.1): an extended and updated framework for modeling biogenic emissions. *Geoscientific Model Development*, 5, 1471-1492.
- GUENTHER, A. B., MONSON, R. K. & FALL, R. 1991. Isoprene and monoterpene emission rate variability: observations with eucalyptus and emission rate algorithm development. *Journal of Geophysical Research: Atmospheres*, 96, 10799-10808.
- HAO WEI, M. & LIU, M. H. 2012. Spatial and temporal distribution of tropical biomass burning. *Global Biogeochemical Cycles*, 8, 495-503.
- HAUSMANN, P., SUSSMANN, R. & SMALE, D. 2016. Contribution of oil and natural gas production to renewed increase in atmospheric methane (2007–2014): top-down estimate from ethane and methane column observations. *Atmospheric Chemistry and Physics*, 16, 3227-3244.
- HE, C., MURRAY, F. & LYONS, T. 2000. Monoterpene and isoprene emissions from 15 Eucalyptus species in Australia. *Atmospheric Environment*, 34, 645-655.
- HELMIG, D., BALSLEY, B., DAVIS, K., KUCK, L. R., JENSEN, M., BOGNAR, J., SMITH, T., ARRIETA, R. V., RODRÍGUEZ, R. & BIRKS, J. W. 1998. Vertical profiling and determination of landscape fluxes of biogenic nonmethane hydrocarbons within the planetary boundary layer in the Peruvian Amazon. *Journal of Geophysical Research: Atmospheres*, 103, 25519-25532.

- HELMIG, D., BOTTENHEIM, J., GALBALLY, I. E., LEWIS, A., MILTON, M. J. T., PENKETT, S., PLASS - DUELMER, C., REIMANN, S., TANS, P. & THIEL, S. 2011. Volatile Organic Compounds in the Global Atmosphere. *Eos, Transactions American Geophysical Union*, 90, 513-514.
- HELMIG, D., MUÑOZ, M., HUEBER, J., MAZZOLENI, C., MAZZOLENI, L., OWEN, R., VAL MARTIN, M., FIALHO, P., PLASS-DUELMER, C., PALMER, P. I., LEWIS, A. & PFISTER, G. 2015. Climatology and atmospheric chemistry of the non-methane hydrocarbons ethane and propane over the North Atlantic. *Elementa: Science of the Anthropocene*, 3, 1-16.
- HELMIG, D., ROSSABI, S., HUEBER, J., TANS, P., MONTZKA, S. A., MASARIE, K., THONING, K., PLASS-DUELMER, C., CLAUDE, A., CARPENTER, L. J., LEWIS, A. C., PUNJABI, S., REIMANN, S., VOLLMER, M. K., STEINBRECHER, R., HANNIGAN, J. W., EMMONS, L. K., MAHIEU, E., FRANCO, B., SMALE, D. & POZZER, A. 2016. Reversal of global atmospheric ethane and propane trends largely due to US oil and natural gas production. *Nature Geoscience*, 9(7).
- HENZE, D. K. & SEINFELD, J. H. 2006. Global secondary organic aerosol from isoprene oxidation. *Geophysical Research Letters*, 33(9).
- HEWITT, C. N., HAYWARD, S. & TANI, A. 2003. The application of proton transfer reaction-mass spectrometry (PTR-MS) to the monitoring and analysis of volatile organic compounds in the atmosphere. *Journal of Environmental Monitoring*, 5, 1-7.
- HEWITT, C. N., LEE, J. D., MACKENZIE, A. R., BARKLEY, M. P., CARSLAW, N., CARVER, G. D., CHAPPELL, N. A., COE, H., COLLIER, C., COMMANE, R., DAVIES, F., DAVISON, B., DICARLO, P., DI MARCO, C. F., DORSEY, J. R., EDWARDS, P. M., EVANS, M. J., FOWLER, D., FURNEAUX, K. L., GALLAGHER, M., GUENTHER, A., HEARD, D. E., HELFTER, C., HOPKINS, J., INGHAM, T., IRWIN, M., JONES, C., KARUNAHARAN, A., LANGFORD, B., LEWIS, A. C., LIM, S. F., MACDONALD, S. M., MAHAJAN, A. S., MALPASS, S., MCFIGGANS, G., MILLS, G., MISZTAL, P., MOLLER, S., MONKS, P. S., NEMITZ, E., NICOLAS-PEREA, V., OETJEN, H., ORAM, D. E., PALMER, P. I., PHILLIPS, G. J., PIKE, R., PLANE, J. M. C., PUGH, T., PYLE, J. A., REEVES, C. E., ROBINSON, N. H., STEWART, D., STONE, D., WHALLEY, L. K. & YIN, X. 2010. Overview: oxidant and particle photochemical processes above a south-east Asian tropical rainforest (the OP3 project): introduction, rationale, location characteristics and tools. *Atmospheric Chemistry and Physics*, 10, 169-199.

- HOPKINS, J. R., LEWIS, A. C. & READ, K. A. 2003. A two-column method for long-term monitoring of non-methane hydrocarbons (NMHCs) and oxygenated volatile organic compounds (o-VOCs). *Journal of Environmental Monitoring*, 5, 8-13.
- HOROWITZ, L. W., WALTERS, S., MAUZERALL, D. L., EMMONS, L. K., RASCH, P. J., GRANIER, C., TIE, X., LAMARQUE, J. F., SCHULTZ, M. G., TYNDALL, G. S., ORLANDO, J. J. & BRASSEUR, G. P. 2003. A global simulation of tropospheric ozone and related tracers: Description and evaluation of MOZART, version 2. *Journal of Geophysical Research: Atmospheres*, 108(D24).
- HOYER, P. O. 2004. Non-negative Matrix Factorization with Sparseness Constraints. *Journal of Machine Learning Research*, 5, 1457-1469.
- HSIEH, C.-C., HORNG, S.-H. & LIAO, P.-N. 2003. Stability of Trace-level VOLatile Organic Compounds Stored in Canisters and Tedlar Bags. *Aerosol and Air Quality Research*, 3, 17-28.
- HUANG, R.-J., ZHANG, Y., BOZZETTI, C., HO, K.-F., CAO, J.-J., HAN, Y., DAELLENBACH, K. R., SLOWIK, J. G., PLATT, S. M., CANONACO, F., ZOTTER, P., WOLF, R., PIEBER, S. M., BRUNS, E. A., CRIPPA, M., CIARELLI, G., PIAZZALUNGA, A., SCHWIKOWSKI, M., ABBASZADE, G., SCHNELLE-KREIS, J., ZIMMERMANN, R., AN, Z., SZIDAT, S., BALTENSPERGER, U., HADDAD, I. E. & PRÉVÔT, A. S. H. 2014. High secondary aerosol contribution to particulate pollution during haze events in China. *Nature*, 514, 218-222.
- HUANG, Y., OU, Q. & YU, W. 1990. Characteristics of flame ionization detection for the quantitative analysis of complex organic mixtures. *Analytical Chemistry*, 62, 2063-2064.
- HUIJNEN, V., WOOSTER, M. J., KAISER, J. W., GAVEAU, D. L. A., FLEMMING, J., PARRINGTON, M., INNESS, A., MURDIYARSO, D., MAIN, B. & VAN WEELE, M. 2016. Fire carbon emissions over maritime southeast Asia in 2015 largest since 1997. *Scientific Reports*, 6(26886).
- IGLESIAS-SUAREZ, F., KINNISON, D. E., RAP, A., MAYCOCK, A. C., WILD, O. & YOUNG, P. J. 2018. Key drivers of ozone change and its radiative forcing over the 21st century. *Atmospheric Chemistry and Physics*, 18, 6121-6139.
- INNESS, A., BAIER, F., BENEDETTI, A., BOUARAR, I., CHABRILLAT, S., CLARK, H., CLERBAUX, C., COHEUR, P., ENGELEN, R. J., ERRERA, Q., FLEMMING, J., GEORGE, M., GRANIER, C., HADJI-LAZARO, J., HUIJNEN, V., HURTMANS, D., JONES, L., KAISER, J. W., KAPSOMENAKIS, J., LEFEVER, K., LEITÃO, J., RAZINGER, M., RICHTER, A., SCHULTZ, M. G., SIMMONS, A. J., SUTTIE, M.,

- STEIN, O., THÉPAUT, J. N., THOURET, V., VREKOUSSIS, M., ZEREFOS, C. & THE, M. T. 2013. The MACC reanalysis: an 8 yr data set of atmospheric composition. *Atmospheric Chemistry and Physics*, 13, 4073-4109.
- ITO, A. & PENNER, J. E. 2004. Global estimates of biomass burning emissions based on satellite imagery for the year 2000. *Journal of Geophysical Research: Atmospheres*, 109(D14).
- JACOBS, M. I., DARER, A. I. & ELROD, M. J. 2013. Rate Constants and Products of the OH Reaction with Isoprene-Derived Epoxides. *Environmental Science & Technology*, 47, 12868-12876.
- JACOBSON, M. Z. 2001. Global direct radiative forcing due to multicomponent anthropogenic and natural aerosols. *Journal of Geophysical Research*, 106(D2).
- JENKIN, M. E., SAUNDERS, S. M. & PILLING, M. J. 1997. The tropospheric degradation of volatile organic compounds: a protocol for mechanism development. *Atmospheric Environment*, 31, 81-104.
- JONES, A. P. 1999. Indoor air quality and health. *Atmospheric Environment*, 33, 4535-4564.
- JONES, C. E., HOPKINS, J. & LEWIS, A. 2011. In situ measurements of isoprene and monoterpenes within a south-east Asian tropical rainforest. *Atmospheric Chemistry and Physics*, 11, 6971-6984.
- JONQUIÈRES, I., MARENCO, A., MAALEJ, A. & ROHRER, F. 1998. Study of ozone formation and transatlantic transport from biomass burning emissions over West Africa during the airborne Tropospheric Ozone Campaigns TROPOZ I and TROPOZ II. *Journal of Geophysical Research: Atmospheres*, 103, 19059-19073.
- KAISER, J., FLEMMING, J., SCHULTZ, M., SUTTIE, M. & WOOSTER, M. 2009. The macc global fire assimilation system: First emission products (gfasv0). *ECMWF Technical Memoranda*, 596, 1-16.
- KAISER, J. W., HEIL, A., ANDREAE, M. O., BENEDETTI, A., CHUBAROVA, N., JONES, L., MORCRETTE, J. J., RAZINGER, M., SCHULTZ, M. G., SUTTIE, M. & VAN DER WERF, G. R. 2012. Biomass burning emissions estimated with a global fire assimilation system based on observed fire radiative power. *Biogeosciences*, 9, 527-554.
- KAMPA, M. & CASTANAS, E. 2008. Human health effects of air pollution. *Environmental Pollution*, 151, 362-367.

- KANSAL, A. 2009. Sources and reactivity of NMHCs and VOCs in the atmosphere: A review. *Journal of Hazardous Materials*, 166, 17-26.
- KARL, M., DORN, H. P., HOLLAND, F., KOPPMANN, R., POPPE, D., RUPP, L., SCHAUB, A. & WAHNER, A. 2006. Product study of the reaction of OH radicals with isoprene in the atmosphere simulation chamber SAPHIR. *Journal of Atmospheric Chemistry*, 55, 167-187.
- KARL, T., GUENTHER, A., YOKELSON ROBERT, J., GREENBERG, J., POTOSNAK, M., BLAKE DONALD, R. & ARTAXO, P. 2007. The tropical forest and fire emissions experiment: Emission, chemistry, and transport of biogenic volatile organic compounds in the lower atmosphere over Amazonia. *Journal of Geophysical Research: Atmospheres*, 112, 1-19.
- KARL, T., POTOSNAK, M., GUENTHER, A., CLARK, D., WALKER, J., HERRICK, J. D. & GERON, C. 2004. Exchange processes of volatile organic compounds above a tropical rain forest: Implications for modeling tropospheric chemistry above dense vegetation. *Journal of Geophysical Research: Atmospheres (1984-2012)*, 109, 1-19.
- KEELING, C. D., WHORF, T. P., WAHLEN, M. & VAN DER PLICHTT, J. 1995. Interannual extremes in the rate of rise of atmospheric carbon dioxide since 1980. *Nature*, 375, 666-670.
- KEELING, R., PIPER, S., BOLLENBACHER, A. & WALKER, J. 2009. Atmospheric carbon dioxide record from Mauna Loa. ESS-DIVE (Environmental System Science Data Infrastructure for a Virtual Ecosystem); Oak Ridge National Laboratory (ORNL), Oak Ridge, TN (United States).
- KELLER, C., LONG, M., YANTOSCA, R., DA SILVA, A., PAWSON, S. & JACOB, D. 2014. HEMCO v1. 0: A versatile, ESMF-compliant component for calculating emissions in atmospheric models. *Geoscientific Model Development*, 7, 1409-1417.
- KESSELMEIER, J., KUHN, U., ROTTENBERGER, S., BIESENTHAL, T., WOLF, A., SCHEBESKE, G., ANDREAE, M. O., CICCIOLO, P., BRANCALEONI, E., FRATTONI, M., OLIVA, S. T., BOTELHO, M. L., SILVA, C. M. A. & TAVARES, T. M. 2002. Concentrations and species composition of atmospheric volatile organic compounds (VOCs) as observed during the wet and dry season in Rondônia (Amazonia). *Journal of Geophysical Research: Atmospheres*, 107(D20).
- KESSELMEIER, J., KUHN, U., WOLF, A., ANDREAE, M., CICCIOLO, P., BRANCALEONI, E., FRATTONI, M., GUENTHER, A., GREENBERG, J. & VASCONCELLOS, P. D.

- C. 2000. Atmospheric volatile organic compounds (VOC) at a remote tropical forest site in central Amazonia. *Atmospheric Environment*, 34, 4063-4072.
- KESSELMEIER, J. & STAUDT, M. 1999. Biogenic volatile organic compounds (VOC): an overview on emission, physiology and ecology. *Journal of Atmospheric Chemistry*, 33, 23-88.
- KHALIL, M. & RASMUSSEN, R. 1992. Forest hydrocarbon emissions: relationships between fluxes and ambient concentrations. *Journal of the Air & Waste Management Association*, 42, 810-813.
- KITAMURA, D., ONO NOBUTAKA, 2016. *Efficient initialization for nonnegative matrix factorization based on nonnegative independent component analysis. Acoustic Signal Enhancement (IWAENC)*. 1-5.
- KITUYI, E., WANDIGA, S., ANDREAE, M. & HELAS, G. 2005. *Biomass burning in Africa: Role in atmospheric change and opportunities for emission mitigation. Climate Change and Africa*. 79-89.
- KOPLITZ, S. N., MICKLEY, L. J., MARLIER, M. E., BUONOCORE, J. J., KIM, P. S., T, L., SULPRIZIO, M. P., DEFRIES, R. S., JACOB, D. J., SCHWARTZ, J., PONGSIRI, M. & MYERS, S. S. 2016. Public health impacts of the severe haze in Equatorial Asia in September–October 2015: demonstration of a new framework for informing fire management strategies to reduce downwind smoke exposure. *Environmental Research Letters*, 11, 094023.
- KROLL, J. H., NG, N. L., MURPHY, S. M., FLAGAN, R. C. & SEINFELD, J. H. 2006. Secondary organic aerosol formation from isoprene photooxidation. *Environmental science & technology*, 40, 1869-1877.
- KRUPNICK, A. J., HARRINGTON, W. & OSTRO, B. 1990. Ambient ozone and acute health effects: Evidence from daily data. *Journal of Environmental Economics and Management*, 18, 1-18.
- KRZYZANOWSKI, M. & COHEN, A. 2008. Update of WHO air quality guidelines. *Air Quality, Atmosphere & Health*, 1, 7-13.
- KUBISTIN, D., HARDER, H., MARTINEZ, M., RUDOLF, M., SANDER, R., BOZEM, H., EERDEKENS, G., FISCHER, H., GURK, C. & KLÜPFEL, T. 2010. Hydroxyl radicals in the tropical troposphere over the Suriname rainforest: comparison of measurements with the box model MECCA. *Atmospheric Chemistry and Physics*, 10, 9705-9728.
- KUHN, U., ANDREAE, M., AMMANN, C., ARAÚJO, A., BRANCALEONI, E., CICCIOLI, P., DINDORF, T., FRATTONI, M., GATTI, L. & GANZEVELD, L. 2007. Isoprene

- and monoterpene fluxes from Central Amazonian rainforest inferred from tower-based and airborne measurements, and implications on the atmospheric chemistry and the local carbon budget. *Atmospheric Chemistry and Physics*, 7, 2855-2879.
- KUMAR, A. & VÍDEN, I. 2007. Volatile Organic Compounds: Sampling Methods and Their Worldwide Profile in Ambient Air. *Environmental Monitoring and Assessment*, 131, 301-321.
- KUNII, O., KANAGAWA, S., YAJIMA, I., HISAMATSU, Y., YAMAMURA, S., AMAGAI, T. & ISMAIL, I. T. S. 2002. The 1997 Haze Disaster in Indonesia: Its Air Quality and Health Effects. *Archives of Environmental Health: An International Journal*, 57, 16-22.
- KURTEN, E. L., BUNYAVEJCHEWIN, S. & DAVIES, S. J. 2018. Phenology of a dipterocarp forest with seasonal drought: Insights into the origin of general flowering. *Journal of Ecology*, 106, 126-136.
- KUZMA, J. & FALL, R. 1993. Leaf Isoprene Emission Rate Is Dependent on Leaf Development and the Level of Isoprene Synthase. *Plant Physiology*, 101, 435-440.
- LAAKSONEN, A., KULMALA, M., O'DOWD, C. D., JOUTSENSAARI, J., VAATTOVAARA, P., MIKKONEN, S., LEHTINEN, K. E. J., SOGACHEVA, L., DAL MASO, M., AALTO, P., PETÄJÄ, T., SOGACHEV, A., YOON, Y. J., LIHAVAINEN, H., NILSSON, D., FACCHINI, M. C., CAVALLI, F., FUZZI, S., HOFFMANN, T., ARNOLD, F., HANKE, M., SELLEGRI, K., UMANN, B., JUNKERMANN, W., COE, H., ALLAN, J. D., ALFARRA, M. R., WORSNOP, D. R., RIEKKOLA, M. L., HYÖTYLÄINEN, T. & VIISANEN, Y. 2008. The role of VOC oxidation products in continental new particle formation. *Atmospheric Chemistry and Physics*, 8, 2657-2665.
- LAMSAL, L. N., MARTIN, R. V., PADMANABHAN, A., VAN DONKELAAR, A., ZHANG, Q., SIORIS, C. E., CHANCE, K., KUROSU, T. P. & NEWCHURCH, M. J. 2011. Application of satellite observations for timely updates to global anthropogenic NO<sub>x</sub> emission inventories. *Geophysical Research Letters*, 38(5).
- LANGFORD, B., MISZTAL, P. K., NEMITZ, E., DAVISON, B., HELFTER, C., PUGH, T. A. M., MACKENZIE, A. R., LIM, S. F. & HEWITT, C. N. 2010. Fluxes and concentrations of volatile organic compounds from a South-East Asian tropical rainforest. *Atmospheric Chemistry and Physics*, 10, 8391-8412.

- LASHOF, D. A. & AHUJA, D. R. 1990. Relative contributions of greenhouse gas emissions to global warming. *Nature*, 344, 529-531.
- LEE, E., CHAN, C. K. & PAATERO, P. 1999. Application of positive matrix factorization in source apportionment of particulate pollutants in Hong Kong. *Atmospheric Environment*, 33, 3201-3212.
- LELIEVELD, J., BUTLER, T., CROWLEY, J., DILLON, T., FISCHER, H., GANZEVELD, L., HARDER, H., LAWRENCE, M., MARTINEZ, M. & TARABORRELLI, D. 2008. Atmospheric oxidation capacity sustained by a tropical forest. *Nature*, 452, 737-740.
- LERNER, B. M., GILMAN, J. B., AIKIN, K. C., ATLAS, E. L., GOLDAN, P. D., GRAUS, M., HENDERSHOT, R., ISAACMAN-VANWERTZ, G. A., KOSS, A., KUSTER, W. C., LUEB, R. A., MCLAUGHLIN, R. J., PEISCHL, J., SUEPER, D., RYERSON, T. B., TOKAREK, T. W., WARNEKE, C., YUAN, B. & DE GOUW, J. A. 2017. An improved, automated whole air sampler and gas chromatography mass spectrometry analysis system for volatile organic compounds in the atmosphere. *Atmospheric Measurement Techniques*, 10, 291-313.
- LESTARI, R. K., MASAHIRO, W., YUKIKO, I., HIDEO, S., ROBERT, D. F., TOSHIHIKO, T. & MASAHIDE, K. 2014. Increasing potential of biomass burning over Sumatra, Indonesia induced by anthropogenic tropical warming. *Environmental Research Letters*, 9, 104010.
- LEWIS, A. C., EVANS, M. J., HOPKINS, J. R., PUNJABI, S., READ, K. A., PURVIS, R. M., ANDREWS, S. J., MOLLER, S. J., CARPENTER, L. J., LEE, J. D., RICKARD, A. R., PALMER, P. I. & PARRINGTON, M. 2013. The influence of biomass burning on the global distribution of selected non-methane organic compounds. *Atmospheric Chemistry and Physics*, 13, 851-867.
- LI, M., ZHANG, Q., KUROKAWA, J., WOO, J. H., HE, K. B., LU, Z., OHARA, T., SONG, Y., STREETS, D. G., CARMICHAEL, G. R., CHENG, Y. F., HONG, C. P., HUO, H., JIANG, X. J., KANG, S. C., LIU, F., SU, H. & ZHENG, B. 2015. MIX: a mosaic Asian anthropogenic emission inventory for the MICS-Asia and the HTAP projects. *Atmospheric Chemistry and Physics Discuss.*, 2015, 34813-34869.
- LIANG, J. & FAIRLEY, D. 2006. Validation of an efficient non-negative matrix factorization method and its preliminary application in Central California. *Atmospheric Environment*, 40, 1991-2001.
- LINDINGER, C., POLLIEN, P., ALI, S., YERETZIAN, C., BLANK, I. & MÄRK, T. 2005. Unambiguous Identification of Volatile Organic Compounds by Proton-

- Transfer Reaction Mass Spectrometry Coupled with GC/MS. *Analytical Chemistry*, 77, 4117-4124.
- LIU, J., D'AMBRO, E. L., LEE, B. H., LOPEZ-HILFIKER, F. D., ZAVERI, R. A., RIVERA-RIOS, J. C., KEUTSCH, F. N., IYER, S., KURTEN, T., ZHANG, Z., GOLD, A., SURRATT, J. D., SHILLING, J. E. & THORNTON, J. A. 2016. Efficient Isoprene Secondary Organic Aerosol Formation from a Non-IEPOX Pathway. *Environmental Science & Technology*, 50, 9872-9880.
- LIU, X., HUEY, L. G., YOKELSON, R. J., SELIMOVIC, V., SIMPSON, I. J., MÜLLER, M., JIMENEZ, J. L., CAMPUZANO - JOST, P., BEYERSDORF, A. J. & BLAKE, D. R. 2017. Airborne measurements of western US wildfire emissions: Comparison with prescribed burning and air quality implications. *Journal of Geophysical Research: Atmospheres*, 122, 6108-6129.
- LOGAN, J. A. 1999. An analysis of ozonesonde data for the troposphere: Recommendations for testing 3 - D models and development of a gridded climatology for tropospheric ozone. *Journal of Geophysical Research: Atmospheres*, 104, 16115-16149.
- LU, K., ROHRER, F., HOLLAND, F., FUCHS, H., BOHN, B., BRAUERS, T., CHANG, C., HÄSELER, R., HU, M. & KITA, K. 2012. Observation and modelling of OH and HO<sub>2</sub> concentrations in the Pearl River Delta 2006: a missing OH source in a VOC rich atmosphere. *Atmospheric chemistry and physics*, 12, 1541-1569.
- LUDWIG, J., MARUFU, L. T., HUBER, B., ANDREAE, M. O. & HELAS, G. 2003. Domestic Combustion of Biomass Fuels in Developing Countries: A Major Source of Atmospheric Pollutants. *Journal of Atmospheric Chemistry*, 44, 23-37.
- MACKENZIE, A., LANGFORD, B., PUGH, T., ROBINSON, N., MISZTAL, P., HEARD, D., LEE, J., LEWIS, A., JONES, C. & HOPKINS, J. 2011. The atmospheric chemistry of trace gases and particulate matter emitted by different land uses in Borneo. *Philosophical Transactions of the Royal Society B: Biological Sciences*, 366, 3177-3195.
- MAEDA, T., ONODERA, S. & OGINO, H. 1995. On-site monitoring of volatile organic compounds as hazardous air pollutants by gas chromatography. *Journal of Chromatography A*, 710, 51-59.
- MAGGS, R., WAHID, A., SHAMSI, S. R. A. & ASHMORE, M. R. 1995. Effects of ambient air pollution on wheat and rice yield in Pakistan. *Water, Air, and Soil Pollution*, 85, 1311-1316.

- MAHOWALD, N. 2011. Aerosol Indirect Effect on Biogeochemical Cycles and Climate. *Science*, 334, 794-796.
- MARAIS, E. A., JACOB, D. J., JIMENEZ, J. L., CAMPUZANO-JOST, P., DAY, D. A., HU, W., KRECHMER, J., ZHU, L., KIM, P. S., MILLER, C. C., FISHER, J. A., TRAVIS, K., YU, K., HANISCO, T. F., WOLFE, G. M., ARKINSON, H. L., PYE, H. O. T., FROYD, K. D., LIAO, J. & MCNEILL, V. F. 2016. Aqueous-phase mechanism for secondary organic aerosol formation from isoprene: application to the southeast United States and co-benefit of SO<sub>2</sub> emission controls. *Atmospheric Chemistry and Physics*, 16, 1603-1618.
- MARAIS, E. A., JACOB, D. J., KUROSU, T., CHANCE, K., MURPHY, J., REEVES, C., MILLS, G., CASADIO, S., MILLET, D. & BARKLEY, M. P. 2012. Isoprene emissions in Africa inferred from OMI observations of formaldehyde columns. *Atmospheric Chemistry and Physics*, 12, 6219-6235.
- MARR, L. C. & HARLEY, R. A. 2002. Modeling the Effect of Weekday-Weekend Differences in Motor Vehicle Emissions on Photochemical Air Pollution in Central California. *Environmental Science & Technology*, 36, 4099-4106.
- MATSUNAGA, S. N., MOCHIZUKI, T., OHNO, T., ENDO, Y., KUSUMOTO, D. & TANI, A. 2011. Monoterpene and sesquiterpene emissions from Sugi (*Cryptomeria japonica*) based on a branch enclosure measurements. *Atmospheric Pollution Research*, 2, 16-23.
- MAUDERLY, J. L. & CHOW, J. C. 2008. Health Effects of Organic Aerosols. *Inhalation Toxicology*, 20, 257-288.
- MAUZERALL, D. L. & WANG, X. 2001. Protecting Agricultural Crops From the Effects of Tropospheric Ozone Exposure: Reconciling Science and Standard Setting in the United States, Europe, and Asia. *Annual Review of Energy and the Environment*, 26, 237-268.
- MCNEIL, B. I. & MATEAR, R. J. 2008. Southern Ocean acidification: A tipping point at 450-ppm atmospheric CO<sub>2</sub>. *Proceedings of the National Academy of Sciences*, 105, 18860-18864.
- MENTEL, T. F., BLEILEBENS, D. & WAHNER, A. 1996. A study of nighttime nitrogen oxide oxidation in a large reaction chamber—the fate of NO<sub>2</sub>, N<sub>2</sub>O<sub>5</sub>, HNO<sub>3</sub>, and O<sub>3</sub> at different humidities. *Atmospheric Environment*, 30, 4007-4020.
- METOFFICE.GOV.UK. 2018. *Relative Humidity- Annual average: 1981-2010* [Online]. UK Met Office. Available: <https://www.metoffice.gov.uk/public/weather/climate/gcwzefp2c> [Accessed 14/05/2018 2018].

- MISZTAL, P. K., NEMITZ, E., LANGFORD, B., DI MARCO, C. F., PHILLIPS, G. J., HEWITT, C. N., MACKENZIE, A. R., OWEN, S. M., FOWLER, D., HEAL, M. R. & CAPE, J. N. 2011. Direct ecosystem fluxes of volatile organic compounds from oil palms in South-East Asia. *Atmospheric Chemistry and Physics*, 11, 8995-9017.
- MOXIM, W. & LEVY, H. 2000. A model analysis of the tropical South Atlantic Ocean tropospheric ozone maximum: The interaction of transport and chemistry. *Journal of Geophysical Research: Atmospheres*, 105, 17393-17415.
- MUDWAY, I. S. & KELLY, F. J. 2000. Ozone and the lung: a sensitive issue. *Molecular Aspects of Medicine*, 21, 1-48.
- NA, K., KIM, Y. P., MOON, I. & MOON, K.-C. 2004. Chemical composition of major VOC emission sources in the Seoul atmosphere. *Chemosphere*, 55, 585-594.
- NG, N., KWAN, A., SURRATT, J., CHAN, A., CHHABRA, P., SOROOSHIAN, A., PYE, H. O., CROUNSE, J., WENNERBERG, P. & FLAGAN, R. 2008. Secondary organic aerosol (SOA) formation from reaction of isoprene with nitrate radicals (NO<sub>3</sub>). *Atmospheric Chemistry and Physics*, 8, 4117-4140.
- NIELSEN, T., JØRGENSEN, H. E., LARSEN, J. C. & POULSEN, M. 1996. City air pollution of polycyclic aromatic hydrocarbons and other mutagens: occurrence, sources and health effects. *Science of The Total Environment*, 189-190, 41-49.
- NÖLSCHER, A., YANEZ-SERRANO, A., WOLFF, S., DE ARAUJO, A. C., LAVRIČ, J., KESSELMEIER, J. & WILLIAMS, J. 2016. Unexpected seasonality in quantity and composition of Amazon rainforest air reactivity. *Nature communications*, 7(10383).
- OCHIAI, N., DAISHIMA, S. & CARDIN, D. B. 2003. Long-term measurement of volatile organic compounds in ambient air by canister-based one-week sampling method. *Journal of Environmental Monitoring*, 5, 997-1003.
- OLESON, K. W., LAWRENCE, D. M., GORDON, B., FLANNER, M. G., KLUZEK, E., PETER, J., LEVIS, S., SWENSON, S. C., THORNTON, E. & FEDDEMA, J. 2010. Technical description of version 4.0 of the Community Land Model (CLM).
- OLIVIER, J., BOUWMAN, A., VAN DER MAAS, C. & BERDOWSKI, J. 1994. Emission database for global atmospheric research (EDGAR). *Environmental Monitoring and Assessment*, 31, 93-106.
- OMAR, A. H., WON, J. G., WINKER, D. M., YOON, S. C., DUBOVİK, O. & MCCORMICK, M. P. 2005. Development of global aerosol models using cluster analysis of

- Aerosol Robotic Network (AERONET) measurements. *Journal of Geophysical Research: Atmospheres*, 110(D10).
- ORTEGA, J., HELMIG, D., GUENTHER, A., HARLEY, P., PRESSLEY, S. & VOGEL, C. 2007. Flux estimates and OH reaction potential of reactive biogenic volatile organic compounds (BVOCs) from a mixed northern hardwood forest. *Atmospheric Environment*, 41, 5479-5495.
- OWEN, S., BOISSARD, C., STREET, R. A., DUCKHAM, S. C., CSIKY, O. & HEWITT, C. N. 1997. Screening of 18 Mediterranean plant species for volatile organic compound emissions. *Atmospheric Environment*, 31, 101-117.
- OWEN, S. M., HARLEY, P., GUENTHER, A. & HEWITT, C. N. 2002. Light dependency of VOC emissions from selected Mediterranean plant species. *Atmospheric Environment*, 36, 3147-3159.
- PACHAURI, R. K., ALLEN, M. R., BARROS, V. R., BROOME, J., CRAMER, W., CHRIST, R., CHURCH, J. A., CLARKE, L., DAHE, Q. & DASGUPTA, P. 2014. *Climate change 2014: synthesis report. Contribution of Working Groups I, II and III to the fifth assessment report of the Intergovernmental Panel on Climate Change*, IPCC. WMO, UNEP.
- PACYNA, J. M. & PACYNA, E. G. 2001. An assessment of global and regional emissions of trace metals to the atmosphere from anthropogenic sources worldwide. *Environmental Reviews*, 9, 269-298.
- PAGE, S. E., SIEGERT, F., RIELEY, J. O., BOEHM, H.-D. V., JAYA, A. & LIMIN, S. 2002. The amount of carbon released from peat and forest fires in Indonesia during 1997. *Nature*, 420, 61-65.
- PAGLIONE, M., SAARIKOSKI, S., CARBONE, S., HILLAMO, R., FACCHINI, M. C., FINESSI, E., GIULIANELLI, L., CARBONE, C., FUZZI, S., MORETTI, F., TAGLIAVINI, E., SWIETLICKI, E., ERIKSSON STENSTRÖM, K., PRÉVÔT, A. S. H., MASSOLI, P., CANARAGATNA, M., WORSNOP, D. & DECESARI, S. 2014. Primary and secondary biomass burning aerosols determined by proton nuclear magnetic resonance (<sup>1</sup>H-NMR) spectroscopy during the 2008 EUCAARI campaign in the Po Valley (Italy). *Atmospheric Chemistry and Physics*, 14, 5089-5110.
- PALMER, P., PARRINGTON, M., LEWIS, A., LEE, J., RICKARD, A. & BERNATH, P. 2013. *Quantifying the impact of Boreal forest fires on Tropospheric oxidants over the Atlantic using Aircraft and Satellites (BORTAS) experiment: design, execution and science overview*. *Atmospheric Chemistry and Physics*, 13, 6239-6261.

- PALMER, P. I., ABBOT, D. S., FU, T. M., JACOB, D. J., CHANCE, K., KUROSU, T. P., GUENTHER, A., WIEDINMYER, C., STANTON, J. C., PILLING, M. J., PRESSLEY, S. N., LAMB, B. & SUMNER ANNE, L. 2006. Quantifying the seasonal and interannual variability of North American isoprene emissions using satellite observations of the formaldehyde column. *Journal of Geophysical Research: Atmospheres*, 111(D12).
- PALMER, P. I., JACOB, D. J., FIORE, A. M., MARTIN, R. V., CHANCE, K. & KUROSU, T. P. 2003. Mapping isoprene emissions over North America using formaldehyde column observations from space. *Journal of Geophysical Research: Atmospheres*, 108(D6).
- PATTEY, E., DESJARDINS, R. L. & ROCHETTE, P. 1993. Accuracy of the relaxed eddy-accumulation technique, evaluated using CO<sub>2</sub> flux measurements. *Boundary-Layer Meteorology*, 66, 341-355.
- PAULOT, F., CROUNSE, J., KJAERGAARD, H., KROLL, J., SEINFELD, J. & WENNBORG, P. 2009a. Isoprene photooxidation: new insights into the production of acids and organic nitrates. *Atmospheric Chemistry and Physics*, 9, 1479-1501.
- PAULOT, F., CROUNSE, J. D., KJAERGAARD, H. G., KÜRTEIN, A., CLAIR, J. M. S., SEINFELD, J. H. & WENNBORG, P. O. 2009b. Unexpected epoxide formation in the gas-phase photooxidation of isoprene. *Science*, 325, 730-733.
- PEDREGOSA, F. V., G. GRAMFORT, A. MICHEL, V. THIRION, B. GRISEL, O. BLONDEL, M. PRETTENHOFER, P. WEISS, R. DUBOURG, V. VANDERPLAS, J. PASSOS, A. COURNAPEAU, D. BRUCHER, M. PERROT, M. DUCHESNAY, E. 2011. Scikit-learn: Machine learning in Python. *Journal of Machine Learning Research*, 12, 2825-2830.
- PEETERS, J., NGUYEN, T. L. & VEREECKEN, L. 2009. HO<sub>x</sub> radical regeneration in the oxidation of isoprene. *Physical Chemistry Chemical Physics*, 11, 5935-5939.
- PENG, C.-Y., LAN, C.-H. & YANG, C.-Y. 2012. Effects of biodiesel blend fuel on volatile organic compound (VOC) emissions from diesel engine exhaust. *Biomass and Bioenergy*, 36, 96-106.
- PENG, Y. P., CHEN, K. S., LAI, C. H., LU, P. J. & KAO, J. H. 2006. Concentrations of H<sub>2</sub>O<sub>2</sub> and HNO<sub>3</sub> and O<sub>3</sub>-VOC-NO<sub>x</sub> sensitivity in ambient air in southern Taiwan. *Atmospheric Environment*, 40, 6741-6751.
- PEÑUELAS, J. & LLUSIÀ, J. 2001. The complexity of factors driving volatile organic compound emissions by plants. *Biologia Plantarum*, 44, 481-487.

- PETERS, A. 2005. Particulate matter and heart disease: Evidence from epidemiological studies. *Toxicology and Applied Pharmacology*, 207, 477-482.
- PHILIP, S., MARTIN, R. V. & KELLER, C. A. 2016. Sensitivity of chemistry-transport model simulations to the duration of chemical and transport operators: a case study with GEOS-Chem v10-01. *Geoscientific Model Development*, 9, 1683-1695.
- POPE, C. A. 2000. Epidemiology of fine particulate air pollution and human health: biologic mechanisms and who's at risk? *Environmental Health Perspectives*, 108, 713-723.
- POPE, C. A., BURNETT, R. T., THURSTON, G. D., THUN, M. J., CALLE, E. E., KREWSKI, D. & GODLESKI, J. J. 2004. Cardiovascular Mortality and Long-Term Exposure to Particulate Air Pollution. *Circulation*, 109, 71-77.
- PORTER, S. 2016. *Can Indonesia's forest fires be put out for good?* [Online]. Available: <http://www.bbc.co.uk/news/business-35770490> [Accessed 2018]. BBC.
- POSTER, D. L., SCHANTZ, M. M., SANDER, L. C. & WISE, S. A. 2006. Analysis of polycyclic aromatic hydrocarbons (PAHs) in environmental samples: a critical review of gas chromatographic (GC) methods. *Analytical and Bioanalytical Chemistry*, 386, 859-881.
- POZZER, A., POLLMANN, J., TARABORRELLI, D., JOCKEL, P., HELMIG, D., TANS, P., HUEBER, J. & LELIEVELD, J. 2010. Observed and simulated global distribution and budget of atmospheric C2-C5 alkanes. *Atmospheric Chemistry and Physics*, 10, 4402-4422.
- PUGH, T. A. M., MACKENZIE, A. R., HEWITT, C. N., LANGFORD, B., EDWARDS, P. M., FURNEAUX, K. L., HEARD, D. E., HOPKINS, J. R., JONES, C. E., KARUNAHARAN, A., LEE, J., MILLS, G., MISZTAL, P., MOLLER, S., MONKS, P. S. & WHALLEY, L. K. 2010. Simulating atmospheric composition over a South-East Asian tropical rainforest: performance of a chemistry box model. *Atmospheric Chemistry and Physics*, 10, 279-298.
- RAMACHER, B., RUDOLPH, J. & KOPPMAN, R. 1997. Hydrocarbon measurements in the spring arctic troposphere during the ARCTOC 95 campaign. *Tellus B: Chemical and Physical Meteorology*, 49, 466-485.
- RAMACHER, B., RUDOLPH, J. & KOPPMANN, R. 1999. Hydrocarbon measurements during tropospheric ozone depletion events: Evidence for halogen atom chemistry. *Journal of Geophysical Research: Atmospheres*, 104, 3633-3653.

- READ, K. A., LEE, J. D., LEWIS, A. C., MOLLER, S. J., MENDES, L. & CARPENTER, L. J. 2009. Intra - annual cycles of NMVOC in the tropical marine boundary layer and their use for interpreting seasonal variability in CO. *Journal of Geophysical Research: Atmospheres*, 114(D21).
- RHEW, R. C. D., M. J. TURNIPSEED, A. A. WARNEKE, C. ORTEGA, J. SHEN, S. MARTINEZ, L. KOSS, A. LERNER, B. M. GILMAN, J. B. SMITH, J. N. GUENTHER, A. B. DE GOUW, J. A. 2017. Ethene, propene, butene and isoprene emissions from a ponderosa pine forest measured by relaxed eddy accumulation. *Atmospheric Chemistry and Physics*, 17, 13417-13438.
- RICH, A. L. & ORIMOLOYE, H. T. 2016. Elevated Atmospheric Levels of Benzene and Benzene-Related Compounds from Unconventional Shale Extraction and Processing: Human Health Concern for Residential Communities. *Environmental Health Insights*, 10(75).
- RINNE, H., GUENTHER, A., GREENBERG, J. & HARLEY, P. 2002. Isoprene and monoterpene fluxes measured above Amazonian rainforest and their dependence on light and temperature. *Atmospheric Environment*, 36, 2421-2426.
- RIZZO, L. V., ARTAXO, P., KARL, T., GUENTHER, A. & GREENBERG, J. 2010. Aerosol properties, in-canopy gradients, turbulent fluxes and VOC concentrations at a pristine forest site in Amazonia. *Atmospheric Environment*, 44, 503-511.
- ROLPH, G., STEIN, A. & STUNDER, B. 2017. Real-time Environmental Applications and Display sYstem: READY. *Environmental Modelling & Software*, 95, 210-228.
- ROSENZWEIG, C. & PARRY, M. L. 1994. Potential impact of climate change on world food supply. *Nature*, 367, 133-138.
- RUDOLPH, J. 1995. The tropospheric distribution and budget of ethane. *Journal of Geophysical Research: Atmospheres*, 100, 11369-11381.
- SAMET, J. M. & UTELL, M. J. 1990. The risk of nitrogen dioxide: what have we learned from epidemiological and clinical studies? *Toxicology and industrial health*, 6, 247-262.
- SANDERSON, M., JONES, C., COLLINS, W., JOHNSON, C. & DERWENT, R. 2003. Effect of climate change on isoprene emissions and surface ozone levels. *Geophysical Research Letters*, 30(18).
- SAWADA, S., TOTSUKA, TSUMUGU 1967. Natural and anthropogenic sources and fate of atmospheric ethylene. *Atmospheric Environment*, 20, 821-832.

- SAXTON, J., LEWIS, A., KETTLEWELL, J., OZEL, M., GOGUS, F., BONI, Y., KOROGONE, S. & SERÇA, D. 2007. Isoprene and monoterpene measurements in a secondary forest in northern Benin. *Atmospheric Chemistry and Physics*, 7, 4095-4106.
- SAYER, J., GHAZOUL, J., NELSON, P. & KLINTUNI BOEDHIHARTONO, A. 2012. Oil palm expansion transforms tropical landscapes and livelihoods. *Global Food Security*, 1, 114-119.
- SCHNITZLER, J. P., LEHNING, A. & STEINBRECHER, R. 2014. Seasonal Pattern of Isoprene Synthase Activity in *Quercus robur* Leaves and its Significance for Modeling Isoprene Emission Rates. *Botanica Acta*, 110, 240-243.
- SCHUH, G., HEIDEN, A., HOFFMANN, T., KAHL, J., ROCKEL, P., RUDOLPH, J. & WILDT, J. 1997. Emissions of volatile organic compounds from sunflower and beech: dependence on temperature and light intensity. *Journal of Atmospheric Chemistry*, 27, 291-318.
- SCHULTZ, M. G. 2015. The Global Atmosphere Watch reactive gases measurement network. *Elementa Science of the Anthropocene*, 67, 1-24.
- SCHULTZ, M. G., SCHRÖDER, S., LYAPINA, O., COOPER, O. R., GALBALLY, I., PETROPAVLOVSKIKH, I., VON SCHNEIDEMESSER, E., TANIMOTO, H., ELSHORBANY, Y., NAJA, M., SEGUEL, R. J., DAUERT, U., ECKHARDT, P., FEIGENSPAN, S., FIEBIG, M., HJELLBREKKE, A.-G., HONG, Y.-D., KJELD, P. C., KOIDE, H., LEAR, G., TARASICK, D., UENO, M., WALLASCH, M., BAUMGARDNER, D., CHUANG, M.-T., GILLETT, R., LEE, M., MOLLOY, S., MOOLLA, R., WANG, T., SHARPS, K., ADAME, J. A., ANCELLET, G., APADULA, F., ARTAXO, P., BARLASINA, M. E., BOGUCA, M., BONASONI, P., CHANG, L., COLOMB, A., CUEVAS-AGULLÓ, E., CUPEIRO, M., DEGORSKA, A., DING, A., FRÖHLICH, M., FROLOVA, M., GADHAVI, H., GHEUSI, F., GILGE, S., GONZALEZ, M. Y., GROS, V., HAMAD, S. H., HELMIG, D., HENRIQUES, D., HERMANSEN, O., HOLLA, R., HUEBER, J., IM, U., JAFFE, D. A., KOMALA, N., KUBISTIN, D., LAM, K.-S., LAURILA, T., LEE, H., LEVY, I., MAZZOLENI, C., MAZZOLENI, L. R., MCCLURE-BEGLEY, A., MOHAMAD, M., MUROVEC, M., NAVARRO-COMAS, M., NICODIM, F., PARRISH, D., READ, K. A., REID, N., RIES, L., SAXENA, P., SCHWAB, J. J., SCORGIE, Y., SENIK, I., SIMMONDS, P., SINHA, V., SKOROKHOD, A. I., SPAIN, G., SPANGL, W., SPOOR, R., SPRINGSTON, S. R., STEER, K., STEINBACHER, M., SUHARGUNIYAWAN, E., TORRE, P., TRICKL, T., WEILI, L., WELLER, R., XU, X., XUE, L. & ZHIQIANG, M. 2017. Tropospheric Ozone Assessment Report, links to Global surface ozone datasets. *Supplement to: Schultz, MG et al. (2017): Tropospheric Ozone Assessment Report: Database and Metrics Data of Global Surface Ozone Observations. Elementa - Science of the Anthropocene*, 5:58, 26 pp, <https://doi.org/10.1525/elementa.244>. PANGAEA.
- SCHUMANN, U. & HUNTRIESER, H. 2007. The global lightning-induced nitrogen oxides source. *Atmospheric Chemistry and Physics*, 7, 3823-3907.
- SCHUUR, E. A. G., BOCKHEIM, J., CANADELL, J. G., EUSKIRCHEN, E., FIELD, C. B., GORYACHKIN, S. V., HAGEMANN, S., KUHR, P., LAFLEUR, P. M., LEE, H.,

- MAZHITOVA, G., NELSON, F. E., RINKE, A., ROMANOVSKY, V. E., SHIKLOMANOV, N., TARNOCAI, C., VENEVSKY, S., VOGEL, J. G. & ZIMOV, S. A. 2008. Vulnerability of Permafrost Carbon to Climate Change: Implications for the Global Carbon Cycle. *BioScience*, 58, 701-714.
- SCHWARZE, P. E., ØVREVIK, J., LÅG, M., REFSNES, M., NAFSTAD, P., HETLAND, R. B. & DYBING, E. 2006. Particulate matter properties and health effects: consistency of epidemiological and toxicological studies. *Human & Experimental Toxicology*, 25, 559-579.
- SCOTT, A. J. & KNOTT, M. 1974. A Cluster Analysis Method for Grouping Means in the Analysis of Variance. *Biometrics*, 30, 507-512.
- SCOTT, C., RAP, A., SPRACKLEN, D., FORSTER, P., CARSLAW, K., MANN, G., PRINGLE, K., KIVEKÄS, N., KULMALA, M. & LIHAVAINEN, H. 2014. The direct and indirect radiative effects of biogenic secondary organic aerosol. *Atmospheric Chemistry and Physics*, 14, 447-470.
- SHAO, M., ZHANG, Y., ZENG, L., TANG, X., ZHANG, J., ZHONG, L. & WANG, B. 2009. Ground-level ozone in the Pearl River Delta and the roles of VOC and NO<sub>x</sub> in its production. *Journal of Environmental Management*, 90, 512-518.
- SHARKEY, T. D., SINGSAAS, E. L., LERDAU, M. T. & GERON, C. D. 1999. Weather Effects on Isoprene Emission Capacity and Applications in Emissions Algorithms. *Ecological Applications*, 9, 1132-1137.
- SHERWEN, T., SCHMIDT, J. A., EVANS, M. J., CARPENTER, L. J., GROSSMAN, K., EASTHAM, S. D., JACOB, D. J., DIX, B., KOENIG, T. K. & SINREICH, R. 2016. Global impacts of tropospheric halogens (Cl, Br, I) on oxidants and composition in GEOS-Chem. *Atmospheric Chemistry and Physics*, 16, 12239-12271.
- SHIRAI, T., BLAKE, D. R., MEINARDI, S., ROWLAND, F. S., RUSSELL - SMITH, J., EDWARDS, A., KONDO, Y., KOIKE, M., KITA, K., MACHIDA, T., TAKEGAWA, N., NISHI, N., KAWAKAMI, S. & OGAWA, T. 2003. Emission estimates of selected volatile organic compounds from tropical savanna burning in northern Australia. *Journal of Geophysical Research: Atmospheres*, 108(D3).
- SILLMAN, S. 1999. The relation between ozone, NO<sub>x</sub> and hydrocarbons in urban and polluted rural environments. *Atmospheric Environment*, 33, 1821-1845.
- SILVA, S. J., HEALD, C. L., GEDDES, J. A., AUSTIN, K. G., KASIBHATLA, P. S. & MARLIER, M. E. 2016. Impacts of current and projected oil palm plantation

- expansion on air quality over Southeast Asia. *Atmospheric Chemistry and Physics*, 16, 10621-10635.
- SIMPSON, D., GUENTHER, A., HEWITT, C. N. & STEINBRECHER, R. 1995. Biogenic emissions in Europe: 1. Estimates and uncertainties. *Journal of Geophysical Research: Atmospheres*, 100, 22875-22890.
- SIMPSON, I. J., AKAGI, S. K., BARLETTA, B., BLAKE, N. J., CHOI, Y., DISKIN, G. S., FRIED, A., FUELBERG, H. E., MEINARDI, S., ROWLAND, F. S., VAY, S. A., WEINHEIMER, A. J., WENNBERG, P. O., WIEBRING, P., WISTHALER, A., YANG, M., YOKELSON, R. J. & BLAKE, D. R. 2011. Boreal forest fire emissions in fresh Canadian smoke plumes: C1-C10 volatile organic compounds (VOCs), CO<sub>2</sub>, CO, NO<sub>2</sub>, NO, HCN and CH<sub>3</sub>CN. *Atmospheric Chemistry and Physics*, 11, 6445-6463.
- SIMPSON, I. J., SULBAEK ANDERSEN, M. P., MEINARDI, S., BRUHWILER, L., BLAKE, N. J., HELMIG, D., ROWLAND, F. S. & BLAKE, D. R. 2012. Long-term decline of global atmospheric ethane concentrations and implications for methane. *Nature*, 488, 490-494.
- SIN, D. W.-M., WONG, Y.-C., SHAM, W.-C. & WANG, D. 2001. Development of an analytical technique and stability evaluation of 143 C3-C12 volatile organic compounds in Summa[registered sign] canisters by gas chromatography-mass spectrometry. *Analyst*, 126, 310-321.
- SINDELAROVA, K., GRANIER, C., BOUARAR, I., GUENTHER, A., TILMES, S., STAVRAKOU, T., MÜLLER, J.-F., KUHN, U., STEFANI, P. & KNORR, W. 2014. Global data set of biogenic VOC emissions calculated by the MEGAN model over the last 30 years. *Atmospheric Chemistry and Physics*, 14, 9317-9341.
- SINHA, V., WILLIAMS, J., LELIEVELD, J., RUUSKANEN, T. M., KAJOS, M. K., PATOKOSKI, J., HELLEN, H., HAKOLA, H., MOGENSEN, D., BOY, M., RINNE, J. & KULMALA, M. 2010. OH Reactivity Measurements within a Boreal Forest: Evidence for Unknown Reactive Emissions. *Environmental Science & Technology*, 44, 6614-6620.
- SIRITHIAN, D., THEPANONDH, S., SATTTLER, M. L. & LAOWAGUL, W. 2018. Emissions of volatile organic compounds from maize residue open burning in the northern region of Thailand. *Atmospheric Environment*, 176, 179-187.
- SOLBERG, S., DYE, C., SCHMIDBAUER, N., HERZOG, A. & GEHRIG, R. 1996. Carbonyls and nonmethane hydrocarbons at rural European sites from the mediterranean to the arctic. *Journal of Atmospheric Chemistry*, 25, 33-66.

- SONG, Y., XIE, S., ZHANG, Y., ZENG, L., SALMON, L. G. & ZHENG, M. 2006. Source apportionment of PM<sub>2.5</sub> in Beijing using principal component analysis/absolute principal component scores and UNMIX. *Science of The Total Environment*, 372, 278-286.
- SPRENGNETHER, M., DEMERJIAN KENNETH, L., DONAHUE NEIL, M. & ANDERSON JAMES, G. 2002. Product analysis of the OH oxidation of isoprene and 1,3 - butadiene in the presence of NO. *Journal of Geophysical Research: Atmospheres*, 107(D15).
- SQUIRE, O., ARCHIBALD, A., ABRAHAM, N., BEERLING, D., HEWITT, C., LATHIÈRE, J., PIKE, R., TELFORD, P. & PYLE, J. 2014. Influence of future climate and cropland expansion on isoprene emissions and tropospheric ozone. *Atmospheric Chemistry and Physics*, 14, 1011-1024.
- ST. CLAIR, J. M., RIVERA-RIOS, J. C., CROUNSE, J. D., KNAP, H. C., BATES, K. H., TENG, A. P., JØRGENSEN, S., KJAERGAARD, H. G., KEUTSCH, F. N. & WENNERBERG, P. O. 2016. Kinetics and Products of the Reaction of the First-Generation Isoprene Hydroxy Hydroperoxide (ISOPOOH) with OH. *The Journal of Physical Chemistry A*, 120, 1441-1451.
- STEIN, A. F., DRAXLER, R. R., ROLPH, G. D., STUNDER, B. J. B., COHEN, M. D. & NGAN, F. 2015. NOAA's HYSPLIT Atmospheric Transport and Dispersion Modeling System. *Bulletin of the American Meteorological Society*, 96, 2059-2077.
- STEINBRECHER, R. & WEIB, E. 2012. Standard operating procedures (SOPs) for air sampling in stainless steel canisters for non-methane hydrocarbons analysis. *GAW Report no. 204*, WMO.
- STOCKWELL, C., VERES, P., WILLIAMS, J. & YOKELSON, R. 2015. *Characterization of biomass burning emissions from cooking fires, peat, crop residue, and other fuels with high-resolution proton-transfer-reaction time-of-flight mass spectrometry. Atmospheric Chemistry and Physics*, 15, 845-865.
- STOCKWELL, C. E., JAYARATHNE, T., COCHRANE, M. A., RYAN, K. C., PUTRA, E. I., SAHARJO, B. H., NURHAYATI, A. D., ALBAR, I., BLAKE, D. R., SIMPSON, I. J., STONE, E. A. & YOKELSON, R. J. 2016. Field measurements of trace gases and aerosols emitted by peat fires in Central Kalimantan, Indonesia, during the 2015 El Nino. *Atmospheric Chemistry and Physics*, 16, 11711-11732.
- STONE, D., EVANS, M. J., EDWARDS, P. M., COMMANE, R., INGHAM, T., RICKARD, A. R., BROOKES, D. M., HOPKINS, J., LEIGH, R. J., LEWIS, A. C., MONKS, P. S., ORAM, D., REEVES, C. E., STEWART, D. & HEARD, D. E. 2011. Isoprene

- oxidation mechanisms: measurements and modelling of OH and HO<sub>2</sub> over a South-East Asian tropical rainforest during the OP3 field campaign. *Atmospheric Chemistry and Physics*, 11, 6749-6771.
- SUN, J., WU, F., HU, B., TANG, G., ZHANG, J. & WANG, Y. 2016. VOC characteristics, emissions and contributions to SOA formation during hazy episodes. *Atmospheric Environment*, 141, 560-570.
- TANI, A., HAYWARD, S. & HEWITT, C. N. 2003. Measurement of monoterpenes and related compounds by proton transfer reaction-mass spectrometry (PTR-MS). *International Journal of Mass Spectrometry*, 223-224, 561-578.
- TARABORRELLI, D., LAWRENCE, M. G., CROWLEY, J. N., DILLON, T. J., GROMOV, S., GROS, C. B. M., VEREECKEN, L. & LELIEVELD, J. 2012. Hydroxyl radical buffered by isoprene oxidation over tropical forests. *Nature Geoscience*, 5, 190-193.
- THELOKE, J. & FRIEDRICH, R. 2007. Compilation of a database on the composition of anthropogenic VOC emissions for atmospheric modeling in Europe. *Atmospheric Environment*, 41, 4148-4160.
- THIRUMALAI, K., DINEZIO, P. N., OKUMURA, Y. & DESER, C. 2017. Extreme temperatures in Southeast Asia caused by El Niño and worsened by global warming. *Nature Communications*, 8, no. 15531.
- THOMPSON, A. M., WITTE, J. C., HUDSON, R. D., GUO, H., HERMAN, J. R. & FUJIWARA, M. 2001. Tropical Tropospheric Ozone and Biomass Burning. *Science*, 291, 2128-2132.
- TIE, X., ZHANG, R., BRASSEUR, G. & LEI, W. 2002. Global NO<sub>x</sub> Production by Lightning. *Journal of Atmospheric Chemistry*, 43, 61-74.
- TINGEY, D. T., MANNING, M., GROTHAUS, L. C. & BURNS, W. F. 1979. The Influence of Light and Temperature on Isoprene Emission Rates from Live Oak. *Physiologia Plantarum*, 47, 112-118.
- TODLING, R. E. A., A 2018. The GMAO Hybrid Ensemble-Variational Atmospheric Data Assimilation System: Version 2.0. *Technical Report Series on Global Modeling and Data Assimilation, Volume 50*, NASA.
- TZOMPA - SOSA, Z. A., MAHIEU, E., FRANCO, B., KELLER, C. A., TURNER, A. J., HELMIG, D., FRIED, A., RICHTER, D., WEIBRING, P. & WALEGA, J. 2017. Revisiting global fossil fuel and biofuel emissions of ethane. *Journal of Geophysical Research: Atmospheres*, 122, 2493-2512.
- UHDE, E. 2007. Application of Solid Sorbents for the Sampling of Volatile Organic Compounds in Indoor Air. *Organic Indoor Air Pollutants*.

- ULBRICH, I. M., CANAGARATNA, M. R., ZHANG, Q., WORSNOP, D. R. & JIMENEZ, J. L. 2009. Interpretation of organic components from Positive Matrix Factorization of aerosol mass spectrometric data. *Atmospheric Chemistry and Physics*, 9, 2891-2918.
- UMUKORO, G. E. & ISMAIL, O. S. 2017. Modelling emissions from natural gas flaring. *Journal of King Saud University - Engineering Sciences*, 29, 178-182.
- UNGER, N. 2014. Human land-use-driven reduction of forest volatiles cools global climate. *Nature Climate Change*, 4, 907-910.
- VADREVU, K., OHARA, T. & JUSTICE, C. 2017. Land cover, land use changes and air pollution in Asia: a synthesis. *Environmental Research Letters*, 12, 120201.
- VAN AARDENNE, J. A., CARMICHAEL, G. R., LEVY, H., STREETS, D. & HORDIJK, L. 1999. Anthropogenic NO<sub>x</sub> emissions in Asia in the period 1990–2020. *Atmospheric Environment*, 33, 633-646.
- VAN DINGENEN, R., DENTENER, F. J., RAES, F., KROL, M. C., EMBERSON, L. & COFALA, J. 2009. The global impact of ozone on agricultural crop yields under current and future air quality legislation. *Atmospheric Environment*, 43, 604-618.
- VÉKEY, K. 2001. Mass spectrometry and mass-selective detection in chromatography. *Journal of Chromatography A*, 921, 227-236.
- VLACHOKOSTAS, C., NASTIS, S. A., ACHILLAS, C., KALOGEROPOULOS, K., KARMIRIS, I., MOUSSIOPOULOS, N., CHOURDAKIS, E., BANIAS, G. & LIMPERI, N. 2010. Economic damages of ozone air pollution to crops using combined air quality and GIS modelling. *Atmospheric Environment*, 44, 3352-3361.
- VOLKAMER, R., JIMENEZ, J. L., SAN MARTINI, F., DZEPINA, K., ZHANG, Q., SALCEDO, D., MOLINA, L. T., WORSNOP, D. R. & MOLINA, M. J. 2006. Secondary organic aerosol formation from anthropogenic air pollution: Rapid and higher than expected. *Geophysical Research Letters*, 33(17).
- VOULGARAKIS, A., NAIK, V., LAMARQUE, J.-F., SHINDELL, D. T., YOUNG, P., PRATHER, M. J., WILD, O., FIELD, R., BERGMANN, D. & CAMERON-SMITH, P. 2013. Analysis of present day and future OH and methane lifetime in the ACCMIP simulations. *Atmospheric Chemistry and Physics*, 13, 2563-2587.
- WANG, S. & HAO, J. 2012. Air quality management in China: Issues, challenges, and options. *Journal of Environmental Sciences*, 24, 2-13.

- WANG, S., XING, J., ZHAO, B., JANG, C. & HAO, J. 2014. Effectiveness of national air pollution control policies on the air quality in metropolitan areas of China. *Journal of Environmental Sciences*, 26, 13-22.
- WANG, T., CHEUNG, T. F., LI, Y. S., YU, X. M. & BLAKE, D. R. 2002. Emission characteristics of CO, NO<sub>x</sub>, SO<sub>2</sub> and indications of biomass burning observed at a rural site in eastern China. *Journal of Geophysical Research: Atmospheres*, 107(D12).
- WANG, Y., RAIHALA, T. S., JACKMAN, A. P. & ST. JOHN, R. 1996. Use of Tedlar Bags in VOC Testing and Storage: Evidence of Significant VOC Losses. *Environmental Science & Technology*, 30, 3115-3117.
- WANG, Y. X., MCELROY, M. B., JACOB, D. J. & YANTOSCA, R. M. 2004. A nested grid formulation for chemical transport over Asia: Applications to CO. *Journal of Geophysical Research: Atmospheres*, 109(D22).
- WARNEKE, C., GOUW JOOST, A., HOLLOWAY JOHN, S., PEISCHL, J., RYERSON THOMAS, B., ATLAS, E., BLAKE, D., TRAINER, M. & PARRISH DAVID, D. 2012. Multiyear trends in volatile organic compounds in Los Angeles, California: Five decades of decreasing emissions. *Journal of Geophysical Research: Atmospheres*, 117(D21).
- WARNEKE, C., HOLZINGER, R., HANSEL, A., JORDAN, A., LINDINGER, W., PÖSCHL, U., WILLIAMS, J., HOOR, P., FISCHER, H., CRUTZEN, P. J., SCHEEREN, H. A. & LELIEVELD, J. 2001. Isoprene and Its Oxidation Products Methyl Vinyl Ketone, Methacrolein, and Isoprene Related Peroxides Measured Online over the Tropical Rain Forest of Surinam in March 1998. *Journal of Atmospheric Chemistry*, 38, 167-185.
- WENBERG, P. O., BATES, K. H., CROUNSE, J. D., DODSON, L. G., MCVAY, R. C., MERTENS, L. A., NGUYEN, T. B., PRASKE, E., SCHWANTES, R. H., SMARTE, M. D., ST CLAIR, J. M., TENG, A. P., ZHANG, X. & SEINFELD, J. H. 2018. Gas-Phase Reactions of Isoprene and Its Major Oxidation Products. *Chemical Reviews*, 118, 3337-3390.
- WENTWORTH, G. R., AKLILU, Y.-A., LANDIS, M. S. & HSU, Y.-M. 2018. Impacts of a large boreal wildfire on ground level atmospheric concentrations of PAHs, VOCs and ozone. *Atmospheric Environment*, 178, 19-30.
- WEST, J. J., SZOPA, S. & HAUGLUSTAINE, D. A. 2007. Human mortality effects of future concentrations of tropospheric ozone. *Comptes Rendus Geoscience*, 339, 775-783.

- WHALLEY, L. K., EDWARDS, P. M., FURNEAUX, K. L., GODDARD, A., INGHAM, T., EVANS, M. J., STONE, D., HOPKINS, J. R., JONES, C. E., KARUNAHARAN, A., LEE, J. D., LEWIS, A. C., MONKS, P. S., MOLLER, S. J. & HEARD, D. E. 2011. Quantifying the magnitude of a missing hydroxyl radical source in a tropical rainforest. *Atmospheric Chemistry and Physics*, 11, 7223-7233.
- WHO 2006. *Air quality guidelines: global update 2005*, World Health Organization.
- WIEDINMYER, C., AKAGI, S., YOKELSON, R., EMMONS, L., AL-SAADI, J., J. ORLANDO, J. & J. SOJA, A. 2010. *The Fire INventory from NCAR (FINN) – a high resolution global model to estimate the emissions from open burning. Geoscientific Model Development*, 4(3).
- WILD, O., ZHU, X. & PRATHER, M. J. 2000. Fast-J: Accurate Simulation of In- and Below-Cloud Photolysis in Tropospheric Chemical Models. *Journal of Atmospheric Chemistry*, 37, 245-282.
- WOLD, S., ESBENSEN, K. & GELADI, P. 1987. Principal component analysis. *Chemometrics and Intelligent Laboratory Systems*, 2, 37-52.
- WOOLFENDEN, E. 2010. Sorbent-based sampling methods for volatile and semi-volatile organic compounds in air: Part 1: Sorbent-based air monitoring options. *Journal of Chromatography A*, 1217, 2674-2684.
- XIAO, Y., JACOB, D. & TURQUETY, S. 2007. Atmospheric acetylene and its relationship with CO<sub>2</sub> as an indicator of air mass age. *Journal of Geophysical Research*, 112(D12).
- YANG, W. & OMAJE, S. T. 2009. Air pollutants, oxidative stress and human health. *Mutation Research/Genetic Toxicology and Environmental Mutagenesis*, 674, 45-54.
- YOKELSON, R. J., SUSOTT, R., WARD, D. E., REARDON, J. & GRIFFITH, D. W. 1997. Emissions from smoldering combustion of biomass measured by open - path Fourier transform infrared spectroscopy. *Journal of Geophysical Research: Atmospheres*, 102, 18865-18877.
- YOU, K.-W., GE, Y.-S., HU, B., NING, Z.-W., ZHAO, S.-T., ZHANG, Y.-N. & XIE, P. 2007. Measurement of in-vehicle volatile organic compounds under static conditions. *Journal of Environmental Sciences*, 19, 1208-1213.
- YU, H., KAUFMAN, Y., CHIN, M., FEINGOLD, G., REMER, L., ANDERSON, T., BALKANSKI, Y., BELLOUIN, N., BOUCHER, O. & CHRISTOPHER, S. 2006. A review of measurement-based assessments of the aerosol direct radiative effect and forcing. *Atmospheric Chemistry and Physics*, 6, 613-666.

- YUAN, B., SHAO, M., LU, S. & WANG, B. 2010. Source profiles of volatile organic compounds associated with solvent use in Beijing, China. *Atmospheric Environment*, 44, 1919-1926.
- YUE, T., YUE, X., CHAI, F., HU, J., LAI, Y., HE, L. & ZHU, R. 2017. Characteristics of volatile organic compounds (VOCs) from the evaporative emissions of modern passenger cars. *Atmospheric Environment*, 151, 62-69.
- YUSOFF, S. 2006. Renewable energy from palm oil – innovation on effective utilization of waste. *Journal of Cleaner Production*, 14, 87-93.
- ZENG, G., PYLE, J. A. & YOUNG, P. J. 2008. Impact of climate change on tropospheric ozone and its global budgets. *Atmospheric Chemistry and Physics*, 8, 369-387.
- ZHANG, L., LIU, L., ZHAO, Y., GONG, S., ZHANG, X., HENZE, D. K., CAPPS, S. L., FU, T.-M., ZHANG, Q. & WANG, Y. 2015. Source attribution of particulate matter pollution over North China with the adjoint method. *Environmental Research Letters*, 10, 084011.
- ZHANG, Q., STREETS DAVID, G., HE, K., WANG, Y., RICHTER, A., BURROWS JOHN, P., UNO, I., JANG CAREY, J., CHEN, D., YAO, Z. & LEI, Y. 2007. NO<sub>x</sub> emission trends for China, 1995–2004: The view from the ground and the view from space. *Journal of Geophysical Research: Atmospheres*, 112(D22).
- ZHANG, R., SUH, I., LEI, W., CLINKENBEARD ANGELA, D. & NORTH SIMON, W. 2000. Kinetic studies of OH - initiated reactions of isoprene. *Journal of Geophysical Research: Atmospheres*, 105, 24627-24635.
- ZHAO, Y., NIELSEN, C., LEI, Y., MCELROY, M. & HAO, J. 2011. Quantifying the uncertainties of a bottom-up emission inventory of anthropogenic atmospheric pollutants in China. *Atmospheric Chemistry and Physics*, 11, 2295-2308.
- ZHENG, C., SHEN, J., ZHANG, Y., HUANG, W., ZHU, X., WU, X., CHEN, L., GAO, X. & CEN, K. 2017. Quantitative assessment of industrial VOC emissions in China: Historical trend, spatial distribution, uncertainties, and projection. *Atmospheric Environment*, 150, 116-125.
- ZHOU, Y., XING, X., LANG, J., CHEN, D., CHENG, S., LIN, W., XIAO, W. & LIU, C. 2017. A comprehensive biomass burning emission inventory with high spatial and temporal resolution in China. *Atmospheric Chemistry and Physics*, 17, 2839.
- ZIEMKE, J. R., CHANDRA, S., DUNCAN, B. N., SCHOEBERL, M. R., TORRES, O., DAMON, M. R. & BHARTIA, P. K. 2009. Recent biomass burning in the

tropics and related changes in tropospheric ozone. *Geophysical Research Letters*, 36(15).